

https://dspace.org/

Performance analysis of plate heat exchangers used as refrigerant evaporators

Huang, Jianchang

2011-05-16
http://hdl.handle.net/10539/9779

Downloaded from a DSpace repository. https://dspace.org/

PERFORMANCE ANALYSIS OF PLATE HEAT EXCHANGERS USED AS REFRIGERANT EVAPORATORS

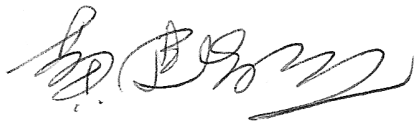
Jianchang Huang

A thesis submitted to the Faculty of Engineering and the Built Environment, University of the Witwatersrand, Johannesburg, in fulfillment of the requirements for the degree of Doctor of Philosophy.

University of the Witwatersrand, Johannesburg
August, 2010

DECLARATION

I declare that this thesis is my own unaided work. It is being submitted to the Degree of Doctor of Philosophy to the University of the Witwatersrand, Johannesburg. It has not been submitted before for any degree or examination to any other University.



.....

24 day of 08 year 2010

ABSTRACT

In this study the heat transfer and frictional pressure drop performance characteristics of plate heat exchangers (PHE's) used as refrigerant liquid over-feed evaporators were investigated. PHE's have been gaining new applications in the refrigeration industry, especially as evaporators, during the last few decades, but the available information in the open literature for operation in this mode is rather limited. This study aims to extend the knowledge of PHE evaporator performance and to develop a model for use in evaluating heat transfer and pressure drop over as wide a range of operating conditions as possible.

A laboratory experimental facility was constructed and the thermal-hydraulic characteristics of three middle-size industrial PHE's were measured. The exchangers all had 24 plates of the same size but with different chevron angle combinations of 28°/28°, 28°/60°, and 60°/60°. Two sets of tests were carried out with the three units: single-phase performance tests with water, and evaporator performance tests with R134a and R507A, for which the exchangers operated as refrigerant liquid over-feed evaporators. The tests with water served to provide accurate water-side heat transfer information for the evaporator performance analysis which is the primary purpose of this study. In the evaporator performance tests, refrigerant flow boiling heat transfer and two-phase pressure drop data were obtained under steady conditions, over a range of heat flux from 1.9 to 6.9 kW/m^2, refrigerant mass flux from 5.6 to 31.4 kg/(m^2s), outlet vapour quality from 0.2 to 0/95, and saturation temperatures from 5.9 to 13.0 °C. Additional field data of thermal performance were collected on an ammonia and a R12 PHE water chiller, operating as thermo-siphon evaporators at their design working conditions.

All experimental data were reduced and analyzed to obtain the refrigerant-side heat transfer coefficients and frictional pressure drops in the PHE evaporators. The heat transfer results showed a strong dependence on heat flux and a weak dependence on mass flux, vapour fraction and the chevron angle. Along with the observations from the ammonia and R12 evaporators, it is concluded that the dominating heat transfer mechanism in this type of evaporator is nucleate boiling rather than forced convection. In contrast to the heat transfer characteristics, the refrigerant two-phase frictional pressure drop was found to be strongly influenced by mass flow rate, vapour fraction and also the chevron angle. An almost linear increase of the frictional pressure drop with the homogeneous two-phase kinetic energy per unit volume was observed for both refrigerants.

Based on the experimental data, correlations were developed for predicting the refrigerant boiling heat transfer coefficient and two-phase frictional pressure drop in PHE liquid over-feed evaporators. Two correlations were developed for boiling heat transfer, one of these reflecting the *h*-*q* relationship in pool boiling, the other with all constants and exponents determined by regression analysis. The mean absolute errors are respectively 7.3% and 6.8% for these correlations. For two-phase frictional pressure drop, data were correlated using two established methods, namely the homogeneous and the Lockhart-Martinelli methods, with means absolute errors of 6.7% and 4.2%, respectively. The homogeneous model showed a slightly higher discrepancy with the experimental data but is likely to be more physically sound for PHE evaporators, and is much simpler to apply. Validation of these correlations with other data has been difficult due to the shortage of published information. For other refrigerants operating at comparable conditions, these correlations should serve as a guide, while more accurate design or evaluation may need to be based on further testing.

The performance analysis carried out in this study was based on systematic experimental investigations and field tests on industrial PHE units. Correlations were developed covering a rather extensive range of flow parameters, plate geometry and various refrigerants. Such correlations have not been reported previously for PHE liquid over-feed evaporators. The results simplify the performance analysis of PHE evaporators and provide a reliable thermal-hydraulic model of PHE liquid over-feed evaporators, which can be used for system modeling of water-chilling machines employing this type of evaporator.

ACKNOWLEDGEMENT

It is difficult to express my gratitude to Professor Thomas J. Sheer, my supervisor, for his support both academically and financially, and for his enormous encouragement and patience during the course of this study. Thank you for your guidance and help, for so long.

I wish to give my sincere thanks to Dr. Michael Bailey-McEwan, my co-supervisor, for his time and all the discussions. Your advice and help had always been valuable to me.

I would also like to convey my gratitude to those who have helped me in any way to finish this work.

To Chunyan Shen, for her encouragement and long-time support.

To the Mechanical Lab staff, especially Mr. John D. Cooper and Mr. Albertus P. Moller, for their considerable assistance with the experimental apparatus.

To Alexander Russell, for his excellent assistance during the water tests.

To Envirocool refrigeration company, for suggestions and building up the experimental infrastructure.

To Mr. Basil Chassoulas, of the School of Chemistry, for his advice on selecting temperature sensors.

To my friends and office neighbors, for all the discussion and leisure talking.

To the University of The Witwatersrand, Johannesburg, for granting me the Postgraduate Merit Award for three years, for the service and facility, and the time and memories I shared with.

CONTENTS

Abstract i

Acknowledgement iii

Contents iv

Nomenclature viii

CHAPTER 1 INTRODUCTION 1

1.1 Background 1

1.2 Objectives, Scope and Methodology 2

1.3 Structure of the Thesis 3

CHAPTER 2 LITERATURE REVIEW 5

2.1 Pool Boiling 5

2.1.1 Overview of Boiling 5
2.1.2 Pool Boiling 6

2.2 Flow Boiling 8

2.2.1 Flow Patterns 9
2.2.2 Flow Boiling in Microchannels 10
2.2.3 Flow Boiling Heat Transfer Correlations 11
2.2.4 Estimation of Boiling Heat Transfer Coefficient of Refrigerant Evaporators 24

2.3 Two-phase Pressure Drop 26

2.3.1 An Overview 26
2.3.2 The Homogeneous Flow Model 28
2.3.3 The Separated Flow Model 31
2.3.4 Two-phase Pressure Drop Correlations 32

2.4 Heat Exchanger Theory 39

2.4.1 Classification of Heat Exchangers 39
2.4.2 Basics of Thermal Characteristics 39

2.5 Plate Heat Exchangers 41

2.5.1 Types of Plate Heat Exchangers 41
2.5.2 Plate Geometry 43
2.5.3 Flow Arrangements 46
2.5.4 Hydraulic diameter, Reynolds Number, and Friction Factor 47

2.6 Single-phase Flow in PHE’s 50

2.6.1 Overall Thermal-hydraulic Performance 50
2.6.2 Single-phase Heat Transfer and Pressure Drop Correlations 53
2.6.3 Flow Distribution 63
2.6.4 Fouling 64
2.6.5 Numerical Simulations 65

2.7 Two-phase Flow in PHE's 66

2.7.1 Adiabatic Two-phase Flow Characteristics 67
2.7.2 Flow Boiling Heat Transfer in PHE's 70
2.7.3 Two-phase Pressure Drop 76
2.7.4 Heat Transfer and Pressure Drop Correlations 80

CHAPTER 3 EXPERIMENTAL INFRASTRUCTURE 87

3.1 Introduction 87

3.2 Brazed Plate Heat Exchangers 88

3.3 Water Test Arrangements 89

3.4 Refrigerant Evaporator Test Arrangements 90

3.4.1 Liquid Over-feed System 90
3.4.2 System Design 93
3.4.3 The Experimental Facility 96

3.5 Instrumentation and Measurement 99

3.5.1 Water Test System 99
3.5.2 Refrigerant Evaporator Test System 101

3.6 Data Acquisition System 104

3.7 Sensor Calibration 108

CHAPTER 4 SINGLE-PHASE PERFORMANCE TESTS WITH WATER 111

4.1 Introduction 111

4.2 Test Procedure 111

4.3 Data Reduction 113

4.3.1 Heat Transfer 113
4.3.2 Pressure Drop 116

4.4 Uncertainty Analysis 119

4.5 Results and Discussion 120

4.5.1 Heat Transfer Characteristics 120
4.5.2 Pressure Drop Characteristics 124

4.6 Conclusion 126

CHAPTER 5 FIELD TESTS ON LARGE-SCALE PHE'S 128

5.1 Introduction 128
5.2 PHE Thermo-Siphon Evaporators 128
5.3 Measurements and Data Reduction 131
5.4 Results and Discussion 132
5.5 Conclusion 134

CHAPTER 6 EVAPORATOR PERFORMANCE TESTS USING R134a AND R507A 136

6.1 Introduction 136
6.2 Test Procedure 138
6.3 Data Reduction 139
6.3.1 Flow Boiling Heat Transfer 139
6.3.2 Two-phase Pressure Drop 141
6.4 Uncertainty Analysis 146
6.5 Results and Discussion 146
6.5.1 Heat Transfer Characteristics 147
6.5.2 Pressure Drop Characteristics 152
6.6 Conclusion 154

CHAPTER 7 DEVELOPMENT OF THERMAL-HYDRAULIC CORRELATIONS FOR PHE EVAPORATORS 155

7.1 Introduction 155
7.2 Flow Boiling Heat Transfer 155
7.3 Two-phase Frictional Pressure Drop 160
7.3.1 Correlation using the Homogeneous Model 160
7.3.2 Correlation using the Lockhart-Martinelli Method 165
7.4 Conclusion 169

CHAPTER 8 CONCLUSIONS AND RECOMMENDATIONS 171

8.1 Conclusions 171
8.2 Suggestions for Future Work 174
8.3 Suggestions on Experimental Facility Design 175

References 177

Appendix A Plate Geometrical Information 190
Appendix B Sensor Technical Data and Wire Connections 193

Appendix C	**Sensor Calibration**	**199**
Appendix D	**Data Acquisition System Specifications**	**207**
Appendix E	**Experiment Results: Water Tests**	**209**
Appendix F	**Experimental Results: Refrigerant Evaporator Tests**	**212**
Appendix G	**Sample Calculation: Refrigerant Evaporator Tests**	**224**
Appendix H	**MATLAB Program Flow Chart: Water Heat Transfer Coefficient**	**229**
Appendix I	**Uncertainty Analysis: General Theory, the ASME and ISO Method**	**232**
Appendix J	**Uncertainty Analysis: Sensor Calibration**	**249**
Appendix K	**Uncertainty Analysis: Water Tests**	**260**
Appendix L	**Uncertainty Analysis: Refrigerant Evaporator Tests**	**270**
Appendix M	**Heat Transfer Surface Partition for a DX Evaporator**	**279**
Appendix N	**Operating Instructions for the Refrigerant Evaporator Test Facility**	**281**

Nomenclature

A	heat transfer area	m^2
A_c	flow channel cross-section area	m^2
A_{ch}	single channel flow cross-section area	m^2
A_p	heat transfer area per plate	m^2
a	acceleration	m/s^2
Bo	boiling number, $\mathrm{Bo} = q/\left(G \cdot i_{fg}\right)$	–
b	plate corrugation depth	m
C	Chisholm parameter	m
c_f	Darcy friction factor, $c_f = \tau_w / \left(\frac{1}{2}\rho u^2\right)$	–
c_p	specific heat at constant pressure	J/(kg·K)
Co	convection number, $\mathrm{Co} = \left(\frac{1-x}{x}\right)^{0.8}\left(\frac{\rho_g}{\rho_f}\right)^{0.5}$	–
D	mass transfer diffusivity	m^2/s
d	diameter	m
d_0	bubble departure diameter, $d_0 = 0.0146\beta\left[\frac{2\sigma}{g(\rho_f - \rho_g)}\right]^{0.5}$	m
d_e	equivalent diameter	m
d_h	hydraulic diameter, $d_h = 4\frac{V}{S}$	m
E	enhancement factor for forced convection	–
e_r	percentage error, $e_r = \frac{\phi_{corr} - \phi_{expe}}{\phi_{expe}}$	–
e_m	mean absolute error, $e_m = \frac{1}{n} \cdot \sum\left(\left\lvert\frac{\phi_{corr} - \phi_{expe}}{\phi_{expe}}\right\rvert\right)$	–
F	1. force	N
	2. log mean temperature difference correction factor	–
	3. suppression factor of nucleate boiling in Chen corr.	–
f	Fanning friction factor, $f = 4c_f$	–
Fr	Froude number, $\mathrm{Fr} = u^2/(gL)$	–
Fr_f	Froude number assuming all mass flow as liquid $\mathrm{Fr}_f = G^2/\left(gd\rho_f{}^2\right)$	–
G	mass velocity	$kg/(m^2 \cdot s)$
g	gravitational constant	m/s^2

g_c	gravitational constant in English units	(ft·lbm)/(s^2·lbf)
h	1. heat transfer coefficient	W/(m^2·K)
	2. specific enthalpy	kJ/kg
h_{tp}	two-phase flow boiling heat transfer coefficient	W/(m^2·K)
h_{nb}	nucleate boiling heat transfer coefficient	W/(m^2·K)
h_f	single-phase convective heat transfer coefficient	W/(m^2·K)
i_{fg}	latent heat of vaporization	J/kg
j	1. phase superficial velocity, $j_i = Q_i / A_c$	m/s
	2. Chilton-Colburn j-factor, $j = \frac{\mathrm{Nu}}{\mathrm{Re}\cdot \mathrm{Pr}^{1/3}} = \frac{\mathrm{Sh}}{\mathrm{Re}\cdot \mathrm{Sc}^{1/3}}$	–
j_{Nu}	heat transfer group, $j_{Nu} = \frac{\mathrm{Nu}}{\mathrm{Pr}^{1/3}\left(\mu/\mu_{wall}\right)^{1/6}}$	–
k	thermal conductivity	W/(m·K)
k_c	mass transfer coefficient	m/s
L	length	m
L_{eff}	effective channel length	m
L_p	port center to port center channel length	m
M	1. molecular weight	kg/mol
	2. mass	kg
$\dot{m}$	mass flow rate	kg/s
N_{ch}	number of channels	–
N_p	number of plates	–
$N_{p,\,eff}$	number of effective plates	–
N_{pass}	number of passes in a PHE	–
n_{RC}	recirculation rate in liquid over-feed system	–
Ntu	heat exchanger number of transfer units	–
Nu	Nusselt number	–
P	pressure	Pa
P_{crit}	critical pressure of fluid	Pa
P_r	reduced pressure, $P_r = P / P_{crit}$	–
ΔP	pressure difference	Pa
Pr	Prandtl number, $\mathrm{Pr} = \mu c_p / k$	–
$\dot{Q}$	total heat transfer rate	W
Q	volumetric flow rate	m^3/s
q	heat flux	W/m^2
R	thermal resistance	m^2·K/W
R_f	fouling factor	m^2·K/W

R_p	surface roughness	m
Re	Reynolds number, $\mathrm{Re} = \rho u d / \mu$	–
Re_{fo}	liquid-only Reynolds number, $\mathrm{Re}_{fo} = Gd / \mu_f$	–
Re_{go}	vapour-only Reynolds number, $\mathrm{Re}_{go} = Gd / \mu_g$	–
r_a	channel aspect ratio, $r_a = L_p / w$	–
S_{wet}	flow channel wetted surface area	m^2
Sc	Schmidt number, $\mathrm{Sc} = \nu / D$	–
Sh	Sherwood number, $\mathrm{Sh} = k_c \cdot L / D$	–
T	temperature	°C
t	time	s
ΔT_{LM}	log mean temperature difference	°C
ΔT_{sat}	excess temperature in boiling, $\Delta T_{sat} = T_{wall} - T_{sat}$	°C
U	over-all heat transfer coefficient	$W/(m^2 \cdot K)$
u	velocity	m/s
	uncertainty	–
V	volume	m^3
$\vec{V}$	velocity vector	m/s
We	Webber number, $\mathrm{We} = G^2 d / (\rho \sigma)$	–
w	channel width	m
x	vapour quality, $x = \dot{m}_g / \dot{m}$	–
x_m	mean vapour quality, $x_m = 0.5(x_{in} + x_{out})$	–
X	Martinelli parameter $X^2 = \left(\frac{dP}{dz}\right)_{fric,\,f} \Big/ \left(\frac{dP}{dz}\right)_{fric,\,g}$	–
Y	parameter used in the Chisholm (1973) correlation $Y^2 = \left(\frac{dP}{dz}\right)_{fric,\,fo} \Big/ \left(\frac{dP}{dz}\right)_{fric,\,go}$	–
z	channel axial co-ordinate	m

Greek

α	1. thermal diffusivity, $\alpha = k / (\rho\, c_p)$	m^2/s
	2. void fraction, $\alpha = A_g / A_c$	–
β	plate corrugation angle (measured from vertical direction)	degrees
δ	thickness	m

ε	heat exchanger effectiveness	–
ϕ	1. plate surface enlargement factor	–
	2. general term for undefined parameter	–
ϕ_{fo}^{2}	two-phase friction multiplier based on pressure gradient assuming total mass flow as liquid	–
ϕ_{f}^{2}	two-phase friction multiplier based on pressure gradient assuming only liquid phase fraction flowing	–
λ	plate corrugation pitch	m
μ	viscosity	Pa·s
$\bar{\mu}$	two-phase mean viscosity	Pa·s
θ	90°- β	degrees
ν	kinematic viscosity, $\nu = \mu / \rho$	m^2/s
ρ	density	kg/m^3
$\bar{\rho}$	two-phase mean density	kg/m^3
σ	surface tension	N/m
τ_w	shear stress at the wall	N/m^2
ψ	heat transfer enhancement factor, $\psi = h_{tp} / h_f$ (introduced in Shah 1976 correlation)	–

Subscripts

0	reference condition	h	hydraulic
acce	acceleration	i	inlet
c	1. cross-section	m	mean
	2. convective	max	maximum
ch	channel	meas	measurement
corr	correlation	min	minimum
crit	critical	nb	nucleate boiling
e	equivalent	o	outlet
eff	effective	p	plate
elev	elevation	port	port
expe	experiment	r	refrigerant
f	liquid phase	sat	saturation
fo	all mass flow as liquid	sub	subcooling
fg	change of phase, liquid to vapour	tp	two-phase
		w	1. water, 2. wall
fric	friction	wall	wall
g	gas/vapour phase		

CHAPTER 1

INTRODUCTION

1.1 Background

Plate heat exchangers (PHE's) were first commercially introduced in the 1920's to meet the hygienic demands of the dairy industry (Seligman, 1963, Carlson, 1992), while some patents existed as early as in the 1870's in Germany (Clark, 1974). Design of this type of exchanger reached maturity in the 1960's with the development of more effective plate geometries, assemblies, and improved gasket material, and the range of possible applications has widened considerably (Kakac S. and Liu H., 2002). PHE's are nowadays widely used in a broad range of heating and cooling applications in food processing, chemical reaction processes, petroleum, pulp and paper, as well as in many water-chilling applications. Some basic features of PHE's include high efficiency and compactness (i.e., high heat transfer capacity per unit volume compared to conventional, shell-and-tube heat exchangers), high flexibility for desired load and pressure drop, easy cleaning, and cost competitiveness.

While PHE's became popular for liquid-to-liquid heat transfer duties, their use in phase-changing applications was not common initially. Before the 1990's such applications were mostly in the fields of concentrating liquid food and drying of chemicals (Usher, 1970, Kumar, 1993). Applications in refrigeration systems were rare, mainly because of concerns over refrigerant leakage, and also because of the pressure limits required, especially on condensation applications. In the last two decades, with the introduction of semi-welded and brazed PHE's, this type of exchanger has been increasingly used in refrigeration systems, from domestic heat pumps to large ammonia installations for water-chilling duties.

Heat exchangers, including PHE's and other types, are designed and employed according to two criteria: heat transfer and pressure drop. Characteristics of the heat exchanger's thermo-hydraulic performance are the primary interest of most investigations. The corrugated channels of PHE's have probably the most complicated geometry of all flow ducts. As the number of applications has

increased, single-phase flows in PHE's have been well investigated in the last few decades. Although a general theory about the influence of some geometric parameters is lacking, due to the complex geometry of the flow channel, a large number of correlations for heat transfer and pressure drop are available in the open literature. The number of published investigations on two-phase heat transfer and pressure drop in PHE's is increasing but is not yet comprehensive. Due to the complexity of the two-phase flow process, a rigorous theoretical analysis is not feasible. The fundamental understanding of the flow boiling mechanism in this type of channel is rather limited. A few two-phase flow boiling heat transfer and frictional pressure drop correlations exist in the literature, obtained from water, R-22, R-134a, R-410a, and ammonia. The coverage of important flow boiling parameters, including the heat flux, mass flux and vapour fraction, is usually limited and unsystematic and the operating conditions vary. As a result, there is not a generally accepted calculation method for flow boiling heat transfer and two-phase pressure drop for PHE evaporators. Although accurate and complex formulations were developed by manufacturers, based on many years of research and systematic testing of specified plates and arrangements, these formulations are confidential and closely guarded.

Vapour-compression refrigerating machines employing PHE evaporators have been used for some years in South African deep mining for water-chilling duties. For the requirement of large cooling loads (well over 1 MW) and also for thermal efficiency, liquid over-feed systems are usually considered rather than direct expansion (DX) systems. System modelling of the water-chilling machines has been difficult due to the shortage of reliable information to model the evaporator performance. Such a need motivated an extensive survey and new research on PHE evaporator performance analysis, to obtain a validated thermal-hydraulic model of PHE evaporators which can be used in the simulation of compete refrigeration systems.

1.2 Objectives, Scope and Methodology

The purpose of the present study is to investigate the performance of plate heat exchangers used as refrigerant liquid over-feed evaporators. The objective is to extend the present knowledge of the thermo-hydraulic performance of PHE evaporators with consideration of flow conditions (mass flux, heat flux, vapour fraction) and channel geometries (chevron angles). This study aims to obtain a generally applicable model, which is able to provide design and operating guidelines for this type of evaporator, and to be used for the simulation of complete refrigeration systems. The specific objectives of this thesis are:

1. To carry out a thorough literature review on plate heat exchangers, their terminology, working principles, single-phase performance characteristics and most importantly the state of the art of evaluating the flow boiling heat transfer and two-phase frictional pressure drop in PHE channels,
2. To obtain single-phase water-water heat transfer and pressure drop data for a range of PHE's. This serves to provide a quantitative understanding of the performance of PHE's in single-phase applications, and to provide accurate water-side heat transfer coefficient information for the PHE evaporators.
3. To obtain flow boiling heat transfer and two-phase frictional pressure drop data, to cover various refrigerants, flow conditions (mass flow rate, heat flux, vapour quality), and channel geometries (chevron angles).
4. As the final and principal aim, to extend the present knowledge of the thermo-hydraulic performance of PHE liquid over-feed evaporators. It is the task of this study to develop general correlations which cover more than one refrigerant and must be able to predict the refrigerant flow boiling heart transfer and frictional pressure drop with reasonable accuracy.

There are a few types of PHE's available, but this study was limited to the chevron (herring-bone) corrugation type. Inlet flow conditioning (normally commercially available via flow distributors) was not considered [1]. A laboratory experimental facility was to be constructed. The facility was to be designed as a liquid over-feed system. This type of system is more flexible for experimental purposes compared with dry expansion and thermo-siphon systems, giving a wide spectrum of possibilities for evaporator running conditions. The experimental equipment was to employ multiple PHE units covering different chevron angles which are typical of industrial applications, and various refrigerants needed to be used. Development of a flow boiling thermo-hydraulic model of the evaporators was to be carried out based on the experimental results, with the assistance of statistical analysis.

1.3 Structure of the Thesis

This thesis contains eight chapters. Chapter 1 provides an introduction to plate heat exchanger applications in refrigeration, followed by the objectives, scope, motivation and methodology of the current study. Chapter 2 provides a critical

[1] Flow distributors are designed to gain uniform flow distribution among channels. This kind of device is more commonly employed in DX evaporators. The Effect of distributors on the thermo-hydraulic performance of a PHE is hard to estimate, and for the sake of clarity and simplicity, distributors are not used in the present study.

review of the literature. This chapter includes a thorough examination of the established theories and methods for flow boiling heat transfer and two-phase pressure drop in general, an in-depth review of plate heat exchanger theory, terminology, working principles, and single-phase performance characteristics, with special attention then paid to flow boiling heat transfer and two-phase frictional pressure drop characteristics in PHE channels. Chapter 3 provides a detailed description of the experimental facility, including the plate heat exchangers, the water test facility and the refrigerant evaporator test facility, instrumentation and the data acquisition system. Chapter 4 describes the single-phase performance tests with water. Chapter 5 analyzes the results of previous field tests on large-scale PHE water-chillers employing ammonia and R12. Chapter 6 presents results of the evaporator performance tests using R134a and R507A. Chapter 7 discusses the results of the data analysis, and presents the development of thermal and hydraulic correlations for PHE liquid over-feed evaporators. Chapter 8 summarizes the overall results and gives suggestion for future work and experimental facility design.

CHAPTER 2

LITERATURE REVIEW

2.1 Pool Boiling

2.1.1 Overview of Boiling

Boiling is a thermodynamic process occurring at a solid-liquid interface in which a fluid is heated by a surface with a temperature above the saturation temperature of the liquid which changes from liquid to vapour phase. *Pool boiling* is the simplest form of boiling with the heating surface being immersed in a large pool of stagnant liquid. If boiling occurs in a liquid that is in motion relative to the surface, it is called *forced convective boiling*, or *flow boiling*. In both types, depending on whether the main body of the liquid in the vicinity of the heated surface is at (or slightly above) or below the saturation temperature, either *saturated boiling* or *subcooled boiling* occurs, respectively.

Boiling occurs only when the temperature of the solid surface T_{wall} exceeds the liquid saturation temperature T_{sat} corresponding to its local pressure. Heat is transferred from the solid surface to the liquid, as can be expressed by Newton's law of cooling:

$$q = h\left(T_{wall} - T_{sat}\right) = h\Delta T_{sat} \qquad (2.\ 1)$$

where $\Delta T_{sat} = T_{wall} - T_{sat}$ is called the excess temperature. Equation (2.1) applies to all types of phase-changing heat transfer, including pool boiling, flow boiling, and condensation. Generally, heat transfer coefficients associated with phase changing, including boiling and condensation, are larger compared with those associated with single-phase forced and natural convection.

The process of boiling is characterized by the formation of bubbles, which grow and detach from the surface. Vapour bubble growth and dynamics depend, in a complicated manner, on the excess temperature, heating surface nature, and

liquid properties (Incropera and DeWitt, 1990). Boiling is a complex phenomenon that is difficult to model analytically. Despite many works on bubble dynamics, boiling nucleation, influence of free convection, etc., a reliable and accurate analytical theory is not available.

2.1.2 Pool Boiling

Nucleate pool boiling is affected by various parameters. In many cases, an accurate quantitative description of those parameters that affect the heat transfer coefficient is very difficult. The three most investigated parameters include heat flux, saturation pressure, and the thermo-physical properties of the working fluid (Pioro et al., 2004). Despite the large number of articles on the subject, a theoretically consistent calculation method on pool boiling heat transfer does not exist (Gorenflo, 1999). The process of pool boiling is best described experimentally by the boiling curve, as available from most heat transfer text books. Briefly, four boiling regimes are found in pool boiling, with unique characteristics, those are natural convection, nucleate boiling, transition boiling, and stable film boiling. Of those, the nucleate boiling region is the primary interest of industry applications.

Data from nucleate pool boiling experiments are usually fitted with expressions such as (Thome, 2003):

$$q \propto \Delta T_{sat}{}^{n} \tag{2. 2}$$

where the exponent n is of the order of 3. Collier (1983) pointed out that the value of n is dependent on the physical properties of the liquid and vapour and on the nucleation properties of the surface, normally in the range of 2 - 4, with a most probable value around 3 to 3.3. With n = 3, it can be obtained from Equations (2.1) and (2.2) that:

$$h \propto q^{2/3} \tag{2. 3}$$

Literally there are hundreds of pool boiling correlations that have been proposed, and those can be classified into several groups according to the assumed dominating mechanism, for example, bubble agitation, reduced pressure, fluid physical properties, etc. Some of the well organized and widely quoted correlations include those of Rohsenow (1952), Stephan and Abdelsalam (1980), Cooper (1984), Gorenflo (1993). Thome (2003) presented a detailed examination of those correlations. Three of those correlations are employed in the present study for comparison purposes, and are given below.

Stephan and Abdelsalam (1980) Correlation

$$\frac{hd_0}{k_f} = 207\left(\frac{qd_0}{k_f T_{sat}}\right)^{0.745}\left(\frac{\rho_g}{\rho_f}\right)^{0.581}\left(\frac{\mu_f c_{p,f}}{k_f}\right)^{0.533} \quad (2.4)$$

where T_{sat} is in K, $d_0 = 0.0146\beta\sqrt{2\sigma/\left[g\left(\rho_f - \rho_g\right)\right]}$ is the bubble departure diameter an β = 35° is the contact angle. For refrigerants, $3\times10^{-3} \le P_r \le 0.78$, mean absolute error = 10.57%.

Equation (2.4) is one of several correlations for classes of fluids including water, organics, refrigerants and cryogens, developed by the authors using statistical regression techniques.

Cooper (1984) Correlation

Cooper proposed the following reduced pressure expression for the nucleate pool boiling heat transfer coefficient:

$$h_{nb} = 55P_r^{\,0.12-0.2\log_{10}R_p}(-\log 10P_r)^{-0.55}M^{-0.5}q^{0.67} \quad (2.5)$$

Note that this is a dimensional correlation in which:
h_{nb}, nucleate boiling heat transfer coefficient, W/(m^2·K),
q, heat flux, W/m^2
P_r, reduced pressure, $P_r = P/P_{crit}$, where P_{crit} is the critical pressure of the fluid,
M, molecular weight of the fluid,
R_p, surface roughness parameter in μm, R_p=1 μm for unspecified surface.

Cooper's correlation is for nucleate pool boiling on plane surfaces; for boiling on horizontal copper tubes, *h* is suggested to be multiplied by a factor of 1.7. The correlation is based on a large range of data, covering reduced pressures from 0.001 to 0.9, and molecular weights from 2 to 200. This correlation has probably the simplest form of all those available for nucleate boiling heat transfer. However, for its accuracy this correlation has gained popularity among many researchers. The very basic *h*-*q* relationship as suggested by Equation (2.3) is clearly evident in this correlation. Collier and Thome (1994) recommended this correlation for water, refrigerants, and organic fluids with poorly defined physical properties. Thome (2003) suggested this correlation for general use.

Gorenflo (1993) Correlation

$$\frac{h}{h_0} = F\left(P_r\right)\left(\frac{q}{q_0}\right)^n\left(\frac{R_p}{R_{p,0}}\right)^{0.133} \qquad (2.6)$$

where
h_0 is the reference heat transfer coefficient, based on $P_r = 0.1$ and $R_{p,0} = 0.4\ \mu$m,
$q_0 = 20$ kW/m^2 is the reference heat flux,
$F\left(P_r\right) = 1.2P_r^{0.27} + 2.5P_r + P_r/\left(1-P_r\right)$, and $n = 0.9 - 0.3P_r^{0.3}$ for all fluids except for water and helium.

The Gorenflo method is based on the concept of reduced pressure but also on a reference heat transfer coefficient at specified standard conditions. The reference value of h_0 are given by the author for a selection of fluids. For fluids outside this selection, additional correlations determining the reference h_0 are needed.

2.2 Flow Boiling

Flow boiling, or forced convective boiling, can have two categories according to the surface geometry: internal flow and external flow. Internal flow boiling is associated with bubble formation at the inner surface of a heated channel through with a liquid flowing. Bubble growth and separation are believed to be strongly influenced by fluid motion, and hydrodynamic effects differ significantly from those corresponding to pool boiling (Incropera and DeWitt, 1990).

The process of flow boiling is associated with the existence of various two-phase flow patterns and is difficult to model. In the literature, it is generally agreed that flow boiling heat transfer has two fundamental components: *nucleate boiling* and *forced convection*. The nucleate boiling part resembles the nucleate pool boiling heat transfer in which heat is transferred into bulk fluid by means of local bubble nucleation, growth and subsequent departure from the surface. The forced convection part is simply assumed as a representation of single-phase heat transfer. The total heat transfer coefficient is calculated by combining the two, with weighting. The combined effects of the two components are not well understood, many hypotheses have been proposed, based on which correlations have been developed. Usually the forced convection part is believed to be enhanced, because the fluid velocity, which is the dominating parameter in single phase convective heat transfer, is higher in two-phase flow than in single-phase

liquid flow given that the channel cross-section is partially occupied by gas (vapour) phase. Other the other hand, the nucleate boiling part is suppressed due to the fact that forced convection effect reduces the thermal boundary layer thickness on the heated surface, and thus suppresses bubble nucleation.

2.2.1 Flow Patterns

Various flow structures are observed in flow boiling, and those are defined as two-phase flow patterns with identifying characteristics. Flow patterns of vertical and horizontal flow generally differ, as flow in horizontal pipes is influenced by the effect of gravity, which acts to stratify the liquid to the bottom and the gas/vapour to the top of the channel. Refrigerant evaporators usually have vertically orientated channels, where two-phase liquid and vapour refrigerant flows in a co-current upward manner.

Four flow patterns are usually identified for vertical up-flows in conventional tubes: bubble, slug (plug), churn, and annular (McQuillan and Whalley, 1985). Figure 2.1 gives the flow patterns in an uniformly heated vertical tube with a low heat flux, with associated wall and fluid temperature variations and heat transfer regions. Churn flow is not present in Figure 2.1, but it can be identified as a highly disturbed flow pattern between slug and annular flow. Flow patterns in horizontal flow will be somewhat different from those shown in this figure. Taitel and Dukler (1976) specified five flow regimes in horizontal two-phase flow, those are smooth stratified, wavy stratified, intermittent (slug and plug), annular and dispersed bubble. It should be pointed out that a two-phase flow pattern is a subjective observation, and there is no general assessing method which identifies and describes flow patterns precisely.

One simple method of representing flow pattern transitions that occur at particular local conditions is by the form of a two dimensional flow pattern map. Respective flow patterns are represented as areas on a graph, with the co-ordinates being most often chosen as superficial phase velocities, j_g and j_f, or other generalized parameters containing these velocities. Coordinates of flow patterns can be arbitrarily chosen, as pointed out by Taitel et al. (1980). Because there was little theoretical basis for selection of coordinates, their generality and accuracy are limited. Nevertheless, flow pattern maps have long been widely used in the industry, the most recognized ones are probably that proposed by Hewitt and Roberts for vertical flow, and that of Baker for horizontal flow.

The channel geometry of a plate heat exchanger is very different from a straight circular tube; flow patterns identified in conventional tubes may not be entirely applicable. For example, due to the highly three-dimensional flow directions,

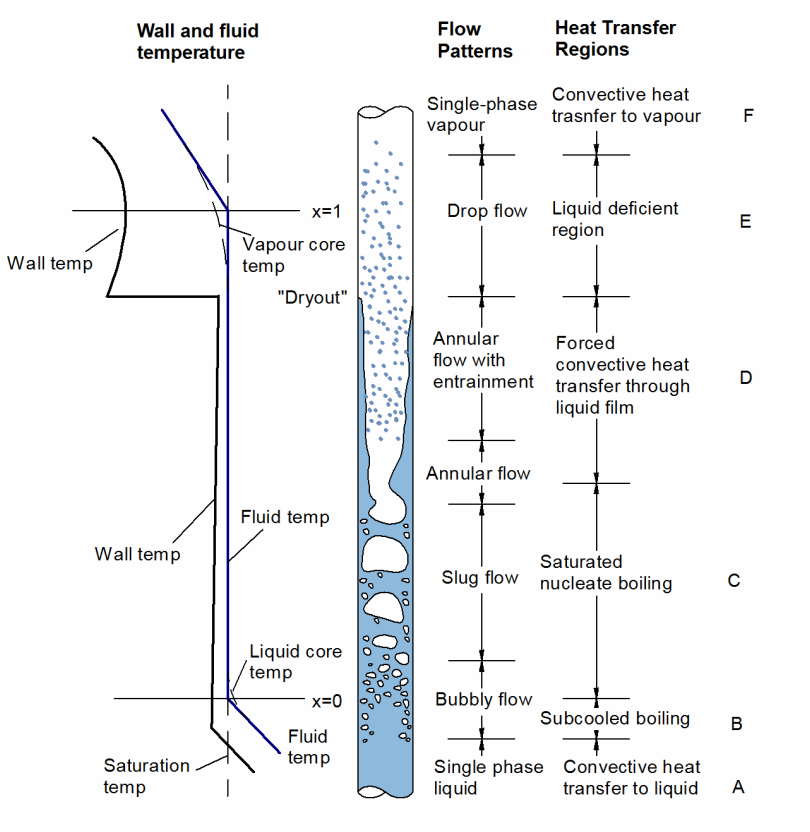


Figure 2.1: Flow patterns with associated heat transfer regions in uniformly heated tube with a low heat flux (Collier and Thome, 1994).

annular flow is not likely to be present. Investigations on flow patterns in plate heat exchangers have been very few, and limited to adiabatic air-water flows, as will be discussed in Section 2.7.1.

2.2.2 Flow Boiling in Microchannels

Channel diameter is an important parameter which has an effect on flow boiling heat transfer. As the channel diameter decreases, the bubble departure diameter reaches that of the flow channel; some macro-scale thermal and fluid phenomena may be suppressed, while others may be enhanced, for example, surface tension forces may become important. Another important difference in two-phase microchannels flows, compared with macro-channel flows, is that the liquid flow is laminar at most conditions, with typical values of Reynolds number from 100 to 4000 (Thome, 2004a, Peters and Kandlikar, 2007). Knadlikar (2004) showed

that the flow boiling phenomena in micro-channels are very similar to the nucleate boiling phenomena, with the periodic dry-out and rewetting of the wall having the same characteristics. Thome (2004) concluded that nucleate boiling controls evaporation in microchannels. Flow boiling heat transfer coefficients are largely dependent on heat flux and saturation pressure while they depend only slightly on mass velocity and vapor quality. It seems clear from the majority of experimental results, as summarized by Bertsch et al. (2008), that nucleate boiling plays a major role in flow boiling in microchannels, while the convective boiling mechanism is diminished.

It should be mentioned that the classification of micro- and conventional channels is not very well agreed in the literature. Many experimental investigations on "micro-" or "small" channels, as termed by different authors, have covered the channel equivalent diameter range from 0.2 to 3 mm, and this range might probably be taken as a rough assessment. Plate heat exchanger channels usually have hydraulic diameters from 3 to 10 mm, and are in the midrange between micro- and conventional size channels.

2.2.3 Flow Boiling Heat Transfer Correlations

To date there is no general theory witch can predict boiling heat transfer coefficients with satisfactory accuracy, due to the deficiencies in the understanding of the complex thermo-hydraulic processes involved. The prediction of heat transfer remains essentially empirical. Numerous correlations have been developed, many of those being inconsistent with others, and should be reviewed critically. For the purpose of the current study, only those most known and verified correlations which are applicable for vertical conduits and for pure substances are introduced in this section.

It is highly important to note that all those correlations give *local* values for the predicted flow boiling heat transfer coefficients. The flow boiling heat transfer coefficient is defined by Equation (2.1). In general there are three types of models existing in the literature for evaluation of flow boiling heat transfer. All types utilize the assumption that two distinct mechanisms: nucleate boiling and forced convection, have contributions to the overall flow boiling heat transfer. These are:

1. The superposition models assuming that the flow boiling coefficient is an additive of nucleate boiling and forced convection contributions, with weighting factors for each. The Chen 1966 correlation is a typical representative of this category of modelling. This type of correlation has the form

$$h_{tp} = S \cdot h_{nb} + E \cdot h_f \qquad (2.7)$$

where h_{tp} is the two-phase flow boiling heat transfer coefficient, h_{nb} is the nucleate boiling heat transfer coefficient, and h_f is the single-phase liquid convective heat transfer coefficient. S and E are suppression and enhancement factors, respectively.

2. Models that use the larger of the two components, h_{nb} and h_f, as the two-phase flow boiling heat transfer coefficient, with h_{nb} calculated by modified correlations. The Shah (1982) correlation is one example of this type.

3. The asymptotic models that combine the two components using a power-law type of equation:

$$h_{tp} = \left({h_{nb}}^n + {h_f}^n \right)^{1/n} \qquad (2.8)$$

The mathematical behavior of the asymptotic model is that at n =1, the model is a superposition model, for large values of n, h_{tp} tends to the larger of the two components. The Steiner and Taborek (1992) correlation is a representative of this type.

Chen (1966) Correlation

Based on 665 data points for water and some hydrocarbons, in the conditions of vertical, saturated flow boiling, Chen (1966) proposed his later widely adopted correlation. It is postulated that two basic mechanisms take part in the heat transfer process for saturated flow boiling: the macro-convective mechanism of single-phase liquid forced convection and micro-convective mechanism associated with bubble nucleation and growth. The flow boiling coefficient is expressed in Equation (2.7), with E being denoted by F in the original paper. In this method, the component of forced convection is calculated by the Dittus-Boelter equation:

$$h_f = 0.023 \left(\mathrm{Re}_f \right)^{0.8} \left(\mathrm{Pr}_f \right)^{0.4} \frac{k_f}{d} \qquad (2.9)$$

where $\mathrm{Re}_f = G(1-x)d / \mu_f$, is the Reynolds number for liquid fraction. h_{nb} is calculated using the Forster and Zuber analysis of nucleate boiling correlation, modified to account for the reduced average superheat in the thermal boundary layer for bubble nucleation at the wall:

$$h_{\mathrm{nb}} = 0.00122\left(\frac{k_{\mathrm{f}}^{0.79} c_{\mathrm{p,f}}^{0.45} \rho_{\mathrm{f}}^{0.49} g_{\mathrm{c}}^{0.25}}{\sigma^{0.5} \mu_{\mathrm{f}}^{0.29} i_{\mathrm{fg}}^{0.24} \rho_{\mathrm{g}}^{0.24}}\right) \Delta T_{\mathrm{sat}}^{0.24} \Delta P_{\mathrm{sat}}^{0.75} \qquad (2.10)$$

where $\Delta T_{\mathrm{sat}} = T_{\mathrm{wall}} - T_{\mathrm{sat}}$ is the excess temperature, ΔP_{sat} is the difference in saturated vapour pressure corresponding to ΔT_{sat}, $\Delta P_{\mathrm{sat}} = P_{\mathrm{sat}}(T_{\mathrm{w}}) - P_{\mathrm{sat}}(T_{\mathrm{sat}})$. It is important to note that Equation (2.10) is derived from non-dimensional equations (Forster and Zuber's correlation for pool boiling), as such, g_{c} is needed only with English units.

As already noted, the effect of forced convection is postulated to be enhanced due to the fact that liquid phase fraction flow velocity is increased, while the nucleate boiling part is suppressed because a sharper temperature gradient at the wall is created by the forced flow, which has an adverse effect on bubble nucleation. The enlargement factor, *F*, is always greater than unity. The author argued that *F* is strictly a flow parameter, and therefore can be assumed as a function of the Martinelli parameter X_{tt}[1]. *S* was estimated as a function of *F* and $\mathrm{Re_f}$. *F* and *S* were both given graphically in the original paper. Collier (1983) later proposed the following curve fitting equations for these two parameters:

$$F = \begin{cases} 1 & \text{for } \dfrac{1}{X_{\mathrm{tt}}} \le 0.1 \\ 2.35\left(\dfrac{1}{X_{\mathrm{tt}}} + 0.213\right)^{0.736} & \text{for } \dfrac{1}{X_{\mathrm{tt}}} > 0.1 \end{cases} \qquad (2.11)$$

$$S = \frac{1}{1 + 2.53\times10^{-6}\left(\mathrm{Re}_{\mathrm{f}}\, F^{1.25}\right)^{1.17}} \qquad (2.12)$$

The Chen correlation is based on 6 different data sources of over 600 data points. The correlation is for vertical flow only, and valid for pressures in the range of 1-35 bar, vapour quality 0-0.7, heat flux 6-2400 kW/m^2, liquid inlet velocity 0.06-4.5 m/s. One shortcoming of Chen's correlation is that a rather large number of physical properties are required, and since the wall temperature is not known beforehand, an iteration procedure is needed in calculation.

Chen's correlation is among the oldest yet most widely used correlations for saturated flow boiling heat transfer in vertical channels. The correlation showed

[1] $X_{\mathrm{tt}} = \left(\dfrac{1-x}{x}\right)^{0.9}\left(\dfrac{\rho_{\mathrm{g}}}{\rho_{\mathrm{f}}}\right)^{0.5}\left(\dfrac{\mu_{\mathrm{f}}}{\mu_{\mathrm{g}}}\right)^{0.1}$ for straight pipes. For more details refer to Section 2.3.3.

excellent agreement with the data analyzed by Chen, however, some later researchers have reported that this correlation did not agree well with their experimental data, such as Kandlikar (1990) and Gungor and Winterton (1986). Especially, large deviations with refrigerant data have been observed (Liu and Winterton, 1990, Kandlikar and Nariai, 1999). Based on the form of Equation (2.7), large numbers of correlations have been proposed since Chen's correlation. Many modifications and analytical examinations of the Chen correlation can be found in the literature in the effort of expanding the correlation to more fluids and operating parameters, for example, Bennett and Chen (1980) and Edelstein et al. (1984).

Shah (1976, 1982) Correlation

Shah in 1976 proposed a general correlation in the form of a graphical chart for the estimation of heat transfer coefficients during saturated boiling at sub-critical heat flux in tubes and annuli, both vertical and horizontal. Equations representing the chart correlation were presented in his 1982 paper. Similar to Chen, he included the two distinct mechanisms: nucleate boiling and forced convection. However, instead of adding the two contributions, this method chooses the larger as the final result. No explicit nucleate boiling term is used in this method, while the two mechanisms are both attributed to a heat transfer enlargement factor ψ. Three flow boiling regions are defined: a nucleate boiling dominant region at low vapour quality x, a convective dominant region corresponding to high x, and in between a bubble suppression region where both mechanisms are significant. In the development of this chart correlation four dimensionless parameters are employed, defined by:

$$\psi = \frac{h_{\mathrm{tp}}}{h_{\mathrm{f}}} \tag{2. 13}$$

$$\mathrm{Co} = \left(\frac{1-x}{x}\right)^{0.8}\left(\frac{\rho_{\mathrm{g}}}{\rho_{\mathrm{f}}}\right)^{0.5} \tag{2. 14}$$

$$\mathrm{Bo} = \frac{q}{Gi_{\mathrm{fg}}} \tag{2. 15}$$

$$\mathrm{Fr}_{\mathrm{f}} = \frac{G^2}{\rho_{\mathrm{f}}{}^2 gd} \tag{2. 16}$$

Co is the convection number, first introduced by Shah in this correlation. Co is proposed to be a replacement of the Martinelli parameter X_{tt}, since the viscosity

ratio was found to have no significant influence. The other three dimensionless parameters have been used in prior correlations. ψ is the heat transfer enhancement factor, Bo is the boiling number and Fr_f is the Froude number assuming all mass flow as liquid. In this method the single-phase liquid heat transfer is calculated, again, by the Dittus-Boelter equation with only the liquid fraction considered. The chart form correlation is very convenient to apply. For the equations representing the chart, the method is shown as follows. First a dimensionless parameter N is defined:

$$N = \begin{cases} \mathrm{Co} & \text{vertical, horizontal with } \mathrm{Fr_f} > 0.4 \\ 0.38\,\mathrm{Fr_f}^{-0.3}\,\mathrm{Co} & \text{horizontal with } \mathrm{Fr_f} < 0.4 \end{cases} \tag{2. 17}$$

Now a second parameter F is defined as:

$$F = \begin{cases} 15.43 & \mathrm{Bo} < 11\times10^{-4} \\ 14.7 & \mathrm{Bo} \geq 11\times10^{-4} \end{cases} \tag{2. 18}$$

Three flow boiling regimes are defined, according to N, which is mainly a function of the vapour quality x. These are the nucleate boiling dominant regime at low x (high Co), the convective boiling (forced convection) dominant regime at high x, and in between a bubble suppression regime. For N >1.0, the heat transfer enhancements are calculated by:

$$\psi_{\mathrm{nb}} = \begin{cases} 230\,\mathrm{Bo}^{0.5} & \mathrm{Bo} > 0.3\times10^{-4} \\ 1 + 46\,\mathrm{Bo}^{0.5} & \mathrm{Bo} < 0.3\times10^{-4} \end{cases} \tag{2. 19}$$

$$\psi_{\mathrm{cb}} = \frac{1.8}{N^{0.8}} \tag{2. 20}$$

The final heat transfer enhancement is the larger of the two:

$$\psi = \max\left(\psi_{\mathrm{nb}}, \psi_{\mathrm{cb}}\right) \tag{2. 21}$$

For $N \leq 1.0$, flow boiling heat transfer is dominated by the boiling suppression region and the convective boiling region. The following equations apply:

$$\psi_{\mathrm{bs}} = \begin{cases} F\,\mathrm{Bo}^{0.5}\,e^{2.74N^{-0.1}} & 0.1 < N \leq 1.0 \\ F\,\mathrm{Bo}^{0.5}\,e^{2.74N^{-0.15}} & N < 0.1 \end{cases} \tag{2. 22}$$

ψ_{cb} is calculated with Equation (2.20). ψ equals to the larger of ψ_{bs} and ψ_{cb}:

$$\psi = \max\left(\psi_{\text{bs}}, \psi_{\text{cb}}\right) \tag{2. 23}$$

Shah's correlation is based on 800 data points from 18 independent experimental studies and found to have a mean deviation of 14%. Those data included most of the common refrigerants in their whole range of applications and water, with pressure between 1 to 170 bar. Almost all common pipe materials, horizontal and vertical, circular and annular, upward and downward were considered, and a wide range of heat and mass flux was covered. Because of its general applicability, the correlation has drawn considerable attention from the research and engineering community since its publication, and has gained great success. The Shah correlation is convenient to apply, and is probably the most widely accepted one.

Gungor and Winterton (1986) Correlation

Gungor and Winterton (1986) proposed a Chen type of correlation, while modifications are made to extend its use in subcooled as well as saturated boiling, and for applications to tubes and annuli for both vertical and horizontal flow. The structure of this correlation is the same as that of the Chen correlation, which is reproduced by:

$$h_{\text{tp}} = S \cdot h_{\text{nb}} + E \cdot h_{\text{f}} \tag{2. 24}$$

The authors argued that the convection heat transfer part is enhanced not only due to the two-phase void fraction, a parameter conventionally correlated by the Martinelli parameter, but also by the generation of vapour itself; the latter can be represented by the boiling number. Therefore, it is postulated that:

$$E = f\left(X_{\text{tt}}, \text{Bo}\right) \tag{2. 25}$$

The suppression factor S is assumed as a function of E and Re_{f}. Both factors are found with iteration procedures. The Forster and Zuber pool boiling correlation used in the Chen correlation is replaced by Cooper's (1984) correlation. For liquid forced convection heat transfer h_{f}, the same Dittus-Boelter equation is used. Using the saturated boiling tube data, E and S are expressed:

$$E = 1 + 24{,}000\,\text{Bo}^{1.16} + 1.37\left(\frac{1}{X_{\text{tt}}}\right)^{0.86} \tag{2. 26}$$

$$S = \frac{1}{1 + 1.15\times10^{-6} E^{2}\,\text{Re}_{\text{f}}^{1.17}} \tag{2. 27}$$

All properties are evaluated at the saturation temperature. For horizontal tubes in which the Froude number is less than 0.05, E should be multiplied by $E_2 = \mathrm{Fr}^{0.1-2\mathrm{Fr}}$, and S multiplied by $S_2 = \sqrt{\mathrm{Fr}}$, for which the Froude number Fr is defined the same way as in the Shah correlation. In subcooled boiling the equations still apply and the expression for E becomes unity since there is no net vapour generation.

The Gungor and Winterton correlation is based on a large data base of 3693 data points, covering water, refrigerants (R11, R12, R22, R113, and R114), and ethylene glycol. The authors compared their correlation with some of the previous correlations including those of Chen (1966), Shah (1982), Bjorge et al, (1982), against the data bank. Good agreement was seen with the Shah correlation for saturated flow boiling, while others showed poor agreement. In the comparison, both the original Chen correlation and a later modification by Bennett and Chen (1980) give poor results with refrigerants.

Gungor and Winterton (1987) Correlation

Gungor and Winterton (1987) modified their 1986 correlation, obtaining a simpler and more accurate one. The new correlation is remarkably simple with the form:

$$h_{\mathrm{tp}} = E \cdot h_{\mathrm{f}} \tag{2. 28}$$

where

$$E = 1 + 3000\,\mathrm{Bo}^{0.86} + 1.12\left(\frac{x}{1-x}\right)^{0.75}\left(\frac{\rho_{\mathrm{f}}}{\rho_{\mathrm{g}}}\right)^{0.41} \tag{2. 29}$$

$$h_{\mathrm{f}} = 0.023\left[\frac{G(1-x)d}{\mu_{\mathrm{f}}}\right]^{0.8}\mathrm{Pr}_{\mathrm{f}}{}^{0.4}\frac{k_{\mathrm{f}}}{d} \tag{2. 30}$$

Compared with the same authors' 1986 correlation, it is noted that the nucleate boiling term is eliminated (see Equation 2.24). While the effect of the nucleate boiling still exists, the authors argued that this effect can be lumped in with the enhancement factor E. Furthermore, since no significant role of the viscosity ratio $\mu_{\mathrm{f}} / \mu_{\mathrm{g}}$ has been reported, for sake of simplicity of the correlation the Martinelli parameter is replaced by quality and density ratios, with exponents of each term determined by experimental data. A similar treatment is found in the Shah (1982) correlation, where a new term, the convection number Co, is introduced by Shah

to replace the Martinelli parameter X_{tt}. The basic difference between the two parameters is that Co does not have the term μ_f / μ_g.

The Gungor and Winterton (1987) correlation is based on 4202 data points for saturated boiling in vertical and horizontal tubes and annuli. The correlation is very simple, and among the most often cited ones. Shah (2006) recently conducted an evaluation of six of the most verified correlations of flow boiling in tubes and annuli, of those only the Shah (1982) and the Gungor and Winterton (1987) correlation gave good agreement with a large database of 30 fluids, at a mean deviation of about 17.5%.

Liu and Winterton (1991) Correlation

Liu and Winterton in 1991 proposed a new flow boiling heat transfer correlation. In this correlation Chen's basic postulate that both forced convection and nucleate boiling mechanisms play a role in flow boiling heat transfer was used; however, whether these two mechanisms are simply additive was questioned. Gungor and Winterton (1987) had previously pointed out, with a detailed comparison with experimental data, that the Chen correlation considerably over-predicts the heat transfer coefficient at high quality regions, and under-predicts that in the low quality regions. Based on this observation, Liu and Winterton postulated that in high quality regions the nucleate boiling mechanism must have been more greatly suppressed than that predicted by the Chen correlation. As a result, a power law type of equation was proposed:

$$h_{TP} = \left[\left(S \cdot h_{nb} \right)^2 + \left(F \cdot h_f \right)^2 \right]^{1/2} \qquad (2.31)$$

Equation (2.31) can be viewed as an asymptotic equation with $n = 2$. The asymptotic equation has the advantage over simple additive equations in that nucleate boiling is further suppressed once $F \cdot h_f$ is appreciably larger than $S \cdot h_{nb}$. h_f is again calculated with the popular Dittus-Boelter equation, however, differently from all previous researchers, Re is calculated with the entire mass flow rate rather than the liquid fraction, this treatment further increases the effect of forced convection. h_{nb} is calculated from Cooper's pool boiling correlation.

It is clear in the development of the Chen type of correlation, including that of Chen (1966) and Gungor and Winterton (1986), also in the Liu and Winterton correlation, that the dominant term is the forced convection term $F \cdot h_f$. In the attempt of developing expressions for the factors F (and E in a later stage), the authors argued that correlations for saturated boiling without an explicit nucleate term but relying only on the boiling number correction do not work for subcooled boiling. Also, a Prandtl number dependence should be included because an

enhancement of the Prandtl number effect is expected, as a result of the sharpened temperature profile across the flow[1]. For these reasons, the boiling number term Bo is completely removed, and a Prandtl number dependence is added. *F* and *E* are found by regression analysis and given by:

$$F = \left[1 + x\,\mathrm{Pr}_{\mathrm{f}}\left(\frac{\rho_{\mathrm{f}}}{\rho_g} - 1\right)\right]^{0.35} \tag{2. 32}$$

$$S = \frac{1}{1 + 0.055F^{0.1}\,\mathrm{Re}_{\mathrm{L\text{-}W}}{}^{0.16}} \tag{2. 33}$$

where $\mathrm{Re}_{\mathrm{L\text{-}W}} = Gd/\mu_{\mathrm{f}}$ is the Reynolds number with the entire mass flow rate flowing as liquid.

The Liu and Winterton correlation used 4300 data points for saturated and subcooled boiling from 28 different sources involving water, refrigerants, and some hydrocarbons. The authors carried out a comparison of their correlation with some other correlations against a large data bank, which showed that only the Liu and Winterton correlation (mean deviation of 21.4%) and the Shah (1982) correlation (mean deviation of 21.9%) give reasonable agreement with all of the saturated boiling data.

Kandlikar (1990) Correlation

Kandlikar (1990) presented a general correlation predicting the heat transfer coefficient in flow boiling. Following the scheme in the Shah correlation, two regions of flow boiling are identified: the nucleate boiling dominant region and the convective boiling dominant region, according to the convection number Co. The final flow boiling coefficient is chosen as the larger of that calculated separately for the two regions. A fluid dependent parameter F_{fl} is newly introduced, for extending the correlation to other fluids. The final form of the correlation is given by:

$$h_{\mathrm{tp}} = \max\left(h_{\mathrm{tp,NBD}}, h_{\mathrm{tp,CBD}}\right) \tag{2. 34}$$

---

[1] $\mathrm{Pr} = \frac{\mu c_{\mathrm{p}}}{k} = \frac{\mu/\rho}{k/\left(\rho c_{\mathrm{p}}\right)} = \frac{\nu}{\alpha} = \frac{\text{momentum diffusivity}}{\text{thermal diffusivity}}$, $\mathrm{Pr} > 1$ physically indicates that momentum diffusivity is greater than the thermal diffusivity, resulting a flatter velocity profile than the temperature profile across the flow. In flow boiling a sharpened temperature profile at the vicinity of the wall is expected, compared with that of single-phase flow heat transfer, because the bulk of the flow is at, or very close to, saturation temperature.

where the subscripts *NBD* and *CBD* refer to the nucleate boiling dominant and the convective boiling dominant regions. The correlation for vertical tubes and horizontal tubes with Froude number, $\mathrm{Fr}_\mathrm{f} > 0.04$, is

$$\begin{cases} \dfrac{h_{\mathrm{tp,NBD}}}{(1-x)^{0.8} h_\mathrm{f}} = 0.6683\,\mathrm{Co}^{-0.2} + 1058.0\,\mathrm{Bo}^{0.7} F_\mathrm{fl} \\ \dfrac{h_{\mathrm{tp,CBD}}}{(1-x)^{0.8} h_\mathrm{f}} = 1.136\,\mathrm{Co}^{-0.9} + 667.2\,\mathrm{Bo}^{0.7} F_\mathrm{fl} \end{cases} \tag{2. 35}$$

The single-phase liquid-only heat transfer coefficient h_f is calculated by the Dittus-Boelter equation, with the Reynolds number computed by the liquid fraction only, i.e., $\mathrm{Re}_\mathrm{f} = Gd(1-x)/\mu_\mathrm{f}$. This treatment is the same as used by Shah. All three dimensionless groups, Co, Fr_fo, and Bo are the same as given in the Shah correlation. Values for the fluid dependent parameter F_fl were reported for 10 fluids including water and some common refrigerants, and later for R134a in another paper (Kandlikar, 1991), those values are shown in Table 2.1. This later paper further reported that all values are applicable to copper tubes only, for stainless steel tubes F_fl =1.

The Kandlikar correlation is based on 5246 data points for water and some refrigerants from 24 sources. Introduction of the fluid dependent parameter F_fl in the nucleate boiling term can be viewed as an important aspect of the Kandlikar correlation. It is clear that this correlation has been developed under the scheme of the Shah correlation; however, not much improvement has been shown in either accuracy or physical basis. The correlation was later extended to microchannels and minichannels by Kandlikar and Steinke (2003) by introducing the use of laminar flow equations, good agreement with experimental data were reported.

Table 2.1: Fluid dependent parameter F_fl in the Kandlikar (1990) correlation

Fluid	F_fl	Fluid	F_fl
water	1	R113	1.30
R11	1.30	R114	1.24
R12	1.50	R134a	1.63
R13B1	1.31	R152a	1.10
R22	2.20		

Steiner and Taborek (1992) Correlation

Steiner and Taborek (1992) proposed a new general correlation for boiling in vertical tubes. The correlation has an open-ended feature, i.e., parts of it might be exchanged to fit the problem at hand without invalidating the final results. The local two-phase flow boiling coefficient is obtained from an asymptotic equation:

$$h_{tp} = \left({h_{nb}}^{n} + {h_f}^{n} \right)^{1/n} \qquad (2.\ 36)$$

The exponent n is to be assigned on empirical grounds to the value that gives the best fit of the data set. n =3 was obtained by the authors on evaluating their large and diversified database. Liu and Winterton (1991) used this type of model in their correlation with n =2. This so called "asymptotic model" is accepted as the most logical model (Darabi et al., 1995). As n approaches infinity, it represents the case of the "greater of the two components", similar to the correlations of Shah (1982) and Kandlikar (1990). For n =1, it represents the superposition model, as that of Chen (1966) and Gungor and Winterton (1986). The local flow boiling heat transfer coefficient is given:

$$h_{tp} = \left[\left(h_{nb,0} F_{nb} \right)^3 + \left(h_{fo} F_{tp} \right)^3 \right]^{1/3} \qquad (2.\ 37)$$

where

$h_{nb,0}$ is the local "normalized" nucleate pool boiling coefficient at standard conditions of heat flux q_0 and reference reduced pressure P_r.

F_{nb} is the nucleate boiling correction factor that compensates for the differences between pool and flow boiling.

h_{fo} is the local liquid phase forced convection coefficient based on the total mass flow as liquid.

F_{tp} is the two-phase multiplier that accounts for the enhancement of convection in a two-phase flow, assumed as a function of vapour quality x and the liquid/vapour density ratio ρ_f / ρ_g.

For $h_{nb,0}$, the standard conditions refer to reduced pressure P_r =0.1, mean surface roughness R_p =1 µm, and the heat flux with specified values for four types of fluid classes (inorganic, hydrocarbons and refrigerants, cryogens, Helium I). $h_{nb,0}$ can be obtained from experimental data or a correlation of the user's choice, for example, the Cooper (1984) pool boiling correlation.

The nucleate boiling correction factor F_{nb} is given by:

$$F_{\mathrm{nb}} = F_{\mathrm{pf}} \left(\frac{q}{q_0} \right)^{\mathrm{nf}} \left(\frac{d}{d_0} \right)^{-0.4} \left(\frac{R_{\mathrm{p}}}{R_{\mathrm{p,0}}} \right)^{0.133} F(M) \qquad (2.38)$$

where,

$$F_{\mathrm{pf}} = 2.816 P_{\mathrm{r}}^{\,0.45} + \left(3.4 + \frac{1.7}{1 - P_{\mathrm{r}}^{\,7}} \right) \cdot P_{\mathrm{r}}^{\,3.7}$$

$$nf = \begin{cases} 0.8 - 0.1 e^{1.75 P_{\mathrm{r}}} & \text{for all fluids except cryogens} \\ 0.7 - 0.13 e^{1.105 P_{\mathrm{r}}} & \text{for cryogens} \end{cases}$$

$$F(M) = 0.377 + 0.199 \ln(M) + 2.8427 \times 10^{-5} M^{2}$$

The authors excluded the notion of F_{nb} as a "nucleate boiling suppression factor", which has been conventionally used for the correction factor for h_{nb}, since no effect of mass velocity and vapour quality on flow nucleate boiling had been observed by the authors, over wide ranges of heat flux and pressure. It is therefore concluded that a nucleate boiling "suppression" does not occur in flow boiling. In Equation (2.38), F_{pf} is a pressure correction factor valid for P_{r} <0.95. $F(M)$ is a correction factor accounting for the effect of molecular weight. The reference tube diameter d_0 is equal to 0.01 m, and reference surface roughness $R_{\mathrm{p,0}}$ is 1 µm which is about the average for commercial tubes.

h_{fo} is calculated with the total mass flow as liquid. The two-phase multiplier F_{tp} is calculated as:

$$F_{\mathrm{tp}} = \begin{cases} \left[(1-x)^{1.5} + 1.9 x^{0.6} \left(\frac{\rho_{\mathrm{f}}}{\rho_{\mathrm{g}}} \right)^{0.35} \right]^{1.1} & 0 \le x \le 0.6 \\ \left\{ \left[(1-x)^{1.5} + 1.9 x^{0.6} (1-x)^{0.01} \left(\frac{\rho_{\mathrm{f}}}{\rho_{\mathrm{g}}} \right)^{0.35} \right]^{-2.2} \right\}^{-0.5} & \\ + \left\{ \left(\frac{h_{\mathrm{go}}}{h_{\mathrm{fo}}} \right) x^{0.01} \left[1 + 8 (1-x)^{0.7} \left(\frac{\rho_{\mathrm{f}}}{\rho_{\mathrm{g}}} \right)^{0.67} \right] \right\}^{-2} & 0.6 \le x \le 1 \end{cases} \qquad (2.39)$$

The terms $x^{0.01}$ and $(1-x)^{0.01}$ were included to arrive at the proper limits at $x = 0$ and $x = 1$.

The Steiner and Taborek (1992) correlation is based on a very extensive data base of 12,607 data points, including 10262 for water and the remaining for four refrigerants (R11, R12, R22 and R113), seven hydrocarbons, three cryogens and

ammonia. Besides, much effort has been placed on the physical basis of the model respecting the established principles of pool and convective boiling, rather than relying on statistical development of correlations. The correlation is well structured with logical basis and currently regarded as the most accurate vertical tube boiling correlation for pure fluids (Thome, 2003, Ghiaasiaan, 2007).

A Summary

It is difficult to predict the boiling coefficient accurately because of the complexities of the mechanisms. The large number of flow boiling correlations available in the literature reveals the fact that the subject is under extensive investigation yet is not well understood. To date a fundamental understanding of the heat transfer mechanism in flow boiling, or any boiling, is still in need. Since the success of Chen's 1966 correlation, it has been widely accepted that two heat transfer mechanisms apply to flow boiling – nucleate boiling and forced convection. Various approaches have been proposed in combining these two contributions, resulting in three types of modelling which essentially cover all correlations available.

All types of correlations were developed empirically, with important functions or constants defined by experimental results. With the accumulation of experimental data in the subject field, later researchers are able to use larger and larger data bases aiding the development of their correlations. Still, there are deficiencies of data available which place limitations on the accuracy of correlations. For example, as pointed out by Gungor and Winterton (1987), there are at least two such limitations, one concerns the difficulty of measuring the sometimes very small temperature differences in boiling heat transfer, another limitation is that the importance of the heat transfer surface condition has not been accounted for adequately; with the lack of this information there is little justification for attempting a complicated correlation procedure. Chisholm (1983) noted that prediction of two-phase flow parameters may carry an uncertainty of 50%, due to the large number of variables encountered.

Comparisons of their correlations are often made by authors with others against the data base from which the new correlation is based. This kind of comparison has always favored the newly developed one. It is always hard to say why one of the approaches should be preferred to the others, since they all possess merits as well as shortcomings. The Chen correlation remains classic and always a popular objective for modification and comparison. The Shah (1982) correlation and Steiner and Taborek (1992) correlation can be regarded as the most accurate ones that are currently available. All correlations have different underlying postulations which could not be fully evaluated with the current knowledge of the

subject (it should be remembered that even the knowledge of single-phase flow is essentially empirical.).

2.2.4 Estimation of Boiling Heat Transfer Coefficient of Refrigerant Evaporators

As already noted, most, if not all, general flow boiling correlations available provide methods to estimate *local* heat transfer coefficients of the liquid. A number of those correlations are recommended by ASHRAE (2005 ASHRAE Handbook: Fundamentals) to estimate local heat transfer coefficients of refrigerants during evaporation, including the Gungor and Winterton (1986), Kandlikar (1999), Shah (1982), and the Chen (1966) correlation. For refrigerant boiling inside tubes, the heat transfer coefficient changes progressively as the refrigerant flows through the tube, mainly as a function of the mass flow rate and vapour quality. It is difficult to develop a single relation to describe the heat transfer performance for evaporation in a tube over the full quality range. Some

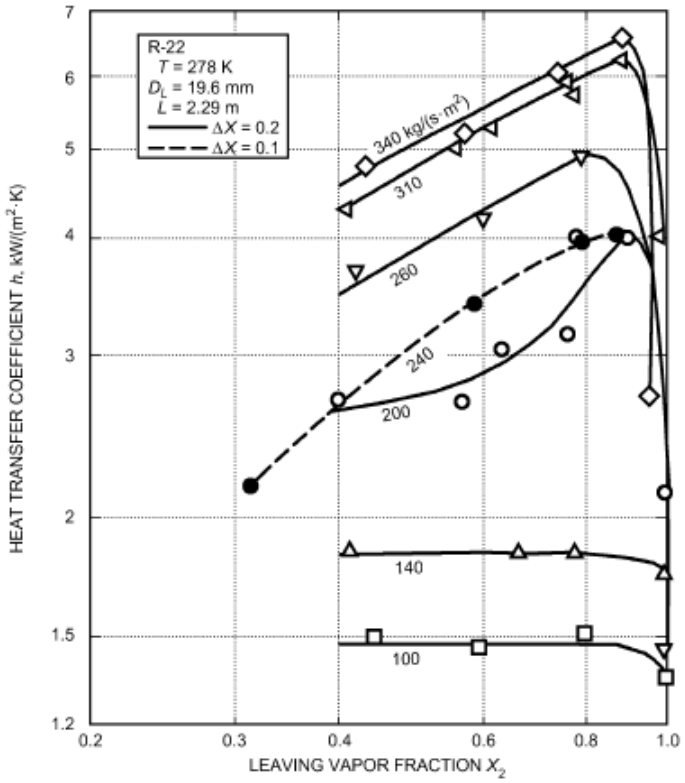


Figure 2.2: Heat transfer coefficient vs. vapour quality for partial evaporation. (ASHRAE Handbook 1997: Fundamentals)

correlations on average heat transfer coefficients for specified refrigerants evaporating in fixed size tubes can be found, for example, Figure 2.2 shows the graphical presentation of the boiling heat transfer coefficient of R22 in a horizontal tube with an outside diameter of 19.6 mm when the quality of refrigerant is varied. However, in general the prediction of heat transfer coefficient is difficult even for a given refrigerant in a certain size tube with specified flow rate (Stoecker, 1998). In the industry, evaporator performance is usually determined by actual testing of the evaporator (Dossat, 1991). It is a common practice for manufacturers and designers of evaporators to provide data of heat transfer coefficients for certain types of evaporators under ranges of operating conditions, and gives the users and application engineers the convenience of selection.

Despite the difficulty of predicting accurately the refrigerant boiling heat transfer coefficient, the trend is clearly known. Figure 2.3 shows the typical refrigerant boiling heat transfer coefficient variation along a DX evaporator tube. The changes in the heat transfer coefficient are associated with changes of flow pattern as a function of the vapour quality and flow velocity that change along the tube. Refrigerant enters the evaporator with a small fraction of flashing vapour as a result of the sudden pressure drop across the expansion valve. Along the tube more refrigerant evaporates progressively and the velocity increases. At the entering section, bubbles and plugs of vapour flow along with the liquid; further along the tube, the flow becomes annular with high-velocity vapour rushing

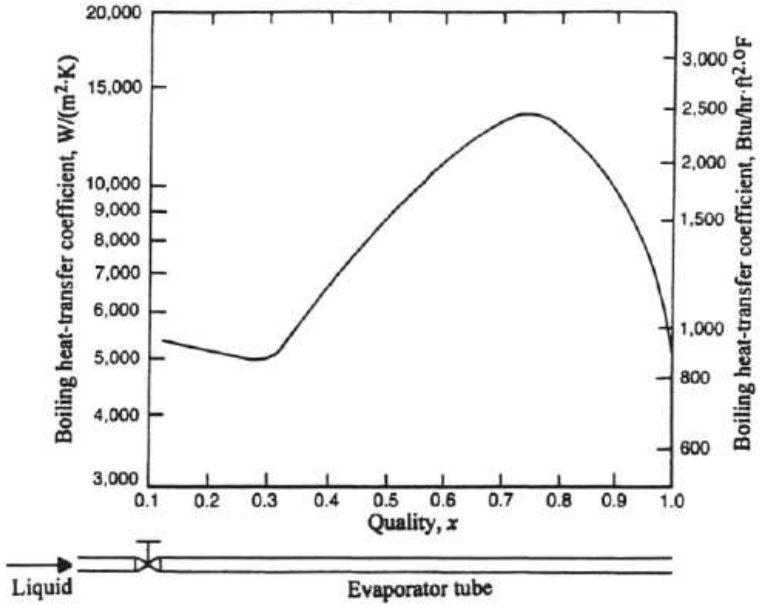


Figure 2.3: Heat transfer coefficient as refrigerant boils in an evaporator tube (Stoecker, 1998)

through the center with liquid clinging to the inside surface of the tube. Still further the flow converts to a mist of non-equilibrium mixture of liquid droplets and superheated vapour (sometimes called dry-out because the surface is no longer wetted by liquid) till all liquid finally evaporates. For DX evaporator tubes, annular flow occurs in most of the tube length (*ASHRAE Handbook 2005: Fundamentals*).

The distribution of heat transfer coefficients as a function of vapour quality helps to understand why flooded and liquid overfeed evaporators have some heat transfer advantages. Single-phase vapour(gas) convection heat transfer is associated with low heat transfer rates. In a DX tube the heat transfer coefficient tends to drop sharply after dry-out and keeps low in the length of super-heating. In flooded and liquid over-feed evaporators the refrigerant side surface area is always wetted by the liquid refrigerant, which results in a higher surface heat transfer coefficient.

2.3 Two-phase Pressure Drop

2.3.1 An Overview

The total pressure drop for two-phase flow in tubes consists of three components: pressure drops due to friction, acceleration (change in momentum), and elevation (gravitation):

$$\left(\frac{dP}{dz}\right)_{\text{total}} = \left(\frac{dP}{dz}\right)_{\text{fric}} + \left(\frac{dP}{dz}\right)_{\text{acce}} + \left(\frac{dP}{dz}\right)_{\text{elev}} \qquad (2.\ 40)$$

The acceleration and gravitation pressure gradient components are due to vapour generation (or degeneration) and non-horizontal orientation of the flow channel. Traditionally, the two most important modelling methods of two-phase gas-liquid flow are the “homogeneous” model and the “separated flow” model. Both methods provide evaluations of the acceleration and gravitational pressure gradient components on a theoretical basis, while the frictional pressure gradient part is usually evaluated empirically, and is the focus of investigations on two-phase pressure drops.

It is convenient and a conventional practice to relate the two-phase *frictional* pressure gradient to that for the flow of the liquid phase (or gas phase) flowing alone in the channel. Four single-phase pressure gradients are thus defined, for the liquid phase:

$\left(\frac{dP}{dz}\right)_{\text{fric, f}}$: liquid *fraction* assumed to flow alone in the whole channel

$\left(\frac{dP}{dz}\right)_{\text{fric, fo}}$: *all* mass flow assumed as liquid

For the gas phase, subscripts of "g" and "go" are to be used. With the single-phase pressure gradients used as reference values, two-phase multipliers are defined accordingly:

$$\begin{cases} \phi_{\text{f}}^{\,2} = \left(\frac{dP}{dz}\right)_{\text{fric}} \Big/ \left(\frac{dP}{dz}\right)_{\text{fric,f}} & (a) \\ \phi_{\text{fo}}^{\,2} = \left(\frac{dP}{dz}\right)_{\text{fric}} \Big/ \left(\frac{dP}{dz}\right)_{\text{fric,fo}} & (b) \end{cases} \tag{2. 41}$$

The single-phase pressure gradients are to be calculated from standard single-phase correlations, for instance, for the liquid phase pressure gradient:

$$\begin{cases} -\left(\frac{dP}{dz}\right)_{\text{fric,f}} = f_{\text{f}} \cdot \frac{\frac{1}{2} G^2 (1-x)^2}{\rho_{\text{f}} d} & (a) \\ -\left(\frac{dP}{dz}\right)_{\text{fric,fo}} = f_{\text{fo}} \cdot \frac{\frac{1}{2} G^2}{\rho_{\text{f}} d} & (b) \end{cases} \tag{2. 42}$$

where f_{f} and f_{fo} are Darcy friction factors, obtained from standard single-phase equations or charts with respective Reynolds numbers. For example, when the Blasius equation ($f = 0.3164 / \text{Re}^{1/4}$) is used,

$$\begin{cases} f_{\text{f}} = \frac{0.3164}{\text{Re}_{\text{f}}^{\,0.25}}, \quad \text{Re}_{\text{f}} = \frac{G(1-x)d}{\mu_{\text{f}}} & (a) \\ f_{\text{fo}} = \frac{0.3164}{\text{Re}_{\text{fo}}^{\,0.25}}, \quad \text{Re}_{\text{fo}} = \frac{Gd}{\mu_{\text{f}}} & (b) \end{cases} \tag{2. 43}$$

The treatment of the two-phase pressure gradient by a single-phase flow assumption and a two-phase multiplier reduces the analytical task to the determination of the two-phase multiplier $\phi_{\text{fo}}^{\,2}$ or $\phi_{\text{f}}^{\,2}$ with independent flow variables, and has proved successful. Many classical works are found in this category, such as the Lockhart-Martinelli (1949) method, that of Chisholm (1973) and Freidel (1979). It shall be noted that the expression of local pressure gradient in terms of $\phi_{\text{fo}}^{\,2}$ is more convenient for evaporating and condensing problems,

where the vapour quality x varies along the tube length and an integration of the local pressure gradients is needed. This is because $(dP/dz)_{\text{fric, fo}}$ is a constant, not a function of the vapour quality, which makes the integration far easier (or indeed possible, for some cases). For this reason, correlations that have been designed for such duties purposely utilize the ϕ_{fo}^2 expression, as seen in correlations of Martinelli-Nelson (1948), and that of Chisholm (1973) which will be later introduced.

2.3.2 The Homogeneous Flow Model

The homogeneous model considers the two phases to flow as a single phase possessing mean fluid properties. Those properties basically include the mean density and mean viscosity. Figure 2.4 shows the momentum conservation in a homogeneous model. The model has been in use in various forms in adiabatic two-phase flow and refrigeration systems for a considerable time (Collier and Thome, 1994). This method has also found its application in two-phase pressure drop calculation in PHE channels, though the treatment for some parameters varies. Two important assumptions in a homogeneous model are:

1. equal vapor and liquid velocities: $\overline{u} = u_{\text{f}} = u_{\text{g}}$,
2. thermodynamic equilibrium between the phases.

Components of pressure gradients can be derived from the momentum conservation equation:

$$-A \cdot dP - F_{\text{fric}} - F_{\text{elev}} = \dot{m} \cdot d\overline{u} \qquad (2.\ 44)$$

The individual forces are:

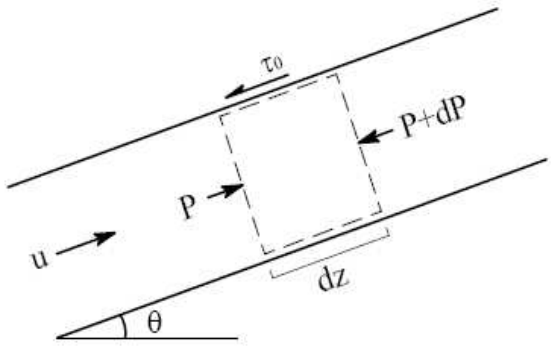


Figure 2.4: Conservation of momentum in a homogeneous model

$$\begin{cases} F_{\text{fric}} = \tau_{\text{w}} S_{\text{wet}} dz = \tau_{\text{w}} \dfrac{4A_{\text{c}}}{d_{\text{h}}} dz = \dfrac{4\tau_{\text{w}}}{d_{\text{h}}} \cdot A_{\text{c}} dz & (a) \\ F_{\text{elev}} = \bar{\rho} g \sin\theta \cdot A_{\text{c}} dz & (b) \\ F_{\text{acce}} = \dot{m} d\bar{u} = G \dfrac{d\bar{u}}{dz} \cdot A_{\text{c}} dz & (c) \end{cases} \tag{2. 45}$$

The pressure gradients are calculated accordingly:

$$\begin{aligned} -\left(\frac{dP}{dz}\right)_{\text{fric}} &= \frac{F_{\text{fric}}}{A_{\text{c}} dz} = \frac{4\tau_{\text{w}}}{d} & (a) \\ -\left(\frac{dP}{dz}\right)_{\text{elev}} &= \frac{F_{\text{grav}}}{A_{\text{c}} dz} = \bar{\rho} g \sin\theta & (b) \\ -\left(\frac{dP}{dz}\right)_{\text{acce}} &= \frac{F_{\text{acce}}}{A_{\text{c}} dz} = G \frac{d\bar{u}}{dz} & (c) \end{aligned} \tag{2. 46}$$

For the frictional pressure gradient, τ_{w} is expressed in terms of a two-phase friction factor:

$$\tau_{\text{w}} = \frac{1}{4} f_{\text{tp}} \left(\tfrac{1}{2} \bar{\rho} \bar{u}^2\right) = \frac{1}{8} \cdot f_{\text{tp}} \frac{G^2}{\bar{\rho}} \tag{2. 47}$$

Now the two-phase frictional pressure gradient can be expressed as:

$$-\left(\frac{dP}{dz}\right)_{\text{fric}} = \frac{4\tau_{\text{w}}}{d} = f_{\text{tp}} \frac{G^2}{2\bar{\rho} d} \tag{2. 48}$$

The two-phase friction factor f_{tp} can be calculated by any single-phase friction factor equations with the Reynolds number determined using mean fluid properties or, alternatively, f_{tp} can be determined directly from measured two-phase pressure drops, the latter usually has higher accuracy for the specified testing conditions.

The homogeneous model assumes the two-phase flow as single-phase, and there are three properties to be defined, namely the two-phase mean velocity, density and viscosity. The mean density $\bar{\rho}$ is defined by the basic conservation of mass:

$$\bar{\rho} = \frac{\dot{m}}{Q} = \frac{\dot{m}}{Q_{\text{g}} + Q_{\text{f}}} = \frac{1}{\dfrac{x}{\rho_{\text{g}}} + \dfrac{1-x}{\rho_{\text{f}}}} \tag{2. 49}$$

The mean velocity $\bar{u}$ is determined accordingly:

$$\bar{u} = \frac{\dot{m}}{\bar{\rho} A_c} \tag{2. 50}$$

The two-phase mean viscosity can be evaluated in many ways, while the following conditions must be satisfied:

$$\begin{cases} x = 0, \bar{\mu} = \mu_f \\ x = 1, \bar{\mu} = \mu_g \end{cases} \tag{2. 51}$$

Three definitions are summarized by Collier and Thome (1994), as given by Equation (2.52). Of those, the most commonly used definition of $\bar{\mu}$ is probably that proposed by McAdams et al, which has the form similar to the definition of $\bar{\rho}$. Another definition of $\bar{\mu}$ often used in the design of water-tube boilers is $\bar{\mu} = \mu_f$ (Chisholm, 1983), but this definition dose not meet the condition specified by Equation (2.51). Still other definitions of mean two-phase viscosity are possible. Collier and Thome (1994) argued that the failure of establishing an accepted definition is that the dependence of the friction factor on viscosity is small.

McAdams et al., 1942: $\bar{\mu} = \left(\frac{x}{\mu_g} + \frac{1-x}{\mu_f} \right)^{-1}$ (*a*)

Cichitti et al., 1960: $\bar{\mu} = x\mu_g + (1-x)\mu_f$ (*b*) (2. 52)

Dukler et al., 1964: $\bar{\mu} = \bar{\rho} \left[x \frac{\mu_g}{\rho_g} + (1-x) \frac{\mu_f}{\rho_f} \right]$ (*c*)

Once the mean fluid properties defined, pressure gradients of the three components can then be integrated stepwise to obtain the pressure drops, provided a number of simplifications are made. Those include assuming f_{tp}, ρ_f, ρ_g as constant and x changes linearly over the channel length. The final form of the integration of the three components can be given as:

$$\begin{cases} -\Delta P_{fric} = \int_{z=0}^{z=L} f_{tp} \cdot \frac{G^2}{2\bar{\rho} d} \cdot dz = f_{tp} \cdot \frac{G^2}{2\rho_f d} \cdot L \cdot \left[1 + \frac{x_i + x_o}{2} \left(\frac{\rho_f}{\rho_g} - 1 \right) \right] & (a) \\ -\Delta P_{acce} = \int_{z=0}^{z=L} G d\bar{u} = G\left(\bar{u}_o - \bar{u}_i \right) = G^2 \left(x_o - x_i \right) \left(\frac{1}{\rho_g} - \frac{1}{\rho_f} \right) & (b) \\ -\Delta P_{elev} = \int_{z=0}^{z=L} \bar{\rho} g \sin\theta \, dz = \frac{\rho_f \rho_g}{\rho_f - \rho_g} \cdot \frac{Lg \sin\theta}{x_o - x_i} \cdot \ln \frac{1 + x_o \left(\frac{\rho_f}{\rho_g} - 1 \right)}{1 + x_i \left(\frac{\rho_f}{\rho_g} - 1 \right)} & (c) \end{cases} \tag{2. 53}$$

The homogeneous model provides a simple method for computing *acceleration* and *gravitational* components of pressure drop and is still a very common method of evaluating two-phase *frictional* pressure gradients. Up until the 1940s, this method, with mean viscosity taken as that of liquid, was used exclusively in designing water-tube boilers with good agreements, but later research indicated this was because of the high mass velocity in such devices (Chisholm, 1983). Different possible treatments of some parameters, for example f_{tp} and $\bar{\mu}$ as shown in the foregoing, result in some variances of this method, but in general the homogenous model tends to under-predict the frictional pressure drop. It is also generally agreed that this method gives reasonable results at high reduced pressure P_r and high mass flux (at more than 2000 kg/(m^2 · s)) for tube flow (Chisholm, 1983, Thome, 2004b). This is probably because at such conditions, the flow is in the regime of dispersed (mist) flow, for which the basic assumptions for the homogeneous model are closely met.

2.3.3 The Separated Flow Model

The separated flow model considers the phases to be artificially segregated into two streams, one of liquid and one of vapour. The most famous and certainly most widely adopted approach in this type of modelling is the Lockhart-Martinelli (1949) method. Basic assumptions of the separated model are:

1. constant but not necessarily equal velocities for vapour and liquid phases,
2. thermodynamic equilibrium between the phases.

Again as for the homogeneous flow model, the frictional pressure gradient can be expressed in terms of the single-phase pressure gradient with a two-phase multiplier:

$$-\left(\frac{dP}{dz}\right)_{\text{fric}} = -\left(\frac{dP}{dz}\right)_{\text{fric, fo}} \cdot \phi_{\text{fo}}{}^2 = -\left(\frac{dP}{dz}\right)_{\text{fric, f}} \cdot \phi_{\text{f}}{}^2 \qquad (2.\,54)$$

For the acceleration pressure gradient consider a control volume (CV). The inertial force applied on a CV is equal to the time rate of change of momentum of the CV, i.e., the net momentum flow rate across the CV, which is expressed as:

$$F_{\text{acce}} = Ma = \frac{D(M\vec{V})}{Dt} = \frac{d\left(\dot{m}_{\text{g}} u_{\text{g}} + \dot{m}_{\text{f}} u_{\text{f}}\right)}{dz} \cdot dz \qquad (2.\,55)$$

Considering $F_{acce} = -dP_{acce} \cdot A_c$, the following is obtained:

$$-\left(\frac{dP}{dz}\right)_{acce} = G^2 \frac{d}{dz}\left(\frac{x^2}{\alpha\rho_g} + \frac{(1-x)^2}{(1-\alpha)\rho_f}\right) \tag{2. 56}$$

The gravitational pressure gradient is obtained from the gravitational force acting on the CV:

$$-F_{elev} = -dP_{elev} \cdot A_c = g \sin\theta\left(\rho_g A_g + \rho_f A_f\right) dz \tag{2. 57}$$

and

$$\left(\frac{dP}{dz}\right)_{elev} = g \sin\theta\left[\rho_g \alpha + \rho_f (1-\alpha)\right] \tag{2. 58}$$

In common with the homogeneous model, a stepwise integration of the pressure gradient components requires simplifying assumptions. The result of integration is given by Equation (2.59), assuming f_{fo}, ρ_f, and ρ_g being constant and a linear change of x over the channel length L:

$$\begin{cases} -\Delta P_{fric} = f_{fo} \cdot \dfrac{\frac{1}{2}G^2}{\rho_f d} \cdot \dfrac{L}{x_o - x_i} \displaystyle\int_{x_i}^{x_o} \phi_{fo}^2 dx & (a) \\ -\Delta P_{acce} = G^2 \left(\dfrac{x^2}{\alpha\rho_g} + \dfrac{(1-x)^2}{(1-\alpha)\rho_f} \right)\Bigg|_{x_i}^{x_o} & (b) \\ -\Delta P_{elev} = g \sin\theta \cdot \dfrac{L}{x_o - x_i} \displaystyle\int_{x_i}^{x_o} \left[\rho_g \alpha + \rho_f (1-\alpha)\right] dx & (c) \end{cases} \tag{2. 59}$$

As is seen the separated model does not supply simple solutions for the acceleration and gravitational components of pressure drop. Additional information is needed for the void fraction α, which brings extra difficulties for the calculation. From considerations of the flow patterns it is expected that this model would be most valid for the annular flow pattern.

2.3.4 Two-phase Pressure Drop Correlations

Numerous correlations on two-phase *frictional* pressure drop are available in the open literature. It is not in the scope of the present study to cover them all; only some of the commonly used and well-cited correlations are compiled and reviewed.

Lockhart-Martinelli (1949) Correlation

Lockhart and Martinelli (1949) presented their classic paper on frictional pressure gradients of two-phase, two-component air-liquid flow. In this method it is assumed that the two phases flow separately without interaction, and pressure drops of the two phases are equal regardless of flow patterns. Four two-phase flow patterns were defined; those are combinations of the liquid and gas phases being individually turbulent or laminar. A new parameter *X*, which was later denoted as the Lockhart-Martinelli parameter (also sometimes called the Martinelli parameter) is defined as:

$$X^2 = \left(\frac{dP}{dz}\right)_{\text{fric, f}} \Big/ \left(\frac{dP}{dz}\right)_{\text{fric, g}} \tag{2. 60}$$

For conventional tubes X^2 is readily calculated with single-phase pressure drop correlations. For example, for the turbulent-turbulent flow region:

$$X_{\text{tt}}^2 = \frac{f_{\text{f}} \cdot \left(\frac{1}{2}\rho_{\text{f}} j_{\text{f}}^2\right)/d}{f_{\text{g}} \cdot \left(\frac{1}{2}\rho_{\text{g}} j_{\text{g}}^2\right)/d} = \left(\frac{\mu_{\text{f}}}{\mu_{\text{g}}}\right)^{0.2} \cdot \left(\frac{1-x}{x}\right)^{1.8} \cdot \frac{\rho_{\text{g}}}{\rho_{\text{f}}} \tag{2. 61}$$

where $j_{\text{f}} = \dot{m}_f / \left(\rho_{\text{f}} A_{\text{c}}\right)$ and $j_{\text{g}} = \dot{m}_g / \left(\rho_{\text{g}} A_{\text{c}}\right)$ are superficial velocities of the two phases. f is the single-phase Darcy friction factor given by: $f = 0.184/\text{Re}^{0.2}$. It is important to recognize that Equation (2.61) has been quoted widely, sometimes without acknowledging that it was obtained for circular tube flow only.

The Martinelli parameter can be expressed in a more general form. This is simply done by defining the Darcy friction factor by $f = a / \text{Re}^{\text{n}}$. The Martinelli parameter is then expressed as:

$$X_{\text{tt}}^2 = \frac{f_{\text{f}} \cdot \left(\frac{1}{2}\rho_{\text{f}} j_{\text{f}}^2\right)/d}{f_{\text{g}} \cdot \left(\frac{1}{2}\rho_{\text{g}} j_{\text{g}}^2\right)/d} = \left(\frac{\mu_{\text{f}}}{\mu_{\text{g}}}\right)^{\text{n}} \cdot \left(\frac{1-x}{x}\right)^{2\text{-n}} \cdot \frac{\rho_{\text{g}}}{\rho_{\text{f}}} \tag{2. 62}$$

Equation (2.62) is applicable for any type of channel as long as the friction factor can be expressed as $f = a / \text{Re}^{\text{n}}$. This is the case for PHE channels.

The core of a separated model is to find the two-phase multiplier ϕ_{f}^2, which has been defined in Equation (2.54), and is represented by:

$$\phi_f{}^2 = \left(\frac{dP}{dz}\right)_{fric} \Big/ \left(\frac{dP}{dz}\right)_{fric,\,f} \tag{2. 63}$$

The two-phase frictional pressure drop can also be expressed in terms of a two-phase multiplier based on the gaseous phase, $\phi_g{}^2$, given by:

$$\phi_g{}^2 = \left(\frac{dP}{dz}\right)_{fric} \Big/ \left(\frac{dP}{dz}\right)_{fric,\,g} \tag{2. 64}$$

The authors successfully correlated $\phi_f{}^2$ and $\phi_g{}^2$ as a unique function of X^2, and the result was presented originally in a graphical form. Chisholm (1967) later conducted a theoretical analysis and developed an equation form of the correlation:

$$\phi_f{}^2 = 1 + \frac{C}{X} + \frac{1}{X^2} \tag{2. 65}$$

where the constant *C*, later known as the Chisholm parameter, has the following values:

Flow pattern	liquid	gas	*C*
tt	turbulent	turbulent	20
vt	viscous	turbulent	12
tv	turbulent	viscous	10
vv	viscous	viscous	5

C = 20 applies for most cases of interest in internal flow in HVAC and refrigeration systems. Citations of the Chisholm parameter *C* in the literature are numerous; many fail to mention that the initial values are restricted to mixtures with gas-liquid density ratios close to air-water. The Chisholm treatment of the Lockhart-Martinelli correlation greatly eases its application in non-regular flow channels and flow conditions other than those tested in the original paper, as *C* can be readily modified to fit experimental data. This approach is also found in two-phase pressure drop investigations in PHE channels, as is introduced in Section 2.7.3.

The Lockhart-Martinelli correlation was developed for two-phase, two-component adiabatic flow of air and liquids including benzene, kerosene, water and various oils in horizontal pipes with diameters from 1.49 to 25.8 mm and at low pressures close to atmosphere. The correlation has also proved to be quite successful when applied to other fluids and for tubes of larger diameters (Chhabra and Richardson, 1999). The Lockhart-Martinelli correlation is the best known separated flow model, it is very simple to use and has long been the most

widely applied correlation for two-phase frictional pressure drop calculations and comparisons.

Chisholm (1973) Correlation

Chisholm (1973) proposed an extensive empirical method applicable to both local pressure gradients and overall evaporating pressure drop calculations. In this method, the liquid-only two-phase multiplier is given as:

$$\phi_{\mathrm{fo}}{}^2 = 1 + \left(Y^2 - 1\right)\left[B \cdot x^{(2-\mathrm{n})/2}\left(1-x\right)^{(2-\mathrm{n})/2} + x^{2-\mathrm{n}}\right] \tag{2. 66}$$

where the parameter Y is determined from

$$Y^2 = \left(\frac{dP}{dz}\right)_{\mathrm{fric,fo}} \Big/ \left(\frac{dP}{dz}\right)_{\mathrm{fric,go}} \tag{2. 67}$$

and n is the exponent of the Reynolds number in the friction factor expression (n = 0.25 for the Blasius equation). B is given by

B	Y	G , kg/(m^2· s)
4.8	≤ 9.5	≤ 500
$2400 / G$		500-1900
$55 / G^{0.5}$		≥ 1900
$520 / \left(YG^{0.5}\right)$	9.5-28	≤ 600
$21 / Y$		≥ 600
$15,000 / \left(Y^2 G^{0.5}\right)$	≥ 28	

The correlation can be extended to evaporating flows. The author argued that where the change in pressure along a tube is sufficiently small in relation to the absolute pressure, Y can be assumed constant, and it is then possible to integrate Equation (2.66), provided the vapour quality x is assumed to vary linearly along the tube length L. The Chisholm correlation is essentially a transformation of some previous correlations including the Lockhart-Martinelli correlation, in forms of $\phi_{\mathrm{fo}}{}^2$ instead of $\phi_{\mathrm{f}}{}^2$, with modifications by data from several sources. This method has the advantage of more convenient applications for both local and phase-changing flows, and is quite simple to use for engineering calculations.

Friedel (1979) Correlation

Friedel (1979) developed a two-phase frictional pressure drop correlation using a large data base. For vertical up-flow and horizontal flow, the two-phase multiplier is given as:

$$\phi_{\mathrm{fo}}{}^2 = E + \frac{3.23F \cdot H}{\mathrm{Fr}^{0.045}\,\mathrm{We}^{0.035}} \qquad (2.\ 68)$$

where

$$E = \left(1-x\right)^2 + x^2 \cdot \frac{\rho_{\mathrm{f}}}{\rho_{\mathrm{g}}} \cdot \frac{f_{\mathrm{go}}}{f_{\mathrm{fo}}}$$

$$F = x^{0.78}\left(1-x\right)^{0.224}$$

$$H = \left(\frac{\rho_{\mathrm{f}}}{\rho_{\mathrm{g}}}\right)^{0.91}\left(\frac{\mu_{\mathrm{g}}}{\mu_{\mathrm{f}}}\right)^{0.19}\left(1-\frac{\mu_{\mathrm{g}}}{\mu_{\mathrm{f}}}\right)^{0.7}$$

$\mathrm{Fr} = \dfrac{G^2}{gd\bar{\rho}^2}$, Froude number

$\mathrm{We} = \dfrac{G^2 d}{\bar{\rho}\sigma}$, Weber number

In the above equations, f_{go} and f_{fo} are friction factors calculated by standard single-phase correlations assuming all mass flow as vapour and as liquid, respectively. $\bar{\rho}$ is the mean two-phase density given by Equation (2.49).

The Friedel correlation is regarded as one of the most accurate, and is recommended for μ_{f} / μ_{g} <1000, which covers most fluids and operating conditions (Collier and Thome, 1994). A comparison of the correlation with a data bank of 25,000 data points (Hewitt, 1983) showed 40-50 % standard deviation, which is regarded as common for two-phase flow correlations.

Müller-Steinhagen and Heck (1986) Correlation

A very simple and purely empirical correlation was proposed by Müller-Steinhagen and Heck (1986). They noted that the two-phase frictional pressure drop increases with x almost linearly up to a maximum at $x \approx 0.85$ and then falls (this is similar to the local flow boiling heat transfer coefficient, see Figure 2.3).

The pressure drop at x=0.5 is nearly always, regardless of mass velocity, identical to that at x=1, which accounts for single-phase gas flow. Based on this information, they proposed:

$$\left(\frac{dP}{dz}\right)_{\text{fric}} = \Lambda\left(1-x\right)^{1/3} + Bx^3 \qquad (2.\ 69)$$

where

$$\Lambda = A + 2\left(B - A\right)x,$$

$$A = \left(\frac{dP}{dz}\right)_{\text{fric,fo}} = f_{\text{fo}} \cdot \frac{G^2}{2\rho_{\text{f}} d},\ B = \left(\frac{dP}{dz}\right)_{\text{fric,go}} = f_{\text{go}} \cdot \frac{G^2}{2\rho_{\text{g}} d},$$

f_{fo}, f_{go} are calculated with standard single-phase correlations.

This method is applicable for $0 \le x \le 1$. Equation (2.69) has the advantage of being easily integrated for evaporating liquids, with the assumption of linear change of x over the tube length.

A comparison was done by the authors of their correlation with fourteen previous correlations against a data bank of 9300 data points covering a variety of fluids and flow conditions. The correlation performed well with 41.9% relative error, with the best correlation giving 32.6% (a very complicated correlation by Bandel, 1973, as given in the authors' paper). The Lockhart-Martinelli correlation gave a relative error of 62.8%. It was concluded by the authors that prediction of frictional pressure drop for two-phase flow in pipes was not satisfactory with the current knowledge, and average deviations of more than 30% should be expected. Tribbe and Müller-Steinhagen (2000) and Ould Didi et al. (2002) have found this correlation worked quite well and is at least as good as others for air/water, air/oil, and several refrigerants.

Other Correlations

Some other well known two-phase frictional pressure drop correlations include those of Dukler et al. (1964), Baroczy (1964) and Grønnerud (1972), among others. Assessment of those correlations can be found in various review articles, for example, Ould Didi et al. (2002).

A Summary

Two-phase flow pressure drop depends on a large number of independent parameters including channel geometry, mass and volume fractions of the individual phases, fluid properties, pressure, mass flux, orientation of the channel (having an influence on the flow patterns), one or two components in the system, adiabatic or with phase-change, etc. Large number of correlations are reported in the literature, to cater for the needs of diverse applications. For improved accuracy, the parameter ranges need to be determined for the problem at hand, and correlations chosen accordingly. Due to the complexity of the problem, mean deviations of as much as 30% are common using these correlations; calculations for individual flow conditions can easily deviate 50% or more from experimental data (*ASHRAE 2005: Fundamentals*). For conditions outside the range of the original data from which these correlations were derived, deviations of more than 100% may be seen. It is then important to realize that the predictions made using these models must be treated with reservation and used only as estimates.

It is seen that a common strategy in both two-phase heat transfer and pressure drop modelling is to begin with a single-phase model and determine an appropriate two-phase multiplier to account for the two-phase effects. This "multiplier concept" approach goes back at least as far as the classic work of Lockhart and Martinelli (1949), and the majority of two-phase frictional pressure drop correlations are found to be falling into this category.

As previously mentioned, of the three components of two-phase pressure gradients, the frictional pressure gradient has been the topic of almost all empirical investigations in the subject. The other two parts are evaluated either by the homogeneous or the separated flow method, with the latter requiring additional information about the void fraction. Investigations were most often carried out on horizontal-adiabatic flow wherein the other two components vanish, but this leaves the effect of flow orientation unattended on application of the correlations obtained. Results of frictional pressure gradient have always been presented with the vapour quality as a primary parameter. To obtain the overall pressure drop in evaporating flow, integration is needed which requires a x-z (vapour quality vs. tube length coordinate) relationship to be determined. Usually a linear change of x over the tube length is assumed which is only strictly satisfied with constant heat flux along the tube but nevertheless has been adopted widely for all other conditions. Examples of this treatment are seen in the correlation of Chisholm (1973) and that of Müller-Steinhagen and Heck (1986). Integration of complex correlations can be carried out numerically, if an explicit mathematical expression is not obtainable.

2.4 Heat Exchanger Theory

A heat exchanger is a heat transfer device that exchanges heat between two (or more) process fluids. Refrigerant evaporators are types of heat exchangers where one of the two fluids undergoes phase-changing.

2.4.1 Classification of Heat Exchangers

Heat exchangers can be classified in many ways. In terms of surface compactness, there are conventional exchangers and compact exchangers. Conventional exchangers largely refer to shell-and-tube exchangers, compact heat exchangers have many sub-categories but all are characterized by a large heat transfer surface area per unit volume, sometimes termed as surface area density. A gas-liquid exchanger is referred to as a compact heat exchanger if it has a surface area density greater than about 700 m^2/m^3 or a hydraulic diameter d_h < 6 mm. A liquid/two-phase fluid heat exchanger is referred to as a compact heat exchanger if the surface area density on any one fluid side is greater than about 400 m^2/m^3 (Shah and Sekulic, 2003). Bergles et al. (2003) recommended hydraulic diameter d_h of 1 to 6 mm for compact heat exchangers and d_h > 6 mm for conventional heat exchangers. A typical process industry shell-and-tube exchanger with plain tubes has a surface area density of less than 100 m^2/m^3 on one fluid side, and two to three times greater than that with finned tubing. Plate-fin, tube-fin, and rotary regenerators are examples of compact heat exchangers for gas flow on one or both fluid sides. Plate heat exchangers (gasketed, welded, brazed) are examples of compact heat exchangers for liquid flows. A typical plate heat exchanger has about twice the average heat transfer coefficient h on one fluid side or the average overall heat transfer coefficient U compared with a shell-and-tube exchanger for water/water applications (Shah and Sekulic, 2003).

2.4.2 Basics of Thermal Characteristics

For any type of exchanger (shell-and-tube, plate, etc), any kind of flow configuration (co-current, counter-current, cross flow, etc), and regardless of type of phase-changing (evaporation or condensation), the basic energy equation is in the form:

$$\dot{Q} = U \cdot A \cdot \Delta T_m \tag{2. 70}$$

where ΔT_m is the mean temperature difference between the two fluids. It can be derived theoretically that for counter-current, co-current, or when temperature of one fluid does not change (the situation approximately met when the fluid undergoes phase-changing, for example, evaporation and condensation):

$$\Delta T_m = \Delta T_{LM} \tag{2. 71}$$

ΔT_{LM} is the familiar log mean temperature difference and defined as:

$$\Delta T_{LM} = \frac{\Delta T_{max} - \Delta T_{min}}{\ln \frac{\Delta T_{max}}{\Delta T_{min}}} \tag{2. 72}$$

where the temperature differences are defined in Figure 2.5 for counter-current flow, but also apply to other types of flow arrangements. For heat exchangers that do not operate in purely co-current or counter-current flow configuration, a correction factor, F, is multiplied by the value of ΔT_{LM} that would be obtained by assuming a counter-current flow configuration, and the mean temperature difference between the two fluids becomes:

$$\Delta T_m = \Delta T_{LM} \cdot F \tag{2. 73}$$

and the energy equation becomes:

$$\dot{Q} = U \cdot A \cdot \Delta T_{LM} \cdot F \tag{2. 74}$$

Analytical relations for F, and their graphical representations, for the most

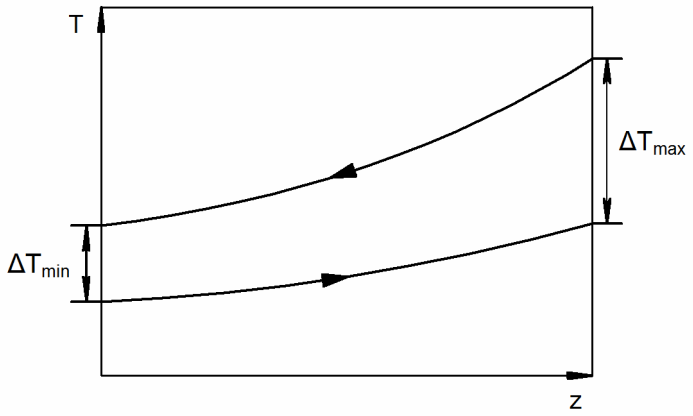


Figure 2.5: Temperature profile in a counter-current heat exchanger

common configurations are available from most heat exchanger design handbooks. For pure co- and counter-current heat exchangers and also for evaporators and condensers, $F = 1$. For any other kind of heat exchangers, $F < 1$. For PHE's with both fluids taking the same number of passes, F is usually in excess of 0.95 (Cooper, 1974 a).

It is important to realize that in applying Equations (2.70) and (2.74), the overall heat transfer coefficient U has to be taken as the average value along the heat exchanger surface. U can be calculated by:

$$U = \frac{1}{\frac{1}{h_1} + \frac{1}{h_2} + \left(\frac{\delta}{k}\right)_{\text{wall}} + R_{\text{f, 1}} + R_{\text{f, 2}}} \qquad (2.\ 75)$$

where h_1 and h_2 are individual convective heat transfer coefficients and R_f are fouling resistances. Equation (2.75) assumes equal heat transfer areas on both sides, this is the case for plate heat exchangers. For cases where the heat transfer areas are not the same on the two sides, for example the tubular exchangers, a simple correction is taken.

The method of using the log mean temperature difference in heat exchangers analysis and design is usually referred to as the *LMTD* method. Another widely used method is the *ε-Ntu* method (not employed in this study), where ε is the heat exchanger effectiveness and *Ntu* is number of transfer units. Details of the two methods can be found in any heat exchanger design handbooks (for example, Shah and Sekulic, 2003, Kuppan, 2000). It shall suffice to mention here that both methods employ the concept of an average value of U along the heat exchanger channels, and for any calculation duties, both methods can be used to obtain equivalent results, though they are each more suitable for certain situations.

2.5 Plate Heat Exchangers

2.5.1 Types of Plate Heat Exchangers

Several types of PHE's are available both for liquid-liquid duties and in refrigeration systems, these being:

1. conventional gasketed plate-and-frame
2. semi-welded plate and frame

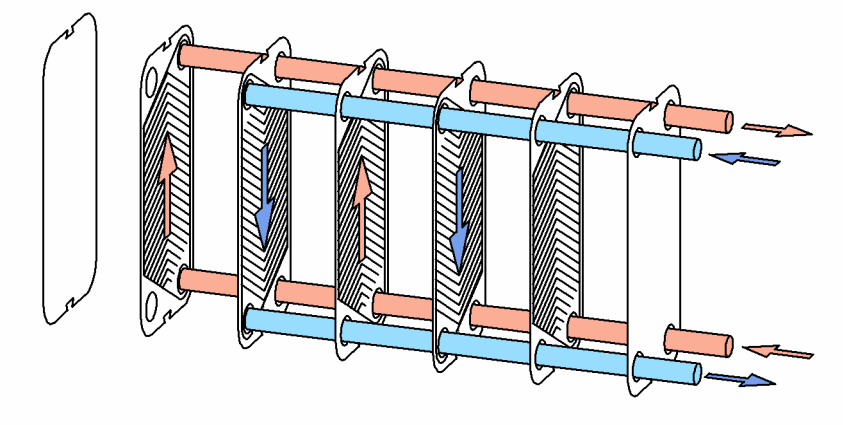


Figure 2.6: Basic flow principle of a PHE in single-pass counter-current flow arrangement

3. brazed plate heat exchangers (BPHE's, also known as compact brazed exchangers, CBE's).

A conventional plate-and-frame heat exchanger consists of a series of thin corrugated metal plates (typically stainless steel, Titanium, or other alloys) between which a number of channels are formed. Channels are sealed with gaskets and corner rings of elastomer materials, most commonly nitrile (Katzel, 2000). The plates and gaskets are held together in a frame by a pressing arrangement. Two fluids flow through alternate inter-plate channels and heat transfer takes place across the plate. The fluids can pass through the heat exchanger either in co-current or counter-current flow, and can be in single-pass or multi-pass arrangement. The basic principle of a single-pass, counter-current flow in a PHE is shown schematically in Figure 2.6. The chevron angle is reversed on adjacent plates so that when plates are assembled together, the corrugations provide numerous contact points. The corrugation on the plates generally perform three functions: they increase the effective surface, they give rigidity and strength, and they promote turbulence (Clark, 1974, Troupe et al., 1960). Normally identical plates are used in one single exchanger pack; however, mixed plates may also be used where there is a demand for balancing heat transfer load and available pressure drop. The design pressure limit of this type of PHE is around 10 bar, and operating temperatures are limited by the availability of suitable gasket materials (Kakac S. and Liu H., 2002). Generally, they are not suited for pressures exceeding 25 bar and temperatures over 250 °C (Raju and Chand, 1980).

The semi-welded PHE is similar to a gasketed plate and frame except the two adjacent plates are welded, usually by laser welding. The welded pair is called a plate cassette, and is sealed at the ports by two ring gaskets (and is thus not gasket-free). Semi-welded channels offer better sealing quality than the frame-

and-plate type, and are designed for high pressure and for aggressive media applications. For the fluid flowing in the welded cassette, temperature limits range from -50 up to 350 °C and operating pressures can be from full vacuum to 40 bar (Reppich, 1999).

Brazed PHE's (BPHE's) have similar plate geometry to the former two types, but gaskets are completely removed and the whole pack is non-opening. In such a unit, plates are brazed together with copper or nickel alloy and the exchanger is completely sealed and leak-tight. Without the limitations brought by the gasket, which has long been a weak point in the design and applications of PHE's, brazed PHE's have typical design temperatures of -160 to 190 °C, and design pressure up to 30 bar (Goldfinch, 1994, Fijas, 1997). This manufacturing solution has greatly increased the exchangers' mechanical resistance, but also eliminated the flexibility and ease of cleaning features available on gasketed PHE's. Nevertheless, the ability to withstand higher pressures and the elimination of sealing problems made the brazed PHE's interesting and applicable for the refrigeration industry, to be used both as evaporators and condensers.

2.5.2 Plate Geometry

Technically, plate corrugations can be of many types, for example, chevron (herringbone), washboard (lateral), wavy-groove, zig-zag. However, over the years, the chevron wave pattern has proved to be the most successful and popular design, and is offered in rather similar shapes by the majority of manufacturers (Carlson, 1992, Martin, 1996). The heat exchangers investigated in this study are of the chevron type, consequently the introduction of this particular type of corrugation pattern is the task of this section.

Chevron Corrugations

Geometrical features of the chevron type of corrugation are given in Figure 2.7. A single plate comprises four corner ports and the corrugated area. The corrugated pattern has a chevron angle β, evaluated as the angle between the corrugation trough to the vertical axis, or in some reports to the horizontal axis. In a PHE unit plates are installed with the apex of the chevron pointing in opposite directions. The chevron design brings four main effects, it

1. increases flow turbulence level,
2. increases the effective heat-transfer area (typically by a factor of 1.1-1.25),
3. increases stiffness of the plate pack,
4. induces turbulence and high wall shear force which reduces fouling.

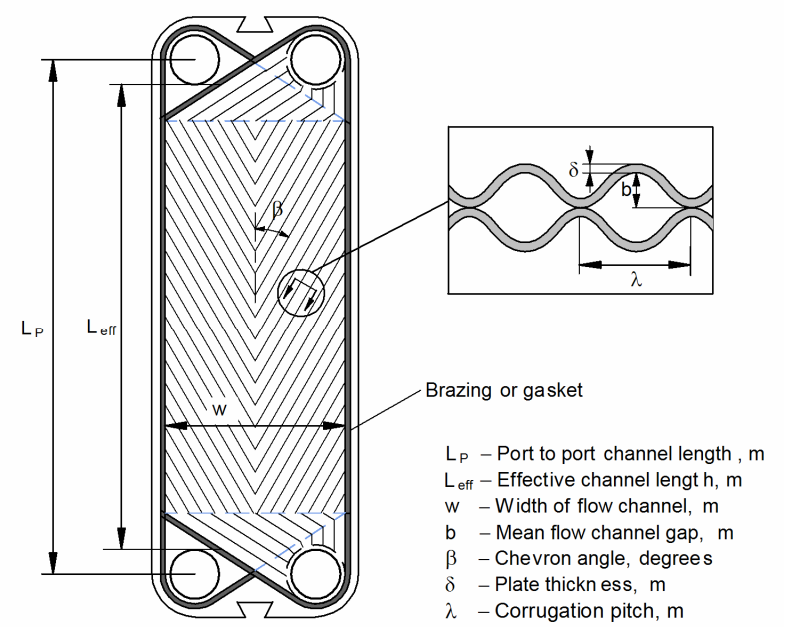


Figure 2.7: Corrugation features of the chevron type plate

The chevron angle of commercially available plates varies between the extremes of about 25 to 65°, and is perhaps the most important geometrical parameter of PHE's relating to thermal and hydraulic performance (Kakac and Liu, 2002). Conventional plates have approximately sinusoidal profiles. Corrugations that are asymmetrical in profile are not common and found to be less efficient (Focke, 1985). The surface enlargement factor, ϕ, is another important parameter, which is defined as the ratio of actual heat transfer area to the projected area. Most commercial plates have enlargement factors usually in a relatively small range of 1.1-1.25 (Kumar, 1984). ϕ can be calculated approximately, for a sinusoidal corrugation profile, from a three-point integration formula (Martin, 1996):

$$\phi \approx \frac{1}{6}\left(1+\sqrt{1+X^2}+4\sqrt{1+\frac{X^2}{2}}\right) \qquad (2.\ 76)$$

where $X = \pi b/\lambda$ is a dimensionless parameter, b is two times the amplitude of the sinusoidal wave (b = mean flow channel gap) and λ is the wave pitch. For a strict sinusoidal wave, ϕ =1.22. The channel aspect ratio is defined as $r_a = L_p/w$. Common industrial plates usually have this ratio around 2, and it is not likely to be much lower than 1.8 (Cooper and Usher, 1983). The heat transfer area of a single plate is calculated by:

$$A = L_{\text{eff}} \cdot w \cdot \phi \qquad (2.\ 77)$$

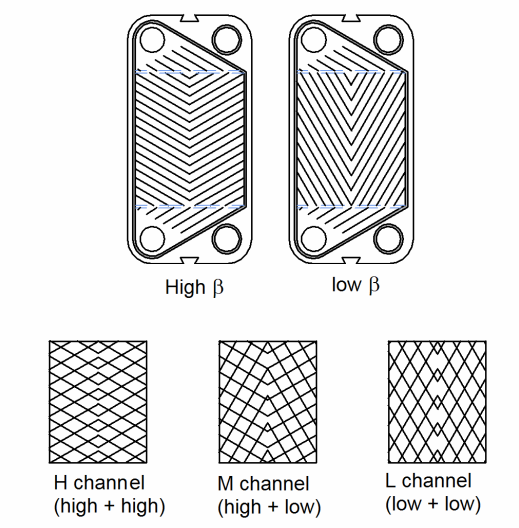


Figure 2.8: Channel of combined plates

where L_{eff} is the effective channel length and *w* the channel width.

Flow Channel Geometry

A flow channel is formed by two adjacent plates, sealed with gaskets, welding or brazing at the edges of plates and ports. The plates are usually identical but positioned with the chevron angle reversed, and the geometry of the flow channel is identical on both sides of the plates. Connecting points are formed at the crests of both plates where they meet. The channel flow area is calculated by:

$$A_{\text{ch}} = w \cdot b \tag{2. 78}$$

Also commonly seen are units with channels which are formed by plates of different chevron angles, this is referred to as the *mixed-angle* arrangement. From the manufacturer's side, the purpose of using mixed plate channels is to achieve the required thermal duty while also using the available pressure drops, and at the same time avoid expenses on pressing tools for a large number of plate types (Raju and Chand, 1980). This solution makes the design work highly flexible, and has long gained popularity in applications as least as early as in the 1970's (Clark, 1974). One of the three units that has been tested in the present study has the mixed angle arrangement, and the other two use identical plates with high and low chevron angles, respectively. These arrangements are shown schematically in Figure 2.8.

Focke (1983) argued that for practical purposes two different plate chevron angles suffice: β=45° at which the ratio of heat transfer/ pressure drop is at its

highest, and β = 72° which results in the maximum heat transfer coefficient value. However, manufacturers usually opt for angles approximately 30° and 60°, presumably to cover low heat transfer rate duties.

2.5.3 Flow Arrangements

The flow arrangement in a PHE can be very flexible. There are basically four types of configurations that can be used, as will be shown below, which are related to flow distribution inside or between channels.

1) **Inside Single Channel**
In a single channel, the flow of one fluid can be either diagonal or parallel, depending on the sealing arrangement on the ports. A diagonal arrangement refers to the flow that enters and leaves the channel at diagonally opposite ports, whereas in the parallel (or vertical, same-side) arrangement the flow enters and leaves on the same side (Kumar et al., 1994). As an example, the gasket set as shown in Figure 2.7 would give a parallel flow if a channel is formed by two such plates.

2) **Pass**
Pass refers to a group of channels in which the flow is in the same direction. The two streams in a PHE unit can have different pass arrangements, single or multiple, with the latter consisting of passes connected in series. Figure 2.9-a shows a 2 pass / 1 pass configuration where one fluid flows in a single pass manner and the other in two.

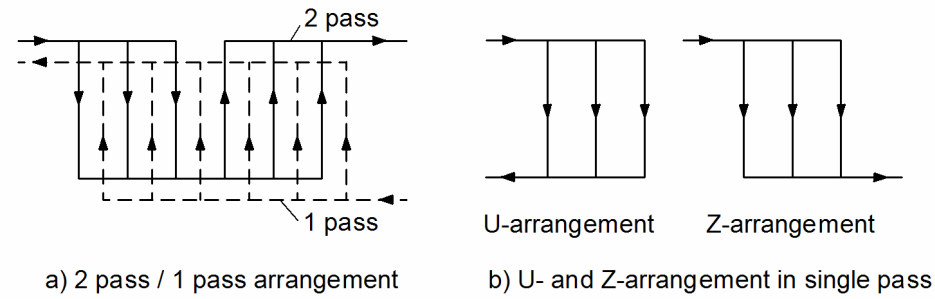


Figure 2.9: Flow arrangement of multi-channel PHE's

3) ***U* and *Z* Type Arrangement in Single-pass Flows**
The so-called *U* and *Z* type arrangements are found in single-pass flows. For any one fluid stream if the inlet and outlet ports are on the same side of the exchanger unit, it is called a *U* type arrangement, otherwise it is a *Z* type, as shown

schematically in Figure 2.9-b. The *U* type permits easy cleaning or repair on the exchanger without disturbing external piping, while the *Z* type offers more uniform flow distribution (Kakac and Liu, 2002). As is clear in the illustration, the *Z* type arrangement assures that liquid streams passing through different channels will cover the same flow distances, while in a *U* type arrangement channels further away from the entrance have longer manifold passages and may thus cause greater pressure drops.

4) **Relative Flows between Two Fluids**
The two fluids can be organized in either co-current or counter-current flow. For single-phase applications, counter-current arrangement is a more favorable choice and gives higher exchanger effectiveness than the co-current flow. This can be shown by a theoretical $\varepsilon - Ntu$ (Effectiveness - Number of transfer units) analysis on pure co- and counter- current flows, which is very well represented by PHE channels.

2.5.4 Hydraulic diameter, Reynolds Number, and Friction Factor

Equivalent vs. Hydraulic Diameter

The corrugated channel found in PHE's is a unique and complex channel; definition of the characteristic diameter of this type of channel has not been agreed on in the research community. Two definitions are found in the open literature, the first one is often called the "equivalent diameter" which is twice the corrugation depth:

$$d_{\mathrm{e}} = 2b \tag{2. 79}$$

A second and possibly more common definition is often named as the "hydraulic diameter", defined in the traditional way for hydraulic diameter of non-circular tubes (four times the volume divided by flow channel wetted surface area) as:

$$d_{\mathrm{h}} = \frac{4V}{S_{\mathrm{wet}}} = \frac{4L_{\mathrm{p}}wb}{2L_{\mathrm{p}}w\,\phi} = \frac{2b}{\phi} \tag{2. 80}$$

where ϕ is the surface enlargement factor.

The hydraulic diameter method of definition seems more physically sound since the surface enlargement factor does change the actual channel cross-section area for a given value of corrugation depth. Furthermore, introducing the enlargement factor to the hydraulic diameter might be a simple and effective way of taking

into account the influence of ϕ on the PHE performance. In the present study, the hydraulic diameter definition is used uniquely as the characteristic diameter for the corrugated channels. For clarity, these two definitions will be distinguished in this study by their subscripts, *e* for equivalent and *h* for hydraulic. It is very important to note that when correlations are quoted the definitions used in the original texts should be mentioned, to avoid confusion or misunderstanding.

Reynolds Number and Other Non-dimensional Groups

Non-dimensional groups are defined with characteristic lengths and velocities. For the chevron type of corrugated channel the characteristic diameter can be either d_e or d_h, as mentioned earlier, but the characteristic velocity is always the nominal flow velocity, or bulk velocity, defined by:

$$u = \frac{Q}{A_{ch}} \tag{2. 81}$$

It shall be noted that the nominal flow velocity obtained is not the true velocity of the fluid, due to the effect of the corrugation. Depending on the particular corrugation pattern, true velocities may be higher by a factor of up to about four (Marriott, 1971). Now, the Reynolds number is defined:

$$\mathrm{Re} = \frac{\rho\, u\, d_h}{\mu} \tag{2. 82}$$

which can also be expressed as $\mathrm{Re} = G \cdot d_h / \mu$, where $G = \dot{m} / (A_{ch} N_{ch})$ is the mass velocity in the vertical direction. With the characteristic length and velocity defined, other non-dimensional groups are now determined accordingly, for example, the Nusselt number is given by:

$$\mathrm{Nu} = \frac{h\, d_h}{k} \tag{2. 83}$$

Friction Factor

Definition of the friction factor can be sometimes confusing, more so when friction factors are mixed freely with different definitions of characteristic diameters and channel lengths, as is the case in the open literature. The two most commonly used definitions of friction factors are the well-known *Darcy* and the *Fanning* types, denoted in this study as f and c_f, respectively, and defined as:

$$f = \frac{\Delta P / L}{\frac{1}{2}\rho u^2 / d} \tag{2. 84}$$

$$c_f = \frac{\Delta P / L}{2\rho u^2 / d} \tag{2. 85}$$

In the above definitions, d is d_e or d_h, whichever is chosen by the investigator. u is the nominal velocity, given by Equation (2.81). L stands for the characteristic length of the flow channel. To make the issue more complicated, there are also two different definitions of L to be found in the literature. In most situations, fortunately, L has been used as the length between upper and lower port centres, denoted as L_p (see Figure 2.7), while in others L can be chosen as the developed flow length defined as the ratio of the actual heat transfer area to the flow width, given by $L = A_p / w$. No reasonable explanations are available for this definition. It is of interest to note that the developed flow length still does not represent the actual fluid flow distance in the channel, since flows are highly three dimensional and directed by corrugation angles, and not along routes normal to the corrugated waves. In this study, the friction factor used is the Darcy type definition f, based on the hydraulic diameter d_h and the projected channel length L_p between the upper and lower ports.

The two friction factors have the simple relationship of $f = 4c_f$ in any case, regardless the geometry of flow channel. Care must be taken to correctly interpret correlations from different authors, as the free choice of two types of characteristic diameters combined with two types of friction factors results in four possible ways to express the friction factor, and all these four are found in the open literature. For clarity, definitions and conversions between the four

Table 2.2: Definitions and conversions of friction factors

Friction factor:	Characteristic diameter	
	$d_h = 2b/\phi$	$d_e = 2b$
$f = \frac{\Delta P / L}{\frac{1}{2}\rho u^2 / d}$	f_h	f_e
$c_f = \frac{1}{4} \cdot \frac{\Delta P / L}{\frac{1}{2}\rho u^2 / d}$	$c_{f,h}$	$c_{f,e}$
Conversion:		
	$f_h = f_e / \phi$	
	$f_h = 4\, c_{f,h}$	
	$f_e = 4\, c_{f,e}$	

expressions are given in Table 2.2.

2.6 Single-phase Flow in PHE's

Over the years, investigations into the single-phase thermo-hydraulic performance of PHE's have become rather extensive. Technical reports on their performance assessment, construction development, and application recommendations are found as early as in the 1960's (for example, Troupe et al, 1960, Dummett, 1964). This is partially due to the PHE's widening applications from the food industry to the chemical industry. There are currently well over 30 correlations available which could be considered as practicable for single-phase duties, mainly for water-water, some for non-Newtonian fluids in laminar flows. PHE's are generally considered not suited for gaseous fluid duties because of high pressure drops, and not for highly viscous fluids due to problems in flow distribution (Kandlikar and Shah, 1989, Raju and Chand, 1980).

2.6.1 Overall Thermal-hydraulic Performance

PHE's are usually much more thermally efficient than their shell-and-tube counterparts, particularly for liquid/liquid duties. Film coefficients can be two to four times those for tubular units of the same duty, at the same or even lower pressure drops (Bond, 1981). At normal working ranges the overall heat transfer coefficient U can be expected to be 2300-5800 W/($m^2 \cdot K$), depending on plate corrugation and flow conditions (Raju and Chand, 1980). The highest U value that could be achieved by a PHE was reported up to 8500 W/($m^2 \cdot K$), making it capable of working with film coefficients three to five times higher than tubular or spiral-plate designs (Carlson, 1992). The augmented heat transfer performance of a PHE is due to several enhancement mechanisms, which directly result from the complex plate surface characteristics. These surface effects include disruption and reattachment of boundary layers, swirling motion of the fluids, continuous change in flow directions and velocity, combining to promote early transition to turbulence and produce exceptionally high film coefficients of heat transfer.

The analogy between heat and momentum transfer would indicate that as the heat transfer is improved there is a higher pressure drop penalty as well. In fact, it is widely noticed that increase of the friction factor is far quicker than that of the Nusselt number with increasing chevron angles. Thonon et al. (1995) reported that at the same Reynolds numbers, when compared with smooth channels the

enhancement of heat transfer is up to 6 times but at the same time the friction factor can be increased by a factor of one hundred. However, in practice for the same heat transfer area or at the same cooling/heating duties, pressure drops in a PHE are usually lower (Troupe et al., 1960), due to the fact that the flow velocities in a PHE unit are usually very low, and the flow channel length is always much shorter than that in tube-type exchangers.

Of all the dimensional parameters that describe a PHE channel, the chevron angle β is probably the most important. Generally both heat transfer and pressure drop increase with higher chevron angles. Mixed plate channels are commonly evaluated with the averaged chevron angle (Bond, 1981, Heavner et al., 1993), though a rigorous examination of this treatment is not found in published works. The surface enlargement factor ϕ might have similar effects, as deeper corrugations increase the effective surface area as well as promote greater swirl and mixing, resulting in higher heat transfer rate and pressure drop. A comparison of experimental data from several sources by Mulley and Monglik (1999) has confirmed this. When the hydraulic diameter $d_h = 2b/\phi$ is used, the effect of ϕ can be regarded as included in that of the hydraulic diameter; in other cases, this effect is usually ignored since an accurate quantitative evaluation of ϕ is difficult to obtain. Another parameter not usually attended to is the channel aspect ratio. While its effect on the exchanger thermal-hydraulic performance is apparent, this parameter has hardly become a consideration in any available correlations. High aspect ratio (a "narrow" channel) at the same heat transfer area will increase the flow velocity for given heat transfer area and thus increase pressure drops; low aspect ratio will bring problems of flow distribution inside individual channels and so will reduce the exchanger efficiency. It is also noticed that in the open literature geometrical parameters are rarely all given in detail.

It is widely recognized in the research community that turbulence is attained in PHE's at much lower Reynolds numbers than in circular tubes, however, the values of the critical Reynolds number, Re_{crit}, are reported differently from various sources from 10 to 500 (Raju and Chand, 1980, Carlson, 1992, Reppich, 1999, etc.). This may partially be due to the particular plate configurations tested. Cooper and Usher (1983) pointed out that it is difficult to predict the flow pattern in a particular PHE unit without testing it. However, it seems quite safe to conclude, from those reported values, that all types of PHE will be in the turbulent flow region at $Re > 500$, and in the laminar region at $Re < 10$. In most cases the transient region is in the Re range of 10-150. The early transition of flow patterns in PHE's might be explained by two main reasons:

1. Corrugation features. Corrugations break down the stagnant insulating film at the plate surface and trigger turbulence (Raju and Chand, 1980). It is

obvious that a higher chevron angle and deeper corrugation will promote higher levels of disturbance and earlier transition.

2. Actual flow velocity. In the corrugated channel, the actual flow would most likely follow the corrugations rather than flow in the vertical direction (Focke et al, 1985). As a result, the actual flow velocity is much higher than the mean value in the vertical direction, which is used to calculate the Reynolds number.

PHE's could be treated as pure co-current or counter-current heat exchangers in principle if end effects are neglected. For a shell-and-tube exchanger this can hardly be the case, due to cross flows resulting from baffles. For a two-channel PHE, pure counter-current flow may be assumed; for multiple channel units, a correction factor of the LMTD (Log Mean Temperature Difference) is sometimes recommended. Buonopane et al. (1963) initially addressed the issue and reported that for lateral-corrugated plates, with packs in a 1 pass/ 1 pass counter-current arrangement, an average correction factor of 0.95 should be applied to the LMTD. Marriott (1971) later presented a chart for approximate values of the correction factor as functions of the Ntu (Number of transfer units) for various pass arrangements, which confirmed Buonopane et al's correction factor value. Kandlikar and Shah (1989) also tabulated correction factor values based on a more refined numerical analysis. Usher (1970) pointed out that corrections are needed when the flow departs from the two-channel equal flow condition, to account for flow ratio, number of passes and end effects of passes, and these can only be determined empirically.

Pressure Drop Components

Pressure drop in a PHE consists of three contributions: (1) frictional pressure drop within the core (plate passages), (2) pressure drop due to elevation change, (3) pressure drop in inlet and outlet manifolds (ports). Of these, the frictional pressure drop is of main interest and has been addressed in various empirical correlations in the open literature. Elevation pressure drop is calculated in a straightforward way by $P=\rho gh$. For the manifold pressure drop, an accurate evaluation method is not available. A very widely cited equation by Shah and Focke (1988) gives an estimation of the manifold pressure drop, without a reference, as:

$$\Delta P_{\text{manifolds}} = 1.5 \cdot \left(\frac{G^2}{2\rho} \right)_{\text{inlet}} \cdot N_{\text{pass}} \tag{2.86}$$

The manifold pressure drop is usually considered much smaller than the other components. Generally the manifold pressure drop is lower than 10% of the

overall pressure drop, but can be as high as 30% or higher in certain designs (Shah and Sekulic, 2003). Bond (1981) pointed out that different port designs, producing variation in manifold roughness, could result in the overall pressure drop to be two to three times higher than the passage pressure drop.

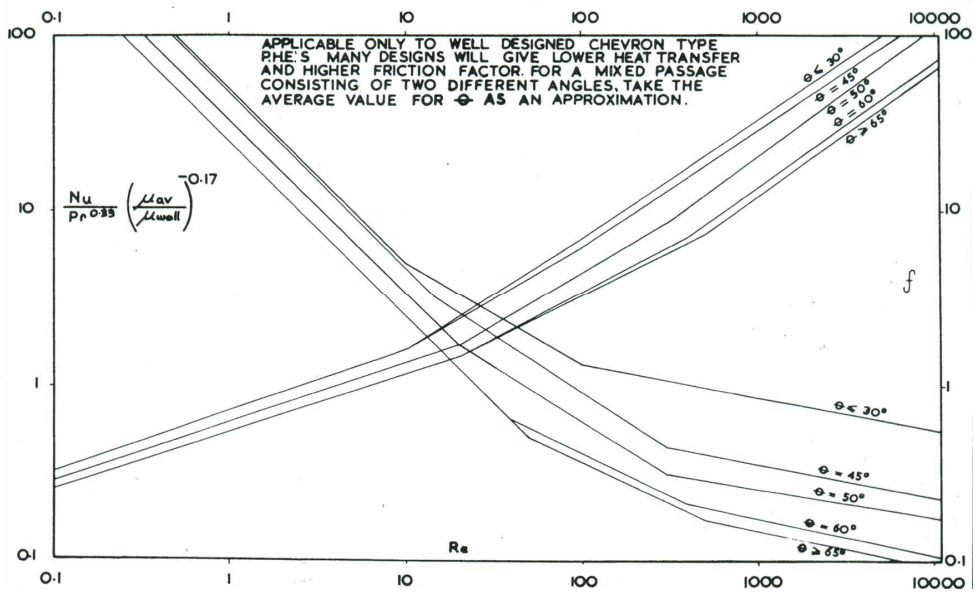
2.6.2 Single-phase Heat Transfer and Pressure Drop Correlations

A considerable amount of research has been conducted to determine heat transfer and flow friction characteristics for the PHE geometry. There are well over 30 correlations available in the open literature, most of which are for a specific plate geometry. Those correlations are generally developed for turbulent water-water duties, with a few for laminar flows of Newtonian and non-Newtonian fluids. Most of them are in forms of the familiar Sieder-Tate type, with modified constants and exponents. Some later correlations express coefficients or exponents of the Reynolds number as functions of the chevron angle and the enlargement factor to cover wider applications. The exponent of Re in most of the water-water correlations is close to 2/3, for all chevron angles. This value was also confirmed by Stasiek et al. (1996) in their tests on turbulent air flow (Re = 400-3500) through air pre-heaters which have very similar geometries to those of PHE channels. It seems clear that correlation forms which have been successfully applied in tube flow are also applicable to PHE's, while a more general one would require considerations of geometrical effects, especially the chevron angle.

Edwards et al. (1974) of the APV Company [1] tested various non-Newtonian fluids including glucose solutions, lubricating oil and poly-acrylamide solutions in one PHE unit with a chevron angle of 60° and very high aspect ratio (≈8). It was found that laminar flow conditions exist up to a Reynolds number of 10, and a very gradual transition to turbulent flow follows, in contrast to pipe flows where the onset of turbulent flow is rapid. The authors had, interestingly, noticed the similarity of channel geometry between a PHE and that of a packed bed of near-spherical particles, in that flow channels are both featured with series of expansions and constrictions. Certain correlations for packed beds were then compared with pressure drop and heat transfer data obtained from the PHE unit and very good agreement was obtained. The authors pointed out that the same measure of agreement would not be expected for plate exchangers having markedly different corrugation patterns. While the analogy of these two types of exchangers remains interesting, verifications of this approach are not found in other works.

[1] APV Company Ltd is an UK based major PHE manufacturer.

Based on extensive test data, Bond (1981) of the APV Company reported PHE heat transfer and pressure drop correlations in graphic form, for β = 25°- 60°, ϕ = 1.14 fixed, and Re = 0.1-10,000. This correlation is reproduced in Figure 2.10, with its basic form expressed in Equation (2.87). The heat transfer relationship in the Bond correlation is of typical Sieder-Tate type, with modified constants accounting for the chevron angle. For each chevron angle the flow is divided into three regions. It is seen that the higher the chevron angle the lower the critical Reynolds number. For β=60°, laminar flow occurs below Re=10. Pressure drops determined from the plots refer to passage pressure drops excluding passage entry and exit losses. The author stated that diverse designs of ports, producing variation in port manifold roughness, could result in the overall pressure drop two to three times the passage pressure drop. Kumar (1984) reported that the accuracy of the Bond correlation is about ±20% except in laminar flow regions, for which greater inaccuracies may occur on account of influence of fluid viscosity. Bond's correlation is one of the earliest with a wide applicability, and remains the only one that is based on manufacturer data covering more than one plate model. This correlation has also become a favorite comparison basis for many later investigations. For the convenience of computation, constants of the correlation were derived in this study from the original graph, and listed in Table 2.3.



θ ($=90^\circ - \beta$) is the angle between corrugation trough to horizontal direction,
f refers to the Fanning friction factor, $d = 2b/\phi$

Figure 2.10: Bond (1981) correlation for chevron-type PHE's

$$\begin{cases} j_{\mathrm{Nu}} = \dfrac{\mathrm{Nu}}{\mathrm{Pr}^{1/3}\left(\dfrac{\mu}{\mu_{\mathrm{wall}}}\right)^{1/6}} = c_1 \mathrm{Re}^{\mathrm{m}} \\ c_{\mathrm{f}} = \dfrac{c_2}{\mathrm{Re}^{\mathrm{p}}} \end{cases} \tag{2.87}$$

Table 2.3: Constants in the Bond (1981) correlation (Equation. 2.87)

β	Re	c_1	m	Re	c_2	p
≤ 25	≤ 20	0.543	0.33	≤ 50	25	1
	$20-500$	0.323	0.50	$50-500$	3.13	0.47
	≥ 500	0.090	0.71	≥ 500	0.62	0.21
30	≤ 20	0.543	0.33	≤ 40	25	1
	$20-400$	0.300	0.53	$40-400$	3.60	0.47
	≥ 400	0.104	0.71	≥ 400	0.742	0.21
40	≤ 20	0.618	0.34	≤ 20	33	1
	$20-300$	0.284	0.60	$20-300$	11.1	0.63
	≥ 400	0.133	0.73	≥ 300	0.78	0.16
45	≤ 20	0.725	0.35	≤ 15	48	1
	$10-100$	0.420	0.59	$15-300$	18.6	0.65
	≥ 100	0.290	0.67	≥ 300	1.30	0.19
≥ 60	≤ 10	0.725	0.35	≤ 10	50	1
	$10-100$	0.375	0.64	$10-100$	19.0	0.58
	≥ 100	0.309	0.68	≥ 100	3.1	0.19

$d_{\mathrm{h}} = 2b/\phi$, $\phi = 1.14$

Table 2.4: Constants in the Heavner et al. (1993) correlation (Equation. 2.87)

β	β_{avg}	c_1	m	c_2	p
45 / 90	67.5	0.278	0.683	1.715	0.0838
23 / 90	56.5	0.308	0.667	1.645	0.1353
45 / 45	45	0.195	0.692	0.810	0.1405
23 / 45	34	0.118	0.720	0.649	0.1555
23 / 23	23	0.089	0.718	0.571	0.1814

$\mathrm{Re} = 400-10{,}000$, $d_{\mathrm{h}} = 2b/\phi$

Heavner et al. (1993) of the APV Company later published test results on five units with different chevron-angle combinations: 23°/23°, 23°/45°, 45°/45°, 23°/90° and 45°/90°. Each unit had 12 channels, other geometrical information was not provided due to commercial considerations. All tests were in turbulent regions with Reynolds number in the range of 400-10000. A correlation was given in the same form as the Bond correlation (Equation (2.87)), with new constants given by Table 2.4. In this correlation, the chevron angle of a mixed-plate channel is evaluated by the average of the two plates. The authors compared their data with the Bond (1981) correlation curves, though chevron angles covered in the two investigations were not identical, and rough agreements were obtained. It is noticed that the Reynolds number index for the heat transfer coefficient is around the value of 0.7 but dose not show much relevance to the chevron angle, which is consistent with the Bond correlation for turbulent flows. For the friction factor it is noticed that the Bond curve has a Re exponent of 0.2, remaining constant for all chevron angle plates, while Heavner et al's data have shown this exponent to decrease with increasing chevron angle. This relationship can be explained, as tried by the authors, by considering the corrugated channel as a rough tube, whose roughness increases with increasing chevron angle. At β = 0° the channel is a collection of smooth vertical tubes which would have a Re exponent of 0.25, as suggested by the Blasius equation ($c_f = 0.79/ \mathrm{Re}^{1/4}$), on the other hand, at β = 90° the exponent reaches 0, as for very rough tubes the friction factor is no longer a function of the Reynolds number (which is also indicated by the familiar Moody chart).

Wanniarachchi et al. (1995) developed a set of more generalized correlations based on the curve correlation of Bond (1981) and data reported by Heavner et al (1993). The correlations are in a third-order asymptotic form, which is given by Equation (2.88). The authors explained that the choice of this form is due to the fact that there was no suitable information to define the critical Reynolds numbers. Mathematically, an asymptotic equation always approaches the larger of the two components and assures a smooth transition. Edwards et al. (1974)'s observation of very gradual transition from laminar to turbulent flow in PHE channels, as opposite to a rapid one in conventional pipes, might have at least partially justified this choice of correlation form.

$$\begin{cases} j_{\mathrm{Nu}} = \left(j_{\mathrm{Nu,\,l}}^3 + j_{\mathrm{Nu,\,t}}^3 \right)^{1/3} \\ c_{\mathrm{f}} = \left(c_{\mathrm{f,\,l}}^3 + c_{\mathrm{f,\,t}}^3 \right)^{1/3} \end{cases} \tag{2.88}$$

where

$$j_{\mathrm{Nu,\,l}} = \frac{3.65}{\theta^{0.455}\,\mathrm{Re}^{0.339}},\quad j_{\mathrm{Nu,\,t}} = \frac{12.6 \cdot \mathrm{Re}^{0.646+0.00111\theta}}{\theta^{1.142}}$$

$$c_{f,l} = \frac{1774}{\theta^{1.026}\,\mathrm{Re}},\ c_{f,t} = \frac{46.6}{\theta^{1.08}\,\mathrm{Re}^{4.23\times10^{-3}\cdot\theta - 2.23\times10^{-5}\cdot\theta^2}},$$

$$\theta = 90^\circ - \beta$$

Valid for $\beta = 23-62$, Re=1-10000

Crozier et al (1964) suggested from investigation on Non-Newtonian flows that, for laminar flow, the Lévêque approximation, initially developed for heat transfer calculations of laminar flow in short pipes, can be used with good results, whereas a clear description of the method was not given. The idea was later developed independently and more successfully by Martin (1996) into a semi-theoretical correlation for turbulent heat transfer and pressure drop in PHE's.

The Lévêque approximation, shown by Equation (2.89), is a purely analytical equation for hydrodynamically developed and thermally developing laminar flows in circular pipes of short lengths. This equation can be found in many heat transfer handbooks (for instance, Bejan and Kraus, 2003, Baehr and Stephan, 2006). Martin proposed a generalized form of this equation, as given by Equation (2.90), based on which his heat transfer correlation for PHE channels was developed. For a circular tube, with $f \cdot \mathrm{Re} = 64$, the generalized Lévêque equation (Equation (2.90)) reduces to the conventional one (Equation 2.89). The author argued that though the Lévêque equation had not been previously applied to turbulent flow, there is no reason to restrict its application to the laminar range. A further analysis on this equation with its applications for the prediction of heat and mass transfer rates from pressure drop can be found in a later paper by the same author (Martin, 2002).

$$\mathrm{Nu} = 1.615\left(\mathrm{Re}\cdot\mathrm{Pr}\cdot\frac{d}{L}\right)^{1/3} \tag{2.89}$$

$$\frac{\mathrm{Nu}}{\mathrm{Pr}^{1/3}} = 0.404\left(f\cdot\mathrm{Re}^2\cdot\frac{d}{L}\right)^{1/3} \tag{2.90}$$

To use Equation (2.90), the friction factor has to be determined first. Martin carried out an analysis on the frictional pressure drop based on the observation (Focke et al., 1985) that there are two kinds of flows coexisting in a corrugated channel: crossing flow following the furrows of adjacent plates and longitudinal flow between two vertical rows of contact points. To obtain an overall friction factor, effects of the two are combined tentatively using a reciprocal square root type of equation, with each part containing constants to be determined by experimental data. The expression for the heat transfer group takes the form of Equation (2.90), with the characteristic length being the distance between two crossings, i.e., $L = \lambda/\sin(2\beta)$, and the leading constant and the exponent for $f \cdot \mathrm{Re}^2$

further refined by experimental data. The final expression of the Martin correlation is:

$$\begin{cases} \dfrac{1}{\sqrt{f}} = \dfrac{\cos\beta}{\sqrt{b\cdot\tan\beta + c\cdot\sin\beta + f_0/\cos\beta}} + \dfrac{1-\cos\beta}{\sqrt{a\cdot f_{1,0}}} & (a) \\ j_{\mathrm{Nu}} = c_{\mathrm{q}}[f\cdot \mathrm{Re}^2\sin(2\beta)]^{\mathrm{q}} & (b) \end{cases} \qquad (2.91)$$

where

$(a,\ b,\ c) = (3.8,\ 0.18,\ 0.36)$

$(c_{\mathrm{q}},\ q) = (0.122,\ 0.374)$

$$f_0 = \begin{cases} \dfrac{64}{\mathrm{Re}} & \mathrm{Re} < 2000 \\ \dfrac{1}{(1.8\log_{10}\mathrm{Re} - 1.5)^2} & \mathrm{Re} \geq 2000 \end{cases}, \quad f_{1,0} = \begin{cases} \dfrac{597}{\mathrm{Re}} + 3.85 & \mathrm{Re} < 2000 \\ \dfrac{39}{\mathrm{Re}^{0.289}} & \mathrm{Re} \geq 2000 \end{cases}$$

for $\mathrm{Re} = 400 - 10{,}000,\ \beta = 0^\circ - 80^\circ,\ d = d_{\mathrm{h}} = 2b/\phi$

The most important implication of Martin's correlation is perhaps the dependency of the heat transfer coefficient on the product $f \cdot \mathrm{Re}^2$, which is a direct measure of the pressure drop: $f\cdot\mathrm{Re}^2 = \Delta P\cdot 2d^3\rho/(L_{\mathrm{p}}\mu^2)$ (from Equation 2.84). It can be shown that the term $\sin(2\beta)$ deviates from its maximum value of 1 by less than 10 percent over the range of $25° \leq \beta \leq 65°$. As a result, Equation (2.91-b) essentially indicates that two PHE units of different chevron angles would have the same heat transfer coefficient if the pressure drops are the same, though the flow rates will differ. This relationship between the heat transfer coefficient and pressure drop for plate heat exchangers was also reported previously by Cooper and Usher (1983) with an exponent of 0.30 for the pressure drop ΔP. The Reynolds number range of validity of Martin's correlation was not given, however it seems that the same range for Heavner et al's correlation should apply, i.e., Re=400-10000, since the analysis of all constants relied heavily on this particular correlation. The chevron angle is in the range of 0-80°. Martin's correlation is well constructed with the author's attempt to generalize the correlation for the Nusselt number by applying a heat transfer-pressure drop analogy through a purely theoretical equation. Several parameters are fitted to experimental data, making it a semi-empirical correlation. Shah and Sekulic (2003) reported ± 40% accuracy for pressure drop and ± 30% for heat transfer coefficients for this correlation. Higher accuracy can be expected if the five constants are further refined with actual detailed plate geometry and certainly with more extensive data. Claesson (2005a) reported excellent fit of this correlation with that supplied by a manufacturer based on extensive tests.

Muley and Manglik (1999) conducted experimental tests on three PHE units with plate chevron angle combinations of 30°/30°, 30°/60° and 60°/60° and enlargement factors of 1.29, in turbulent flows of Re > 1000. The conventional Sieder-Tate form (Equation (2.87)) was again used, with the slight difference of the viscosity ratio exponent being 0.14 instead of 0.17. In the effort to obtain a general correlation that covers all the three units, the lead coefficients and Re exponents were described as functions of the chevron angle β. The effect of the enlargement factor ϕ was included by using a third-order polynomial correlated with more data from other sources. The final correlation shows:

$$\begin{cases} j_{\mathrm{Nu}} = \dfrac{\mathrm{Nu}}{\mathrm{Pr}^{1/3}\left(\mu/\mu_{\mathrm{wall}}\right)^{1.14}} = c_1 \mathrm{Re}^{\mathrm{m}} \\ c_{\mathrm{f}} = \dfrac{c_2}{\mathrm{Re}^{\mathrm{p}}} \end{cases} \tag{2.92}$$

where

$c_1 = \left(0.2668 - 0.006967\beta + 7.244\times10^{-5}\beta^2\right)\cdot\left(20.78 - 50.94\phi + 41.16\phi^2 - 10.51\phi^3\right)$

$m = 0.728 + 0.0543\sin(\pi\beta/45 + 3.7)$

$c_2 = \left(2.917 - 0.1277\beta + 0.002016\beta^2\right)\cdot\left(5.474 - 19.02\phi + 18.93\phi^2 - 5.341\phi^3\right)$

$p = 0.2 + 0.0577\sin(\pi\beta/45 + 2.1)$

β in degrees, $\pi\beta/45 + 3.7$ and $\pi\beta/45 + 2.1$ are in radians.

For $\mathrm{Re} \geq 1000$, $\beta = 30 - 60$, $\phi = 1 - 1.5$, $d = d_{\mathrm{e}} = 2b$

The agreements for Nusselt number and friction factor with the experimental data were claimed as 10% and 5%, respectively. However, the accuracy of this correlation needs verification by more tests, since it was based on only three different PHE's. Moreover, the treatment of the effect of the enlargement factor in Muley and Manglik's correlation can be arguable. The third order polynomial expressions accounting for ϕ, in both the Nusselt number and the friction factor equations, were based on a very limited number of data points (less than 10) with relatively big scatters. A simple calculation would indicate that in the range of ϕ=1.1-1.25, which is typical for industrial plates (Kumar, 1984), the correlation gives an increment of 52% for Nu and 143% for f. Even though reports on the effect of ϕ have not been quantitatively conclusive in the literature, those figures are likely to be exaggerated. It can be shown that when the enlargement factor is smaller than its tested value, i.e., 1.29, the Muley and Manglik correlation tends to give continuously lower values of Nu and f than those predicted by most other correlations.

Focke and his coworkers conducted a series of experimental studies on PHE's including flow visualizations (Focke and Knibbe, 1986), optimum PHE surface

patterns selection (Focke, 1986) and performance assessment of asymmetrically corrugated PHE plates (Focke, 1985). Based on *mass* transfer and pressure drop data, Focke et al. (1985) reported a correlation for *heat* transfer and friction factor. The heat transfer rate is evaluated not by direct measurement data but by heat-mass transfer analogy theory, with the Colburn *j*-factor which states: $j = \mathrm{Sh}/(\mathrm{Re}\cdot\mathrm{Sc}^{1/2}) = \mathrm{Nu}/(\mathrm{Re}\cdot\mathrm{Pr}^{1/2})$ [1]. The testing unit consisted of a single channel machined in sinusoidal corrugation shape with an enlargement factor of 1.464, which is considerably higher than most commercially available industrial plates. Care should be taken when using this correlation as the heat transfer data are based on the projected and not the developed transfer surface area. This is a rather unusual treatment, but explanations were not given in the paper. The correlation is found to give exceptionally high Nu when compared with others, while the friction factor is fairly similar.

Some other correlations are available, though less cited and usually lack generality. A total of 28 correlations were summarized by Ayub (2003) in his review article [2], which brings a good and brief introduction. It is recommended here, however, that for the details and applicability of a particular correlation, reference should be made to the original source, as the obscure terminology and mixed use of various parameters often causes not only confusion but also erroneous quotations.

It might be worthwhile, for the sake of a straightforward perception, to compare the introduced correlations against each other. Figure 2.11 shows the calculation curves of Nu and f against the Reynolds number in the range of Re=100-10000, at β = 45° and ϕ = 1.14, from six correlations as introduced in this section. Valid ranges of those correlations are given in Table 2.5. The chevron angle of 45° is covered by all correlations while the enlargement factor of 1.14 is not, this value is chosen for a fairest possible comparison basis for all. Disagreements between those correlations are clear, being relatively greater at low Reynolds numbers. The Nu predicted by Focke et al's correlation is significantly different, which could possibly be explained by their heat-mass transfer analogy treatment of experimental data, also with the tested channel's large enlargement factor. Muley and Manglik's correlation gives a Nu number lower than all the others, possibly because of an exaggerated effect of the enlargement factor.

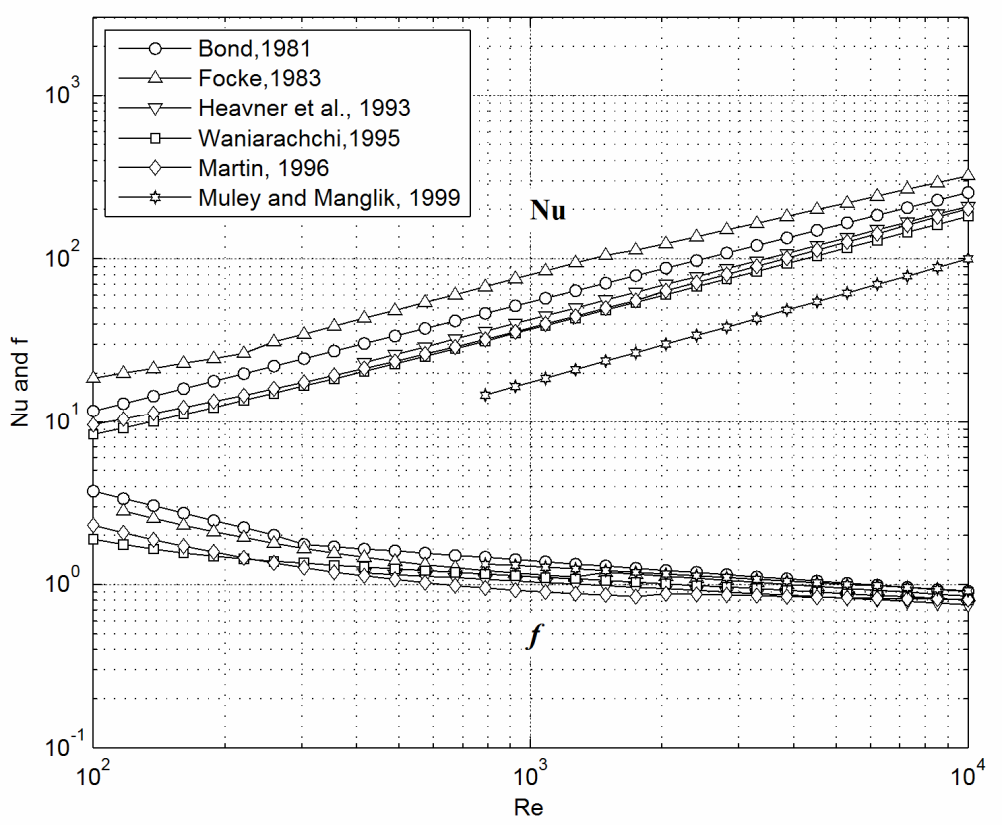
---

[1] The familiar Chilton-Colburn analogy states, as seen in many heat transfer textbooks:

$$j = \frac{\mathrm{Nu}}{\mathrm{Re}\cdot\mathrm{Pr}^{1/3}} = \frac{\mathrm{Sh}}{\mathrm{Re}\cdot\mathrm{Sc}^{1/3}}$$

It is noticed that Focke et al. (1985) has chosen the exponent of the Pr number as 1/2, instead of 1/3, no explanation of this treatment was given.

[2] Reproduction of those correlations in Ayub's paper was not without mistakes. Besides typographical errors, one apparent cause has been, for certain correlations, the author's incorrect interpretation of the various characteristic length and friction factors used by different authors. The use of particular correlations is thus recommended to refer to the original papers.



Calculation based on β =45°, ϕ =1.14, at Pr =6.13 (water at 1bar, 25°C)

f is Darcy friction factor, characteristic diameter is $d = 2b/\phi$

Figure 2.11: A comparison of six correlations

Table 2.5: Some single-phase PHE correlation with their validity ranges

Correlation	Re	β, degrees	ϕ	$N_{ch} \times$ Pass	$L_p \times w$ (mm)	Description
Bond, 1981	0.1-10,000	25, 30, 40, 45, 60	1.14	–	–	
Focke et al., 1983	90-56,000	0, 30, 45, 60, 72, 80, 90	1.464	Single channel	440×100	Heat transfer data based on mass transfer measurement
Heavner et al., 1993	400-10,000	23/23, 23/45, 45/45, 23/90, 45/90	–	12×1/12×1	–	PHE typical of modern designs
Wanniarachchi et al., 1995	1-10,000	23-67.5	–	–	–	Based on Bond and Heavner et al. data
Martin, 1996	All range	0-80	All range	–	–	Heavily based on Heavner et al data
Muley and Manglik, 1999	>1,000	30/30, 30/60, 60/60	1-1.5	12×1/12×1	392×163	ϕ =1.29 for the tested units

A Summary

In contrast with the established knowledge and standards for heat transfer and pressure drop in straight pipes and conventional heat exchangers, a generally accepted theory, or correlation, for PHE design and performance assessment has not yet become available. This is certainly attributed to the highly complex nature of the PHE channel, in terms of its corrugation-featured geometry, also in terms of the almost infinite combinations of many other parameters including the aspect ratio, channel depth, port size, flow distribution, plus many types of optional flow arrangements. Plate corrugation is not an industry standard, there are over 60 different corrugation patterns from different manufacturers (Cooper and Usher, 1983). Although it is true that the chevron-type corrugation is dominant, geometries of those plates from different manufacturers are not identical, a typical example is the types of patented corrugation features around the entrance region aiming at more uniform flow distributions. It is believed that the only accurate correlations are those produced by manufacturers, based on many years of research and extensive tests of specified plates and arrangements but those are usually kept confidential (Cooper, 1974a, Reppich, 1999). Such correlations, once available, are still to be regarded as case studies with restricted applications for specified conditions.

With all this in consideration, the task of achieving a general solution seems hopeless. On the other hand, however, a generally applicable correlation could have to focus only on important and common features while omitting minor and irregular ones, at the expense of lower accuracy. From the most widely accepted correlations, including all that have been reviewed in this section, it is seen that chevron angle is (of course) a priority, enlargement factor is an option, other geometrical parameters and the effect of any flow arrangements are usually not considered. Of those correlations, there is currently no suitable information one can rely on to judge which one is more accurate than others, and it is usually difficult to explain the disagreements between them, as those disagreements may have resulted from, among others, geometry differences, incorrect treatment in the data reduction, and measurement errors. It is not unusual to find calculations using some of those correlations to differ by more than ±30% or even over 100% especially at lower Reynolds numbers. As such, correlations shall be chosen according to the plate geometry and used as rough estimates only. For rigorous assessments and for situations where high accuracy is required, it is always preferable to conduct individual performance tests.

2.6.3 Flow Distribution

The concept of flow distribution, in the case of plate heat exchangers, refers to that between channels and thus applies only to multi-channel units. Although the flow distribution inside an individual channel can be another important technical issue, it is rarely addressed in the open literature. Thermo-hydraulic theories and correlations for PHE's largely work on the assumption of uniform flow distribution between channels, this is however not the case in practice. It is generally accepted that flow maldistribution can increase the overall pressure drop and decrease the thermal performance. There is, however, no generally accepted quantitative determination method accounting for this effect.

Flow distribution is determined by inlet and exit manifold pressure profiles, for which two factors can have influences: frictional force and momentum change. Frictional force always causes pressure drops, the momentum change may however have two different effects: in the inlet manifold the deceleration of fluid, due to outflow (into channels), results in actually a pressure *rise*, whereas in the exit manifold the fluid confluence gives pressure *drop* in the flow direction. The net effect of the two mechanisms depends on many factors, most importantly channel pressure drop characteristics which determines the flow rate of the fluid leaving the manifold and entering the channels, fluid flow rate, and port size which determines the frictional losses in the manifolds. Most industrial PHE units are arranged in single-pass *U* or *Z* type flows; effects of friction loss and momentum change on the pressure profile in these two arrangements are schematically illustrated in Figure 2.12. A vertical line between the two pressure profile lines represents the pressure drop. Even distribution of pressure drops means even distribution of flow, since all channels are identical.

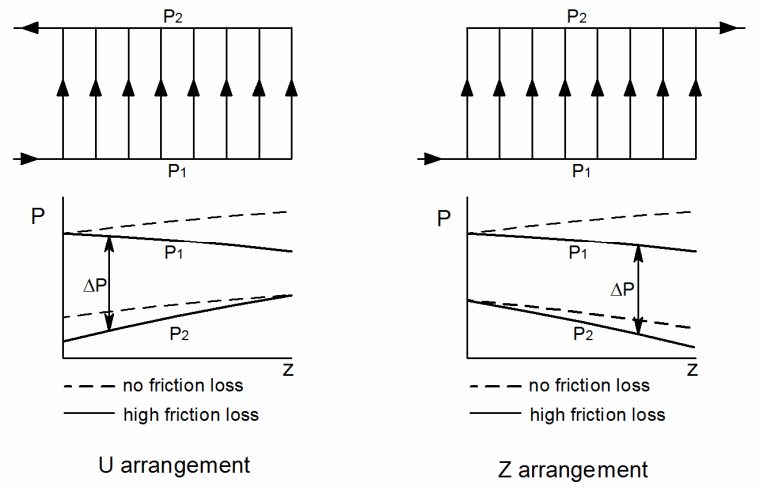


Figure 2.12: Manifold pressure and channel flow distribution

As introduced earlier (Section 2.5.3), the *Z*-type arrangement is normally expected to give more uniform flow distributions than the *U*-type (Kakac and Liu, 2002). This was confirmed by Wilkinson (1974) in his test on units of six channels with pressure measurement on each individual channel. The result also indicated that in the *U*-type arrangement the liquid stream always "favors" channels closer to the inlet nozzle, more so at higher volume flow rates. The author further pointed out that this holds true also for large units.

Bassiouny and Martin (1984 a, 1984 b) carried out a theoretical analysis on the flow distribution and pressure drop in PHE's, based on the assumption that the friction loss in the manifolds is negligible. The direct result from this assumption is that pressure always rises in the inlet manifold along the flow direction, and consequently the *Z*-type arrangement always suffers more severe maldistribution than the *U*-type. This is because, with such an assumption, pressure profiles in the Z-type arrangement always tend to diverge, while in a U-type they tend to remain relatively parallel (see Figure 2.12). While this assumption remains itself highly arguable, Rao and Das (2004) concluded using this same model that maldistribution is more severe in the *Z*-type compared with the *U* type. They conducted tests of overall pressure drop with the two arrangements, but no obvious difference of the overall pressure drop at the two conditions could be seen.

2.6.4 Fouling

Predicting the fouling resistance accurately is essential for any rigorous performance analysis or design of heat exchangers. For refrigeration applications as in the current study, the refrigerant flows in a closed loop and is usually assumed as clean, information of fouling is needed for the water side.

In practice, scale or deposits on heat exchanger surfaces cause a decrease in thermal performance during operation due to reduced overall heat transfer coefficient. The effect of fouling is evaluated by a fouling factor, R_f, which is defined as the thermal resistance across the fouling substance. Fouling is found to be considerably less in PHE's than in other types of exchangers. The main reason for this is the high degrees of turbulence which maintain solids in suspension and removes foulant (Marriott, 1971). R_f can be generally expected to be about 10-20% of that in a tubular exchanger, from reported data available in the open literature (Cooper, 1974a, Marriott, 1971, Stromblad, 1989, Panchal and Rabas, 1999). It is evident but worth stressing that an over-estimated value of the fouling factor will have a much greater effect on the overall coefficient of a high-efficiency exchanger such as a PHE than on that of an exchanger having a low overall thermal efficiency. In the current study typical values of fouling factors

Table 2.6: Recommended fouling resistances of PHE's vs. TEMA values

Process fluid	R_f - PHE $\times 10^{-3}$ m^{2}K/W		R_f - TEMA $\times 10^{-3}$ m^{2}K/W
	Marriott, 1971	Panchal and Rabas, 1999	Panchal and Rabas, 1999
Water			
soft	0.018	0.018	0.18-0.35
hard	0.043	-	-
Cooling tower water	0.034	0.044	0.18-0.35
Sea water	0.026	0.026	0.18-0.35
River water	0.043	0.044	0.35-0.53
Lubricant oil	0.017-0.043	0.053	0.36
Organic solvents	0.009-0.026	0.018-0.053	0.36
Steam	0.009	0.009	0.18
Process fluids, general	0.009-0.052	-	-

for plate heat exchangers as quoted from two sources, along with those of the tubular exchangers for the convenience of comparison, are given in Table 2.6. The fouling factors of tubular exchangers are quoted from the TEMA (Tubular Exchanger Manufacturers Association) standard as provided by Panchal and Rabas (1999).

There are currently no standard values of fouling factors available for PHE's, in contrast to those for tubular exchangers. Considering the great variety of corrugation patterns, it is reasonable to assume a geometry-related fouling factor applicable to a specific exchanger. Under the circumstance where this information is lacking, values provided in Table 2.6 can be used as a general and best estimation.

2.6.5 Numerical Simulations

Numerical simulation, or in other terms, computational fluid dynamics (CFD), has been the subject of recent interest for many heat exchanger analysts, due to the vast computational resources available and development of numerical solution techniques particularly in the last thirty years (Nithiarasu, 2005). Numerical simulation of any heat transfer problem essentially involves the solution of the Navier-Stokes equations with the continuity and energy equations, by commercial or specially developed software. Simplifications are necessary, of mathematical expressions and geometrical conditions of the problem.

There are a number of CFD simulations on the flow pattern or heat transfer in plate heat exchangers, e.g., Trifonov (1998), Mehrabian and Poulter (2000), Kanaris et al. (2004), Pelletier et al. (2005). The majority of those concern heat transfer and pressure drop in a single unitary cell or a simplified single channel with only one corrugated plate, due to the highly complex channel geometry. No numerical simulation of a complete PHE channel has been found. CFD modeling has the advantage, among others, of being able to show local behaviour and interactions, such as of temperature and velocity vector profiles, usually in graphical interfaces. On the other hand, however, those simulated results are difficult to validate, especially for flows in confined and limited spaces such as a PHE. Validations and engineering applications of the CFD simulation method in plate heat exchangers have so far been limited, though it is known that some manufacturers have used this method in their product development process for years.

2.7 Two-phase Flow in PHE's

A brief history review shows that PHE's were not normally considered as suitable for refrigerant evaporators and condensers before the 1990's. Concerns included leakage from gasket materials, pressure limits (especially for condensers), freezing risk, and high pressure drops of generated, or in the case of a condenser, entering, vapour in both the manifolds and plate passages. Early applications of PHE's in two-phase flow duties commonly involved heating process fluids using condensing steam (Cooper, 1974b, Kumar, 1983) with usually moderate pressure on the steam side, one typical example of this kind is pasteurizing milk. PHE's were also used as evaporators for liquid food concentration and sea water desalination (Kumar, 1993). Even though some of the major manufacturers had started development programs on PHE's as refrigerant evaporators and condensers since the middle of 1970's, as initiated by the first energy crisis (Strömblad, 1989), applications of this type of exchanger in refrigeration systems only became popular after the invention of semi-welded PHE's and brazed PHE's in the early 1990's. Meanwhile, the ozone-depletion issue in the mid-1980s also became a factor promoting the use of PHE's in refrigeration systems because their compactness would result in a low refrigerant charge (Ayub, 2003). In the last two decades, with their inherent advantage of high efficiency and compactness, it is believed that PHE's have enjoyed a rapidly increasing market in the refrigeration industry with applications including liquid chillers, indirect systems, residential heat pumps, and absorption chillers (Mencke et al, 2005).

Investigations on two-phase flow in PHE's are increasing but not are yet extensive. Due to the complex nature of two-phase flow, fundamental understandings of the flow boiling mechanism in this unique type of channel (actually, in any type of channel) is rather limited. In contrast to the thermal-hydraulic process in single-phase flow, flow boiling is controlled by some additional parameters, most importantly heat flux, vapour quality and local flow regimes. Of the few empirical correlations available in the open literature, coverage of those important parameters is usually limited and unsystematic and the operating conditions vary. As a result, there is not a generally accepted calculation method for two-phase heat transfer and pressure drop in PHE channels. Some manufacturer-published information can help, but this is either too general or restricted to a few aspects of certain products (Ayub, 2003).

2.7.1 Adiabatic Two-phase Flow Characteristics

Investigations on adiabatic flows have mainly focused on pressure drop characteristics and sometimes on flow visualization. The air-water system is most often used. It has been a common practice to model a liquid with its vapour by water and air for two-phase flows in conventional pipes. This strategy normally helps to ease the experimental arrangements.

It is widely agreed that PHE's are not suitable for gas applications due to high pressure drops. At the same time, the topic is rarely addressed in any depth in the open literature. With the lack of information on gaseous fluid pressure drop in PHE channels, one question may rise: could the friction factor correlations obtained from liquid (water) flow be applicable to gaseous fluids (air)? This question becomes important when two-phase pressure drop calculation is concerned, in adiabatic or phase-changing flows. Most, if not all, empirical methods employing the separated flow concept require pressure drop determination of both the liquid and gaseous phases when they flowing alone in the channel. One would naturally assume that the same correlation should apply for both phases. This is the case for conventional tubular channels, and has been adopted by many investigators for PHE channels without questioning. Experimental results from a few reports may have supported this assumption. In a test of air flow in corrugated channels by Gaiser and Kottke (1989), the friction factors at Re = 2000 were compared with Focke et al.(1985)'s data using water. Good agreement was obtained with deviations smaller than 20% for all six chevron angles in the range of β = 20°-77.5°. Laboratory machined plates were used in both investigations where ϕ = 1.57 and 1.46, respectively. In another test by Stasiek et al.(1996) on air flow in an industrial power plant regenerator, which

has corrugated passages very similar to those of a PHE, the friction factor at Re = 500 - 4000 and fixed β =30° would give close agreement to that of Focke et al., with deviations smaller than 10% for most data points. Reports on air flow pressure drops in industrial PHE units were not found. On the other hand, in an effort of calculating PHE condenser pressure drop, Kumar (1983) obtained different correlations for liquid and vapour phase:

$$\begin{cases} f_{\mathrm{f}} = A / \mathrm{Re}^{0.2} & \text{liquid} \\ f_{\mathrm{g}} = B / (\mathrm{Re} \cdot \mu)^{0.3} & \text{vapour} \end{cases} \tag{2.93}$$

where A and B are geometry-dependent constants, unique for each plate. Kumar's expression for liquid friction factor was in agreement with the correlation suggested by Bond (1981). More specific investigations on gas pressure drop in PHE's were not found. Nevertheless, information available may have indicated that a single correlation could be applied to both phases without serious error, and most investigators have used this treatment.

Some fundamental issues need to be considered in adiabatic flow pressure drop:

1. the dependence of two-phase pressure drop on mass flux G and mixture quality x,
2. applicability of correlations from conventional channels for PHE's,
3. influence of geometrical parameters, particularly chevron angle.

Creissig and Müller-Steinhagen (1992) measured port-to-port pressure drops of air/water flow in an Alfa-Laval commercial PHE with β = 60°, in the range of Re=4000-64000. Considerable pressure drops were observed at such high flow Reynolds numbers, single phase air pressure drop was 90 kPa/m at Re = 4000 and 300 kPa/m at Re = 8000, for instance. It was found that the pressure drop increases almost linearly with the mixture quality x, which differs from tubular flow where maximum pressure drops are normally observed at x = 0.8 - 0.9. Four correlations previously established for conventional channels were tried to predict the data, three of which are based on separated flow concepts including the Lockhart-Martinelli (1949) correlation and that of Müller-Steinhagen and Heck (1986). All of those tend to over-predict the pressure drop data but the Dukler (1964) correlation, which is based on the homogeneous model, gave reasonable agreement, being better at high mixture qualities. The authors argued, reasonably, that the complicated flow geometry in a PHE would keep the two phases well mixed, therefore heterogeneous flow patterns which are often seen in tubular flow (most commonly annular flow), are unlikely to occur.

Winkelmann et al. (1999) experimentally investigated air-water down-flow in a corrugated channel with β = 27°. At two mass fluxes of 50 and 100 kg/($m^2 \cdot s$) (air and water combined), it was observed that the frictional pressure drop

increases almost linearly with the mixture quality x. This observation agrees with that of Creissig and Müller-Steinhagen (1992). The authors correlated their data by the Lockhart-Martinelli method using the original Chisholm type of equation (see Equation (2.65)), an average value of $C = 6$ was obtained for all data points covering $x = 0.05$ to 0.9. The reported accuracy of the calculation is within 25% of the measured values of two-phase pressure drop.

Tribbe and Müller-Steinhagen (2001a, 2001b) investigated air-water flow in typical industrial PHE's in greater depth. Measurements of pressure drop in the corrugated section, using thin needles interested through the gasket, were taken on three chevron angle combinations of 30°/30°, 30°/60° and 60°/60°, under constant mass flux conditions in the range of 50 to 600 kg/($m^2 \cdot s$). It was found that regardless of channel geometry, the measured total pressure drop tended toward a linear function of mixture quality x except at very low qualities. They found that, upon applying the Lockhart-Martinelli method, the Chisholm parameter C varies considerably as a function of the Martinelli parameter X, and they recommended not to use a unique value for C [1].

Claesson and Simanic (2003) experimentally investigated pressure drop of R134a adiabatic flow inside a BPHE channel. Plate geometry information was not given, but it was reported that in the range of $x = 0.1$-0.7 and $G = 18$-48 kg/($m^2 \cdot s$), the frictional pressure drop is almost linear with the quality x. The pressure drops were high, for example, 100 kPa at $G = 48$ kg/($m^2 \cdot s$) and $x = 0.3$. A general correlation was not obtained due to the small number of data points, but efforts were made to correlate the two-phase multiplier ϕ_f to the Martinelli parameter X and a power law type of $\phi_f - X$ relationship was suggested. A constant C approach of the Chisholm method would not succeed because of large variations.

Vlasogiannis et al. (2002) investigated air/water mixture down-flow in an Alfa-Laval P-01 PHE with 6 channels and a chevron angle of 60°. Four flow regimes were identified based on visual observations through a Plexiglas plate, embossed with the same corrugation and placed as the last plate of the exchanger pack. At water superficial velocity j_f lower than 0.025 m/s, liquid mainly moves at the bottom of corrugation furrows leaving a continuous gas phase flowing in the major part of the channel space (regime A). At $j_f > 0.1$ m/s and low j_g, dispersed flow was observed where small bubbles flow inside a liquid continuous stream (regime B). At other superficial velocities of both phases the flow was interpreted

[1] Upon using the Lockhart-Martinelli approach, the $\phi_f - X$ relationship could be given in graphical form (as in the original paper, and Kumar(1984) for PHE condensation), by the Chisholm C constant, or in other forms. The authors proposed a new empirical correlation for the $\phi_f - X$ relationship. Though they suggested not to use the C constant method, as an unique value of C would result in large errors, a close examination shows that when a C value of 4.00 is used the maximum deviation from their suggested correlation is -23.7%, not so large a value for two-phase pressure drop predictions.

as combinations of the two. In another flow visualization investigation by Shiomi et al. (2004), only dispersed flow was observed in the range of j_f =0.01-0.56 and j_g, = 0.14-1.2 m/s, on three PHE's of 30°/30°, 30°/60° and 60°/60° chevron angles.

Flow visualization investigations had often used transparent materials as a cover plate, and it is noticed that pictures are always vague and blurry because of metal reflection, a problem not suffered by investigations on pipe flows. This affects flow pattern identifications which are already heavily associated with subjective judgments.

2.7.2 Flow Boiling Heat Transfer in PHE's

Flow boiling heat transfer is a very complex process and the physics of this process is still not well understood. Practical applications require quantitative prediction of the flow boiling coefficient. Since it is not possible at present to solve boiling heat transfer problems by analytical or numerical solutions of the conservation laws, the coefficient is always obtained through experimental studies and expressed by empirical correlations. The flow boiling heat transfer coefficient is a complex function of transfer surface finish, fluid thermo-physical properties but most importantly two-phase flow parameters, including primarily mass flux, heat flux, vapour quality, and system pressure. Conventional treatments involve the combination of two contributions: nucleate boiling and forced convection (for more details refer to Section 2.2.3). For circular pipes, these two are usually treated as additive or in other forms. For PHE channels, while the same two components are considered to present, their contributions are not clearly known. It is also generally agreed that two-phase heat transfer and pressure drop are flow pattern dependent, but most conventional models have ignored this effect. Flow pattern related investigations on two-phase flow in PHE channels are very scarce, and there is no heat transfer associated modelling currently available.

Overall Performance and Basic Features

Panchal et al.(1983) investigated the overall performance of two industrial PHE's used as refrigerant evaporators. A series of tests were conducted with ammonia and R22 at various exit vapour qualities, chevron angles, heat flux, and mass flow rates. In general, ammonia showed better performance than R22 with higher overall heat transfer coefficients and lower pressure drops at same heat flux and exit qualities. The two major conclusions were:

1. nucleate boiling is a major mode of heat transfer, but forced-convection will be more important for the upper region. Results showed that the overall heat transfer coefficient is not substantially influenced by the refrigerant flow rate and relatively insensitive to the chevron angle, both indicating a nucleate boiling dominant process.

2. the controlling heat transfer resistance is on the refrigerant side. As a result, increasing the water side flow rate (and thus h_w) did not significantly increase the overall heat transfer coefficient. A test was conducted on one exchanger unit before and after a nucleate boiling promoting surface was coated on the heat transfer surface; the overall heat transfer coefficient was increased by a factor of 2 or more at the same heat fluxes.

Since only overall performance was tested, water and refrigerant side heat transfer coefficients were not individually determined, and the relative contribution of nucleate boiling and forced convection could not be determined because local measurements were not made. Nevertheless, the results are important in academic value as well as for engineering practice. It might be inferred from Panchal et al's observations that PHE evaporators will not benefit from high angle plates, which only marginally increase the heat transfer rates but significantly increase water-side pressure drop. In a later report Panchal and Rabas (1993) confirmed that nucleate boiling is the dominant evaporation mechanism up to the upper part of a PHE evaporator. As such, a nucleate boiling promoting coating on the refrigerant side can be applied but is only necessary to the lower half of the plates. More data were reported on individual film coefficients of both fluid sides of a 60° chevron angle unit in this latter report, and it was shown that the porous surface coating increased the ammonia side heat transfer coefficient from 5700 to 29000 W/($m^2 \cdot K$), with the water side coefficient remains as high as 15000 W/($m^2 \cdot K$) and resulted in an overall heat transfer coefficient increase from 3500 to 8100 W/($m^2 \cdot K$).

Engelhorn and Reinhart (1990) conducted a series of tests on a R22 direct expansion (DX) PHE evaporator with and without an inlet flow distributor. The influence of vapour exit conditions was also investigated, the overall heat transfer values U for superheated refrigerant at the exit were approximately 25% lower than those of the saturated state. Evaporator performance was considerably improved after the installation of a flow distributor. Experimental results showed that the refrigerant heat transfer coefficient h_r had a strong dependence on heat flux q, and no significant influence of mass flow rate or evaporating pressure was observed. Data points of h_r were explained quite well by methods for nucleate pool boiling.

Kumar (1993) reported two basic conclusions for evaporation of water where the heat source is condensing steam: 1. overall heat transfer coefficient U is invariant

with water mass flow rate G, and 2. U is significantly lower at low evaporating pressures P. Boccardi et al. (2000) tested three refrigerants (R134a, R407C and R410A) and it was found that R410A had the best overall thermal performance under the same working conditions, while the other two had similar performances. More recently Thonon (2008) reviewed experimental work on propane evaporation in BPHE's, it was concluded that the refrigerant side heat transfer coefficient for hydrocarbons is usually lower than for R22 due to their specific physical properties. For example, the higher latent heat of propane implies a lower flow rate. Propane heat transfer coefficients of 1700-2750 W/($m^2 \cdot K$) were reported in normal working ranges of heat flux of q = 6-10 kW/m^2.

Dominant Flow Boiling Process in PHE: Forced Convection or Nucleate Boiling?

Flow boiling heat transfer in pipe flow is established to be the combination of two basic mechanisms: forced convection and nucleate boiling, which well represent the term "flow boiling". Conventionally, the nucleate boiling contribution is often calculated from pool boiling correlations, sometimes with a suppression factor introduced, while the forced convection contribution is calculated from single-phase correlations. For compact heat exchangers including PHE's, it is generally admitted that the two basic mechanisms occur during flow boiling, but no general predictive method is available (Thonon et al., 1997).

There are four most important working parameters to be considered in flow boiling in any channel geometries: evaporating pressure P, heat flux q, local vapour quality x, and the mass velocity G. Pool boiling heat transfer is a strong function of P and q, plus surface roughness R_p, which is a fixed feature for a certain channel. In general, nucleate boiling heat transfer coefficients increase with increasing P, q, and R_p. On the other hand, single-phase forced convection heat transfer coefficients are mainly a function of flow velocity, which is directly relevant to the mass velocity G and local vapour quality x; P and q have only marginal effects via fluid thermal-physical properties. The influence of those parameters on the overall heat transfer performance indicates the contribution of relative heat transfer mechanisms.

Thonon et al. (1997) concluded from experiments on R22 and R134a vaporization in PHE's that the heat transfer coefficients could be either in a nucleate or a convective boiling regime. The transition between these two basic mechanisms depends on flow characteristics and also on channel geometry. It was concluded that for PHE's running as DX evaporators, the dominant boiling mechanism is forced convection. The authors suggested a transition criterion, $Bo \cdot X_{tt}$:

$$\begin{aligned} &\mathrm{Bo}\cdot X_{\mathrm{tt}} > 0.15\times10^{-3} \quad \text{Nucleate boiling dominant} \\ &\mathrm{Bo}\cdot X_{\mathrm{tt}} < 0.15\times10^{-3} \quad \text{Forced convection dominant} \\ &\text{where } X_{\mathrm{tt}} = \sqrt{\Delta P_{\mathrm{f}} / \Delta P_{\mathrm{g}}} \end{aligned} \tag{2.94}$$

In the above equation $Bo \cdot X_{\mathrm{tt}}$ is a product of the boiling number and the Martinelli parameter, this criterion takes into account the operating parameters but not the geometrical effects.

Ayub (2003) pointed out that in PHE flooded evaporators it is possible that the majority of the heat transfer is through forced convection rather than local nucleate boiling, due to the narrow complex passages, but nucleate boiling probably plays its role in the lower sections. Stromblad (1989) argued that high shear and homogeneous two-phase flow characteristics in corrugated channels result in rapid suppression of nucleate boiling, and as a consequence, in the entire channels the boiling process takes place by two-phase convective heat transfer. While both statements are technically reasonable, later experimental observations of various authors suggested otherwise. Panchal et al. (1983) observed that in an ammonia liquid-overfeed system the overall heat transfer coefficient is not changed significantly by increasing the ammonia flow rate. Engelhorn and Reinhart (1990) found that data points in a R22 evaporator showed strong dependence on q. Kumar (1993)'s test on water flow boiling showed that U is invariant with water flow rate G, Panchal et al. (1983) and Uehara et al. (1997) both obtained very high overall heat transfer coefficients applying nucleate boiling-promoting material on the refrigerant side. All those observations seem to suggest a nucleate boiling dominant process in PHE evaporators. Claesson and Palm (1999) experimentally determined the evaporating and superheating regions of a brazed PHE R22 DX evaporator using thermochromic liquid crystal (TLC, a material which changes colour with temperature) techniques. In the range of q = 6-15 kW/m^2 with superheating of 1-10°C the *evaporating region* heat transfer coefficient was only a function of the boiling heat flux and not the mass flux, which led to the authors' conclusion that the boiling process in this type of heat exchanger is mainly in the nucleation boiling region.

From the foregoing, it seems clear that nucleate boiling will be a dominant boiling process in a liquid-overfeed PHE where a liquid-deficient region is not likely to occur. For DX systems two-phase forced-convection evaporation may become important for the upper part. There are two factors which are unique in a PHE evaporator and need some consideration. Firstly the flow velocity in a PHE evaporator is usually significantly lower than that in pipe flow at comparable mass flow rates (cooling loads), due to the wide flow area, and this effect favours local nucleate boiling. Secondly, most, if not all, PHE evaporators are arranged in

single-pass configuration for the refrigerant side and the flow length is very short. Consequently, when dry-out occurs, even for a short length of the channel, it will occupy a considerable portion of the channel and bring a severe effect on the overall heat transfer coefficient. The latter feature was seen in a number of investigations. Panchal et al. (1983) observed that at in a R22 evaporator, at comparable heat flux and both water and refrigerant side mass velocities, the overall heat transfer coefficient dropped 44% when the exit quality changed from 0.63 to 0.98. Claesson and Palm's test (1999) showed that when the exit superheat changed from 1°C to 10°C, the evaporating area dropped sharply from 90% of the total surface to 20%. The same authors (Claesson and Palm, 2002) in a later paper pointed out that when there are two regions present – boiling and superheating regions, those two need to be treated individually in predicting the evaporator performance. Sterner and Sunden (2006) and Jokar et al.(2006) divided the PHE DX evaporator into two regions in their experimental analysis. The basic method of determining the individual areas of these two regions, which was also outlined by all groups of authors, is given in *Appendix M*. However, Claesson and Palm (2002) had pointed out that this method tends to underestimate the area of the superheating region when compared with measured areas using the TLC (Thermochromic Liquid Crystals) technique. Other accurate calculation methods for determining the areas of these two regions have not been available.

Sterner and Sunden (2006) argued that for small channels of d_h = 2.5-3 mm the channel dimension plays a critical role in determining heat transfer mechanisms, and conflicting data interpretations and conclusions could be drawn depending on whether the channel size is greater or less than some critical space dimension. This is a reasonable statement, but may not be the main cause of the issue. Most industrial plates are in a rather small range of corrugation depth and hydraulic diameters d_h are usually well beyond 3 mm; in cases where laboratory machined plates are used, those are often of similar or scaled-up corrugations. Plam and Claesson (2006) in another paper noticed the complexity of flow boiling and disagreement of different authors, they stated that the difference in opinion seems not to be explained by differences in the geometric parameters or in the flow conditions. They further reported that for DX evaporators there is a dominating influence of heat flux and only a minor influence of mass flux and vapour fraction, but this does not necessarily mean that nucleation is an active process under all conditions; thin film evaporation might be an important heat transfer mechanism which is also a heat flux dominating process.

It is evident that local flow structure has the strongest influence on the local boiling mechanism. It is also possible that the effects of heat flux and mass flux on the heat transfer coefficient only become significant when those parameters are greater than certain magnitudes. The choice of the mass flux in a PHE evaporator is flexible even at comparable heat fluxes using the same refrigerant

because of the free choice of the number of channels. For DX evaporators there is a direct connection between heat flux and mass flux, which makes it very difficult to distinguish between the two contributions.

The question of which mechanism is dominating in a PHE evaporator has not gained an agreed answer and thus remains open. Results from various investigators have led to different, and sometimes conflicting conclusions. There is no in-depth and systematic investigation devoted to this topic in the open literature. All correlations available are based on statistical analysis without regard to the physics of the boiling process that occurs in this type of channel.

Heat Transfer Enhancement in PHE Evaporators

It is a well known fact that liquid over-feed, or flooded, evaporators are more thermally effective than direct expansion (DX) evaporators. This also applies to other types of evaporators. One of the reasons for this improvement is certainly due to the fact, as is also known for pipe flow, that dry-out occurs at the upper section of the transfer surface of a DX evaporator. The situation is more severe for a high performance evaporator, bearing in mind that in normal one-pass working conditions the flow channel is already short. One other reason, not usually addressed, might be attributed to the inlet flow distribution. A DX evaporator has liquid-vapour mixtures at the inlet, due to liquid flashing at the thermal expansion device. Hewitt et al. (1993) conducted an excellent analysis on the liquid/vapour interface in the manifold. They demonstrated that from the inlet port along the flow direction, vapour would rise first and then the liquid. As a result, a certain number of channels would contain vapour and the remainder pure liquid, and this effectively leads to the "under-utilizing" of the heat exchanger. This analysis gives a reasonable perspective of the two-phase maldistribution at the PHE evaporator inlet, while its effect on the overall heat transfer rate depends on two things: number of plates and inlet vapour quality. In a test by Kedzierski (1995) on a DX evaporator of 36 plates with R22 as the working fluid, the effect of flow maldistribution was investigated by feeding both saturated and subcooled entering refrigerants; in the latter case the amount of subcooling was set to offset pressure drops that would occur and cause flashing, however, no significant difference in the heat transfer performance of the evaporator was observed.

Some authors (Engelhorn and Reinhart, 1990, Sterner and Sunden, 2006) have reported heat transfer improvement by the installation of an inlet refrigerant distributor[1], all concerning DX systems. This is justifiably so according to the

[1] A distributor basically consists of a tube with small bores, one per channel. But there are various patented designs. Installation of a distributor is a convenient option usually offered by manufacturers.

analysis above, and it could possibly be said that a distributor would not be as effective for a liquid-overfeed evaporator since this type of evaporator does not suffer from liquid/vapour maldistribution in the first place. Stromblad (1989) reported that the largest liquid-overfeed evaporators have about 300 refrigerant channels (600 plates for the exchanger pack), while for DX systems the number of channels should not be excessive (maximum numbers not given).

Promotion of heat transfer on the refrigerant side has proved effective in increasing the PHE evaporator overall heat transfer rate. This is because PHE evaporators usually have the major thermal resistance on the refrigerant side. Panchal et al. (1983) obtained an increase of the overall heat transfer coefficient by a factor of 2 after application on the refrigerant side (ammonia) of a porous surface coating specially designed for promoting nucleate boiling. Uehara et al. (1997) tested a R22 shell-and-plate evaporator (plate geometries very similar to that of a PHE) where the refrigerant side was coated with aluminium powder, very high overall heat transfer coefficients of 3200-4800 W/(m^2 · K) were observed. Longo et al. (2004) obtained improved R22 heat transfer coefficient by 30% - 40% using a "cross-grooved plate surface". It is established that the water side heat transfer coefficient h_w can be several times greater than that of the refrigerant side, h_r, as Gray (1984) stated: PHE evaporators usually confer *very high* heat transfer coefficients on the liquid side and *good* coefficients on the boiling side. According to various sources (Marriott, 1971, Raju and Chand, 1980, Panchal et al., 1983, Stromblad M., 1989, Engelhorn and Reinhart, 1990), at normal conditions, values of h_w = 3000 - 12000 W/(m^2 · K) for water, and h_r = 1000 - 3000 W/(m^2 · K) for R22 and 2000 - 5000 W/(m^2 · K) for ammonia can be expected.

2.7.3 Two-phase Pressure Drop

Two-phase pressure drop in a PHE unit has many components. Under common conditions pressure measurements are taken at the inlet and exit of the unit, and the total pressure drop (measured value) includes four parts: pressure drop due to the channel friction ΔP_{fric}, pressure drop at the ports and manifolds ΔP_{port}, pressure drop due to momentum change (acceleration) ΔP_{acce} and pressure drop due to gravity (elevation) ΔP_{elev}. Of those the frictional pressure drop is by far the major part and almost the sole interest of all investigations. Evaluation methods of those components are reviewed in this section.

Frictional Pressure Drop

For the calculation of two-phase frictional pressure drop in PHE channels, many authors have chosen the Lockhart-Martinelli method. Others have used the homogeneous model treatment. The Lockhart-Martinelli method has been reviewed in detail in Section 2.3.3; this method requires determination of the ϕ_f-X, i.e., two-phase multiplier and Martinelli parameter, relationship. This relationship can be given in many ways, for example, it can be in graphic forms (as in the original paper), or by the Chisholm method with a C constant (Equation (2.65)), or other equation forms as found suitable for the experimental results. The Chisholm method is widely employed; however, different values of the Chisholm constant C have been reported with large variations.

Cooper (1974b) of the APV company might be the first in the literature who proposed the Lockhart-Martinelli method in PHE two-phase flow applications. The author reported that for steam condensation the use of the Lockhart-Martinelli formulation gave the best fit of the data among a number of correlations tried; ϕ_g was used instead of ϕ_f and the ϕ_g –X relationship was obtained by curve fits but not given in the paper. Kumar (1983) of the same company later reported more details in applying this method for steam condensation pressure drop calculations. A figure form of the ϕ_f –X and also ϕ_g –X relationship was presented, which yields non-fixed values of the C parameter ($C \approx 5.4$ at $X = 1$) if the Chisholm method is to be used. It is important to note that Kumar had used different correlations for the liquid and vapour phase pressure drops in his method. The Martinelli parameter X is determined from its original definition, as given by Equation (2.60), which gives different values than if determined by the widely recognized equation for circular tubes, Equation (2.61).

Thonon et al.(1995) reported that for two-phase pressure drop in corrugated channels the original Chisholm equation can be used with C=8 to obtain good estimation of the two-phase flow multiplier ϕ_f. The Martinelli parameter X was however evaluated by the circular pipe flow Equation (2.61) and no information on the channel geometry was given. Winkelmann et al. (1999) later reported C = 6 for air-water adiabatic flow in a single corrugated channel with chevron angle of 27°. Asano et al.(2004) reported C = 2.73 for air-water adiabatic flow in a single channel with chevron angle of 60°. Tribbe and Muller-Steinhagen (2001) observed that in their air-water adiabatic flow experiments the data obtained could not be represented by the Chisholm equation with a unique value of C, and a form of ϕ_f –X correlation was suggested. Claesson (2005b) used the Chisholm method for calculation of refrigerant pressure drop in DX evaporators, the Chisholm parameter was fitted from the experimental data in the form $C = f(\mathrm{Re}_{fo}, X)$. Palm and Claesson (2006) later reported that a single value of C=4.67

correlated the data reasonably well. Sterner and Sunden (2006) applied the Chisholm parameter for their ammonia DX evaporators, C was found as a function of the liquid-only Reynolds number, i.e., $C = f(\mathrm{Re}_{\mathrm{fo}})$.

It is seen that many investigators have favoured using the Lockhart-Martinelli approach in calculating two-phase frictional pressure drop in PHE channels, especially for adiabatic two-phase flows. However the $\phi_{\mathrm{f}} - X$ relationship, or value of the Chisholm parameter C where used, could not be agreed upon. The disagreement is certainly relevant to the variety of channel geometries tested. Another possible reason, among others, could be due to the difficulty of accurately predicting the single-phase gaseous pressure gradient. Confirmation is still needed whether correlations obtained from single-phase water are applicable to refrigerant liquid and vapours. It is important to note that where the Lockhart-Martinelli method is used for phase-changing calculations, such as evaporation and condensation, the channel length must be split into several zones; in each zone the individual liquid and vapour component pressure drops are to be calculated using pertinent correlations. This is because the method is for the adiabatic flow condition only. With modern computation facilities available, a stepwise integration can be carried out numerically by dividing the flow length into a great number of subsections, say 100 or more.

Other methods have also been proposed. In fact most proposed frictional factor correlations from experiments on PHE evaporators have been based on homogeneous theory, with the friction factor being a function of local mean vapour quality and liquid-only Reynolds number. This is seen in a list of empirical correlations available, as given in Table 2.7 in the following section. Yan and Lin (1999) first proposed a simple two-phase friction factor correlation (Equation 2.98), followed by Hsieh and Lin (2002, 2003) and Han et al. (2003) with similar forms (see Equations (2.101), (2.103) and (2.105)). Ayub (2003) presented a very simple correlation for two-phase Fanning friction factor which is a function of vapour-only Reynolds number and chevron angle (Equation 2.107). Jassim et al. (2005) observed from R134a adiabatic flow in a single chevron-type channel with β=60° that a linear relationship between pressure drop ΔP and homogeneous kinetic energy $G^2/(2\rho_{\mathrm{m}})$ exists in the two-phase flow at a given quality in the whole range of x = 0-1. Longo and Gasparella (2007) also reported the same linear relationship between ΔP and $G^2/(2\rho_{\mathrm{m}})$, from their tests on R134a, R410A and R236fa evaporation in a BPHE with β=65°. If the observations from those two groups of authors could be validated, calculation of two-phase frictional pressure drop in PHE channels will be greatly simplified by using the homogeneous model with a relatively fixed friction factor.

There is no published information available for the effect of flow maldistribution on two-phase pressure drops, since most two-phase investigations were carried out in just a few channels and no severe flow maldistributions were present. One

would assume that the same type of pressure-profile-driving flow distribution may also occur for two-phase flow. In the case of an evaporator, vapour flows at much higher velocity than that of liquid in the exit manifold; the pressure profile should be changing more steeply than in the case of single-phase flow, hence the flow maldistribution would be expected to be more severe. This can not, however, be taken as conclusive without verifications from experimental work.

Other Pressure Drop Components

There are basically three other pressure drop components: acceleration pressure drop ΔP_{acce}, elevation pressure drop ΔP_{elev} and port pressure drop ΔP_{port}. The first two components can be readily calculated by the homogenous model as given by Equation (2.53.b) and (2.53.c), or alternatively they can be calculated by the separated model as given by Equation (2.59.b) and (2.59.c), but in the latter the void fraction α needs to be determined using additional empirical correlations. The port pressure drop is usually evaluated by the single-phase correlation, Equation (2.86), assuming homogeneous flow. This equation gives:

$$\Delta P_{\text{port}} = 1.5\left(\tfrac{1}{2}\rho u^2\right)_{\text{m}} \tag{2.95}$$

where *m* indicates that density and port velocity are to be evaluated by homogeneous mean values. Equation (2.95) was suggested first by Yan and Lin (1999) and followed by a number of other investigators. Ayub (2003) proposed another simple correlation:

$$\Delta P_{\text{port}} = 1.1\left(\tfrac{1}{2}\rho u^2\right)_{\text{g}} \tag{2.96}$$

Equation (2.96) is a conversion from the original one which was in English units. The equation accounts for pressure drop in both inlet and outlet ports.

Sometimes the calculation of overall pressure drop is further complicated when a flow distributor is present, whose effect on pressure drop is very difficult to evaluate without relevant information from the manufacturer. As it is seen that some of the pressure drop components are evaluated by empirical methods, the accuracy and thus their effect on the final frictional pressure drop is hard to evaluate. Fortunately, it has been found that the frictional pressure drop component is by far the largest part, usually being more than 90% (Yan and Lin, 1999, Han et al., 2003, Lango and Gasparella, 2007) of the measured overall pressure drop.

2.7.4 Heat Transfer and Pressure Drop Correlations

A handful of correlations are available in the open literature, for various flow and plate geometry conditions. None of these have been verified for a wide range of applications. Some of the correlations are reviewed in this section; for clarity, details of these correlations reviewed are tabulated in Table 2.7.

Yan and Lin (1999) investigated local R134a flow boiling heat transfer and pressure drop in a two-channel PHE with a chevron angle of 60°, in the quality range of x = 0.1-0.8 with quality change of Δx = 0.09-0.18. They observed that at low values of vapour quality (x < 0.45), mass flux had a small influence on h_r, while beyond that, h_r increased rapidly with x. Heat flux had very little effect on the overall heat transfer performance. The authors proposed two-phase refrigerant Nu and f correlations, which are among the earliest published and one of a few based on *local* vapour qualities. However, difficulties in applying those correlations have been reported. It is noticed that the heat transfer correlation (Equation (2.97)) shows very poor agreement with the authors' own data (given in graphic form in the paper) with the predicted value falling far below the data points. This problem was also reported by Donowski and Kandlikar (2000). There might be typographical errors in the published version, or perhaps direction on the proper use of their correlation is needed from the authors. More recently Garcia-Cascales et al. (2007) used this correlation in a comparison work and the predicted heat transfer coefficient needed to be multiplied by a factor of 8 to match it to the experimental results obtained.

Donowski and Kandlikar (2000) used Yan and Lin's data and proposed an improved correlation. The new correlation, given by Equation (2.99), is based on the form of the Kandlikar correlation (1991) for augmented tubes but exponents for Bo, Co and (*1*-x) are re-evaluated from best-fits to the experimental data. The original Kandlikar correlation is given by Equation (2.35). Good agreement was reported for the improved correlation with a mean error of 16%.

Hsieh and Lin (2002), following Yan and Lin and on the same experimental apparatus, carried out an investigation on R410A saturated flow boiling heat transfer and pressure drop. They observed that both h_r and ΔP increase almost linearly with heat flux q, and that mass flux G had a significant effect on h_r only at higher q. Empirical correlations were provided for Nu and f, given by Equations (2.100) and (2.101). In their test the R410a inlet quality was always preset to be saturated liquid, while outlet qualities were not given. This makes their observations less valuable and the reported correlation is lacking a comparison basis to others, since the tested conditions were neither as a whole at standard conditions for refrigerant evaporators (DX or liquid-overfeed) nor with locally specified x or range of Δx. The same authors (Hsieh and Lin, 2003) in a

later report presented R410a evaporation performance data based on local mean vapour qualities, at x_m = 0.1-0.8 and Δx = 0.126-0.337, and a new set of correlations was presented, shown by Equations (2.102) and (2.103). The new correlation for h_r, however, was noticed to be a complete adoption of the Gungor and Winterton 1986 correlation (see Equations (2.24) through (2.27)) for tube flow without any modification. The single-phase liquid heat transfer coefficient h_f and the Martinelli parameter X_{tt}, as required by the method, were both evaluated using smooth circular tube flow equations. Acceptable agreement with data was claimed by the authors but this treatment remains certainly questionable, and no explanation of its physical basis was given.

Han et al. (2003) performed experiments on three BPHE's of different chevron angles with two refrigerants, R22 and R410A. Evaporation heat transfer coefficients and pressure drops were measured with varying P, q, G and local x. Heat transfer coefficients were observed to increase with increasing vapour quality in all units. Empirical correlations were obtained which are given by Equations (2.104) and (2.105). Han et al.'s correlation is another one that is based on local mean vapour qualities, but the determination of this local quality was not clearly given. A tentative calculation, for example, for the testing condition of R410A at G = 27 kg/(m^2 · s) and q = 5.5 kW/m^2, showed that Δx is 0.5, this brings the question whether the result can be regarded as "local", it is also confusing as the range of data points covered x_m = 0.2-0.95 at such a Δx ($x_m \pm 0.5\ \Delta x$ will be out of the range of x = 0-1, at extreme points). Explanations of those questions could not be found in the paper.

Ayub (2003) presented heat transfer coefficient and two-phase friction factor correlations, based on a decade of design and field experience, and data collected from a number of ammonia and R22 installations. The correlation for heat transfer is independent of heat flux, but a leading constant takes different values for flooded or DX systems. The correlations were originally in English units, which were converted into Metric units and given by Equations (2.106) and (2.107). Ayub's correlations are so far the most universal for PHE evaporators, they cover the two most widely used refrigerants, two types of systems (DX and liquid overfeed), and any type of commercially available plates with any chevron angles. The correlation for heat transfer is however of dimensional form, which is easy to use by field engineers but dimensionally inconsistent.

Sterner and Sunden (2006) investigated ammonia heat transfer and pressure drop on five commercial PHE's with different geometrical configurations. Three sets of correlations were obtained using linear regression analysis for the five evaporator units, those are given by Equations (2.108) and (2.109). All tests were performed under realistic DX conditions where the ammonia inlet quality is in the range of 0.05-0.1 and outlets were at superheats of 2-10 °C. The correlations gave reasonable accuracy in the range over which they were developed, however

any application outside those conditions should be done with caution. They are not likely to be suitable for liquid-overfeed and any systems employing halocarbon (HCFC, CFC) refrigerants, the reasons being:

1. The mass flux G has a high value of exponent of 1.05-1.41. In a liquid-overfeed system where the recirculation rate (and thus G) is high, this correlation will give unreasonably high values of the heat transfer coefficient. Also, under comparable cooling loads, CFC refrigerant mass flux will be 5-10 times higher than that of ammonia, which will result in a 5-26 times higher heat transfer coefficient by this correlation.
2. The parameter $1/x$-1 (in the Co number) has an exponent of 1.44-2.24. In DX systems, the value of x is between 0.53-0.55 (corresponding to inlet vapour quality of 0.05 and 0.1, as in Sterner and Sunden's (2006) paper), while in liquid overfeed systems x is usually around 0.25-0.35 (corresponding to outlet quality of 0.5 to 0.7). It can be shown that this again will bring the heat transfer coefficient up to 6 times higher.

Jokar et al. (2006) carried out a dimensional analysis on two-phase flow in corrugated channels and presented empirical correlations based on data collected from a PHE DX evaporator using R134a. The authors reported that in correlating heat transfer coefficient with flow parameters the Chen type of correlation, i.e., the summation of the two terms of forced convection and nucleate boiling, did not work well. For pressure drops, the Lockhart-Martinelli model was found not suitable, while the homogeneous model best described the experimental data. Empirical correlations were proposed for Nu and two-phase c_f as given by Equations (2.110) and (2.111). The authors reported average deviations of 31% for the Nu correlation and 46% for c_f, which are higher than in most other reported correlations. Again, the form of Jokar et al's correlation for heat transfer coefficient indicated that it is not suitable for liquid-overfeed systems, as the term $1/x$ has an exponent of 2 on h_r. Moreover, the vapour quality x had to be evaluated by the inlet and outlet mean (0.4 and 1 in their test) since no local measurements were taken. This type of treatment makes the effect of local vapour quality more obscure than clear, and at times when a large exponent is assigned to the mean vapour quality by means of regression analysis, as in this correlation, a change of x_m due to change of working conditions will result in much greater or even unreasonable changes of the heat transfer coefficient calculated. The authors made a comparison between their data with the Yan and Lin (1999) correlation, and (surprisingly) it showed consistency in trend and magnitudes. It has been reported earlier in this section that Yan and Lin's correlation, at least in its equation form as given in the original paper, has major errors and deviates significantly from their own data. The agreement of Jokar et al's data with this correlation is confusing, which makes the application of this correlation questionable.

Palm and Claesson (2006) recommended that for flow boiling heat transfer the Cooper (1984, Equation 2.5) pool boiling correlation is to be used with a correction factor of 1.5. It was concluded that the flow boiling in a DX PHE evaporator is a heat flux dominant process; as such, the Cooper correlation showed good accuracy for a number of refrigerants, PHE's and pressure level, and is very simple to use. For two-phase frictional pressure drop calculations, the Lockhart-Martinelli method was suggested with a fixed Chisholm parameter *C* set to 3.

Longo and Gasparella (2007) experimentally investigated heat transfer and pressure drop of R134a, R410A and R236fa in a small BPHE. As outlet vapour quality was a controlling parameter, there is a direct connection between heat flux and mass flux and their contributions could not be separated. The heat transfer coefficients showed great sensitivity to heat flux (and corresponding mass flux), weak sensitivity to evaporating pressure, and dropped markedly when outlet superheat was increased. The authors concluded that dry-out occurs in the upper part of the evaporator and the decrease of the heat transfer coefficient is due to the increase in the superheating portion of the heat transfer surface. R410A showed heat transfer coefficients 40-50% higher than R134a and 50-60% higher than R236fa under the same operating conditions. No correlation was proposed for the flow boiling heat transfer coefficient, but experimental results were compared with two well known correlations for nucleate boiling: the Cooper (1984, Equation 2.5) and Gorenflo (1993, Equation 2.6) correlations. It was found that both correlations were able to predict R134a and R410A data with acceptable agreement, with the Cooper correlation performing better (approximately ±20% deviation), whereas both under-predict R236fa data. The authors assumed that this is due to the fact that R134a and R410A evaporating data were controlled by nucleate boiling, whereas R236fa data is affected by both nucleate boiling and forced convection. This assumption was justified by applying the criterion suggested by Thonon et al (Equation 2.94). Two-phase pressure drop was well predicted by the homogeneous model, but an explicit correlation for friction factor was not given.

García-Cascales et al. (2007) compared six correlations with experimental results obtained for R22 and R290 from two PHE evaporators. Those correlations included that of Yan and Lin (1999, with h_r multiplied by 8), Hsieh and Lin (2002), Han et al.(2003), the Cooper (1984) pool boiling correlation, and two others traditionally applied to fin and tube heat exchangers but adapted by the authors to plate heat exchangers. Good results were obtained with the Cooper correlation which led to the conclusion that that nucleate boiling plays an important role in the test cases.

A Summary

It is noticed that most correlations available were developed by the investigators to represent their own data, covering usually limited plate geometry and working conditions. A few authors made comparisons of their correlations with those of others, but none have gained wide validation to any practical extent. All correlations are based heavily or entirely on statistical analysis, which makes their application beyond their tested range highly risky. As demonstrated for some, doing so can brought unreasonable results.

To date a general method or correlation for predicting reliably the flow boiling heat transfer and pressure drop in PHE evaporators has not become available. Predictions by different correlations can give very different results at specified conditions. In terms of generality, Ayub's correlation (2003) is the most promising one, which covers two of the most common refrigerants, two evaporator types, any plate chevron angle, over a wide range of practical conditions. The Donowski and Kandlikar (1999) correlation also remains promising. This correlation works with local heat transfer coefficients which makes it preferable for wider applications. It is based on the form of one that has gained some popularity for round and augmented tubes. The good agreement of this correlation with data might indicate that compact heat exchangers could be treated as augmented tubes, with introduced augmentation factors accounting for surface enhancements. This correlation was developed for a chevron angle of 60° only and different sets of constants might be needed for other plate geometries; moreover, the employment of a fluid-dependent parameter in this correlation may restrict its use with certain refrigerants.

Table 2.7: PHE two-phase heat transfer and pressure drop correlations

Investigator	Correlation	Details
Yan and Lin, 1999	$\mathrm{Nu_r} = 1.926 \cdot \mathrm{Re_{eq}} \cdot \mathrm{Re_{fo}}^{-0.5} \cdot \mathrm{Bo_{eq}}^{0.3} \cdot \mathrm{Pr_f}^{0.33}$ (2.97) for $2{,}000 < \mathrm{Re_{eq}} < 10{,}000$ $c_{\mathrm{f,\,tp}} = \begin{cases} \dfrac{6.947\times10^5}{\mathrm{Re_{eq}}^{1.109} \cdot \mathrm{Re_{fo}}^{0.5}} & \mathrm{Re_{eq}} < 6{,}000 \\ \dfrac{31.21 \cdot \mathrm{Re_{eq}}^{0.04557}}{\mathrm{Re_{fo}}^{0.5}} & \mathrm{Re_{eq}} \geq 6{,}000 \end{cases}$ (2.98) $\mathrm{Nu_r} = h_r d / k_f$, $\mathrm{Re_{fo}} = Gd / \mu_f$, $\mathrm{Bo} = q / (G \cdot i_{fg})$, $\mathrm{Re_{eq}} = \mathrm{Re_{fo}} \cdot C_x$, $\mathrm{Bo_{eq}} = \mathrm{Bo} / C_x$ $C_x = 1 - x + x\left(\rho_f / \rho_g\right)^{0.5}$, $d = d_e = 2b$,	R134a/water, 2 channels, β=60°, ϕ=1.22, 2b=5.8mm local, Δx= 0.09-0.18, x_m=0.1-0.8 q=11-15 kW/m^2, G_r=55, 70 kg/(m^2· s)

Donowski and Kandlikar, 2000	$\frac{\mathrm{Nu_r}}{(1-x)^{0.003}\cdot \mathrm{Nu_{r,f}}} = 1.184\cdot \mathrm{Co}^{-0.3} + 225.5\cdot F_{\mathrm{fl}}\cdot \mathrm{Bo}^{2.8}$ (2.99) $\mathrm{Nu_{r,f}} = 0.2875\cdot \mathrm{Re_f}^{0.78}\,\mathrm{Pr_r}^{1/3}$, single-phase liquid F_{fl} is a fluid dependent parameter.	Yan and Lin's data
Hsieh and Lin, 2002	$h_{\mathrm{r,sat}} = h_{\mathrm{r,f}}\left(88Bo^{0.5}\right)$ (2.100) $\mathrm{Nu_{r,f}} = 0.2092\cdot \mathrm{Re_f}^{0.78}\cdot \mathrm{Pr_r}^{1/3}\cdot\left(\frac{\mu}{\mu_{\mathrm{wall}}}\right)^{0.14}$ single-phase liquid $c_{\mathrm{f,tp}} = \frac{61{,}000}{\mathrm{Re_{eq}}^{1.25}}$ (2.101) $d = d_{\mathrm{e}} = 2b$ $\mathrm{Re_{eq}}$ see Yan and Lin (1999) correlation	R410A/water Plate geometry same as Yan and Lin, 1999, x_{in}=0, x_{out} unknown, q=5-35 kW/m^2, G_{r}=50-125 kg/(m$^2\cdot$ s), P=10.8, 12.5, 14.4 bar
Hsieh and Lin, 2003	$h_{\mathrm{r}} = E\cdot h_{\mathrm{f}} + S\cdot h_{\mathrm{pool}}$ (2.102) $h_{\mathrm{f}} = 0.023\,\mathrm{Re_f}^{0.8}\,\mathrm{Pr}^{0.4}\left(k_{\mathrm{f}}/d\right)$ h_{pool} by Cooper 1981 correlation, Equation (2.5) $E = 1 + 24{,}000\,\mathrm{Bo}^{1.16} + \frac{1.37}{X_{\mathrm{tt}}^{0.86}}$ $S = \left(1+1.15\times10^{-6}\cdot E^2\cdot \mathrm{Re_f}^{1.17}\right)^{-1}$ $f_{\mathrm{tp}} = \frac{23{,}820}{\mathrm{Re_{eq}}^{1.12}}$ (2.103) $\mathrm{Re_{eq}}$ same in Yan and Lin (1999) correlation	R410A/water Plate geometry same as Yan and Lin, 1999 Local, x_{m}=0.1-0.8, Δx=0.126-0.337, q=10, 20 kW/m^2, G_{r}=50-100 kg/(m$^2\cdot$ s), P=10.8, 12.5bar
Han et al., 2003	$\mathrm{Nu_r} = \mathrm{Ge_1}\,\mathrm{Re_{eq}}^{\mathrm{Ge_2}}\,\mathrm{Bo_{eq}}^{0.3}\,\mathrm{Pr_f}^{0.4}$ (2.104) $f_{\mathrm{tp}} = Ge_3\,\mathrm{Re_{eq}}^{\mathrm{Ge_4}}$ (2.105) $\begin{cases}\mathrm{Ge_1} = 2.81(\lambda/d)^{-0.041}\,\beta^{-2.83}\\ \mathrm{Ge_2} = 0.746(\lambda/d)^{-0.082}\,\beta^{0.61}\\ \mathrm{Ge_3} = 64{,}710(\lambda/d)^{-5.27}\,\beta^{-3.03}\\ \mathrm{Ge_4} = -1.314(\lambda/d)^{-0.62}\,\beta^{-0.47}\end{cases}$ β in radian, $d = d_{\mathrm{h}} = 2b/\phi$, $\mathrm{Re_{eq}}$ and $\mathrm{Bo_{eq}}$ same in Yan and Lin (1999) correlation	R22/water, R410A/water, 3 BPHE's, all 5 channels, β=45°, 55°, 70°, ϕ=1.17, 2b=4.3mm, Local, x_{m}=0.15-0.9 q=2.5-8.5 kW/m^2, G_{r}=13-34 kg/m$^2\cdot$ s, T_{sat}=5-15 °C
Ayub, 2003	$h_{\mathrm{r}} = 0.025\cdot C\cdot\left(\frac{k_{\mathrm{f}}}{d_{\mathrm{h}}}\right)\left(\frac{\mathrm{Re_{fo}}^2\, i_{\mathrm{fg}}}{L_{\mathrm{P}}}\right)^{0.4124} P_{\mathrm{r}}^{0.12}\left(\frac{65}{\theta}\right)^{0.35}$ (2.106) C=0.1121 for flooded and thermo-siphon, C=0.0675 for DX,	Ammonia, R22, Flooded and Dx, for any type of commercially available plates with all chevron angles.

	$P_r = P / P_{crit}$, $\theta = 90^\circ - \beta$, $d = d_h = 2b/\phi$ $c_{f,tp} = \frac{n}{\mathrm{Re}_{go}^{\ m}}\left(-1.89 + 6.56R - 3.69R^2\right)$ (2.107) $R = 30/\theta$, for ΔP_{fric} , entire flow considered as vapour, $m = 0.137$ $n = 2.99$ for $\mathrm{Re} \le 4{,}000$ $m = 0.172$ $n = 2.99$ for $4{,}000 < \mathrm{Re} \le 8{,}000$ $m = 0.161$ $n = 3.15$ for $8{,}000 < \mathrm{Re} \le 16{,}000$ $m = 0.195$ $n = 2.99$ for $\mathrm{Re} > 16{,}000$	
Sterner and Sunden, 2006	$\mathrm{Nu} = c_1 \cdot \mathrm{Re}_{fo}^{\ c_2} \cdot \mathrm{Ja}^{c_3} \cdot \mathrm{Co}^{c_4}$ (2.108) $C = \frac{c_5}{\mathrm{Re}_{fo}^{\ c_6}}$ (2.109) $\mathrm{Re}_{fo} = Gd/\mu_f$, $\mathrm{Re}_{fo} = Gd/\mu_f$, $\mathrm{Ja} = \frac{c_{p,f} \cdot \Delta T_{in}}{h_{fg}} \cdot \frac{\rho_f}{\rho_g}$, $d = d_e = 2b$ $\Delta T_{in} = T_{w,in} - T_{r,in}$ (count-current), $\mathrm{Co} = \left(\frac{1-x}{x}\right)^{0.8}\left(\frac{\rho_g}{\rho_f}\right)^{0.5}$ C is the Chisholm parameter	Ammonia/water, or ethylene glycol-water, 5 PHE's, 1 with distributor, β=59° for 4, 65° for 1 $2b$=3.6, 5, 5.6 mm N_{ch}=63-99 DX, overall, x_{in}=0.05-0.1, x_{out}=1, ΔT_{sup}=2-10°C, q not given, G_r=0.5-9.5 kg/(m^2· s) T_{sat}=-3-6°C
Jokar et al., 2006	$\mathrm{Nu}_r = 0.603\mathrm{Re}_{fo}^{\ 0.5}\,\mathrm{Pr}_f^{\ 0.1}\left(\frac{G^2}{\rho_f^{\ 2} c_{p,f}\Delta T_{sat}}\right)^{-0.1}$ $\left(\frac{\rho_f^{\ 2} i_{fg}}{G^2}\right)^{-0.5}\left(\frac{\rho_f \sigma}{\mu_f G}\right)^{1.1}\left(\frac{1}{x}\cdot\frac{\rho_f}{\rho_f - \rho_g}\right)^2$ (2.110) $c_{f,r} = 3.521\times10^4 \frac{1}{\mathrm{Re}_{fo}^{\ 1.35} C_x}$ (2.111) for $70 \le \mathrm{Re}_{fo} \le 420$ $d = d_e = 2b$ C_x same in Yan and Lin (1999) correlation	R134a/ glycol-water, β=60°, $2b$=4 mm, N_p >30 DX, overall, x_{in}≈0.4, x_{out}=1, P= 200-600 kPa, q and G_r not clearly given.

CHAPTER 3

EXPERIMENTAL INFRASTRUCTURE

3.1 Introduction

The experimental infrastructure in this study has two systems:

1. the water test system, where three brazed plate heat exchanger (BPHE) units operate as single-phase water-water heat exchangers,
2. the refrigeration test system, where the same BPHE's operate as refrigerant evaporators, with water as process liquid.

Using the two systems, two sets of experiments were carried out: the water test and the refrigeration system test. The water test serves to provide heat transfer information on the water side which is to be used for the refrigerant evaporator analysis. The water test system was designed and built in such a way that both thermal characteristics and pressure drops of water can be tested. Pressure drop data on single-phase water are not necessary for evaporator analysis; however, the information helps to understand the hydraulic performance of the corrugated channels in general.

The refrigeration test arrangement was built as a liquid over-feed system; experimental facilities were designed in order to study the detailed global performance of the brazed plate heat exchangers and to generate data which can be used to evaluate the developed model. Two circuits are included in this system: the water flowing on one side of the corrugated channel and the refrigerant flowing on the other. The two circuits were designed to provide stable controlled conditions in the desired range of temperatures, fluid flows, and thermal capacities.

Measuring instrumentation was selected and installed to quantify all physical variables necessary for determining the exchangers' thermal capacity and hydraulic resistances, with high accuracy. A data acquisition system with PC based data logging was developed. Detailed descriptions of the measuring instruments are presented in the following sections.

3.2 Brazed Plate Heat Exchangers

Three BPHE units of the herring-bone type were tested in this study. All plates are made of stainless steel AISI 316. The three units have different chevron angle combination: 28°/28°, 28°/60°, and 60°/60°. Plate surface geometry is characterized by the chevron angle β, corrugation depth b, and the surface enlargement factor ϕ (ratio of actual corrugated surface area to the projected area of the plate). The enhanced heat transfer is directly related to these features, which provide increased effective heat transfer area, disruption and reattachment of boundary layers, and swirl flow generation.

Figure 3.1 shows the geometry of a single plate. All important geometric parameters of the tested plate heat exchanger units were doubly confirmed, in addition to the manufacturer-supplied information. Refer to *Appendix A* for details of this information on the dimensions and how they were confirmed. Some important geometrical and operational parameters are summarized in Table 3.1. For the fluid on any one side, the BPHE unit is manufactured in a single-pass U-type arrangement (inlet and outlet at the same side of the exchanger unit), and the ports are positioned in a parallel (as opposed to diagonal) manner.

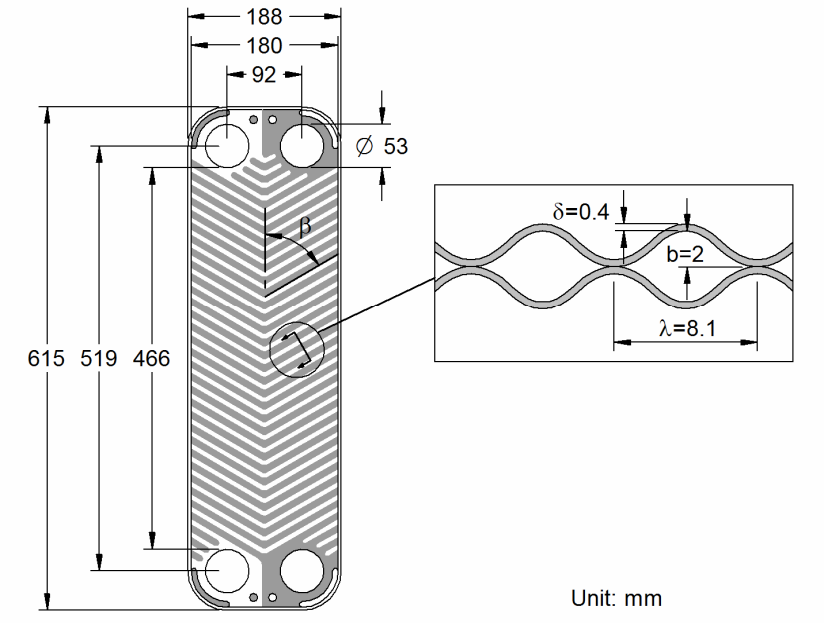


Figure 3.1: Single plate geometry

Table 3.1: Summary of three BPHE units' geometrical and operating parameters

Number of plates:	$N_p = 24$
Number of effective plates:	$N_{p,eff} = N_p - 2 = 22$
Number of channels:	$N_{ch} = N_p - 1 = 23$, Side 1 (Refrigerant): 12, Side 2 (water): 11
Volume per channel:	$V_{ch} = 0.201$ l
Heat transfer area per plate:	$A_p = 0.095$ m^2
Design pressure:	30 bar
Design temperature:	-196 to 200 °C
Port to port channel length:	$L_p = 519$ mm
Effective channel length:	$L_{eff} = 466$ mm
Width of flow channel:	$w = 180$ mm
Plate port diameter:	$d_{port} = 53$ mm
Corrugation depth:	$b = 2$ mm
Plate thickness:	$\delta = 0.4$ mm
Chevron angle:	28°/28°, 28°/60°, 60°/60°
Corrugation wavelength:	$\lambda = 8.1$ mm
Enlargement factor:	$\phi = 1.14$
Single channel flow area:	$A_{ch} = wb = 3.6\times10^{-4}$ m^2
Equivalent diameter:	$d_e = 2b = 2\times2 = 4$ mm
Hydraulic diameter:	$d_h = 2b/\phi = 3.51$ mm
Total heat transfer area:	$A = A_p N_{p,eff} = 0.095\times22 = 2.09$ m^2

3.3 Water Test Arrangements

The water test system consists of one BPHE, two water tanks, water pump and pipe lines, and the instrumentation. The system was designed in such a way that one BPHE is tested at one time. This arrangement brings the inconvenience of replacing the BPHE's when more than one unit is tested, but simplifies the system design. Counter-current arrangement is implemented for the two water streams. Hot water is circulated from the water tank to the PHE and flows upwards. Cold water is pumped from the water sump to the PHE and flows downwards. The experimental apparatus is shown schematically in Figure 3.2. The hot and cold water streams were thus arranged so that the cold water flows in

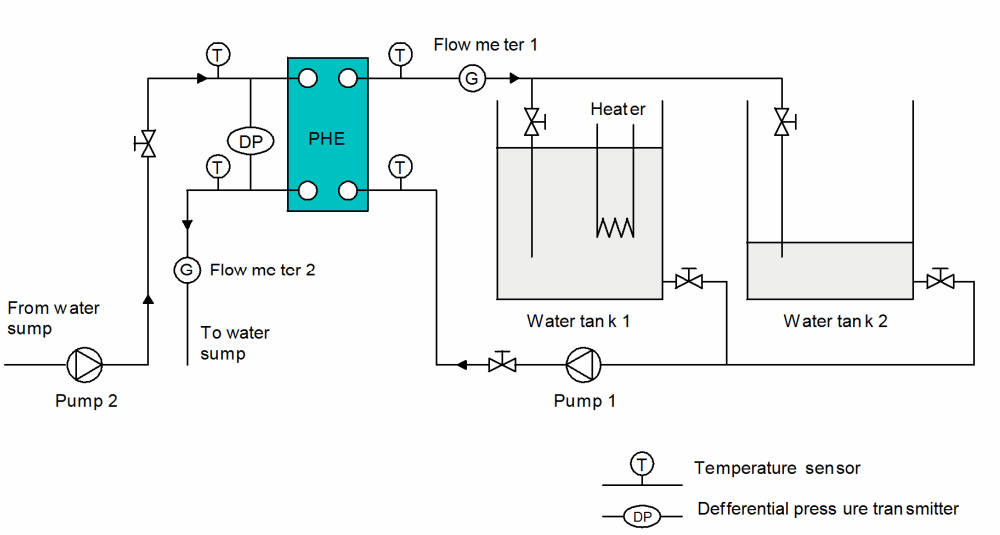


Figure 3.2: Schematic diagram of water test facility layout

the same direction both in this single-phase performance test and later in the refrigerant evaporator tests. In the evaporator tests refrigerant flows upwards and water (from the water sump, as used here for the cold side) downwards, forming a counter-current flow arrangement. Because the water side heat transfer coefficient of the evaporator is to be evaluated by a correlation based on the current cold side data, it is preferable to keep the cold water flow in the same flow direction in both set of tests, to reduce experimental errors on the water side for the evaporator test.

The two water tanks have volumes of 1.3 m^3 and are well insulated to ensure that water is supplied at constant temperature during the test. It was observed that during any single test (about 45 minutes) the water temperature change was less than 0.5 °C. Two centrifugal pumps were used to circulate the two water streams. Hot water supply was obtained by using four immersed heaters with a capacity of 2 kW each; water temperature is raised to the desired value, around 55 °C, before each test run. PVC pipes with an inside diameter of 28 mm are used for all water piping.

3.4 Refrigerant Evaporator Test Arrangements

3.4.1 Liquid Over-feed System

The evaporator feeding method was designed to be the liquid over-feed type, with liquid refrigerant being circulated by a liquid pump. Liquid over-feed systems

refer to those in which “excess liquid is forced, either mechanically or by gas pressure, through organized flow evaporators, separated from the evaporator, and returned to the evaporators” (*ASHRAE 2006*). Figure 3.3 shows a typical liquid over-feed system.

There are generally two types of evaporator feeding methods applicable to PHE evaporators: direct expansion (or dry expansion, DX) and liquid over-feed. From an experimental point of view, the liquid overfeed system is preferable to a DX system, in that some important parameters are more freely adjustable and independent of the cooling load, these include: refrigerant flow rate $\dot{m}_r$ (feeding rate), inlet and outlet vapour quality x_{in} and x_{out}, and evaporating pressure. The refrigerant flow rate is controlled by a liquid pump and can be in a wide range, the evaporating pressure will depend on the surge drum pressure. Inlet vapour quality is also controllable provided a pre-heater is installed upstream of the evaporator (this arrangement is not employed in the present study). On the other hand, in a DX evaporator these parameters are always coupled and not individually adjustable, because certain degrees of superheat required at the exit of the evaporator will determine the operation of the expansion valve, resulting in a simultaneous change of refrigerant flow rate, evaporating pressure, and inlet vapour quality.

From an industrial point of view, almost all large units invariably use over-feed systems where PHE evaporators are involved. Halocarbon refrigerants are not commonly used in large over-feed systems, the reasons for this can be:

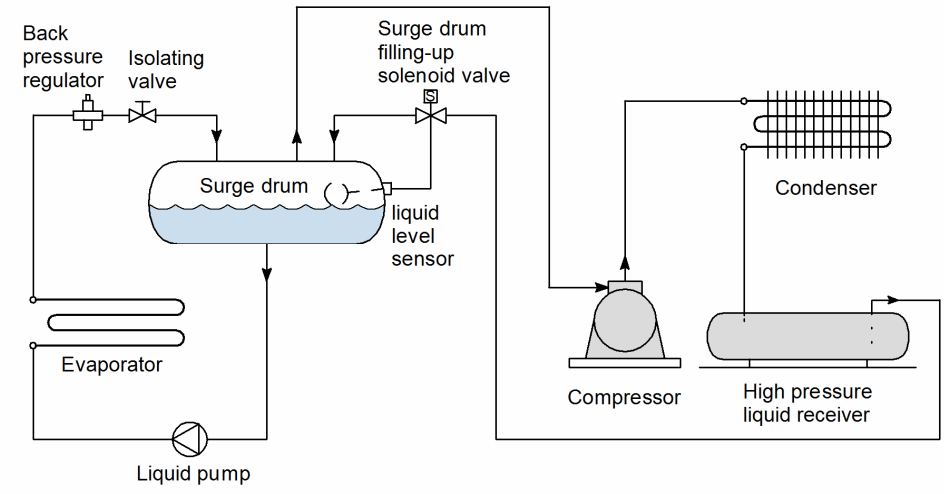


Figure 3.3: Typical liquid over-feed system

1. oil returning problems;
2. high density of halocarbon refrigerants requires high pump power input;
3. low latent heat requires more refrigerant to be pumped for the same cooling duties.

Ammonia is usually the choice for large-scale liquid overfeed installations for the above reasons. In the current study, however, halocarbon refrigerant was used in a liquid overfeed system, but the focus of the investigation was on the flow boiling mechanism rather than on any specified feeding method (to this aim, it would also be desirable to test other refrigerants in further experiments).

It might be worthwhile to make the concept clear that liquid overfeed systems are those in which a greater rate of liquid refrigerant is delivered to the evaporator than evaporated. At the exit of the evaporator a mixture of liquid and vapour flows out. Liquid overfeed systems are characterized by having a low-pressure receiver, also sometimes called a surge drum, from which the liquid refrigerant is circulated through the evaporator either mechanically or by thermo-siphon. What is normally called a flooded evaporator is a shell-and-tube exchanger where chilled process liquid flows in the tubes which are submerged in boiling refrigerant in the shell. Vapour refrigerant is discharged from the top of the evaporator and directed to the compressor. The difference between an overfeed and a flooded evaporator is that in the latter only vapour leaves the evaporator, instead of a two-phase mixture, and for this purpose it is necessary to design a dropout area inside or install an eliminator at the top of the evaporator, to separate the liquid refrigerant from the vapour. A liquid overfeed evaporator can be either a shell-and-tube exchanger or a PHE, while a flooded evaporator is always a shell-and-tube exchanger with refrigerant boiling on the shell side. It is also important to note that sometimes the terms “flooded” and “liquid overfeed” are mixed freely and may refer to the same evaporator, possibly because the liquid overfeed evaporator operates also in a flooded “manner”.

Thermo-siphon evaporators are another example in the liquid overfeed category, these types of evaporators operate by means of natural density differences in the refrigerant liquid and vapour and a liquid pump is not used. Thermo-siphon systems are more commonly seen in large-sized industrial installations. Field tests were carried out on two large-scale thermo-siphon units using ammonia and refrigerant R12, which are described in Chapter 5.

In a liquid overfeed system, the overfeed extent is evaluated by the recirculation rate n_{RC}, which is defined as the mass ratio of liquid entering to the amount of liquid vaporized in the evaporator :

$$n_{RC} = \dot{m} / \dot{m}_{g,\,out} = 1 / x_{out} \qquad (3.1)$$

Typical values of recirculation rate for conventional evaporators are 2 to 7 (ASHRAE 2006), while for PHE liquid over-feed evaporators the common value of recirculation rate is 1.2-1.5 (Stromblad, 1989, Hanssen, 1997), corresponding to outlet vapour quality of 0.67-0.83. The current system was designed for this range of recirculation rate. With fine adjustment of the system operating parameters, i.e., water and refrigerant flow rates and the surge drum pressure, it is also possible to obtain fully vaporized or superheated outlet conditions, where the liquid-overfeed system will run as a dry system and the recirculation rate is 1 in this case.

3.4.2 System Design

Feeding Method

The experimental facility serves for experimental investigation of the refrigerant flow boiling mechanism in corrugated channels of the plate heat exchangers under various flow conditions. To this aim, the equipment had to be able to control, in a certain range, some of the important operating parameters; those basically include flow rate, outlet vapour quality, evaporating pressure, and the cooling load. The evaporator feeding method was chosen to be the liquid overfeed type; as mentioned previously, this feeding method gives the system the flexibility that a DX system does not offer.

Choosing the PHE Type

Choosing the PHE type is another task in the system design. There are mainly three types of PHE's applicable to refrigeration duties, namely frame-and-plate, semi-welded plate pack, and brazed PHE's (BPHE's). The frame-and-plate type of PHE is widely used for liquid-liquid duties and its applications in refrigeration duties are not commonly seen nowadays, mainly due to the concerns of refrigerant leakage. With chosen gasket material compatible with the refrigerant applied, this type of PHE can be used as refrigerant evaporators. The frame-and-plate type exchanger has many virtues when used as testing equipment. The plates can be replaced to obtain different channel geometries; the number of flow channels can be changed by adding or removing plates when there is a need of cooling load change; needle-type pressure tappings can be inserted through the gasket at certain locations if local pressure is to be measured. Moreover, plates for this type of PHE usually have the widest product spectrum from manufacturers, compared with the other two. However, when used in a refrigeration system, the evaporator requires high levels of sealing quality; new

gasket sets need to be used if new plates are to be tested. This type of exchanger is not considered in the present study.

Semi-welded PHE's are refrigerant leakage-proof and can work under higher pressure and temperature limits. For a testing rig, one shortcoming for semi-welded units is that the plate geometries to choose from are usually limited. Mixed-plate channels are possible to obtain from manufacturers when special orders are made, but this will depend on the available plate geometrical patterns.

BPHE's are widely used in refrigeration systems as evaporators and condensers, where the plates are brazed together as an integral pack which makes it not possible to change channel geometry without using new sets of PHE's. Some BPHE's are equipped with flow distributors, and because the effect of distributors on flow distribution, pressure drop, and heat transfer are not well understood, the installation of a distributor may not be desirable for experimental purposes. For this study, three sets of BPHE units with different chevron angles were used, flow distributors were not fitted.

Refrigerants

The system used in this study was initially designed for refrigerant R134a, which is gaining an increasing application worldwide in the refrigeration industry. R507A was used for additional tests with new lubricant oil. R410A was a consideration but not used due to its high working pressure.

Oil Return

Oil return is a critical design parameter in all refrigerant systems; it is more so in a liquid overfeed system using halocarbon refrigerants. Liquid overfeed systems typically use a surge drum to feed the evaporator, either by gravity or by a liquid pump. No matter how efficient the oil separator is, some lubricant oil will always find its way into the low pressure side of the system and will inevitably accumulate in the surge drum. The approach to returning oil in an ammonia system is relatively simple because ammonia and mineral oil are not miscible (to be accurate, miscible to a very limited extent) and because the oil has a greater density than liquid ammonia, when oil passes on to the surge drum it separates from the refrigerant and settles to the bottom. An oil sump installed at the bottom of the surge drum can then collect the oil and a drain line on the sump will direct the oil back to the compressor. In halocarbon systems, however, the refrigerant and lubricant oil are at least partially miscible, the miscibility depends on refrigerant type, temperature and pressure. For partially miscible oil/refrigerant solutions, for instance mineral oil/R22, the two substances are miscible above a certain temperature, below that temperature there is a separation, and because the

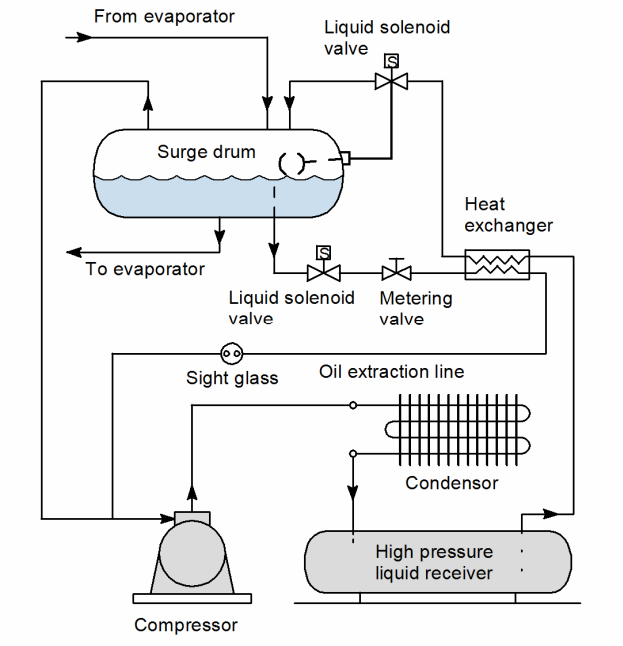


Figure 3.4: Schematic of the oil returning arrangement

oil-rich layer is less dense than the halocarbon-rich layer, it rises to the top of the liquid mass. For mutually soluble pairs such as Polyol Ester (POE)/R134a, the two substances are completely soluble. For these reasons, oil return must be handled differently than in an ammonia system (Stoecker, 1998).

In the current R134a system, a flow of liquid refrigerant and its dissolved oil is extracted from an outlet of the surge drum (it could also be on a point of the feeding line to the evaporator), and directed to the suction line. Because there is liquid refrigerant in this mixture that should not be permitted to return to the compressor, a liquid/extraction heat exchanger is located on the liquid line connecting the compressor discharge and the surge drum. This method will not return all the oil in the surge drum, but the amount of oil in the surge drum will be maintained at a certain level in any stable running condition. Figure 3.4 shows the schematic of the oil return system.

The amount of extraction is controlled by a metering valve and should be kept small. To ensure that a suitable return flow is taken and at the same time no liquid refrigerant is passing to the compressor, some additional components are required:

Upstream of the heat exchanger:

- A liquid solenoid valve, actuated by the compressor, to prevent flow of liquid refrigerant to the suction line when the compressor is idle;

- A metering valve, to control the extraction flow rate.

Downstream of the heat exchanger:

- A sight glass in which no liquid should be observed.

Also very important is that where a riser is needed in the suction line, the sizing of the riser is to be carefully designed to make sure that a high vapour flow velocity is obtained sufficient to carry the oil back to the compressor, as in the case of a direct expansion system.

3.4.3 The Experimental Facility

The refrigeration test facility consists principally of two circuits: the water circuit and the refrigerant circuit. Each circuit has independent control. The test facility has been designed to give controllable and stable working conditions for the refrigeration cycle, and to provide desired evaporating pressure and liquid refrigerant recirculation rates n_{RC} for the evaporator. The system layout is given schematically in Figure 3.5, and the equipment shown in Figure 3.6.

Water Circuit

The water circuit circulates water at the environment temperature (between 17 and 25 °C, depending on season) from the water sump through the brazed plate heat exchangers and back to the water sump, at a position away from the point of water suction. This is to ensure that the supply water temperature will not be affected by the retuning cooled water. The water sump has a large volume of clean water collection (more than 40 m^3) and constant feeding temperature during the testing period is assured. Water flows downwards in the exchanger to form a counter-current flow arrangement. Water flow rate was mutually controlled by a gate valve on the feeding line and a ball valve on the by-pass line.[1] To reduce water side fouling on the exchangers' surface, two fine-mesh filters were fitted at the pump suction and pump outlet.

[1] A by-passing arrangement is more preferable in flow rate control than a single regulating valve fitted in the main line. Centrifugal pumps can run stably in a certain range of flow rates, below that, vibration and flow fluctuation usually occur. A by-passing arrangement can effectively reduce the flow rate in the main line without much effect on that of the pump; this can be very useful if stable and small flow rates are desired from a relatively large capacity pump.

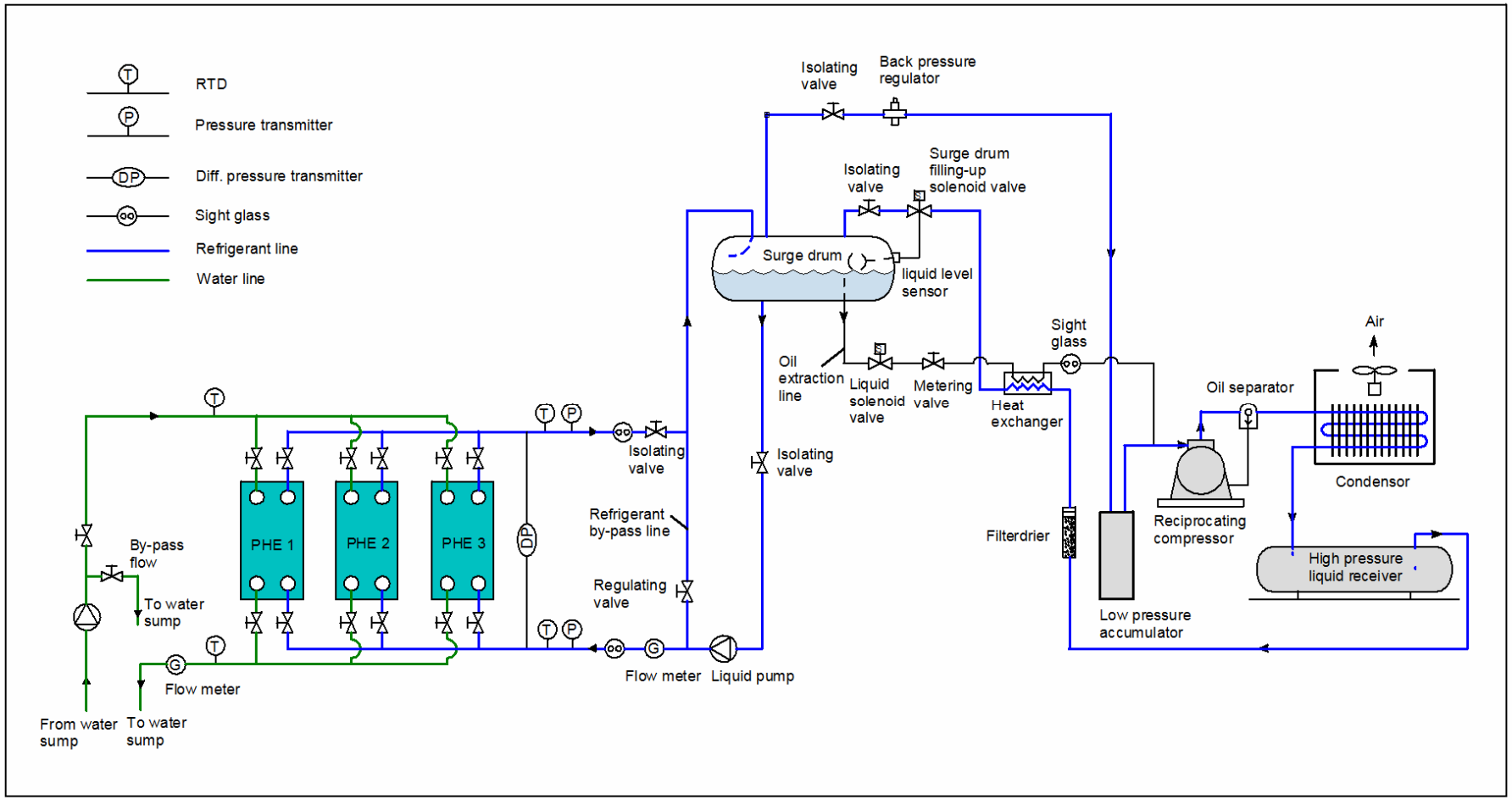


Figure 3.5: System layout of the refrigeration system test facility



Figure 3.6: The experimental equipment of the refrigerant evaporator tests

Refrigerant Circuit

The refrigerant circuit consists of the BPHE evaporators, the condensing unit with reciprocating compressor and air-cooled condenser, the surge drum, a high pressure receiver, the oil returning system, and other accessories necessary for system running. The three brazed plate heat exchangers were organized in a parallel manner; each unit can be conveniently isolated from the system by shutting down two isolating valves positioned in the inlet and outlet pipe lines. Refrigerant liquid enters the evaporator at the bottom and flows upwards, being heated by the process water when flowing through the channel. The refrigerant flow rate was controlled by a by-pass arrangement. A by-pass line is installed at a point between the refrigerant liquid pump and the flow meter; the line joins the refrigerant returning line from evaporator and returns to the surge drum. Refrigerant flow rate in the evaporator feeding line is thus controlled by a regulating valve fitted on the by-pass line. A back pressure regulator is installed at the surge drum outlet on the compressor suction line; this regulator controls the surge drum pressure, which determines the evaporating pressure in the evaporator.

Cooling Load

At design conditions, the system has a cooling capacity of 13.5 kW minimum and 24 kW maximum, in the range of evaporating temperature of 1-15 °C and condensing temperature of 35-45 °C. The refrigerant flow rate is in the range 3.9-7.6 l/min, giving recirculation rates of 1-1.4 at the given cooling loads.

For a specific evaporator with fixed heat transfer area, cooling load is determined by the mean temperature difference ΔT_{LM} between the two fluids and the overall heat transfer coefficient U . Water inlet temperature is not a controllable quantity, however, on the refrigerant side, the evaporating temperature can be controlled in a range by adjusting the surge drum pressure, via a back pressure regulator installed at the surge drum outlet on the compressor suction line. The overall heat transfer coefficient U depends largely on the water and refrigerant side heat transfer coefficient components, and can be controlled to a certain extent by changing the water flow rate, an operation conveniently available.

3.5 Instrumentation and Measurement

The instrumentation used in the experimental facility was selected and applied for the measuring of all the variables necessary for determining the performance of the heat exchangers. The quantities measured, in both water and refrigeration system tests, basically included temperatures, pressures, and flow rates. There are 14 sensors that were employed in the study, of those 7 were used for the water test, 9 for the refrigeration test, some of which were used for both tests. All instruments have analogue outputs which are logged onto a PC via the data acquisition system. A description of the measuring instruments is presented in this section, organized separately for the water test system and the refrigeration test system. For detailed technical data and wire connections, *Appendix B* refers.

3.5.1 Water Test System

Temperature *T*

Temperatures are measured at four points, i.e., at inlets and outlets of both hot and cold water streams, approximated 200 mm from the PHE ports. Measurements were taken by sensors located at pertinent points with LM35DZ semi-conductor sensors, which are integrated circuit sensors that give electrical

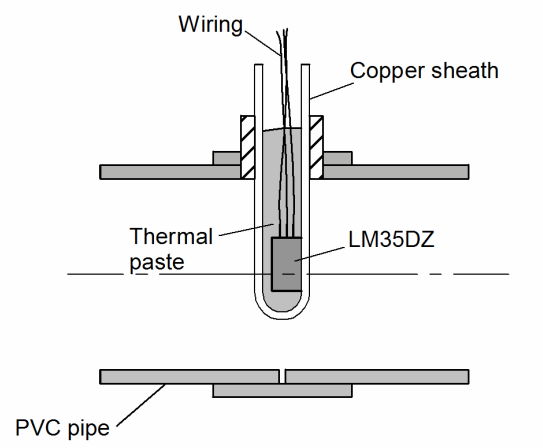


Figure 3.7: Temperature probe structure

voltage output proportional to the temperature in Celsius. The sensors are each powered by a 9V battery and give a 0-1 V signal corresponding to 0-100 °C temperature spectrum, via a three wire system.

The LM35DZ sensor is a tiny semi-conductor with a plastic tip. To use this sensor for the measurement of water temperature, a probe needed to be made which encloses the sensor in a copper sheath and thus can be inserted into the water pipe. The temperature sensor probe is shown schematically in Figure 3.7.

Volumetric flow rate *Q*

Volumetric flow rates of water on both sides are measured with two RS 257-026 turbine flowmeters. These flow meters have a rotor which spins when liquid passes through the flowmeter. The speed of the rotor is directly proportional to the flow velocity. As the rotor spins, the stainless steel blade tips pass a magnetic field and an AC voltage is induced in a coil, which is converted into an output 4-20 mA current signal proportional to the flow. The two flowmeters have the capacity of 0-100 l/min and were, for the present experimentation, calibrated in the range of 0-60 l/min.

Many piping configurations and fittings generate disturbances with unknown characteristics, for this reason, flow conditioning, i.e., minimum length of straight pipe runs before and after the meter, is required for certain types of flowmeters. This information is not available from the manufacturer's data sheet, therefore as a general rule, a minimum length of 20 diameters of straight run piping (Feener, 1999) was applied.

Differential Pressure ΔP

Differential pressure is the pressure drop between the PHE inlet and outlet, on the cold water side in the test. The pressure drop is measured by a Rosemount 3051 CD differential pressure transmitter. The transmitter has a working range of 0-80 kPa and was calibrated in the same range using water. Figure 3.8 shows the layout of the measurement arrangement.

It is important to note that the measured pressure drop has many components, and is not the frictional pressure drop ΔP_{core} in the corrugated channel, which is of the interest of the test. Evaluations of other components and an extraction procedure are required to obtain ΔP_{core}, as will be given in Chapter 4.

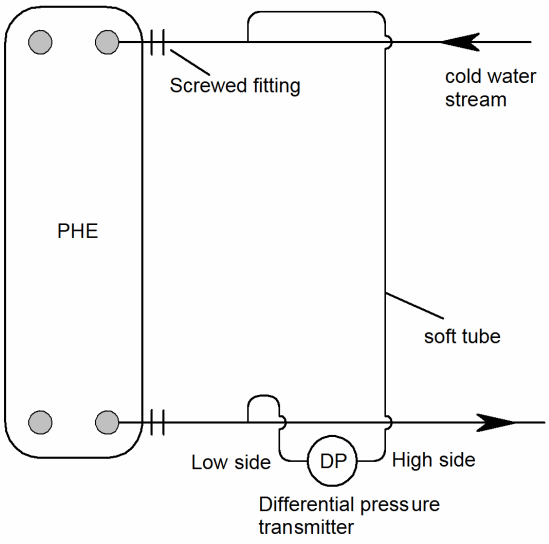


Figure 3.8: Layout of the pressure drop measurement in water test

3.5.2 Refrigerant Evaporator Test System

Temperature *T*

Temperatures are measured at four points: inlets and outlets of both refrigerant and water. Four resistance temperature detectors (RTD's) are used for the measurements. All the RTD sensors use a VDC 24V power supply and give standard 4-20 mA current signals. On the water pipe line, two RTD's are

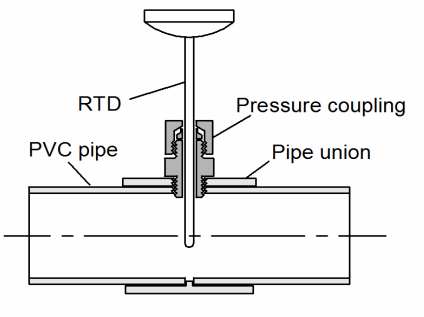


Figure 3.9: Water line RTD mounting

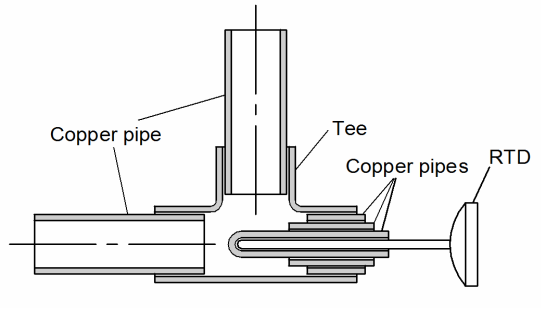


Figure 3.10: Refrigerant line RTD mounting

mounted using pressure couplings. On the refrigerant pipe line, the two sensors are mounted in well insulated T-connections where sealed copper pipes are brazed into a Tee and the sensors are inserted into the pipes. All sensors were extended approximately to the pipe center lines. Schematics of the mounting arrangement are shown in Figures 3.9 and 3.10.

Refrigerant Absolute Pressure P

Static pressures at the refrigerant inlet and outlet are measured by two WIKA pressure transmitters. The two sensors are mounted in well insulated T-connections on the pipe line. Also on the compressor suction line a pressure gauge is fitted on the back pressure regulator, for monitoring of the surge drum pressure. Both the WIKA sensors and the pressure gauge give readings of the "gauge pressure", which is the absolute pressure less the local atmosphere pressure. The WIKA sensors use a VDC 24V power supply and give 4-20 mA current signals.

Refrigerant Differential Pressure ΔP

The pressure drop through the evaporator is measured with a differential pressure transmitter 3051 CD, from Rosemount Inc. Careful consideration is needed for this measurement. The inlet refrigerant is liquid and the outlet refrigerant is a liquid and vapour mixture. The transmitter can not simply be installed with vertical connection between the inlet and outlet pipe lines because the connection could be partially filled with liquid and vapour. The unknown liquid column in the pressure connection can exert static pressure and thus has an effect on the measured result. For heavy refrigerants such as R134a this could be of the order

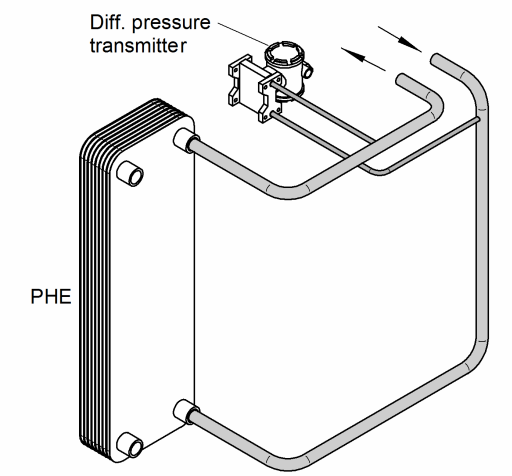


Figure 3.11: Connection of the differential pressure transmitter

of the measurement itself. To solve this problem, all sensor connection tubes must be horizontally oriented, and the evaporator outlet port and the sensor low-side connection must be at the same height. The arrangement in the current facility is shown schematically in Figure 3.11. This arrangement eliminates the influence of refrigerant fluids in the connecting tubes on the pressure measurement.

Water Volumetric Flowrate Q_{w}

Volumetric flow rate of water on the process liquid sides is measured with one RS 257-026 turbine flowmeter, which is one of the two flowmeters which were used for the water test. The flowmeter was positioned at the water pipe line exit. The same flow conditioning was applied for this flowmeter, namely a minimum length of 20 diameters of straight run piping provided on both sides.

Refrigerant Volumetric Flow rate Q_{r}

The flow rate of the liquid refrigerant is measured with a Trimec MP 15S multipulse flowmeter, from Trimec Industries (Australia). The flow meter utilizes the oscillating-piston principle for measuring the flow rate. The passage of liquid causes a piston to oscillate smoothly in a circular motion within the round measuring chamber. Each piston cycle displaces a known volume of liquid

from the inlet to the outlet port, while small high energy magnets in the piston activate a reed switch and a solid state sensor (Hall effect sensor), which provides pulse outputs for remote flow monitoring. The flowmeter has a flow rate range of 0.2-10 l/min, the calibration was done in the range of 0-8.5 l/min for the current study.

This flowmeter is insensitive to viscosity changes and does not require flow conditioning. The manufacturer's instruction states that the flowmeter does not create pulses in the flow, however, pulsation of the water stream was observed during the calibration (refer to *Appendix C*), more apparent at relatively smaller flow rates. The device uses a 5-24V VDC power supply and gives a variable frequency signal. The frequency signal is converted to a current signal via a converter (Model 1100P, IQ Instruments cc, South Africa), and then sent to the data acquisition system.

3.6 Data Acquisition System

Sensors and Data Acquisition

It is generally accepted in the field of measurement that sensors which give electrical signals are termed as "transducers", while transducers which give 4-20 mA signal ranges are called "transmitters". All sensors used in this study have electrical analog signal outputs. The four temperature sensors used in the water test give voltage signals in the range of 0-1 V. All other sensors are standard transmitters and give current output signals of 4-20 mA.

Outputs from the sensors need to be converted into a meaningful quantity, for example, the output from the turbine flowmeter, which is a current signal, needs to be converted into volumetric flow rate. In most cases, measuring transmitters are linearized devices; the conversion rate is given in the manufacturer's instruction, along with its accuracy specifications. For higher accuracy, a calibration process needs to be carried out with a properly designed procedure.

The data acquisition system used in the present study is the National Instruments' NI PCI-6224 DAQ system along with the operating software LabVIEW (version 8.0). Most data acquisition systems read voltage signals only, including the NI PCI-6224 system. Therefore, it is necessary to make an arrangement in electrical connection which can give voltage signals. Because current output is the same at any point in the circuit, it can be converted to a voltage output for measurement purposes at any point in the circuit by adding a load resistor in series. The basic

circuit for measuring the output of a transmitter is then to connect a power supply, a precision load resistor and the transmitter in series. The analogue signal is measured indirectly by connecting a voltmeter (built-in with the data acquisition system) across the load resistor which produces a voltage drop and is proportional to the 4 to 20 mA current loop. This is shown in Figure 3.12. The load resistor brings extra uncertainty to the measurement accuracy. However, a calibration procedure can compensate for this uncertainty if the measurement channel, including the sensor and all connections, is calibrated as one integrated unit.

General Features of the Data Acquisition System Used

The NI PCI-6224 data acquisition system is one of the M series products from National Instruments. Voltage signals are the only analogue signals that can be read by the device. Three types of analogue input ground-reference settings are supported, namely: Differential mode, Referenced single-ended mode, Non-referenced single-ended mode. Depending on the ground-reference mode, 16 or 32 channels in total are supported (16 channels for differential mode, 32 for other modes). The Differential mode reduces noise pickup and should be used whenever possible; this was used in these tests.

It is recommended by NI that the M-Series device should be self-calibrated after installation and whenever the ambient temperature changes. Self-calibration should be performed after the device has warmed up for the recommended time period (15 minutes for NI 6224). This function measures the onboard reference voltage of the device and adjusts the self-calibration constants to account for any errors caused by short-term fluctuations in the environment. In the process of self-calibration all external signals need to be disconnected.

Multichannel Scanning Considerations

In multichannel scanning applications, accuracy is affected by settling time. Settling time refers to the time the device takes to amplify the input signal to the desired stability before it is sampled.

Several factors can increase the settling time which decrease the accuracy of measurements. To ensure fast settling times, the following should be considered (in order of importance):

- **Use low impedance sources**
  Large source impedances increase the settling time. To ensure fast settling times, the signal sources should have an impedance of less than 1kΩ. If the source impedance is high, the scan rate can be decreased to allow more time to settle. The NI 6224 has a default settling time of 14 µs, but this was manually adjusted to 1000 µs in the current study. For sensors that have a current signal output, the signal source is actually a 47 ohm resistor and will thus not cause a problem.

- **Use short high-quality cabling**
  Short high-quality cables can minimize several effects including crosstalk, transmission line effects, and noise. It is recommended by NI to use individually shielded, twisted-pair wires that are 2m long or less to connect analogue signals to the device.

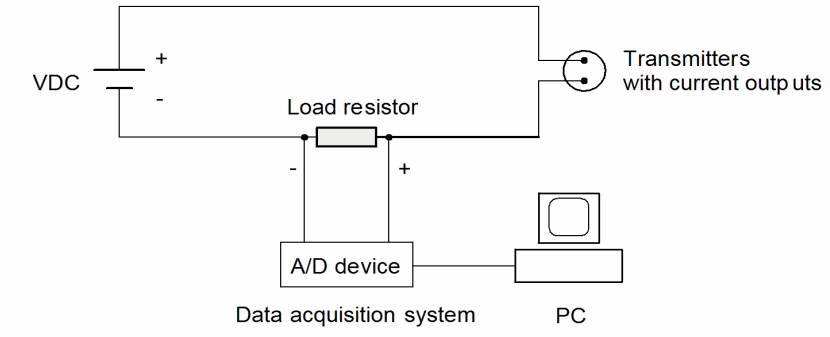


Figure 3.12: Connection loop of transmitters with current

- **Carefully choose the channel scanning order**
  a. Avoid switching from a large to a small input range. Switching from a channel with a large input range to a channel with a small input range can greatly increase the settling time. In the current study, all channels have an input range of 1 V.
  b. Minimize the voltage step between adjacent channels. When scanning between channels that have the same input range, the settling time increases with the voltage step between channels. If the expected input range of the signals is known, then similar expected ranges should be scanned together in groups.

- **Avoid scanning faster than necessary**
  Scanning slower gives the system more time to settle to a more accurate level. There are two cases to consider:

  a. Averaging large number of samples can increase the accuracy by reducing noise effects but it also decreases the required settling time.

  b. If the time relationship between channels is not critical, it is preferable to scan the same channel multiple times and scan less frequently.

Technical Specifications and Analogue Input Circuitry

For more detailed information on technical specifications and analogue input circuitry of the data acquisition system, refer to *Appendix D*.

Scanning Settings and Channel Assignments

The data acquisition system was set to have a sampling rate of 100 Hz for each channel, and the samples were filtered by a built-in third order Butterworth low-pass filter, the filtered signals were then further averaged over every 50 sample. Finally two readings per second were obtained. This setting was maintained throughout all the calibrations and tests.

Channel assignments for the water and refrigeration system tests are given in Tables 3.2 and 3.3, respectively. The channel-sensor pairs must be kept unchanged for all calibration and measurement procedures.

Table 3.2: Channel assignment in water test

Physical channel	Sensor	Measuring quantity

AI 0	Temperature sensor No.1	Hot inlet
AI 1	Temperature sensor No.2	Hot outlet
AI 2	Temperature sensor No.3	Cold outlet
AI 3	Temperature sensor No.4	Cold inlet
AI 4	Water flowmeter No.1	Hot water stream (at outlet)
AI 5	Water flowmeter No.2	Cold water stream (at outlet)
AI 6	Diff. pressure transmitter	Cold water (between outlet and inlet)

Table 3.3: Channel assignment in refrigeration system test

Physical channel	**Sensor**	**Measuring quantity**
AI 16	RTD No.1	Water outlet
AI 17	RTD No.2	Water inlet
AI 18	RTD No.3	Refrigerant inlet
AI 19	RTD No.4	Refrigerant outlet
AI 20	Refrigerant flowmeter	Refrigerant flow rate
AI 21	Pressure transmitter No.1	Refrigerant outlet
AI 22	Pressure transmitter No.2	Refrigerant inlet
AI 4	Water flowmeter No.1	Water flow rate
AI 6	Diff. pressure transmitter	Refrigerant (between outlet and inlet)

3.7 Sensor Calibration

Calibration Procedure and Range

All 14 sensors were carefully calibrated before the experimentation. A best fitting curve was obtained for each sensor and used in the measurements. As a summary, Table 3.4 gives a list of all the sensors with their manufacturer-specified and calibration ranges. Refer to *Appendix C* for details of the calibration procedures and evaluation of the fitting curves. Uncertainty analysis for sensor calibration is given in *Appendix J*.

It is very important to note that the sensors and data acquisition channels had to be calibrated together, and to be used together for any measurements afterwards. This is because an individual channel brings its own error. A data acquisition channel includes the wire connections, load resistance, and the data acquisition system physical channel with all its settings. Channel-sensor pairs should be kept unchanged, for example, if channel No.1 is used for sensor No.1 in the calibration, then the same pair should remain for any further measurements.

Calibration helps to improve the sensors' accuracy, in addition to that provided by the manufacturer's product specifications. Although sensors with factory calibration certificate can be used straight away, it must be noted that the accuracy level degrades after a period of time, normally 1 year after the calibration is taken. This same time period applies to calibrations carried out by the experimenter.

Table 3.4: Summary of sensor calibration range

Sensor	Measuring quantity	Manufacturer-specified working range	Calibration range
RS flowmeter 1	Q, l/min	0-100	0-65.0
RS flowmeter 2	Q, l/min	0-100	0-65.1
LM35DZ 1	T, °C	0-100	0-63.3
LM35DZ 2	T, °C		
LM35DZ 3	T, °C		
LM35DZ 4	T, °C		
RTD 1	T, °C	0-100	0-59.5
RTD 2	T, °C	0-100	
RTD 3	T, °C	0-200	
RTD 4	T, °C	0-200	

WIKA 1	P , Pa	0-1000k	0-840k
WIKA 2	P , Pa		
Rosemount 1151 CD	ΔP , Pa	0-80k	0-73.3k
Trimec flowmeter	Q , l/min	0.2-10	0-8.5

Calibration Uncertainty

For the sensor calibration, and also in the following experimental measurements, the uncertainties were calculated according to the ISO (ISO/1995) method. For clarity, only a summary of the analysis results is presented here, as given by Table 3.5. Extended details of the uncertainty analysis for the sensor calibration are given in *Appendix J*.

Table 3.5: Summary of sensor calibration uncertainty

sensor	Maximum uncertainty
LM35DZ temperature sensors (4 in total)	± 0.08 °C
RTD's (4 in total)	± 0.08 °C
RS 257-026 Turbine Flow Meters (2 in total)	± 0.65 %
Trimec MP15S Flowmeter	± 0.29 %
Rosemount 3051 CD Diff. Pres. Transmitter	± 1.9 %
WIKA Static Pressure Transmitters (2 in total)	± 0.72 %

CHAPTER 4

SINGLE-PHASE PERFORMANCE TESTS WITH WATER

4.1 Introduction

The experimental results on the three BPHE units operating as water-water heat exchangers are reported in this chapter. Correlations for Nu and isothermal friction factor f are developed, based on the experimental data. The obtained correlations are compared with seven other published correlations, and discussions on the thermal and hydraulic performance of PHE's are given.

The tests with water have three main purposes:

1. to obtain an overall understanding of the performance of PHE's operating in single-phase water-water applications;
2. to obtain accurate water side heat transfer coefficient information. This was needed for the subsequent performance analysis of the same units when used as water-cooling evaporators;
3. to obtain single-phase water pressure drop data, for the evaporator pressure drop analysis when the separated model (the Lockhart-Martinelli method) is used.

The Reynolds number range in these tests was relatively small, from 280 to 1100. As discussed in Section 2.6.1, single-phase flows in this range can be considered to fall in the turbulent flow region for PHE's.

4.2 Test Procedure

The water test facility and arrangements have been described in detail in Section 3.3. BPHE units were configured in a single-pass U-type (inlet and outlet at the same side of the exchanger units), counter-current arrangement. Experiments on

heat transfer and pressure drop were carried out separately. In each set of experiments, tests were carried out on the three BPHE units individually, following the same procedure. Measurements were taken in a range of flow rates, as summarized in Table 4.1.

For tests on the heat transfer performance, hot water flow was maintained at fixed flow rates for each unit, and was kept at high Reynolds numbers to ensure turbulent flow. Cold water was supplied in a range of flow rates. Hot water was maintained at approximately 55 °C for all tests, and the cold water was supplied at around 18 °C from the water sump. It is to be noticed that hot water achieves a higher Reynolds number than the cold water at the same flow rate, due to the temperature-dependent characteristics of water viscosity. For both the hot and cold water streams, measurements were taken for volumetric flow rates and inlet and outlet temperatures. All data were taken under steady-state conditions, this was confirmed by:

1. Stable fluid outlet temperatures. Variation of outlet temperatures of the two water streams were within 0.1 °C during a 2 minute time period before each measurement was taken.
2. Close energy balance. The heating and cooling load $\dot{Q}$ calculated from the hot and cold sides did not differ by more than 2%.

For tests on the pressure drop performance, adiabatic flow conditions were maintained with only cold water flowing through the exchangers at the environment temperature (around 20°). A differential pressure transmitter was positioned to measure the pressure drop across the PHE's, at various volumetric flow rates. Again all data were taken under steady-state conditions.

Table 4.1: Summary of water-water performance tests of the three PHE units

	Test	PHE Chevron angle	No. of data	Hot side		Cold side	
				Re	T_{in} , °C	Re	T_{in} , °C
Heat transfer	1	28°/28°	22	510-560	55.0-56.0	280-1100	18.4-19.3
	2	28°/60°	18	450-510	55.0-55.5	330-1110	18.4-19.2
	3	60°/60°	16	430-460	56.0-56.5	350-1030	18.3-19.1
Pressure drop	4	28°/28°	17	–	–	280-1010	18.0-22.0
	5	28°/60°	16	–	–	220-990	19.0
	6	60°/60°	18	–	–	210-840	18.0

4.3 Data Reduction

Experimental data for the heat transfer coefficient were processed by a MATLAB code, using data reduction methods described in this section. The program flowchart is given in *Appendix H*. Water properties were evaluated according to a NIST Standard Reference Database (Lemmon et al., 2005). All fluid properties are calculated at the bulk mean temperature:

$$T_{\text{mean}} = \tfrac{1}{2}\left(T_{\text{in}} + T_{\text{out}}\right) \tag{4. 1}$$

4.3.1 Heat Transfer

The primary measurements consist of six parameters, namely the volumetric flow rates and the inlet and outlet temperatures of both streams. Heat loads (total heat transfer rates) on the hot and cold side are calculated by:

$$\begin{cases} \dot{Q}_{\text{hot}} = -\dot{m}_{\text{hot}} \int_{\text{in}}^{\text{out}} c_{\text{p}}\, dT \\ \dot{Q}_{\text{cold}} = \dot{m}_{\text{cold}} \int_{\text{in}}^{\text{out}} c_{\text{p}}\, dT \end{cases} \tag{4. 2}$$

Under ideally steady conditions and provided that the measurements are absolutely accurate, there is an energy balance between the two streams:

$$\dot{Q} = \dot{Q}_{\text{hot}} = \dot{Q}_{\text{cold}} \tag{4. 3}$$

In the real experiment, due to flow conditions not reaching equilibrium and measurement errors, there will always be some discrepancy between the two. Either the arithmetical average of the two or the one which has a smaller measurement uncertainty can be used as the heat load of the exchanger. In the present study, the hot side has stable flow rates during one test run which led to a smaller measurement uncertainty and is thus chosen. For all measurement points the discrepancy of the heat load does not exceed 2%. The overall heat transfer coefficient is determined by

$$U = \frac{q}{\Delta T_{\text{LM}}} \tag{4. 4}$$

where $q = \dot{Q} / A$ is the heat flux. ΔT_{LM} is the log-mean-temperature-difference defined by Equation (2.72).

The film coefficient h is not a direct measurement quantity, and must be extracted from the overall heat transfer coefficient, through a proper reduction procedure . (Although a direct method is possible to find the film coefficient, this will involve the measurement of wall temperatures, a condition not conveniently available in most situations.) The overall heat transfer coefficient can be expressed in terms of thermal resistances by:

$$\frac{1}{U} = \frac{1}{h_{\text{hot}}} + \frac{1}{h_{\text{cold}}} + R_{\text{wall}} + R_{\text{fouling, hot}} + R_{\text{fouling, cold}} \tag{4. 5}$$

Where h_{hot} and h_{cold} are the film coefficients on the hot and cold side, respectively. R_{wall} is the wall thermal resistance determined by:

$$R_{\text{wall}} = \left(\frac{\delta}{k}\right)_{\text{wall}} \tag{4. 6}$$

Fouling resistances can be found from reference books or published information. Information from two selected sources is given in Section 2.6.4. Since brand new PHE units were used in the experiment, the fouling resistances were assumed to be negligible.

To determine h_{hot} and h_{cold} from Equation (4.5), some assumptions must be made, especially for the expression form of the film coefficient. A new method is proposed here which has not been found in the open literature, as described below.

Step 1: Determine the form of the equation for heat transfer coefficient h. It is customary to express the Nusselt number in the following form, as seen in much of the literature:

$$\text{Nu} = c\,\text{Re}^{\text{m}}\,\text{Pr}^{0.33}\left(\frac{\mu}{\mu_{\text{w}}}\right)^{0.17} \tag{4. 7}$$

which can be rewritten as:

$$h = c\,\text{Re}^{\text{m}}\,\text{Pr}^{0.33}\left(\frac{\mu}{\mu_{\text{w}}}\right)^{0.17}\left(\frac{k}{d}\right) \tag{4. 8}$$

Step 2: Assume that the same form of expression for film coefficient applies on both sides. This requires that during the test, the two fluid streams shall be at sufficiently high Reynolds numbers and thus are both in the turbulent region. The trend of the Nu-Re relationship curve changes

when flows change from laminar to turbulent regions[1], and so does the correlation equation. In the current experiment, this change was observed at Reynolds number around 360 for the low-angle PHE unit, but not for the mixed and high-angle PHE units at similar Re numbers. For this reason, only data obtained at Reynolds number beyond 360 are used for the low-angle PHE, and the developed correlation applies to turbulent flow conditions only.

Step 3: Assume a value of m in Equation (4.7), and find the wall temperature to evaluate μ_w. The heat flux q is expressed as:

$$q = \frac{T_{\text{wall, hot}} - T_{\text{wall, cold}}}{R_{\text{wall}}} = h_{\text{hot}}(T_{\text{hot}} - T_{\text{wall, hot}}) = h_{\text{cold}}(T_{\text{wall, cold}} - T_{\text{cold}}) \quad (4.9)$$

Using Equation (4.9), an iteration program is carried out to find $T_{\text{wall, hot}}$ and $T_{\text{wall, cold}}$:

1. set initial value of $T_{\text{wall, cold}}$ as $\left(T_{\text{wall, cold}}\right)^0$, for each measurement point of flow rate
2. $T_{\text{wall, hot}} = \left(T_{\text{wall, cold}}\right)^0 + \frac{q}{R_{\text{wall}}}$
3. find iteration value of $T_{\text{wall,c}} = \left(T_{\text{wall, cold}}\right)^1$, where

   $\left(T_{\text{wall, cold}}\right)^1 = T_{\text{cold}} + (T_{\text{hot}} - T_{\text{wall, hot}})\frac{h_{\text{hot}}}{h_{\text{cold}}}$

   where $h_{\text{hot}} / h_{\text{cold}}$ is obtained by Equation (4.8), the constant c_1 cancelled in the ratio.
4. If $e = \left(T_{\text{wall, cold}}\right)^1 - \left(T_{\text{wall, cold}}\right)^0 < 0.1$, iteration finished, otherwise $\left(T_{\text{wall, cold}}\right)^0 = \frac{1}{2}\left[\left(T_{\text{wall, cold}}\right)^0 + \left(T_{\text{wall, cold}}\right)^1\right]$, and repeat 2-4.

Step 4: Use linear regression to find the leading constant c. To make the regression possible, some rearrangements are needed. The film coefficient is rewritten as:

$$h_0 = \frac{h}{c} = \text{Re}^{\text{m}}\,\text{Pr}^{0.33}\left(\frac{\mu}{\mu_{\text{w}}}\right)^{0.17}\left(\frac{k}{d}\right) \quad (4.10)$$

[1] The Nu−Re curve is generally flatter in the laminar region and steeper in the turbulent region, according to the current experimental observations and correlations from open literature. This is the same trend as shown in the better-known circular tube heat transfer mechanisms, where for the two extreme cases of constant wall temperature and constant heat flux, laminar flows have constant Nusselt number, though with different values in each case.

note that h_0 is now obtained with the assumed m. Substitute Equation (4.10) into equation (4.5) and rearrange:

$$\left(\frac{1}{U}-R_{\text{wall}}\right)=\frac{1}{c}\left(\frac{1}{h_{0,\text{ hot}}}+\frac{1}{h_{0,\text{ cold}}}\right) \tag{4. 11}$$

Let $x=\left(\frac{1}{h_{0,\text{ hot}}}+\frac{1}{h_{0,\text{ cold}}}\right)$ and $y=\left(\frac{1}{U}-R_{\text{wall}}\right)$, use linear regression (least square fitting) to find the constant for $y = ax$. The data size for x and y is the number of experimental measurement points. Now c is obtained by $a = 1/ c$.

Step 5: Determine m. Every pre-assumed m value would have resulted in a corresponding c, and therefore solely determines the fitting curve by the regression as shown in step 4. The best value for m is the one from which the resulted fitting curve best fits the experimental data. Generally the goodness of a fitting is evaluated by two parameters, the Root Mean Square Error (RMSE) and the Coefficient of Multiple Determination (usually called R-square). In the present method, the best m is determined by trial-and-error: values from 0.01 to 2 with a step of 0.01 were tried, the one which has the smallest RMSE was chosen.

4.3.2 Pressure Drop

Contributions of the Total Pressure Drop

For single-phase flow, the total pressure drop across a plate heat exchanger consists of three contributions:

1. pressure drop associated with the inlet and outlet manifolds and ports, ΔP_{port},
2. friction pressure drop within the core, ΔP_{core},
3. pressure drop due to the static water head (elevation change), ΔP_{elev}.

Summing all contributions, the total pressure drop across a plate heat exchanger is given by:

$$\Delta P_{\text{ PHE}}=\Delta P_{\text{core}}+\Delta P_{\text{port}}+\Delta P_{\text{elev}} \tag{4. 12}$$

The elevation pressure drop (or rise, depending on flow direction) is due to the static water head, and is calculated by:

$$\Delta P_{\text{elev}} = \rho g \Delta h \tag{4. 13}$$

where Δh is the water head, measured as the vertical distance between the upper and lower port centre line. The pressure drop in the manifolds and ports is calculated by an empirical equation (Shah and Sekulic, 2003):

$$\Delta P_{\text{port}} = 1.5\left(\frac{G_{\text{port}}^2}{2\rho}\right) \tag{4. 14}$$

The frictional pressure drop within the core is the purpose of the investigation, and is usually by far the major part of the total pressure loss. The pressure drop measurement arrangement is given in Figure 3.8. The measured value of pressure drop is not directly the total pressure drop across a PHE but has extra contributions, as can by expressed by:

$$\Delta P_{\text{measured}} = \Delta P_{\text{PHE}} + \Delta P_{\text{pipe}} + \Delta P_{\text{fittings}} - \Delta P_{\text{elev}} \tag{4. 15}$$

Note that in this equation the term of the elevation pressure drop has a negative value; this is because the static pressure due to the water head in the transmitter connection tube will counteract that in the PHE. Combining Equation (4.12) and (4.15), we have:

$$\Delta P_{\text{measured}} = \Delta P_{\text{core}} + \Delta P_{\text{port}} + \Delta P_{\text{pipe}} + \Delta P_{\text{fittings}} \tag{4. 16}$$

The dimensions of the pipeline and the fittings are given in Figure 4.1. The pressure loss along the inlet and outlet pipelines, ΔP_{pipe}, is calculated by

$$\Delta P_{\text{pipe}} = f \cdot \left(\frac{L}{d} \cdot \frac{1}{2}\rho u^2\right)_{\text{pipe}} \tag{4. 17}$$

where f can be obtained from the Moody Chart, or any fluid mechanics text book. For convenience of numerical calculation, the well-known Blasius equation is used which states:

$$f = \frac{0.3164}{\text{Re}^{0.25}} \tag{4. 18}$$

for smooth tube, $3000<\text{Re}<10^5$

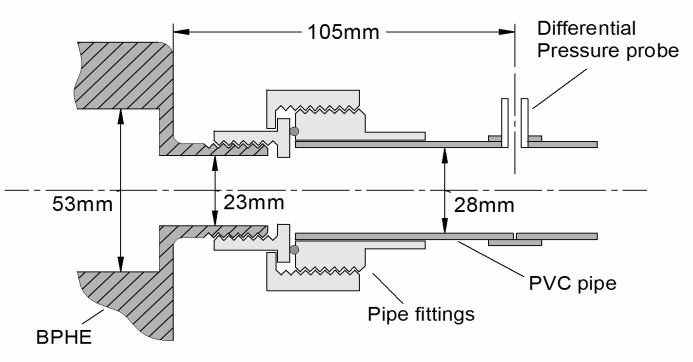


Figure 4.1: Pipe and fitting dimensions for pressure drop calculation

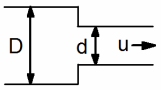
Local losses from pipe fittings, $\Delta P_{\text{fittings}}$, can be evaluated by the empirical "velocity head" method. In this method, the term $\rho u^2/2$ is used which has the dimension of pressure and is commonly called a "velocity head". Local losses are reported as a number of velocity heads. The local pressure loss in the present study has only one major component, this is the sudden flow area change between that of the pipeline and the PHE manifold. This can be treated as a sudden enlargement and contraction when a water stream enters and exits the PHE. Those losses are evaluated from the following equations:

$$\Delta P_{\text{local}} = K \cdot \tfrac{1}{2} \rho u^2 \qquad (4.\ 19)$$

The K values are given in Table 4.2 (Avallone and Baumeister, 1996). For the experimental arrangement used, K = 0.66 is taken for the contraction (from pipe to PHE), and 0.39 for the expansion (from PHE to pipe).

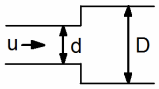
Table 4.2: K values for sudden contraction and expansion

sudden contraction



D/d	1.5	2.0	2.5	3.0	3.5	4.0
K	0.28	0.36	0.40	0.42	0.44	0.45

Sudden enlargement



$$K = \left[1-(d/D)^2\right]^2$$

Frictional Pressure Drop and Friction Factor

The frictional pressure drop, ΔP_{core}, is the purpose of the investigation. Once it is obtained, the Darcy friction factor is determined conveniently by

$$f = \frac{DP / L}{\frac{1}{2}\rho u^2 / d} \tag{4. 20}$$

A common practice, which is often seen in the literature and also justified by the current study, is to correlate the friction factor to Reynolds number by the form:

$$f = \frac{c_2}{\mathrm{Re}^{\mathrm{p}}} \tag{4. 21}$$

The constant c_2 and p are determined by linear regression analysis.

4.4 Uncertainty Analysis

For sensor calibration and experimental measurements presented in this study, the uncertainties were analyzed according to the ISO (ISO/1995) method. There are two widely accepted methods from two organizations: the ASME method (ANSI/ASME PTC 19.1, 2005) and the ISO method (ISO/1995). For a detailed

Table 4.3: Summary of experimental measurement uncertainties

Parameter	Maximum absolute percentage uncertainty, $\left[u(\phi_i)/\phi_i\right]_{max}$		
	β = 28°	β = 28°/60°	β = 60°
Mass flow rate, $\dot{m}_{hot}$ (kg/s)	0.43 %	0.45 %	0.46 %
Mass flow rate, $\dot{m}_{cold}$ (kg/s)	1.13 %	1.4 %	1.36 %
ΔT_{LM} (°C)	0.5 %	0.8 %	1.6 %
Pressure drop, ΔP (Pa)	1.9 %	2.4 %	1.0 %
Heat flux, q_{hot} (W)	1.2 %	1.2 %	1.1 %
Heat flux, q_{cold} (W)	1.5 %	1.7 %	1.7 %
Overall heat transfer coefficient, U, (W/m^{2}K)	1.3 %	1.4 %	1.9 %
heat transfer coefficient, h_{cold}, (W/m^{2}K)	1.3 %	1.5 %	2.1 %
Re	1.7 %	1.9 %	1.9 %
Nu	1.6 %	1.7 %	2.2 %
f	3.1 %	3.1 %	2.3 %

discussion of the ASME and ISO methods, along with the basic principles of uncertainty analysis in general, refer to *Appendix I*. Extended details of the uncertainty analysis for the water test results are given in *Appendix K*. For clarity, only a summary of the analysis result is presented here in Table 4.3.

4.5 Results and Discussion

Experimental observations and developed correlations on heat transfer and pressure drop characteristics are presented in this section. PHE's represent two symmetric ($\beta = 28^\circ / 28^\circ$ and $\beta = 60^\circ / 60^\circ$) and one mixed ($\beta = 28^\circ / 60^\circ$) plate arrangements, where the mixed-plate chevron angle can be approximated by $\beta = 44^\circ$, according to some authors. Experimental observation and calculation results are recorded in *Appendix E*.

4.5.1 Heat Transfer Characteristics

The measured overall heat transfer coefficient U at various volume flow rates is presented in Figure 4.2. For heating of cold water which flows in the testing turbulence range, the experimental data can be correlated as:

$$\mathrm{Nu} = c_1 \mathrm{Re}^{\,m} \mathrm{Pr}^{0.33} \left(\frac{\mu}{\mu_{\mathrm{wall}}} \right)^{0.17} \qquad (4.\ 22)$$

where the constants c_1 and m are:

	c_1	m	RMSE*
β = 28°	0.0508	0.78	2.218×10^{-5}
β = 28°/60°	0.215	0.65	4.114×10^{-6}
β = 60°	0.759	0.53	3.048×10^{-6}

* Refer to Equation (4.11) for variables of y vs. x of the fitting curve.

The result from Equation (4.22) is compared with a selection of seven published correlations, which are among the most widely quoted and recognized from over 30 correlations that are available in the open literature. Some of those correlations can be found in detail in Section 2.6.2. The comparison result is shown in Figure 4.3. For the comparison to be possible, the heat transfer group j_{Nu}, as defined below, instead of Nu, is plotted against Re for each correlation.

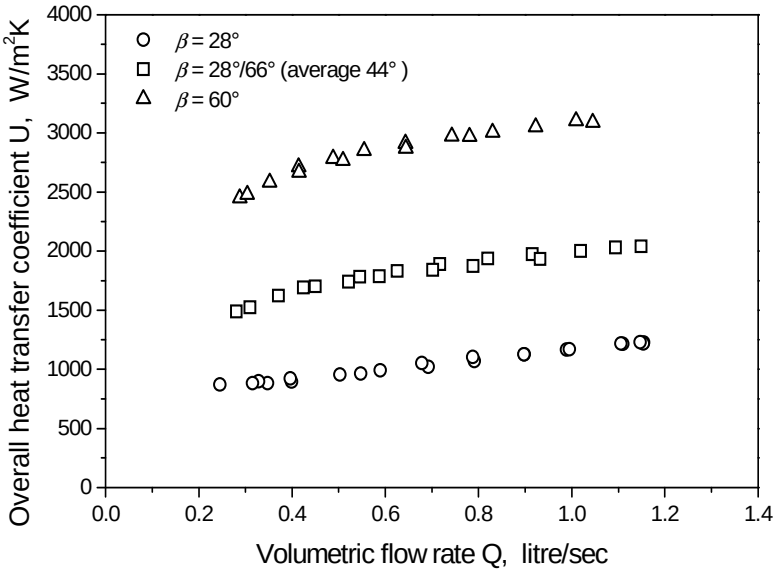


Figure 4.2: Measured overall heat transfer coefficient vs. volume flow rates

$$j_{\mathrm{Nu}} = \frac{\mathrm{Nu}}{\mathrm{Pr}^{0.33}\left(\frac{\mu}{\mu_{\mathrm{w}}}\right)^{0.17}} \qquad (4.\ 23)$$

Note that some correlations do not have the term μ / μ_{w}, and this is simply ignored in the calculation of j_{Nu} in that case. Also in some correlations the exponents for Pr and μ / μ_{w} are not the values as used in Equation (4.22) (for example, Focke et al.'s correlation has a Pr exponent of 0.5, Muley and Monglik's correlation uses 0.14 for μ/μ_{w}), and the j_{Nu} is calculated accordingly using the values as specified in the original correlation. For clarification, the result for each BPHE unit is presented separately. For correlations which do not cover the exact chevron angle as used in the present experiments, the nearest chevron angle covered in that correlation is chosen.

It is apparent from the result that higher Nusselt numbers are obtained with increasing chevron angles, which reflects the increasing intensity of flow turbulence generated by the corrugations. Also note that the Nu-Re relationship is well represented by Equation (4.22).

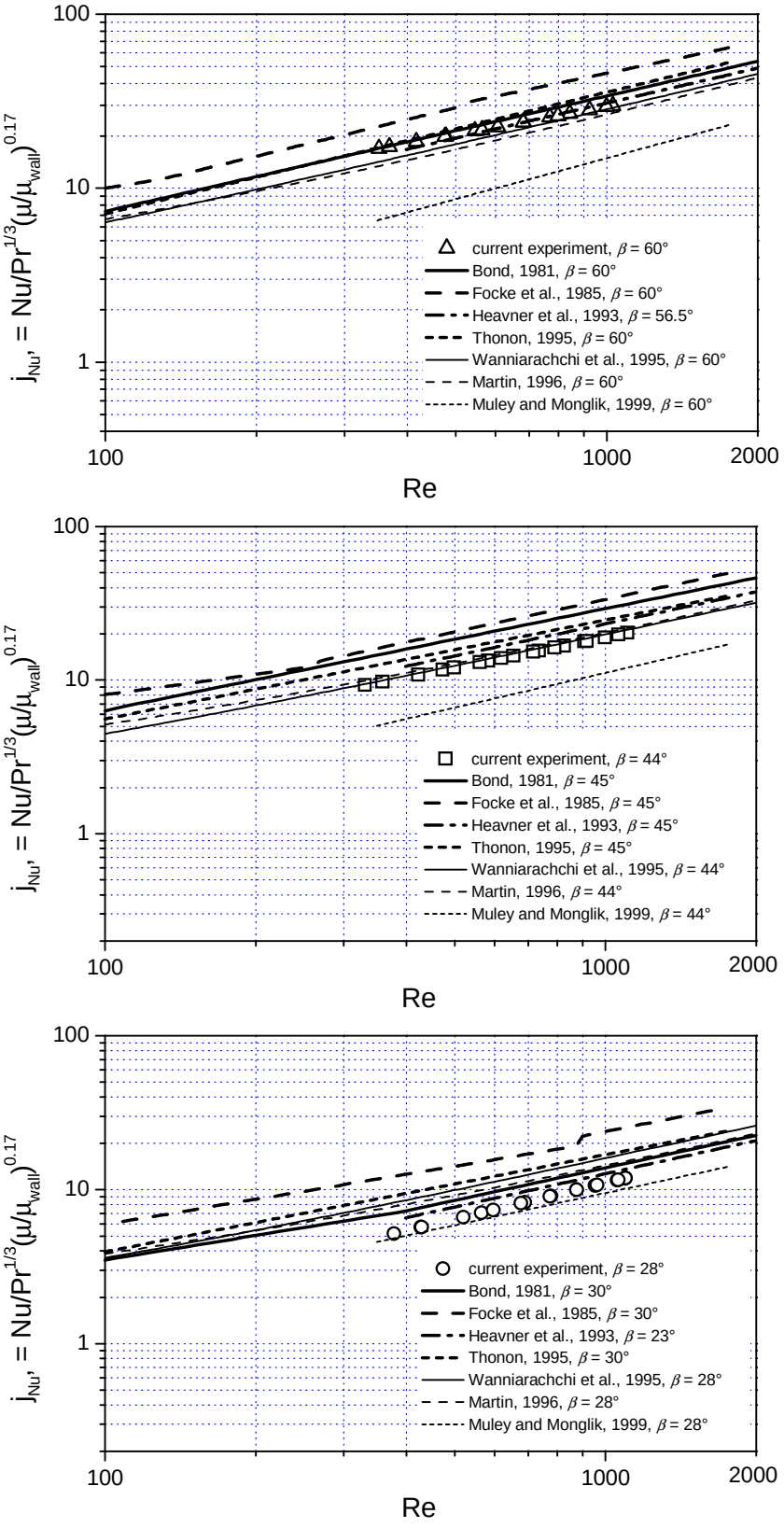


Figure 4.3: Comparison of j_{Nu}-Re result against correlations
(a) β = 60°, (b) β = 44°, (c) β = 28°

The comparison shows good agreement of the experimental data with correlations from Heavner et al (1993) and Martin (1996), in all three cases. Results from Bond (1981), Wanniarachchi (1995), and Thonon (1995) are also in reasonable range, but tend to over-predict the experimental data at lower chevron angles. Focke et al's result are much higher than those of the present study for all cases, while Muley and Monglik (1999)'s equation is always much lower than all others. Focke et al (1985)'s heat transfer correlation was based on mass transfer experiments and therefore is not as reliable as those based on direct measurements. For Muley and Monglik's correlation, it is obvious that the authors have put considerable weight on the enlargement factor ϕ (refer to Section 2.6.2 for the correlation), which gives a 37% drop for Nu when the enlargement factor changes from 1.29 (for Muley and Monglik's rig) to 1.14 (in the present study). As discussed in Section 2.5.4, the use of the hydraulic diameter which involves the enlargement factor as a component, is physically sound and might be a simple and effective way of introducing its influence on Nu and *f*. Muley and Monglik's approach, in which the effect of ϕ is accounted for by cubic polynomials, might easily give more weight to this parameter than appropriate.

It seems that there is not a generally accepted correlation in the open literature which meets all requirements. It is important to note that there is no suitable information one can rely on to judge which one is more accurate than others. The disagreement, as clearly shown in Figure 4.3, between results from various authors can perhaps be attributed to, among other factors, non-physical treatment of variables in data reduction, and certainly measurement errors. Another possible fact, which can not be ignored, is that the complexity of the PHE channel, in terms of its corrugation-featured geometry, and also in terms of the very many combinations of important parameters including the aspect ratio, port size, flow arrangement of ports (vertical or diagonal), flow arrangement of channels (single pass, multiple passes), flow arrangement of streams (co-current or count-current), flow distribution between channels, flow distribution around ports, and many others, all make it almost impossible to have two units that are identical. This may have partially explained why a "general" correlation is hard to obtain, for this type of exchanger.

Only turbulent flow is considered in the current study, and this involves the criterion of the critical Reynolds number, which indicates the transition from laminar to turbulent flow. A discussion on the critical Reynolds number is given in Section 2.6.1. It suffices to mention here that the Reynolds number for heat transfer tests was maintained at 280-1100, which can be considered as in the turbulent region. The transition from laminar to turbulent flow was observed only for the low-angle unit (β = 28°) at a Reynolds number around 360. This transition was not found for the other two units in the testing range of flow rates.

4.5.2 Pressure Drop Characteristics

The measured pressure drops are plotted against the volume flow rates in Figure 4.4. Pressure drop measurements were carried out under isothermal conditions, where only cold water at the environment temperature (around 20°) was supplied to the exchangers.

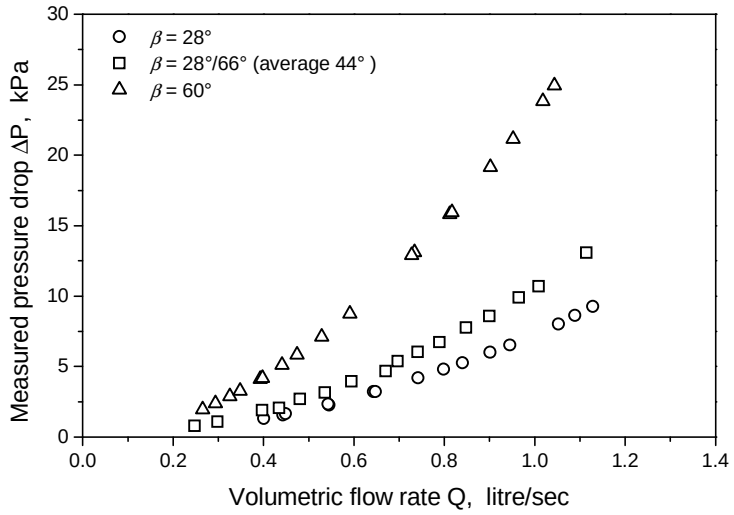


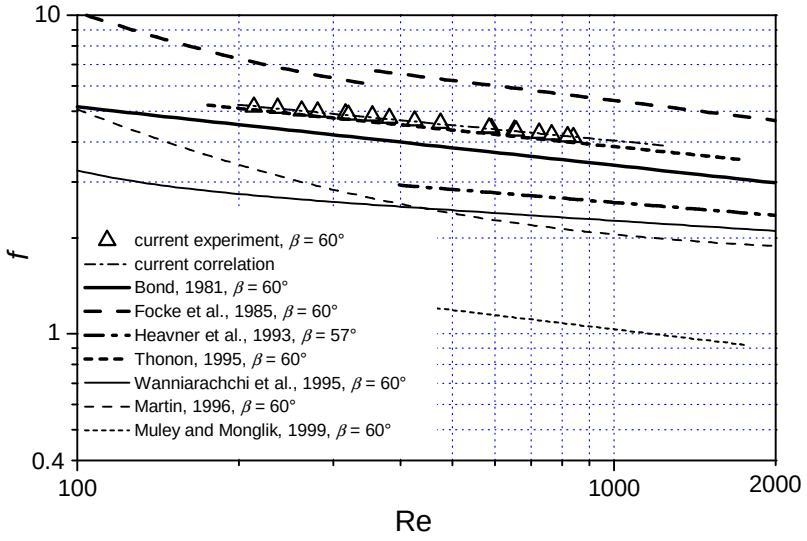
Figure 4.4: Measured pressure drop vs. volume flow rate

In the testing range of flow rates, which corresponded to Reynolds number of 210-1000, the experimental data could be correlated as:

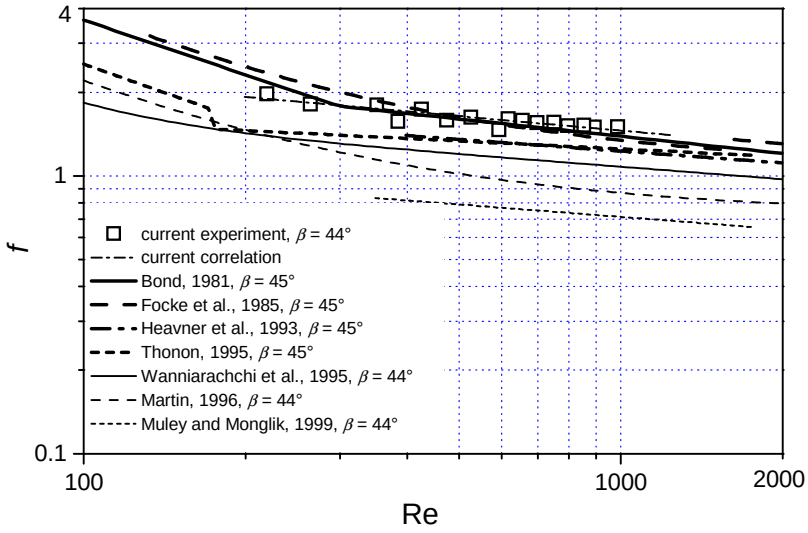
$$f = \frac{c_2}{\mathrm{Re}^{\,p}} \tag{4. 24}$$

where the constants c_2 and p are:

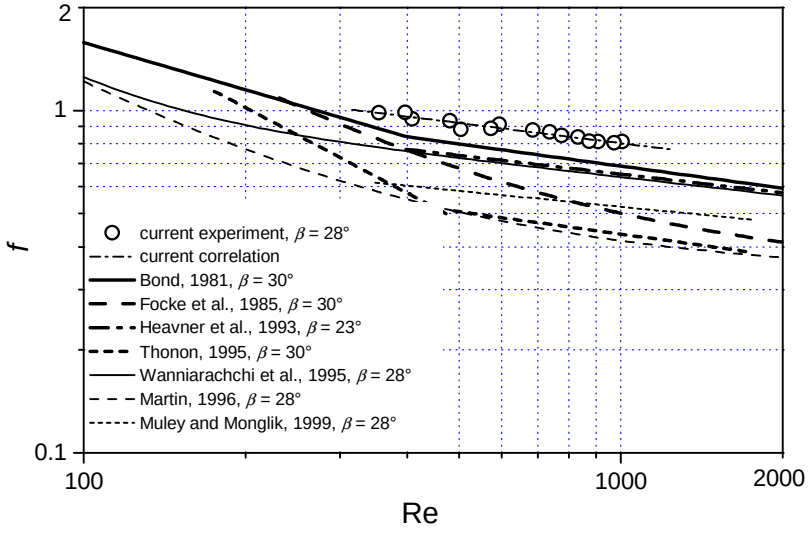
	c_2	p	RMSE
β = 28°	3.11	0.196	0.01751
β = 28°/60°	4.81	0.173	0.06703
β = 60°	12.28	0.161	0.02353



(a)



(b)



(c)

Figure 4.5: Comparison of f-Re result against correlations
(a) $\beta = 60°$, (b) $\beta = 44°$, (c) $\beta = 28°$

As for Nu, the result from Equation (4.24) is compared with the same seven correlations, as given in Figure 4.5. Bond (1980)'s correlation agrees with the results of the present experiments fairly well, for all three units. However, in general the comparison reveals much larger differences between the various correlations than those observed for Nu, more so at higher chevron angles. For example, at β = 60°, the highest predicted result (from Focke et al., 1985) is more than 2.5 times higher than the lowest (from Martin, 1996). Muley and Monglik (1999)'s correlation again tends to under-predict the friction factor compared with most other correlations. Martin's is the only semi-empirical correlation of the seven, which agreed well with the current experiment in predicting Nu, failed to do so for the friction factor *f*. This correlation consistently tends to under-predict the current experimental results by approximately 50% for all three units.

It is difficult to explain the disagreements between those correlations, as for the case of Nu. However, one may reason that the final frictional pressure drop is obtained through a subtraction procedure, wherein many local losses are evaluated by empirical equations. This might have brought extra errors, but would still not suffice to explain the big discrepancy between different correlations, because the local and port pressure drops are relatively much smaller than the frictional core pressure drop (refer to *Appendix E* for values of those components).

4.6 Conclusion

Experimental results of the thermo-hydraulic performance of three BPHE's are presented. Single-phase turbulent flow of water under heating conditions is considered for heat transfer characteristics, and isothermal turbulent flow is considered for frictional pressure drop characteristics. The units have three sets of different chevron plate arrangements: two symmetric with β=28°/28° and β=60°/60°, and one mixed with β=28°/60°. Based on the experimental data, correlations for Nu and isothermal *f* are developed and further compared with a collection of seven correlations from the open literature.

The experimental results clearly show that chevron angle has a strong influence on the heat transfer and pressure drop performance of the exchanger units. Both high overall heat transfer coefficients and friction factors are observed. A comparison shows that certain published correlations agreed with the results from the current study fairly well. However, in general the high level of disagreement between those correlations, including that developed in the present study, indicates that a general correlation might be difficult to achieve.

The current study has been constrained, due to pump capacities, to water flows within Reynolds number ranges of 280-1100 for Nu and 210-1000 for pressure drop. This is a relatively small range in industrial applications. The obtained correlations are accurate in this particular range, while applications beyond that are not recommended.

CHAPTER 5

FIELD TESTS ON LARGE-SCALE PHE'S

5.1 Introduction

Field measurements were carried out on two large industrial PHE water chillers (both having heat transfer areas greater than 500 m^2) to evaluate their thermal performance. The machines were installed at South African gold mine and both were fed by the thermo-siphon (gravity-feed) method. The refrigerants employed were ammonia and R12, tested in February 1994 and June 1996, respectively. This chapter reports the results of the heat transfer performance evaluation of those evaporators. All data presented are based on two technical reports (Bailey-McEwan, 1994, Bailey-McEwan et al., 1996). During the tests the chillers were operating at their design working conditions, i.e., at fixed mass flow rates and cooling loads. The performance assessment was therefore based on these conditions only.

5.2 PHE Thermo-Siphon Evaporators

Thermo-siphon evaporators operate by means of density differences between the refrigerant liquid and vapour. A surge drum is positioned at a suitably higher level than the refrigerant inlet and liquid exits from the bottom of the surge drum and flows into the evaporator. When it boils a mixture of liquid and vapour is formed which is lighter than the liquid alone, therefore gravity circulation takes place. A high heat transfer rate is normally achieved because the surface is thoroughly wetted. Overall heat transfer coefficients have been reported to be in the range of 2500-4500 W/(m^2K) for ammonia, and 1500-3000 W/(m^2K) for CFC refrigerants when plates are clean (Stromblad, 1989). Overfeeding ensures that the vapour exiting the evaporator will be close to saturation, not superheated, which gives lower compressor temperatures and more efficient operation of the condenser. The overfeed extent is evaluated by the *recirculation rate* n_{RC}, which is defined as the mass ratio of liquid entering to the amount of liquid vaporized in

the evaporator ($n_{RC} = \dot{m} / \dot{m}_{g,out} = 1/x_{out}$). Typical values of recirculation rate for conventional evaporators are 2 to 7 (ASHRAE Handbook 2006: Refrigeration), while for PHE flooded evaporators the common value of recirculation rate is 1.2-1.5 (Stromblad, 1989, Hanssen, 1997). The evaporators tested in the present study were designed and operated at a recirculation rate around 1.4.

Because single-phase liquid refrigerant with low velocity is fed into the inlet manifold, flows are relatively evenly distributed between channels without distribution devices, which means that a large number of plates can be installed. For this reason, PHE flooded evaporators are generally operated for large cooling capacities over 500 kW. The two PHE thermo-siphon evaporators tested in this study were operating at cooling loads between 4 and 8 MW. Direct-expansion (DX) PHE evaporators are more commonly found in smaller installations, where a flow distributor is usually employed in the inlet manifold, which can result in better flow distribution and heat transfer performance, but also brings higher pressure drops.

Thermo-siphon evaporators are normally expected to have a higher heat transfer coefficient than DX evaporators. Ammonia evaporators are smaller than HCFC and CFC evaporators under comparable cooling loads, due to the high latent heat and thermal conductivity of ammonia. It is evident that nucleate boiling is more likely to occur in a PHE flooded evaporator than in a DX evaporator, since most of the heat transfer surface is "flooded", i.e. submerged, in liquid refrigerant and the exit vapour quality is always low (normally around 0.7, depending on the recirculation rate) in the entire channel. Subcooling at the channel entrance region should be taken into account when flow rates are high, since the increased static

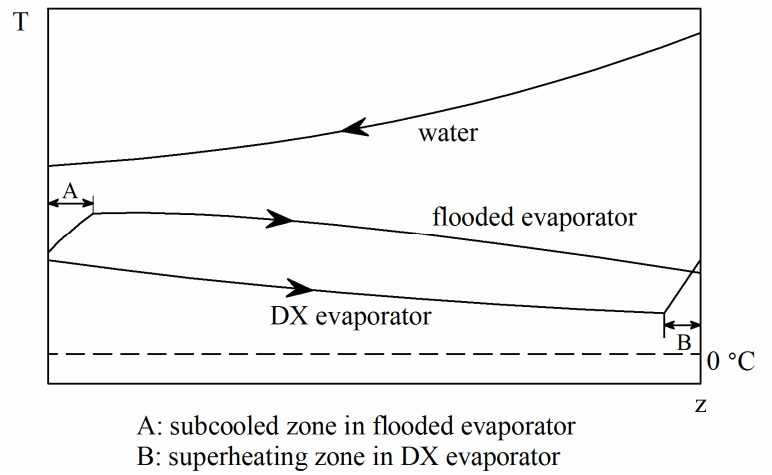


Figure 5.1: Typical temperature profile in PHE liquid-overfeed and DX evaporators for water chilling

liquid head will cause the liquid at the evaporator inlet to be subcooled, resulting in the preheating section taking up a considerable part of the heat transfer area. Figure 5.1 shows a typical temperature profile in PHE flooded and DX evaporators for water chilling applications.

The Water Chillers Tested

Both of the tested water chillers employed semi-welded plates; no entrance distributors were installed. The plate types were the same for the two evaporators. There were two evaporators in the R12 installation, a twin refrigerant exit arrangement was employed with the water flow in series and the refrigerant flow in parallel, and measurements were taken on evaporator No.1. The plant layout of these thermo-siphon systems is shown schematically in Figure 5.2, the exchanger information is summarized in Table 5.1.

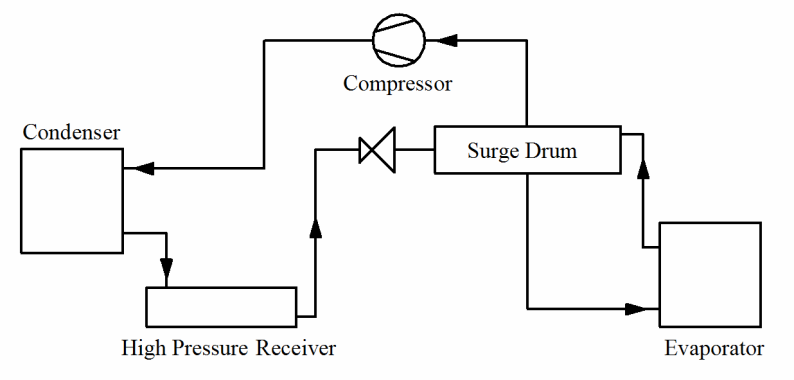


Figure 5.2: Schematic diagram of the thermo-siphon system

Table 5.1: PHE geometrical information

	Ammonia	R12
PHE type	AX30-BW-FD	AX30-B-FD
Plate geometry	$\beta = 60°$, $\phi = 1.22$, $b = 5$ mm	
Plate size	$L_p \cdot w = 1.8 \times 0.94$ m^2	
No. Plates, N_p	444	316
No. Effective plates, $N_{p,\,eff}$	442	314
No. channels (total), N_{ch}	443	315
No. Water channel, $N_{ch,\,w}$	222	158
No. Refrigerant channel, $N_{ch,\,r}$	221	157
Heat transfer area, A, m^2	712	505.8
Plate thickness δ_p, mm	0.8	0.6
Plate material	AISI 316	AISI 316

5.3 Measurements and Data Reduction

Measurements of five quantities were taken at stable running conditions of the two chillers, these being the inlet and outlet temperatures of both water and refrigerant and the volumetric flow rate on the water side. Six readings were taken of each quantity during a time period at certain intervals. The experimental measurements are given in Figures 5.3 and 5.4, for tests carried out on the chillers employing ammonia and R12, respectively. The final results for each quantity were taken as the average of all six readings, and are given in Table 5.2 along with their measurement uncertainties.

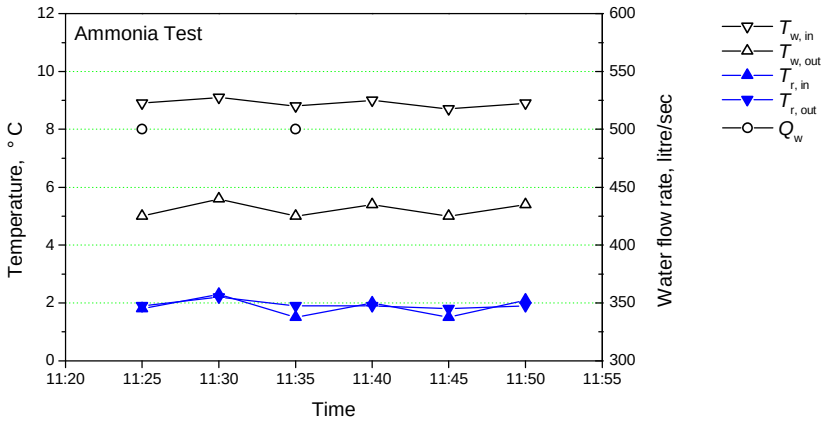


Figure 5.3: Ammonia water chiller measurements

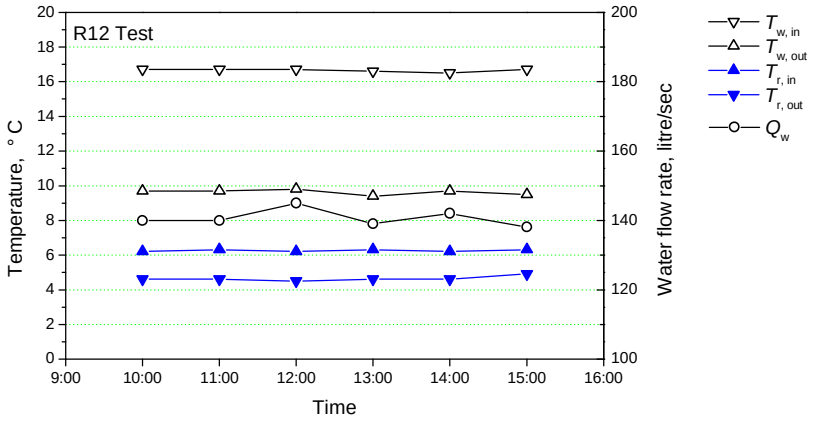


Figure 5.4: R12 water chiller measurements

The overall heat transfer coefficient between the two fluids can be expressed as:

$$U = \frac{\dot{Q}}{A \cdot \Delta T_{\mathrm{LM}}} \tag{5. 1}$$

where $\dot{Q} = \dot{m}_{\mathrm{w}} c_{\mathrm{p.\,w}} \left(T_{\mathrm{w,\,in}} - T_{\mathrm{w,\,out}} \right)$ is the evaporator cooling load.

To find the value of the individual heat transfer coefficients, U is expressed in the form of thermal resistance:

$$\frac{1}{U} = \frac{1}{h_{\mathrm{w}}} + \frac{1}{h_{\mathrm{r}}} + \left(\frac{\delta}{k} \right)_{\mathrm{plate}} + R_{\mathrm{fouling}} \tag{5. 2}$$

The refrigerant heat transfer coefficient can now be calculated using Equations (5.1) and (5.2). The water side transfer coefficient was evaluated using the Martin correlation (1996) as given by Equation (2.91). Fouling factors recommended by Panchal and Rabas (1999), as given in Table 2.6, were taken for the ammonia chiller. The R12 chiller had been renovated with new plates prior to the test, therefore the water side fouling was neglected for this chiller.

Table 5.2: Measurement results of Ammonia and R12 chillers

Parameter	Ammonia	R12
Q_{w}, m^3/s	0.5 ± 9.4%	0.141 ± 7 %
$T_{\mathrm{w,\,in}}$, °C	8.88 ± 0.2	16.7 ± 0.2
$T_{\mathrm{w,\,out}}$, °C	5.23 ± 0.2	9.7 ± 0.2
$T_{\mathrm{r,\,in}}$, °C	1.86 ± 0.2	6.3 ± 0.2
$T_{\mathrm{r,\,out}}$, °C	1.93 ± 0.2	4.6 ± 0.2
Cooling load, kW	7656 ± 12%	4131 ± 8%
ΔT_{LM}, °C	4.95	6.85

5.4 Results and Discussion

The obtained flow boiling heat transfer coefficients of ammonia and R12 are given in Table 5.3, along with values that were calculated by some published correlations from the literature. All correlations are given in Table 2.7, except for

Cooper's pool boiling correlation which is given by Equation (2.5). It is worth mentioning that because different channel equivalent diameter were used by different authors, care must be taken when those correlations are used. The comparisons between the measured and predicted values are evaluated by the percentage error, which is defined as:

$$e_r = \frac{h_{corr} - h_{expe}}{h_{expe}} \tag{5. 3}$$

It is shown from the comparison that a number of correlations could predict the refrigerant heat transfer coefficients with reasonable accuracy. The refrigerant used does not appear to cause a particular trend in the accuracy of the correlations. The good agreement between Hsieh and Lin's correlation with the experimental value for ammonia might be in some way coincidental as this correlation, originally developed for halocarbon R410A, failed to predict the R12 data with comparable accuracy. Yan and Lin's correlation is one of the earliest published for evaporation heat transfer in PHE channels and it did not predict the

Table 5.3. Comparison between tested and calculated values of refrigerant heat transfer coefficient

	Original testing condition	Ammonia		R-12	
		h_r W/(m^2·K)	e_r, %	h_r W/(m^2·K)	e_r, %
Current experiment	β=60°	4371	0	1744	0
1. Cooper, 1984 Eq. (2.4)	Pool boiling	3807	-12.9	1522	-12.7
2. Yan and Lin, 1999 Eq. (2.88)	Single channel β=60°, R134a,	1028	-76.5	299.2	-82.8
3. Donowski and Kandlikar 2000, Eq. (2.90)	Single channel β=60°, R134a	4686	7.21	2391	37.1
4. Hsieh and Lin, 2002 Eq. (2.91)	Single channel β=60°, R410A	4374	0.1	2583	48.1
5. Han et. al., 2003 Eq. (2.95)	2 channels R410A	3600	-17.6	1723	-1.2
6. Ayub, 2003 Eq. (2.97)	Flooded ammonia	5570	27.4	1281	-26.5
7. Sterner and Sunden, 2006 Eq. (2.99)	DX, β=59° ammonia	38300	776	127000	7182
8. Jokar et. al., 2006 Eq. (2.101)	DX, β=60° R134a	12050	176	2035	16.7

experimental values adequately. A further check of this correlation shows very poor ability to predict the authors' own data; calculated values fall far below their experimental data (the verification can be carried out with Figure 6 in Yan and Lin's paper). As is discussed in Section 2.7.4, either there is an error in this correlation as published, or a direction on the proper use of the correlation is needed.

Very high values of h_r are observed with the correlations from both Sterner and Sunden (2006) and Jokar et al. (2006). This may particularly be due to the fact that both of those correlations were developed for DX evaporators. In Sterner and Sunden's correlation the term $(1/x_m-1)$ has a power of 1.624, which will result in sharp increments of h_r with small decrements of x_m. Note that for a DX evaporator x_m is in the range of 0.52-0.55 (corresponding to inlet vapour quality of 0.05-0.1), while in the current test x_m is around a value of 0.35 (corresponding to exit vapour quality of 0.7). Also, this correlation has an exponent of 1.41 on the mass flux, which makes it unsuitable for CFC refrigerants as CFC refrigerants would have a much higher mass flux compared with that of ammonia under comparable cooling loads. In Jokar et al.'s correlation the term $1/x_m$ has a power of 2; calculations for small changes of the circulation rate have shown very high changes of heat transfer coefficient. These two correlations might be accurate for their specified ranges of conditions, but they are not recommended for flooded evaporators.

Cooper's nucleate pool boiling correlation shows good ability to predict the heat transfer coefficients for both ammonia and R12 evaporators, with essentially the same deviations. The correlations from Han et. al. (2003) and Ayub (2007) also give fairly good agreements for both cases. These two correlations are also superior to all others with plate geometry being taken into account and are applicable for various chevron angles.

5.5 Conclusion

In the thermal performance tests carried out on two large-scale thermo-siphon PHE evaporators, the ammonia evaporator showed a refrigerant heat transfer coefficient of 4371 W/(m^2·K), which is 2.5 times higher than that of the R12 evaporator. A comparison between the measured and calculated values of heat transfer coefficients using some published correlations indicates that these correlations are likely to become inaccurate outside their original ranges. Of those, correlations developed for DX systems gave the highest discrepancy with the current test data. Cooper's (1984) pool boiling correlation appears to predict the

heat transfer coefficient quite accurately for both evaporators. It might be concluded that this correlation is suitable for large-scale PHE thermo-siphon evaporators, notwithstanding the fact that the dominant boiling mechanisms in PHE channels remain a matter of debate.

CHAPTER 6

EVAPORATOR PERFORMANCE TESTS USING R134a AND R507A

6.1 Introduction

The experimental results of the thermal and hydraulic performance of the three BPHE units operating as liquid over-feed evaporators are reported in this chapter. A schematic diagram of the experimental apparatus is given in Figure 3.5. Two refrigerants, R134a and R507A, were used, following basically the same experimental procedure but with slightly different ranges of cooling loads and system pressures.

A detailed description of the liquid over-feed system is given in Section 3.4.1. The testing range of the two refrigerants, as allowed by the system maximum capacity, is summarized in Table 6.1. In total there are 175 measurement data points obtained for the tests using R134a and 60 for R507A. Each data point contains measurements of nine variables including temperatures at the water inlet and outlet and those at the refrigerant inlet and outlet, volumetric flow rates of both the water and refrigerant streams, and the two static pressures at, and the differential pressure between, the refrigerant inlet and outlet. It is desirable to give some explanation regarding the selection of experimental data. No data have been discarded simply because they do not fit the developed correlation. However some data were discarded because they did not meet all of the following conditions:

- Data were taken under stable conditions.
  All data for analysis were to be obtained under steady-state conditions, confirmed by observing a stable water outlet temperature changing by not more than 0.1 °C during approximately a 10 minutes time period. In a few cases the obtained data showed greater divergence and were thus discarded. Tests were repeated for that testing condition in such cases whenever possible.

Table 6.1: Testing Range for R134a and R507A

	R134a	R507A
Heat flux, q, kW/m^2	1.85 - 6.50	3.79 - 6.88
Mass flux, G, kg/(m^{2}s)	5.60 - 30.30	15.94 - 31.39
Outlet vapour quality, x_{out}	0.20 - 0.95	0.40 - 0.95
Saturation temperature, °C	5.9 - 13.04	7.8 - 12.6

- For heat transfer data, the refrigerant superheat at the evaporator exit was less than 0.3 °C.
  Theoretically for a liquid over-feed evaporator the refrigerant temperature at exit is slightly lower than that at the entrance, due to the pressure drop across the evaporator with a corresponding saturation temperature reduction. However in an actual test, superheat at the evaporator exit could sometimes be observed. This could be explained by the fact that the refrigerant mixture downstream of the evaporator was not in equilibrium across the pipe cross-section while the temperature sensor probes were positioned at the pipe centre line and measured the vapour-phase temperature. In the present study most data have inlet and outlet temperature differences less than 0.2°C for R134a and 0.3 °C for R507A.

- For pressure drop data, the differential pressure transmitter had a positive reading.
  Differential pressure transmitters are designed for the measurement of positive pressure differences. When the transmitter works at low or even negative pressure differences, the readings are expected to have high errors. In the tests carried out in this study, the actual pressure drop across the evaporator was always positive, however the measured value could be negative because the liquid leg in the feeding line, which is downstream of the transmitter high side connection point (see Figure 3.11), imposed a pressure rise for the measurements. This situation was encountered only in a few occasions for the tests with R134a at very low flow rates.

The experimental data were reduced to obtain the refrigerant-side heat transfer coefficient and frictional pressure drop. The effect of flow maldistribution, for both water and refrigerant streams, was not considered. For the effect of the lubricant oil in the system no detailed information is available. An oil separator was installed in the system, however, oil finds its way into the evaporator no matter how efficient the separator is. Oil concentration less than 2% might be expected in the evaporators. All thermo-physical properties and the performance assessment of the refrigerant/oil mixture have been based on the assumption of pure refrigerant.

6.2 Test Procedure

The test facility of the evaporators has two circuits: the refrigerant circuit, with refrigerant flowing upwards on one side of the exchanger and the water circuit, with water flowing downwards on the other, forming a counter-current flow arrangement. The two circuits were designed to provide stable controlled conditions in the desired ranges of temperatures, fluid flows, and thermal capacities. Water was supplied from the water sump at environmental temperatures. Due to the large volume of the water sump which exceeds 40 m^3, the water supplying temperature changes very slightly on a daily basis, normally within 0.1°C. Details of all the measurements and sensor mounting arrangements are given in Section 3.5.2. The evaporator performance tests were carried out on the three BPHE units individually, as summarized in Table 6.2.

The effects of three parameters, namely the imposed heat flux q, the refrigerant mass flux G_r, and the outlet vapour quality x_{out}, on the evaporator heat transfer and pressure drop performance were investigated. Different heat fluxes were obtained mainly by controlling the condenser air flow rate and also with operating the surge drum feeding valve and the compressor back pressure regulator. At each fixed heat flux, the refrigerant mass flux G_r was adjusted from maximum to minimum as allowed by the system capacity. Different outlet vapour fractions x_{out} resulted according to the different flow rates. The effect of the system pressure P was not investigated due to its small range in the current tests. P was determined by the water supply temperature at the given cooling loads. During the tests the water flow rate was maintained at fixed values, this helped to improve the consistency in the calculation of the cooling load and water-side heat transfer coefficient. All data were obtained under steady-state conditions, confirmed by observing a stable water outlet temperature changing by not more than 0.1 °C during approximately a 10 minute time period. The experimental

Table 6.2: Summary of evaporator performance tests of the three PHE units

Refrigerant	Test	PHE Chevron angle	No. of data points	G_w kg/(m^2s)	$T_{w,in}$ °C	G_r kg/(m^2s)	T_{sat} °C	q kW/m^2
R134a	1	28°/28°	58	201-203	13.7-16.0	5.6-30.3	5.9-12.2	1.85-6.10
	2	28°/60°	58	200-203	13.8-15.9	5.7-27.1	6.7-12.8	1.86-6.44
	3	60°/60°	59	200-203	13.8-15.9	5.8-27.0	7.4-13.0	1.86-6.50
R507A	4	28°/28°	22	200-204	16.3-16.6	16.0-29.8	7.8-10.6	3.8-6.4
	5	28°/60°	18	200-204	16.2-16.3	16.0-31.4	8.6-10.9	3.8-6.7
	6	60°/60°	20	202-203	16.2-16.3	17.6-31.4	9.2-12.6	4.7-6.9

measurements and some selected calculated parameters are given in *Appendix F*. Operating instructions of the refrigerant evaporator test facility can be found in *Appendix N*.

6.3 Data Reduction

All experimental data for the analysis were processed by MATLAB codes specially developed for the current study. Water properties were evaluated according to a NIST Standard Reference Database (Lemmon et al., 2005) at the bulk mean temperature:

$$T_{\text{mean}} = \tfrac{1}{2}\left(T_{\text{in}} + T_{\text{out}}\right) \tag{6. 1}$$

For the refrigerants the physical properties were evaluated at the saturation temperature T_{sat}, according to *ASHRAE Handbook 2005*. Both the water and refrigerant property values were determined by linear interpolation from property tables as provided by the reference sources. A sample calculation, via the methods provided in this section, of the data reduction is given in *Appendix G*.

6.3.1 Flow Boiling Heat Transfer

The evaporator cooling load is calculated by:

$$\dot{Q} = \dot{m}_{\text{w}} c_{\text{p, w}} \left(T_{\text{w, in}} - T_{\text{w, out}}\right) \tag{6. 2}$$

The refrigerant vapour quality at the evaporator inlet is assumed as zero for all tests, and the vapour quality at exit is determined from

$$x_{\text{out}} = \frac{\dot{Q}}{\dot{m}_{\text{r}} i_{\text{fg}}} \tag{6. 3}$$

The overall heat transfer coefficient U for the evaporators is found from

$$U = \frac{\dot{Q}}{A \Delta T_{\text{LM}}} \tag{6. 4}$$

where ΔT_{LM} is the log mean temperature difference between the two streams:

$$\Delta T_{\mathrm{LM}} = \frac{\Delta T_{\max} - \Delta T_{\min}}{\ln\left(\frac{\Delta T_{\max}}{\Delta T_{\min}}\right)} \tag{6. 5}$$

Equation (6.5) applies to all types of heat exchanger. For the current evaporators with counter-current flow, the temperature differences are

$$\begin{aligned} \Delta T_{\max} &= T_{\mathrm{w,\,in}} - T_{\mathrm{r,\,out}} \\ \Delta T_{\min} &= T_{\mathrm{w,\,out}} - T_{\mathrm{r,\,in}} \end{aligned} \tag{6. 6}$$

The refrigerant at the evaporator inlet is in the liquid state and slightly subcooled. This subcooling is due to the liquid leg in the feeding line (see Figure 3.11) which imposes additional pressure on the saturated liquid flowing downstream from the surge drum. The evaporator should strictly be regarded as having two regions: a single-phase region and a two-phase flow boiling region. The two regions have different temperature profiles and should be treated separately. The partition of the two regions follows the procedure similar to that given in *Appendix M*, first by assuming single-phase heat transfer coefficients for the refrigerants. In the real experiment in the current study, however, the heat transfer rate in the single-phase region, $\dot{Q}_{\mathrm{subcooling}}$, is very small, being less than 1% of the total cooling load for most cases. Therefore, the evaporator is treated as a single region of two-phase saturation boiling and Equation (6.5) applies for the whole exchanger. $\dot{Q}_{\mathrm{subcooling}}$ is calculated by

$$\dot{Q}_{\mathrm{subcooling}} = \dot{m}_{\mathrm{r}} c_{\mathrm{p,\,r}} \Delta T_{\mathrm{sub}} \tag{6. 7}$$

where ΔT_{sub} is the degrees of subcooling, taken as the corresponding temperature difference caused by the static pressure of the liquid leg. The magnitude of ΔT_{sub} is 0.6 °C for R134a and 0.3 °C for R507A at the liquid leg height of 0.66 m. Additionally, the saturation temperature T_{sat} is used instead of the inlet temperature $T_{\mathrm{r,\,in}}$, for the calculation of the log mean temperature difference in Equation (6.6), considering that the two-phase region accounted for more than 99% of the heat transfer. The saturation temperature is calculated by:

$$T_{\mathrm{sat}} = T_{\mathrm{r,\,in}} + \Delta T_{\mathrm{sub}} \tag{6. 8}$$

The refrigerant-side heat transfer coefficient is now determined from:

$$\frac{1}{h_{\mathrm{r}}} = \frac{1}{U} - \frac{1}{h_{\mathrm{w}}} - R_{\mathrm{wall}} - R_{\mathrm{f}} \tag{6. 9}$$

In this equation the water-side heat transfer coefficient h_w is determined from Equation (4.22), as obtained from the single-phase tests with water. Values for the water side fouling factor R_f are taken as recommended by Panchal and Rabas (1999), given in Table 2.6. R_{wall} is the wall thermal resistance defined by:

$$R_{wall} = \left(\frac{\delta}{k} \right)_{wall} \tag{6. 10}$$

6.3.2 Two-phase Pressure Drop

Components of the Measured Pressure Drop

The measured pressure drop ΔP_{meas} consists of many components, including pressure drops inside the channel ΔP_{PHE}, frictional pressure losses through the pipeline with all its bends and fittings, and elevation components of any vertical lines between the sensor's two connections. For the pressure measurement arrangement, Figures 3.5 and 3.11 refer. ΔP_{meas} is expressed by:

$$\Delta P_{meas} = \Delta P_{PHE} + \Delta P_{pipe,\,fric} + \Delta P_{pipe,\,local} + \Delta P_{pipe,\,elev} \tag{6. 11}$$

where the total pressure drop across a plate heat exchanger is given by:

$$\Delta P_{PHE} = \Delta P_{fric} + \Delta P_{port} + \Delta P_{acce} + \Delta P_{elev} \tag{6. 12}$$

In the above equations, the frictional pressure drop across the channel, ΔP_{fric}, is the purpose of investigation, and is usually the major part of the measured value of pressure drop. To obtain ΔP_{fric}, all other components have to be evaluated and extracted from ΔP_{meas}. In this study the acceleration and gravitational pressure losses inside the PHE, ΔP_{acce} and ΔP_{elev}, are evaluated theoretically by the homogeneous model with Equations (2.53 b) and (2.53 c), respectively. The pressure drops across the inlet and outlet ports and manifolds are evaluated using the empirical correlation suggested by Shah and Focke (1988), as given by Equation (4.14). This equation was initially proposed for single-phase water, but has been adopted by many investigators for the estimation of two-phase pressure drop across the ports and manifolds in PHE channels assuming homogeneous flow. Since there is no better information available for the calculation of this pressure loss, this method is adopted here and ΔP_{port} is calculated by:

$$\Delta P_{\text{port}} = 0.75\left[\left(\frac{G_{\text{port}}{}^2}{2\rho}\right)_{\text{in}} + \left(\frac{G_{\text{port}}{}^2}{2\bar{\rho}}\right)_{\text{out}}\right] \tag{6. 13}$$

where $\bar{\rho}$ is the two-phase mean density defined by Equation (2.49).

Lengths of the evaporators' refrigerant feed and return lines are given schematically in Figure 6.1. Calculation of pressure drops in the feeding line follows the same procedure given by Section 4.3.2, as the refrigerant is in the liquid state in this line. For the return line which contains a two-phase mixture of the refrigerant, the frictional pressure drop of the pipe is calculated using the classic Lockhart-Martinelli method as given in Section 2.3.4. For local losses across bends and fittings, the methods summarized by Collier and Thome (1994) are used. This calculation method for local pressure losses is based on the separate flow model and is very similar to the Lockhart-Martinelli method for straight pipes. The two-phase pressure drop across a pipe fitting which does not change flow section (i.e., no enlargement or contraction downstream of the fitting) is given by:

$$\frac{\Delta P_{\text{tp}}}{\Delta P_{\text{f}}} = 1 + \frac{C}{X} + \frac{1}{X^2} \tag{6. 14}$$

where C is the Chisholm parameter given by:

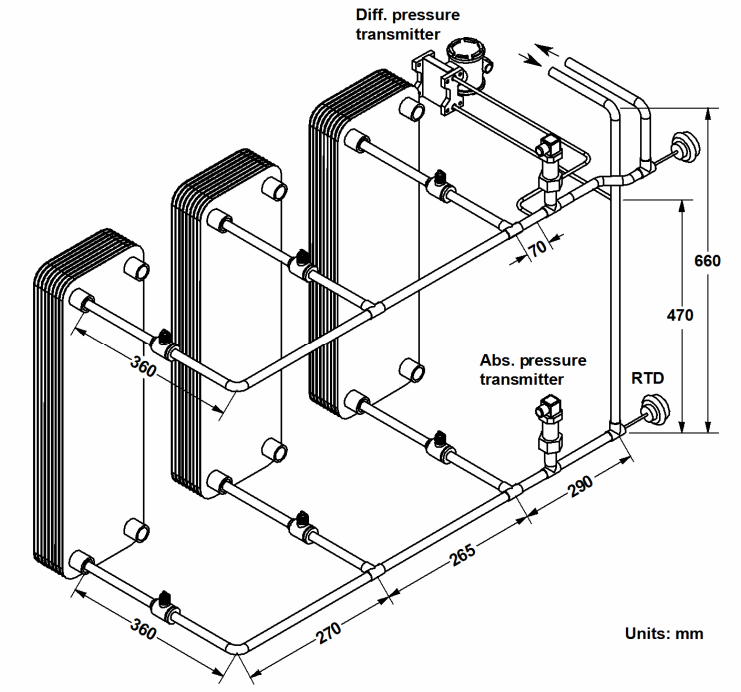


Figure 6.1: Lengths of the feed and return pipelines

$$C = \left[\lambda + (c_2 - \lambda)\left(1 - \frac{\rho_g}{\rho_f}\right)^{0.5} \right] \left[\left(\frac{\rho_f}{\rho_g}\right)^{0.5} + \left(\frac{\rho_g}{\rho_f}\right)^{0.5} \right] \qquad (6.15)$$

where c_2 and λ are constants to be determined for different types of fittings. X in Equation (6.14) is the Martinelli parameter determined by Equation (2.61). ΔP_f is the pressure drop assuming only the liquid fraction flowing in the pipe. There are two methods available to calculate ΔP_f , both commonly seen for calculation of single-phase pressure loss across pipeline fittings:

$$\begin{aligned} \Delta P_{local} &= K\left(\tfrac{1}{2}\rho u^2\right) \qquad (a) \\ \Delta P_{local} &= f \cdot \left(\frac{L}{d}\right)_{eq} \cdot \left(\tfrac{1}{2}\rho u^2\right) \qquad (b) \end{aligned} \qquad (6.16)$$

The parameter K in method (a) (Equation 6.16 a) is called the "resistance coefficient", and $(L/d)_{eq}$ in method (b) (Equation 6.16 b)is called the "equivalent length in pipe diameters". In the present study method (b) is adopted with values of $(L/d)_{eq}$ taken from those recommended by Avallone and Baumeister (1996), and Equation (6.16 b) is rewritten as:

$$\Delta P_f = f_f \cdot \left(\frac{L}{d}\right)_{eq} \cdot \frac{G^2(1-x)^2}{2\rho_f} \qquad (6.17)$$

For the fittings and bends in the current experimental apparatus, values for c_2 and λ in equation (6.15) and $(L/d)_{eq}$ in Equation (6.17) are summarized in Table 6.3.

Table 6.3: Values of $(L/d)_{eq}$, c1 and λ for pipe fittings and bends

		$(L/d)_{eq}$	c_2	λ
	Tee branch	60	1.75	1
	Tee run	20	1.5	1
	Bend	30	2.0	1
	Ball valve	20	1.5	1

Friction Factor and the Chisholm Parameter

Once the frictional pressure drop is obtained, the two-phase friction factor f_{tp} and

the Chisholm parameter C can be calculated using the homogeneous model and the Lockhart-Martinelli method, respectively. Both methods were tried in this study to find which one is more suitable to the experimental data.

f_{tp} is calculated straightforwardly assuming homogeneous flow:

$$f_{tp} = \frac{\Delta P_{fric} / L_p}{G^2 / 2\bar{\rho} d_h} \tag{6. 18}$$

where $\bar{\rho}$ is the two-phase mean density calculated by Equation (2.49) with mean vapour quality of $x_m = 0.5\ (x_{in} + x_{out})$.

As reviewed in Section 2.3.4, the Lockhart-Martinelli method is based on adiabatic flow for which the vapour quality x is a constant. To apply this method for refrigerant evaporators where x changes along the channel length, local values of x have to be assumed and a stepwise integration of the pressure gradient obtained at local x is needed to obtain the total pressure drop. The assumption of linear change of x along the channel length is the simplest option and is used in this study. Sterner and Sunden (2006) also adopted this treatment. The Lockhart-Martinelli method essentially consists of the determination of the ϕ_f - X relationship for irregular channels, where the Martinelli parameter X is a function of local vapour quality. The ϕ_f - X relationship can be found experimentally and can be given:

a) using the Chisholm parameter C, i.e., Equation (2.65)
b) in graphic form
c) in other equation forms.

Of these the method (a) is popular and is regarded as standard for circular channels. The latter two require the measurement of pressure drops at local x, which is a common practice for adiabatic flow tests but is not practicable for tests on evaporators where usually only overall measurements are taken with x changing in a certain range. For these reasons the method (a) is adopted in this study and the Chisholm constant C is obtained via a MATLAB program code following the procedure:

1. For numerical integration, artificially divide the channel length L_p into N parts (N = 1000 in this study). Assume linear change of x along L_p.

$$\frac{dx}{dz} = \frac{x_{out} - x_{in}}{L_p} \tag{6. 19}$$

2. At each local x (one of 1000), calculate the Martinelli parameter X by its original definition:

$$X = \sqrt{\frac{dP_{\text{fric, f}}}{dz} / \frac{dP_{\text{fric, g}}}{dz}} \tag{6. 20}$$

where, $\frac{dP_{\text{fric, f}}}{dz} = f_{\text{f}} \cdot \frac{G^2(1-x)^2}{2\rho_{\text{f}} d_{\text{h}}}$, $\frac{dP_{\text{fric, g}}}{dz} = f_{\text{g}} \cdot \frac{G^2 x^2}{2\rho_{\text{g}} d_{\text{h}}}$

$f_{\text{f}} = \frac{a}{\text{Re}_{\text{f}}^{\,b}}$, $f_{\text{g}} = \frac{a}{\text{Re}_{\text{g}}^{\,b}}$, values for a and b are taken from Equation (4.24), as in the friction factor correlation obtained from the single-phase water tests. The same correlation is used for liquid and vapour phases.

$\text{Re}_{\text{f}} = \frac{G(1-x)d_{\text{h}}}{\mu_{\text{f}}}$, $\text{Re}_{\text{g}} = \frac{Gxd_{\text{h}}}{\mu_{\text{g}}}$.

3. Find the Chisholm parameter C.

3.1 Assume an initial value of C

3.2 Calculate the two-phase friction pressure drop

$$\phi_{\text{f}}^{\,2} = 1 + \frac{C}{X} + \frac{1}{X^2} \tag{6. 21}$$

$$\frac{dP_{\text{fric}}}{dz} = \phi_{\text{f}}^{\,2} \cdot \frac{dP_{\text{fric, f}}}{dz} \tag{6. 22}$$

$$\Delta P_{\text{fric}} = \int_0^{L_{\text{p}}} \frac{dP_{\text{fric}}}{dz} \cdot dz = \frac{L_{\text{p}}}{x_{\text{out}} - x_{\text{in}}} \int_{x_{\text{in}}}^{x_{\text{out}}} \phi_{\text{f}}^{\,2} \cdot \frac{dP_{\text{fric, f}}}{dz} \cdot dx \tag{6. 23}$$

Alternatively, C could be determined using $\phi_{\text{g}}^{\,2}$ and Equation (2.64), with the same results, as verified in this study.

3.3 Compare the calculated ΔP_{fric} with experimental data, if the two differ more than a preset value say 0.5%, modify the value of C and repeat step 3.2 until the right value of C is found. This is an iteration approach. Alternatively, as used in the current program, C is found by trial-and-error, values of C were tried starting from 0 and growing upwards with a step of 0.01 until the calculated ΔP_{fric} exceeds the experimental value, and the last smallest C was chosen. In the current program the discrepancy between the calculated ΔP_{fric} and the experimental data is smaller than 0.5%.

6.4 Uncertainty Analysis

For the experimental data and calculated parameters, the uncertainty analysis was carried out according to the ISO (ISO/1995) method. This method, along with the ASME (ANSI/ASME PTC 19.1, 2005) method, which are among the most widely used, is introduced in *Appendix I*. Extended details of the uncertainty analysis for the refrigerant evaporator test results are given in *Appendix L*. For clarity, only a summary of the analysis results is presented here in Table 6.4.

Table 6.4: Summary of experimental measurement uncertainties

Parameter	Max. Abs. percentage uncertainty, $\left[u(\phi_i)/\phi_i\right]_{max}$					
	R134a Test			R507A Test		
	β = 28°	β =28°/ 60°	β = 60°	β = 28°	β =28°/ 60°	β = 60°
Water mass flow rate, $\dot{m}_w$, (kg/s)	0.43 %	0.42 %	0.42 %	0.42 %	0.42 %	0.42 %
Refrigerant mass flow rate, $\dot{m}_r$ (kg/s)	1.8 %	1.9 %	2.0 %	0.5 %	0.6 %	0.9 %
Heat flux, q (W)	4.3 %	4.3 %	4.3 %	3.4 %	3.4 %	3.5 %
ΔT_{LM} (°C)	1.9 %	2.3 %	2.9 %	1.2 %	1.9 %	2.3 %
Overall heat transfer coefficient, U, (W/m^{2}K)	4.7 %	4.9 %	5.1 %	3.6 %	3.9 %	4.2 %
Refrigerant heat transfer coefficient, h_r, (W/m^{2}K)	7.6 %	7.0 %	6.7 %	6.5 %	7.9 %	8.6 %
Outlet vapour quality, x_{out}	4.6 %	4.6 %	4.5 %	3.3 %	3.3 %	3.4 %
Frictional pressure drop, ΔP_{fric}, (Pa)	12.4 %	12.1 %	11.6 %	12.4 %	12.5 %	12.8 %
Two-phase friction factor, f_{tp}	12.5 %	12.2 %	11.7 %	12.5 %	12.6 %	12.9 %

6.5 Results and Discussion

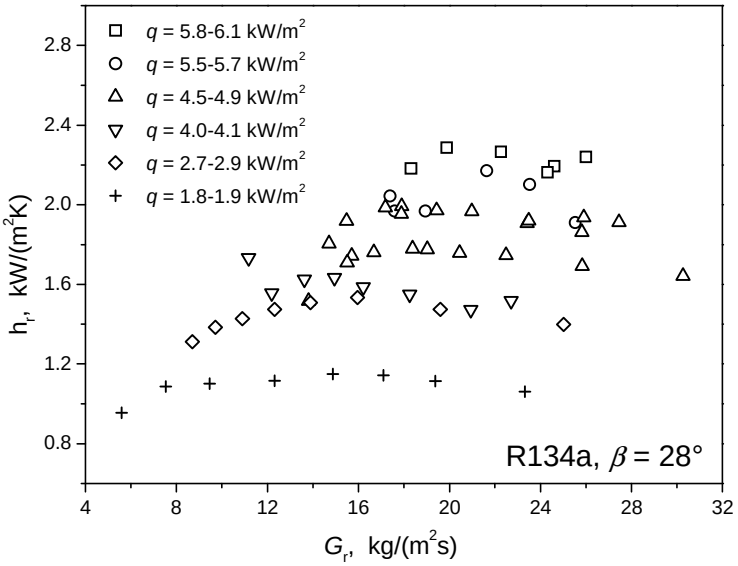
The experimental results of the thermal and hydraulic performance of the three BPHE units operating as liquid over-feed evaporators are reported and discussed in this section. Calculated results can be found in *Appendix F*.

6.5.1 Heat Transfer Characteristics

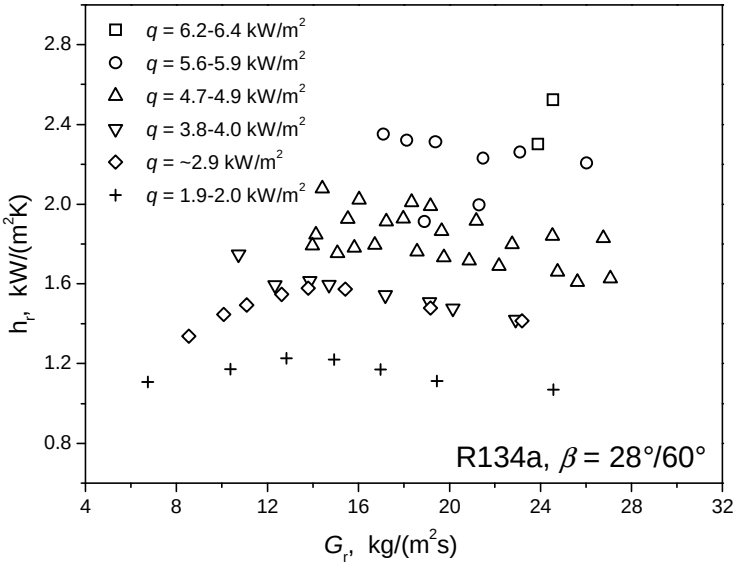
The primary interest in the heat transfer performance analysis is the refrigerant flow boiling heat transfer coefficient h_r. The purpose of the analysis is the quantitative evaluation of this parameter, and its dependence on relevant flow properties (mainly q, x, G and P_{sat}), channel geometry (primarily the chevron angle β), and the refrigerant thermo-physical properties. The experimental data of h_r are presented in Figures 6.2 and 6.3 for R134a and R507A tests, respectively, plotted versus the refrigerant mass flux rate G_r, at fixed heat fluxes. It is observed that for both refrigerants in the test range, the heat transfer coefficient shows a strong dependence on the heat flux, and a relatively weak dependence on mass flux. The two refrigerants showed similar heat transfer coefficients at comparable heat fluxes in the range of 1.9 - 6.9 kW/m^2.

It is also observed, as seen in Figures 6.2 and 6.3, that the chevron angle exerted a very small effect on the flow boiling heat transfer coefficient at comparable q and G_r. It is known that the chevron angle is the most important geometrical parameter for single-phase heat transfer in PHE's, but in the current tests, the flow boiling heat transfer coefficients for different chevron angle units are quite close to each other at same heat fluxes. The unit with the highest chevron angle of 60° does not show improved heat transfer rates compared with that with the lowest angle of 28°. This indicates an insignificant forced convection contribution to the total heat transfer rate.

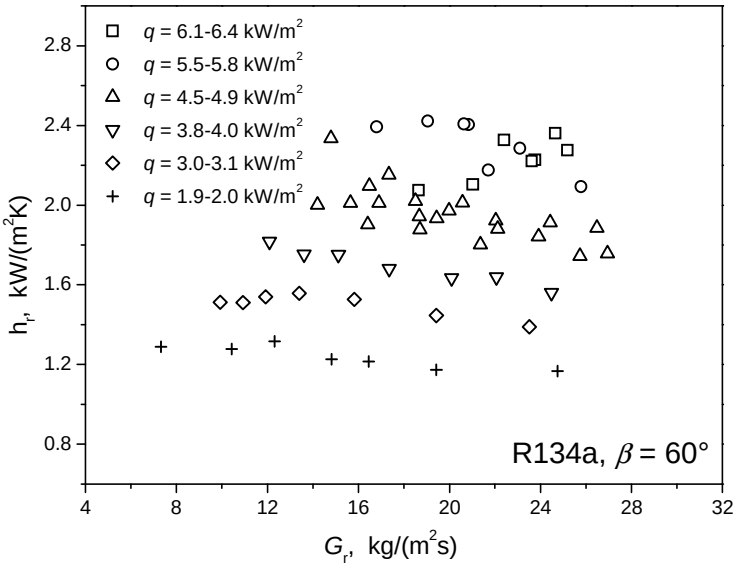
The influence of the vapour quality x on the refrigerant heat transfer coefficient is not explicitly shown in Figures 6.2 and 6.3. As stated earlier, the two parameters of refrigerant mass velocity G_r and the outlet vapour quality x_{out} were coupled in the present experiments, as tests were carried out at fixed values of heat flux for which the outlet vapour quality changed correspondingly with the mass flux. The relationship of the two parameters is demonstrated by Equation (6.3). Quantitative evaluations of the influence of G_r and x_{out} on the refrigerant heat transfer coefficient h_r could not be individually obtained due to this restriction. Nevertheless, all data obtained in the testing range indicated that this influence is insignificant. For example, in the test of R134a with β = 28°, at an imposed heat flux of 4.0-4.1 kW/m^2, h_r changed in the narrow range of 1.52 – 1.73 kW/(m^{2}K) when G_r varied from 22.7 to 11.2 kg/(m^{2}s) and x_{out} from 0.44 to 0.92. Figure 6.4 shows the R134a experimental data of h_r at q ~ 4 kW, plotted versus x_{out}., and a weak dependence of h_r on x_{out} can be seen for all three units with different chevron angles. It is understood that at higher mass flux and vapour quality the two-phase mixture flows at higher velocity, which promotes convective heat transfer. In the current experiment this effect is relatively small, and again it indicates insignificant contribution of forced convection contribution to the total heat transfer rate.



(a)



(b)



(c)

Figure 6.2: R134a experimental h_r vs. G_r at various heat fluxes

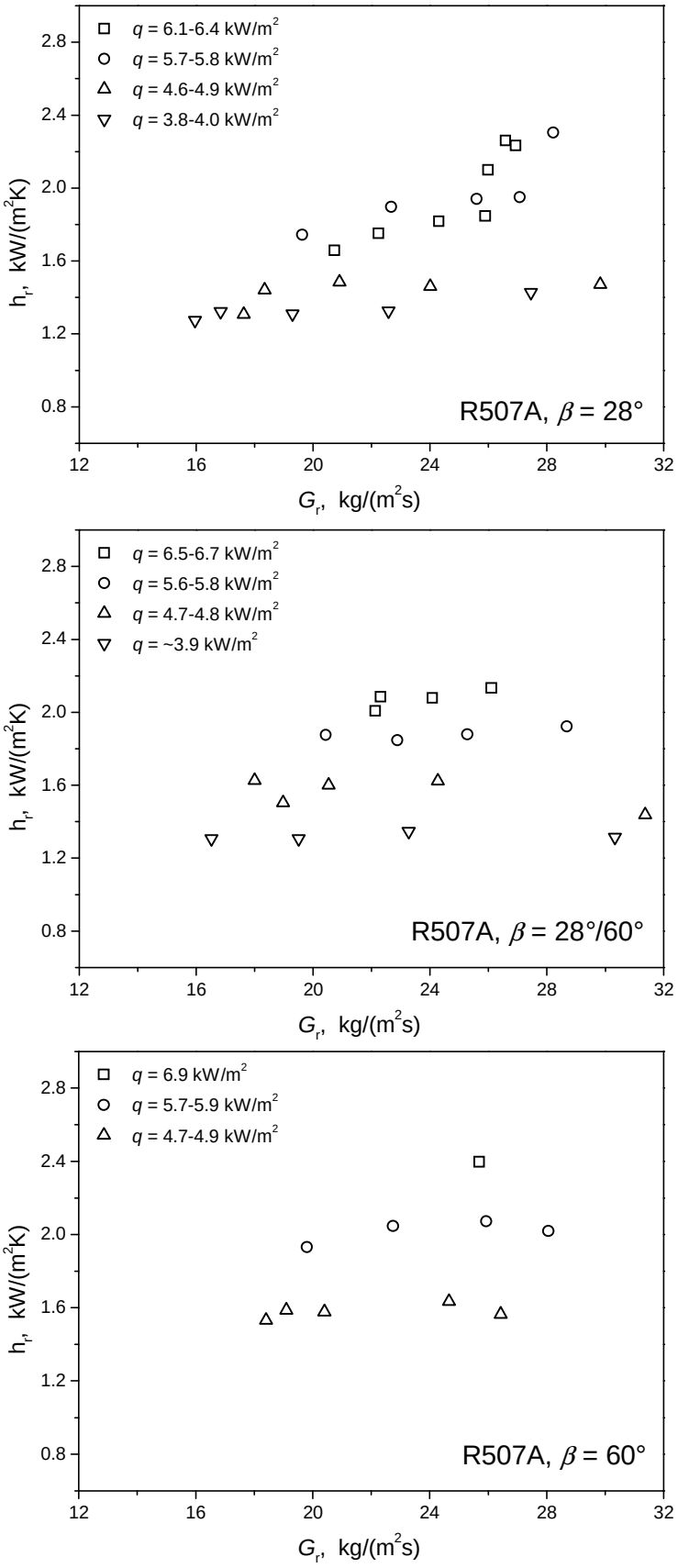


Figure 6.3: R507A experimental h_r vs. G_r at various heat fluxes

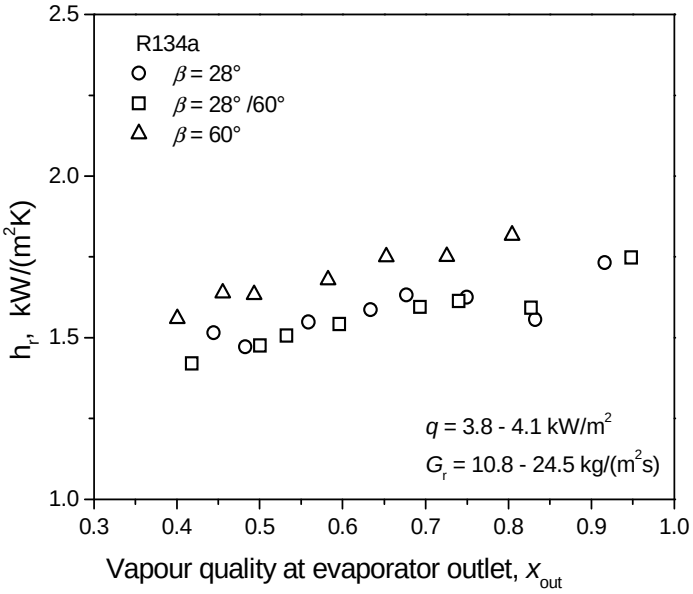


Figure 6.4: Influence of x_{out} on h_r at fixed heat flux

The experimental data of h_r are plotted versus the heat flux q in Figures 6.5 and 6.6, for R134a and R507A respectively. For both refrigerants in the test range of G_r, h_r increases with q and the trend shows a strong dependence. Also presented in these figures, the experimental data of R134a and R507A are compared with three selected pool boiling correlations including the Stephan and Abdelsalam (1980) correlation, the Cooper (1984) correlation and the Gorenflo (1993) correlation [1]. The comparison is for the purpose of finding out whether the heat transfer process in the PHE evaporator units is nucleate-boiling dominated. These three reference correlations are given by Equations (2.4) through (2.6), and are among the most widely recognized in the literature. It is observed that for R134a, predictions by the three correlations are quite close to each other. Of these correlations, The Cooper (1984) correlation was developed for nucleate pool boiling on horizontal plane surfaces, the author suggested that for boiling on horizontal copper tubes, h is to be multiplied by a correction factor of 1.7. While no resemblance could be recognized between the two type of channels, the Cooper (1984) pool boiling correlation for horizontal copper tubes (the original correlation multiplied by 1.7) fits rather well with the current experimental data of R134a flow boiling in PHE evaporators, with a mean absolute error of 7.5%., defined by

[1] In the calculation using the three correlations, all physical properties are evaluated at T_{sat} = 8.6 °C for R134a and 9.1 °C for R507A, respectively, which are the average values of the tested ranges of saturation temperature.

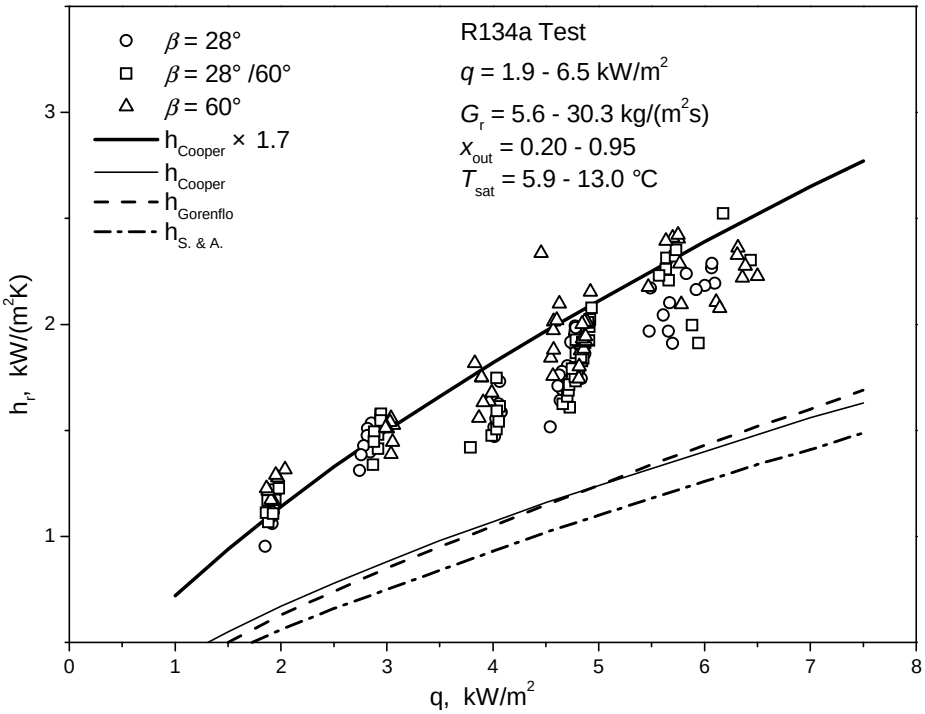


Figure 6.5: R134a flow boiling heat transfer coefficient versus heat flux

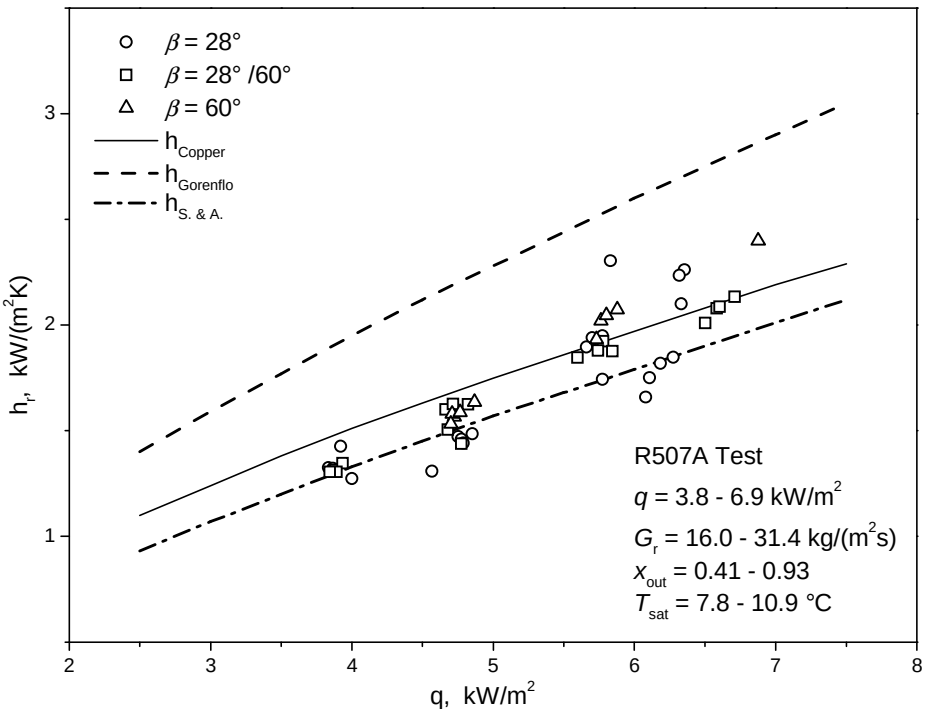


Figure 6.6: R507A flow boiling heat transfer coefficient versus heat flux

$$e_{\mathrm{m}} = \frac{1}{n} \cdot \sum \left(\left| \frac{h_{\mathrm{corr}} - h_{\mathrm{expe}}}{h_{\mathrm{expe}}} \right| \right) \tag{6. 24}$$

where n is the number of data points. For R507A, the three correlations showed greater disagreement on the predicted heat transfer coefficient, with the Gorenflo (1993) correlation giving much higher h_{r} than the other two. R507A is a relatively new refrigerant which is not covered by the original databases of these three correlations. The original Cooper correlation (Equation 2.5) fits reasonably well with the R507A data, with a mean absolute error of 9.3%.

It is observed that even though the data for R134a and R507 could not be all correlated by a single pool boiling correlation, the trend of h_{r} with q is well predicted. Along with the observation that forced convection heat transfer has an insignificant contribution to the total heat transfer rates, it might be concluded at this point that the flow boiling process in PHE liquid over-feed evaporators is nucleate-boiling dominated.

6.5.2 Pressure Drop Characteristics

The pressure drop across a refrigerant evaporator has many contributions, among which the two-phase frictional pressure drop is by far the largest. It is the purpose of this study to evaluate this pressure drop and find its dependency on relevant flow and geometrical parameters.

In general, the two-phase frictional pressure drop of the refrigerants showed strong dependence on mass flux and vapour quality, and increased with higher chevron angles. This is distinct from the heat transfer coefficient results on which the flow parameters and chevron angle showed an insignificant influence. The frictional pressure losses of both refrigerants were observed to increase almost linearly with the homogeneous two-phase kinetic energy per unit volume, $E_{\mathrm{k,\,tp}}$, which is defined by

$$E_{\mathrm{k,\,tp}} = \frac{G^2}{2\rho_{\mathrm{m}}} \tag{6. 25}$$

where ρ_{m} is the homogeneous two-phase mean density calculated by Equation (2.49) with mean vapour quality x_{m}. For a clearer perception of the term $E_{\mathrm{k,\,tp}}$, Equation (6.25) is expanded to:

$$E_{\mathrm{k,\,tp}} = \frac{G^2}{2\rho_{\mathrm{f}}}\left[\left(\frac{\rho_{\mathrm{f}}}{\rho_{\mathrm{g}}}-1\right)x_{\mathrm{m}}+1\right] \qquad (6.\ 26)$$

where $x_{\mathrm{m}} = 0.5\left(x_{\mathrm{in}} + x_{\mathrm{out}}\right)$.

The experimental data of frictional pressure drop ΔP_{fric} are plotted versus $E_{\mathrm{k,\,tp}}$ in Figure 6.7, for all R134a and R507 data. A relatively linear relationship is clearly seen. This relationship between ΔP_{fric} and $E_{\mathrm{k,\,tp}}$ was also reported by Jassim et al. (2005) for R134a adiabatic flow in a single chevron-type channel with β = 60° in the whole range of x = 0 - 1, and by Longo and Gasparella (2007) from tests on R134a, R410A and R236fa evaporation in a BPHE with β = 65 °. The current data cover a wider range of chevron angles. All data showed the same trend and for each refrigerant the frictional pressure drop is higher at higher chevron angles. From an analytical point of view, the relatively linear increase of frictional pressure drop with the kinetic energy suggests that an inertial effect is dominating, rather than viscous effects. This phenomenon resembles that of single-phase pipe flow in the "fully rough turbulent flow" region. It is a well known fact that in single-phase pipe flow when the Reynolds number exceeds a certain transition

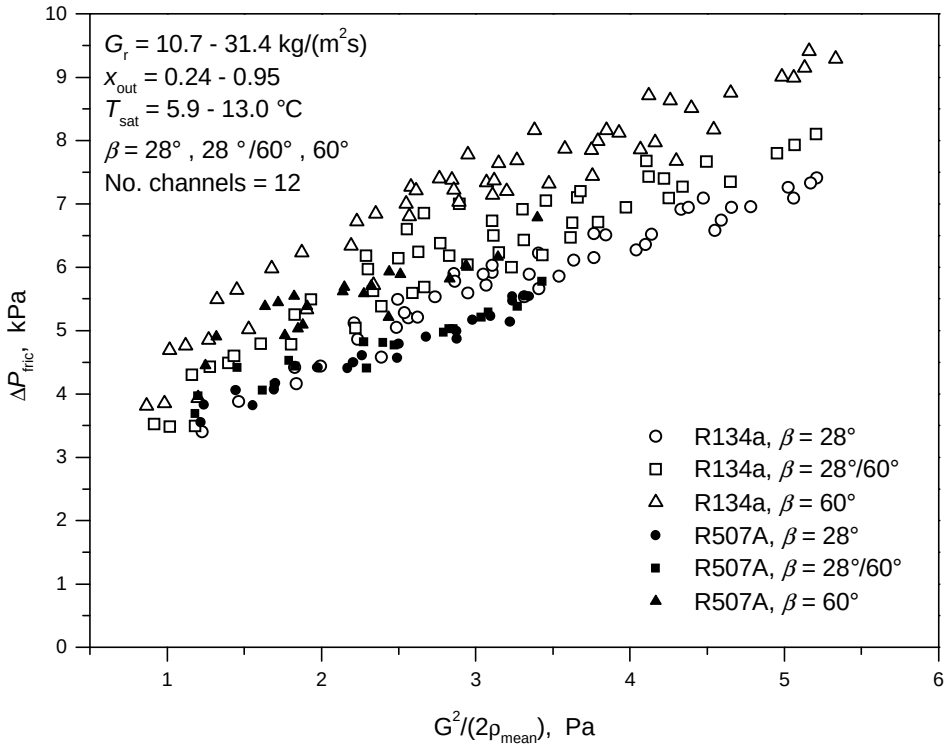


Figure 6.7: R134a and R507A experimental data of frictional pressure drop versus two-phase kinetic energy for

criterion, the frictional pressure loss becomes linearly dependent on the kinetic energy $\rho u^2/2$. The criterion of this transition starts earlier for rougher pipes, as demonstrated clearly by the Moody Chart. For single-phase flow the corrugated channels of PHE's could be considered as a rough tube, whose roughness increases with increasing chevron angle (Heavner et al., 1993). It seems that this assumption has also found some validation from the current data of two-phase frictional pressure drops. Also, the strong relationship between the frictional pressure drop and the homogeneous two-phase kinetic energy indicates a potential application of the homogeneous flow model for this type of channel.

6.6 Conclusion

Experimental results of refrigerant heat transfer and pressure drop performance of three BPHE units using R134a and R507A are presented and discussed. The units were arranged in parallel but were operated and tested individually as liquid over-feed evaporators.

The heat transfer data suggest a nucleate boiling-dominated process in the evaporators. For both refrigerants in the test range, the heat transfer coefficient showed a strong dependence on the heat flux, and a weak dependence on mass flux, vapour quality, and the chevron angle. The observed refrigerant-side heat transfer coefficients are essentially of the same magnitude for the two refrigerants, being 1 - 2.5 kW/(m^{2}K) in the test range of q at 1.9 - 6.9 kW/m^2. On the other hand, the two-phase frictional pressure drop of the refrigerants showed strong dependence on mass flux and vapour quality, and increased substantially with higher chevron angles. The frictional pressure loss with both refrigerants was observed to increase almost linearly with the homogeneous two-phase kinetic energy per unit volume, $G^2/2\rho_m$.

CHAPTER 7

DEVELOPMENT OF THERMAL-HYDRAULIC CORRELATIONS FOR PHE EVAPORATORS

7.1 Introduction

Correlations predicting the refrigerant flow boiling heat transfer and two-phase frictional pressure drop in PHE liquid over-feed evaporators are developed in this chapter. The heat transfer correlations are based on 222 data points, covering the experimental data of R134a, R507A and the field testing data of ammonia and R12. The pressure drop correlations are based on 206 data points covering R134a and R507A, and two methods are considered: the homogenous method and the Lockhart-Martinelli method.

7.2 Flow Boiling Heat Transfer

The Cooper (1984) pool boiling correlation can fit rather well with the experimental data of R134a and R507A, as given in Chapter 6, with different correction factors for the two refrigerants tested, being 1.7 for R134a and 1.0 for R507A, respectively. The application of this particular pool boiling correlation for PHE evaporators has been suggested in a few other occasions, for example, Claesson and Palm (1999) found this correlation suitable for a R22 direct expansion evaporator when multiplied by a factor of 1.5. Also, the field measurement data obtained for ammonia and R12 PHE water chillers, as presented in Chapter 5, suggested a leading coefficient of 1.14 for both refrigerants. It is the task of this study to find a general correlation which covers more than one refrigerant and which must be able to predict the refrigerant boiling heat transfer with reasonable accuracy.

In the development of a general correlation of many experimental data, various approaches are possible, for example, to improve or modify existing correlations

considered appropriate or suitable for the data at hand, or to derive new forms of correlation using dimensional analysis then adapt the constants and exponents using a statistical regression methods. Some difficulties are encountered when trying the first approach:

1. There is no flow boiling heat transfer correlation for PHE channels which has gained wide validation and approval. Consequently no correlation developed for PHE channels to date could be regarded as sufficiently sound for general use.
2. Conventional flow boiling correlations developed for regular pipes showed inconsistency with the current experimental observations. As pointed out earlier, it is observed in the current study that the flow boiling process in the liquid over-feed PHE evaporators is nucleate boiling-dominated. As such, conventional forms of correlations are not entirely applicable to the current case where the contribution of forced convection is negligibly small.
3. On the other hand, no pool boiling correlation could be modified to accommodate all data obtained from different refrigerants, although the general trend of h_r versus q could be predicted by those correlations.

Consequently, the second approach is adopted in this study, i.e., correlating the experimental data by means of statistical regression. This approach is essentially finding the best fitting constants and exponents of a known number of non-dimensional groups, obtained from dimensional analysis. It is understood that the heat transfer process is characterized by a number of flow and heat transfer parameters including q, T_{sat}, G, x, P, and fluid physical properties including ρ, μ, c_p, k, σ, i_{fg}. Now a set of non-dimensional groups is obtained from those variables, using dimensional analysis:

$$X_1 = \frac{qd_0}{k_f T_{sat}},\ X_2 = \frac{i_{fg} d_0^{\,2}}{\alpha_f^{\,2}},\ X_3 = \mathrm{Re}_f = \frac{Gd_h}{\mu_f},\ X_4 = \mathrm{Re}_{tp} = \frac{Gd_h}{\mu_{tp}}$$

$$X_5 = \frac{\rho_f}{\rho_g},\ X_6 = \mathrm{Pr} = \frac{\mu_f c_{p,f}}{k_f},\ X_7 = \mathrm{Nu} = \frac{hd_0}{k_f},\ X_8 = P_r = \frac{P_{sat}}{P_{crit}}$$

where T_{sat} is in K, not in °C,

$d_0 = 0.0146\beta\left[\dfrac{2\sigma}{g(\rho_f - \rho_g)}\right]^{0.5}$, is the bubble departure diameter,

β is the contact angle, taken as 35° for hydrocarbon and refrigerants,

$\alpha = k/(\rho c_p)$ is thermal diffusivity, in m^2/s.

Some of these non-dimensional groups have been employed by other authors, for example, X_1 and X_2 by Stephan and Abdelsalam (1980), X_8 by Cooper (1984) and

Gorenflo (1993), and some have been familiar in single-phase heat transfer correlations. It is to be noted that this list of non-dimensional groups is not complete. For example, at least another three quantities including the latent heat i_{fg} could be defined: $X_9 = i_{fg} / \left(c_{p,f} T_{sat} \right)$, $X_{10} = i_{fg} d_0^2 / \nu_f^2$ where $\nu = \mu / \rho$ is the kinematic viscosity, and $X_{11} = \mathrm{Bo} = q / \left(G i_{fg} \right)$. Furthermore, the two-phase Reynolds number Re_{tp} could have as many as three expressions, with the two-phase viscosity being defined by Equations (2.52 a) through (2.52 c). It remains the task of the investigator to find the most relevant and pertinent non-dimensional groups in the analysis. As pointed out by Stephan and Abdelsalam (1980), the non-dimensional numbers need not necessarily include all possible ones but essential properties must be included in those numbers.

Experimental data of refrigerant boiling heat transfer obtained for this study include 171 data points for R134a, 49 for R507A, 6 for ammonia and 6 for R12. For the latter two refrigerants, i.e., ammonia and R12, all 6 measurements were taken at certain time intervals under fixed design working conditions, and those measurements are averaged and reduced to one data point for the analysis. Details of the complete dataset for all four refrigerants are given in Table 7.1.

Table 7.1: Description of the heat transfer data

Refrigerant	No. data points	Chevron angle	q, kW/m^2	G, kg/m^{2}s	x_{out}	T_{sat}, °C
R134a	58	28°	1.85-6.10	5.60-30.27	0.21-0.92	5.9-12.2
	57	28°/ 60°	1.86-6.44	6.74-27.07	0.20-0.95	6.7-12.8
	56	60°	1.86-6.50	7.32-26.95	0.20-0.85	7.4-13.04
R507A	22	28°	3.84-6.36	15.96-29.83	0.45-0.92	7.8-10.6
	17	28°/ 60°	3.84-6.71	16.53-31.37	0.41-0.93	8.6-10.9
	10	60°	4.70-6.88	18.40-28.06	0.56-0.91	9.2-10.5
ammonia	1	60°	10.75	8.22	0.71	1.9
R12	1	60°	8.17	52.25	0.71	5.5

Based on the complete set of data, the following equations were obtained.

Correlation 1:

$$\mathrm{Nu}_{\mathrm{r}} = \frac{h_{\mathrm{r}} d_0}{k_{\mathrm{f}}} = 1.18\times10^{-4} \cdot \left(\frac{q d_0}{k_{\mathrm{f}} T_{\mathrm{sat}}} \right)^{0.67} \left(\frac{i_{\mathrm{fg}} d_0^{\,2}}{\alpha_{\mathrm{f}}^{\,2}} \right)^{0.42} \left(\frac{\rho_{\mathrm{f}}}{\rho_g} \right)^{-0.10} \mathrm{Pr}_{\mathrm{f}}^{\,0.31} \qquad (7.\ 1)$$

Mean absolute error 7.3% for all data. Specially, the percentage error is 6.4% for ammonia and 11.1% for R12.

Correlation 2:

$$\mathrm{Nu}_{\mathrm{r}} = \frac{h_{\mathrm{r}} d_0}{k_{\mathrm{f}}} = 1.87\times10^{-3} \cdot \left(\frac{q d_0}{k_{\mathrm{f}} T_{\mathrm{sat}}} \right)^{0.56} \left(\frac{i_{\mathrm{fg}} d_0^{\,2}}{\alpha_{\mathrm{f}}^{\,2}} \right)^{0.31} \mathrm{Pr}_{\mathrm{r}}^{\,0.33} \qquad (7.\ 2)$$

Mean absolute error 6.8% for all data. Specially, the percentage error is 4.1% for ammonia and 8.9% for R12.

Correlation 1 was developed with the exponent of the heat flux group fixed at 0.67. This value was specifically chosen to reflect the commonly accepted *h-q* relationship in pool boiling heat transfer, as given by Equation (2.3) and discussed in Section 2.1.2. For Correlation 2, all constants and exponents were determined by regression analysis. It is to be noticed that in both correlations the heat flux *q* imposes a strong influence on the Nu number, comparable to that as in pool boiling correlations (for example, those given by Equations 2.4 through 2.6). Flow parameters such as Re and vapour quality *x* and also information on plate geometry, especially the chevron angle, are excluded from the analysis as a result of their negligible influence on the heat transfer rates. The two correlations are developed from, and thus only cover, refrigerants, plate geometries and evaporator working ranges as specified in Table 7.1.

Calculated Nu_{r} values using Correlation 1 and Correlation 2 are compared with experimental data of R134a, R507A, ammonia and R12, and are presented in Figures 7.1 and 7.2, respectively. As shown in the figures, both correlations are able to predict the data fairly well, with Correlation 2 giving better agreement for both refrigerants and showing a better consistency with the data at low heat fluxes. For Correlation 2, 75% of the data fall within 10% deviation bands, and 97.3% within 20% deviation bands.

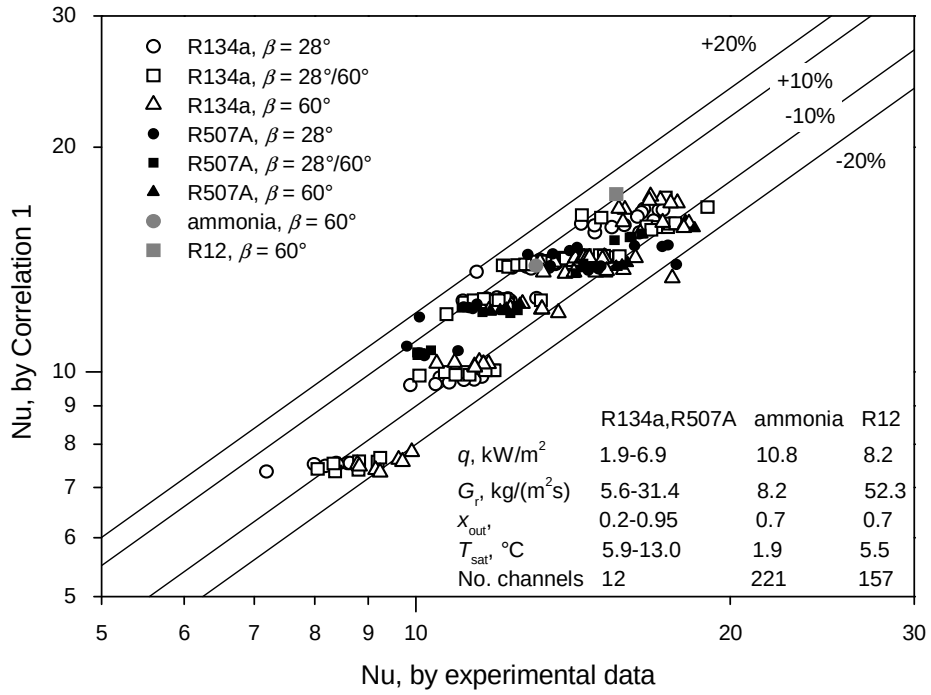


Figure 7.1: Comparison of predictions of Nu using Correlation 1 with experimental data

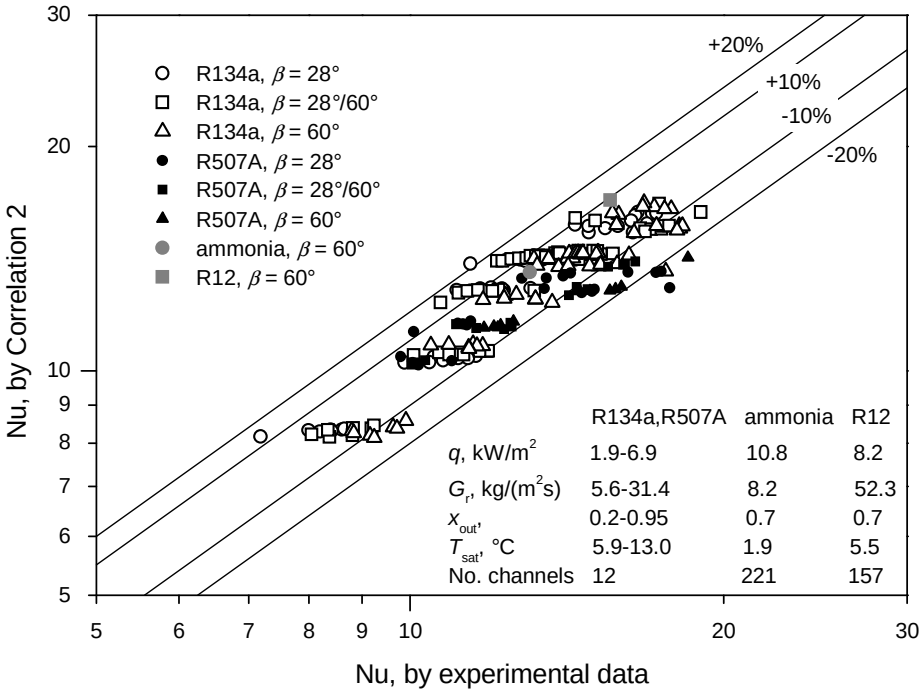


Figure 7.2: Comparison of predictions of Nu using Correlation 2 with experimental data

7.3 Two-phase Frictional Pressure Drop

Correlations were developed to predict the two-phase frictional pressure drops in PHE channels using two methods : the homogeneous method and the Lockhart-Martinelli method. Experimental data of the refrigerant two-phase frictional pressure drop include 146 data points for R134a and 60 for R507A. Details of the complete data set are given in Table 7.2.

Table 7.2: Description of the frictional pressure drop data

Refrigerant	No. data points	Chevron angle	G, kg/m^2s	x_{out}	T_{sat}, °C
R134a	44	28°	13.62-30.27	0.25-0.82	5.9-12.2
	50	28°/ 60°	10.74-27.07	0.24-0.95	6.7-12.8
	52	60°	10.89-26.95	0.25-0.90	7.4-13.0
R507A	22	28°	15.96-29.83	0.45-0.92	7.8-10.6
	18	28°/ 60°	15.94-31.37	0.41-0.93	8.6-10.9
	20	60°	17.61-31.39	0.40-0.95	9.2-12.6

7.3.1 Correlation using the Homogeneous Model

Based on the experimental data of R134a and R507A, correlations were developed to predict the two-phase frictional pressure drops in the corrugated channels. The homogeneous model defines the two-phase friction factor in the form:

$$f_{tp} = \frac{a}{\mathrm{Re}_{tp}^{\,b}} \tag{7. 3}$$

where a and b are constants that can contain fluid properties and geometrical information. There are two considerations arising when using the homogeneous model to correlate experimental data:

1. Local x versus mean x.
   The total pressure drop ΔP_{fric} can be calculated by integration of local pressure gradients:

$$-\Delta P_{\text{fric}} = \int_0^{L_p} f_{\text{tp}} \cdot \frac{G^2}{2\bar{\rho} d_{\text{h}}} \cdot dz \tag{7. 4}$$

where $\bar{\rho}$ is determined by local x, and f_{tp} is the adiabatic two-phase friction factor which is also a function of local x. This calculation method is difficult to obtain from evaporator test data where local measurements are not available, and inconvenient to apply due to the integration procedure. Alternatively, ΔP_{fric} could also be calculated by a mean vapour quality for the evaporation process:

$$\Delta P_{\text{fric}} = f_{\text{tp}} \cdot \frac{L_p}{d_{\text{h}}} \cdot \frac{G^2}{2\rho_{\text{m}}} \tag{7. 5}$$

where ρ_{m} is two-phase mean density using mean vapour quality: $x_{\text{m}} = 0.5\left(x_{\text{in}} + x_{\text{out}}\right)$. This method is also commonly used in pressure drop evaluation of refrigerant evaporators (for example, by Pierre, 1964). As no integration is needed, this method is usually much simpler than the one using local x, both in obtaining and applying the correlation equations.

In the current study, both approaches using local and mean x are investigated, with the latter found to have better agreement with the experimental data.

2. Definition of the two-phase Reynolds number Re_{tp}.
   The two-phase Reynolds number is defined simply by the equation

$$\text{Re}_{\text{tp}} = \frac{G d_{\text{h}}}{\mu_{\text{tp}}} \tag{7. 6}$$

   Because of the free and flexible choice of the two-phase viscosity μ_{tp}, at least five definitions of Re_{tp} are available, namely with μ_{tp} being the viscosity of liquid phase, the vapour phase, and the three definitions given by Equations (2.52 a) thought (2.52 c). In the current study, the Dukler et al. definition (Equation 2.52 c) of the two-phase viscosity gives the best fit to the experimental data, for both methods using local and mean vapour qualities.

For R134a and R507A data, the following correlation was obtained using the homogeneous model with mean vapour quality:

$$f_{\mathrm{tp}} = \frac{3.81\times10^{4}\cdot F_{\mathrm{R,f}}}{\mathrm{Re}_{\mathrm{tp}}^{\,0.90}\left(\dfrac{\rho_{\mathrm{f}}}{\rho_{\mathrm{g}}}\right)^{0.16}} \qquad (7.7)$$

where

$\mathrm{Re}_{\mathrm{tp}} = Gd_{\mathrm{h}} / \mu_{\mathrm{tp}}$.

$$\mu_{\mathrm{tp}} = \rho_{\mathrm{m}}\left[x_{\mathrm{m}}\frac{\mu_{\mathrm{g}}}{\rho_{\mathrm{g}}} + (1-x_{\mathrm{m}})\frac{\mu_{\mathrm{f}}}{\rho_{\mathrm{f}}}\right],$$

$$\rho_{\mathrm{m}} = \left[x_{\mathrm{m}}/\rho_{\mathrm{g}} + (1-x_{\mathrm{m}})/\rho_{\mathrm{f}}\right]^{-1}.$$

$x_{\mathrm{m}} = 0.5(x_{\mathrm{in}} + x_{\mathrm{out}})$

$F_{\mathrm{R,f}}$ is a geometrical parameter catering for different chevron angles:

$F_{\mathrm{R,f}} = 0.183R^{2} - 0.275R + 1.10,\ R = \beta / 30^{\circ}$

The correlation given by Equation (7.7) for the two-phase friction factor is plotted against the two-phase Reynolds number in Figure 7.3. It is seen that the correlation agrees well with the experimental data, but discrepancy is greater at low Reynolds numbers, this might be explained by the higher percentage error of the experimental frictional pressure drop at low flow rates. The calculated two-phase frictional pressure drop ΔP_{fric} using Equation (7.7) is compared with the experimental data in Figure 7.4. For this correlation, 75.2% of the data fall within

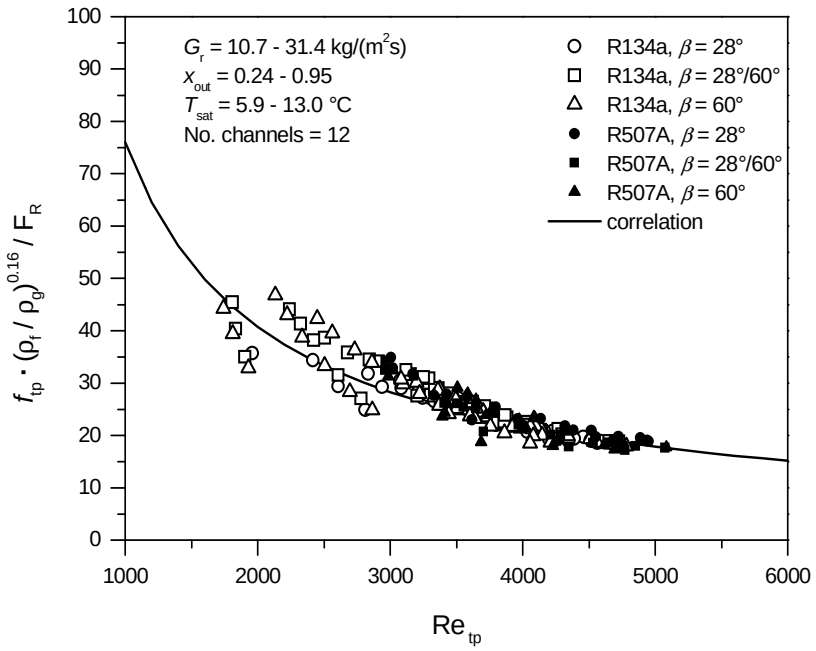


Figure 7.3: Calculated f_{tp} versus $\mathrm{Re}_{\mathrm{tp}}$ compared with experimental data

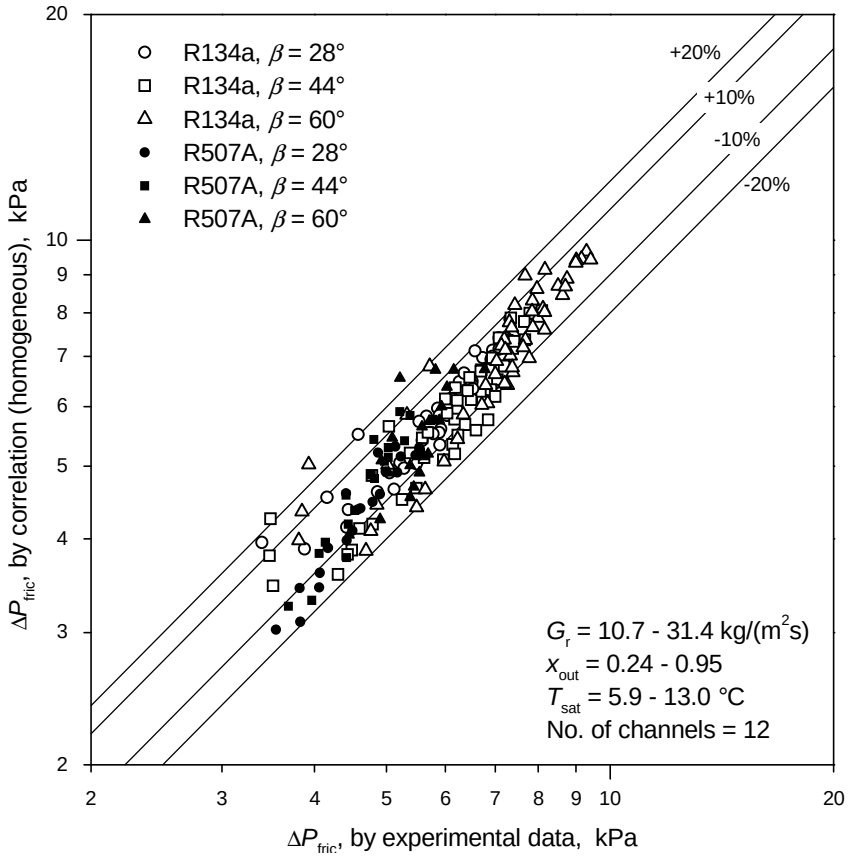


Figure 7.4: Comparison of predictions of ΔP_{fric} using the homogeneous model with experimental data

10% deviation bands, and 98.1% within 20% deviation bands. The mean absolute error is 6.7%.

It is to be noticed that the data set for the frictional pressure drop is not exactly the same as that used for the boiling heat transfer coefficient. As described previously in this chapter, the differential pressure transmitter gave readings close to zero or even negative magnitudes on a few occasions with very low flow rates, due to the existence of the liquid leg in the feeding line. Those data were believed to have higher measurement errors and eliminated for this analysis. Even though the pressure drop could, theoretically, be determined by the subtraction of the readings from the two static pressure transmitters located at the evaporator inlet and outlet, this method brings higher uncertainty and inconsistency of the results, and is not used.

The obtained correlation covers R134a and R507A for the conditions specified by Table 7.2. Application of the correlation to other refrigerants could not be

evaluated as no such data are available in the literature for a validation. Also, comparisons of the current correlation with existing ones could not be carried out on any fair basis as those correlations (some selected ones are given in Table 2.7) were developed for different refrigerants, evaporator geometry, and various flow conditions. None of those has claimed applicability beyond its tested range. Nevertheless, a qualitative comparison is made between the current one and those by Yan and Lin (1999) and Jokar et al.(2006). Both these other correlations were developed for R134a and for chevron angle of 60°, and both employ the homogeneous theory, but different forms and components are used expressing the friction factor. For the comparison to be possible, some parameters have to be set. The comparison is shown in Figure 7.5, with the plate geometry, fluid properties and vapour quality set as according to the current experimental conditions, and f_{tp} is plotted versus liquid-only Reynolds number Re_{fo} in the correlations' application range. It is seen that the Jokar et al. correlation, which was obtained from DX evaporators with more than 30 plates, agrees reasonably well with the current correlation. The Yan and Lin correlation, which was obtained for flow in a single channel and at G = 55 and 70 kg/(m^{2}s) only, gives much higher predictions of f_{tp} than the other two, especially at low Re. Calculations showed that this correlation is unsuitable to represent the current data.

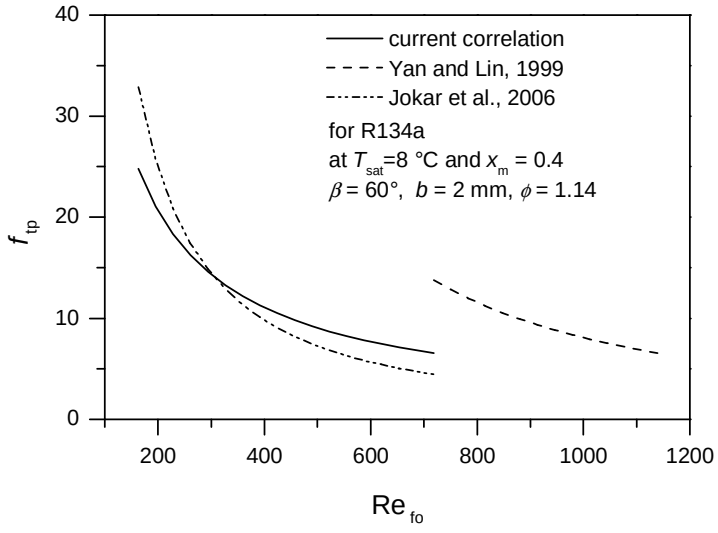


Figure 7.5: Comparison of the predicted f_{tp} by the current correlation with that by Yan and Lin (1999) and Jokar et al. (2006) correlation

7.3.2 Correlation using the Lockhart-Martinelli Method

The Lockhart-Martinelli method using the Chisholm constant *C* is investigated here for its ability of to predict the experimental data. As this method is based on adiabatic flow, the application of the method for refrigerant evaporator pressure drop calculation requires:

1. Local values of *x*. *x* is assumed to increase linearly along the channel length *z* from inlet to outlet. This assumption is only strictly correct at uniform heat flux conditions but nevertheless has been commonly used for all types of refrigerant evaporators,
2. The total pressure drop to be calculated by stepwise integration of pressure gradients obtained at local *x*.

The central part of this method is to find the value of *C* at local *x*, and the total frictional pressure drop is then calculated using Equations (6.19) through (6.23). *C* is a constant for turbulent flow in conventional pipes, but has been reported with different values in a rather wide range for adiabatic and also phase-changing flow in PHE channels, as reviewed in Section 2.7.3. Of those, some reported

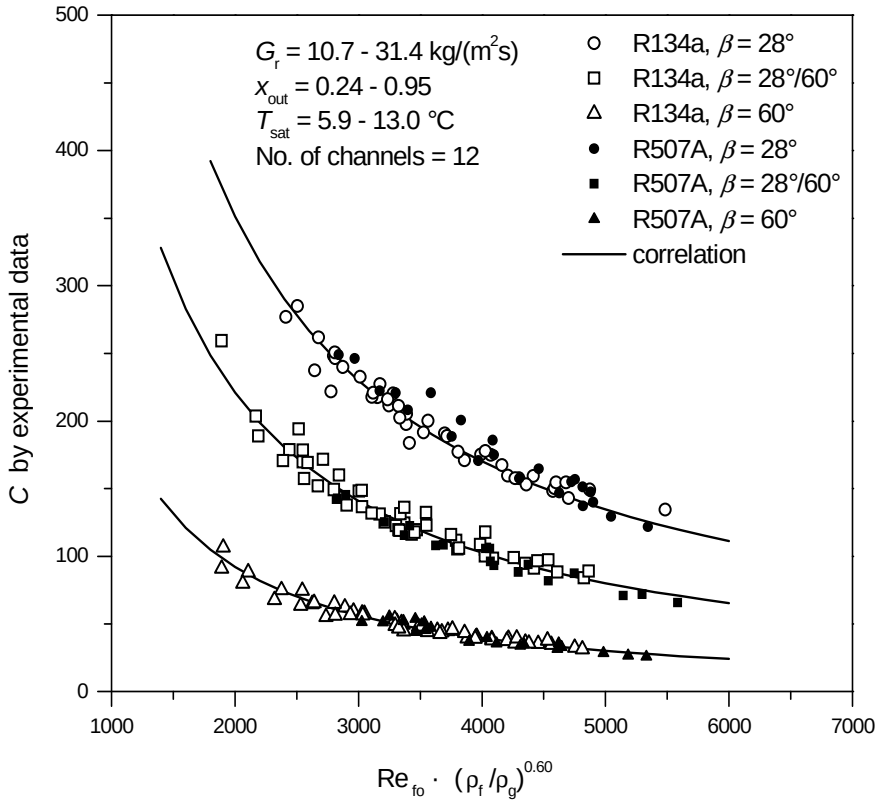


Figure 7.6: Chisholm parameter *C* versus liquid-only Reynolds number

fixed values of C, and some reported C as a function of the Reynolds number, or in other forms. In this study, the experimental data for R134a and R507A showed that C varies with the mass flux G, and can be correlated with either the liquid-only or the vapour-only Reynolds number ($\mathrm{Re_{fo}}$ or $\mathrm{Re_{go}}$). Figure 7.6 shows C versus the liquid-only Reynolds number $\mathrm{Re_{fo}}$ for the heat exchangers. C is also found to be dependent on the chevron angle, which has not been reported previously in the literature. Based on the experimental data, the following correlation is obtained:

$$C = \frac{1\times10^{6}}{\left[\mathrm{Re}_{\mathrm{fo}}\cdot\left(\rho_{\mathrm{f}}/\rho_{\mathrm{g}}\right)\right]^{F_{\mathrm{R,C}}}} \tag{7. 8}$$

where $\mathrm{Re}_{\mathrm{fo}} = Gd_{\mathrm{h}}/\mu_{\mathrm{f}}$ is the liquid-only Reynolds number,

$F_{\mathrm{R,C}}$ is a geometrical parameter catering for different chevron angles:

$F_{\mathrm{R,C}} = 0.0951R^{2} - 0.114R + 1.07,\ R = \beta/30^{\circ}$

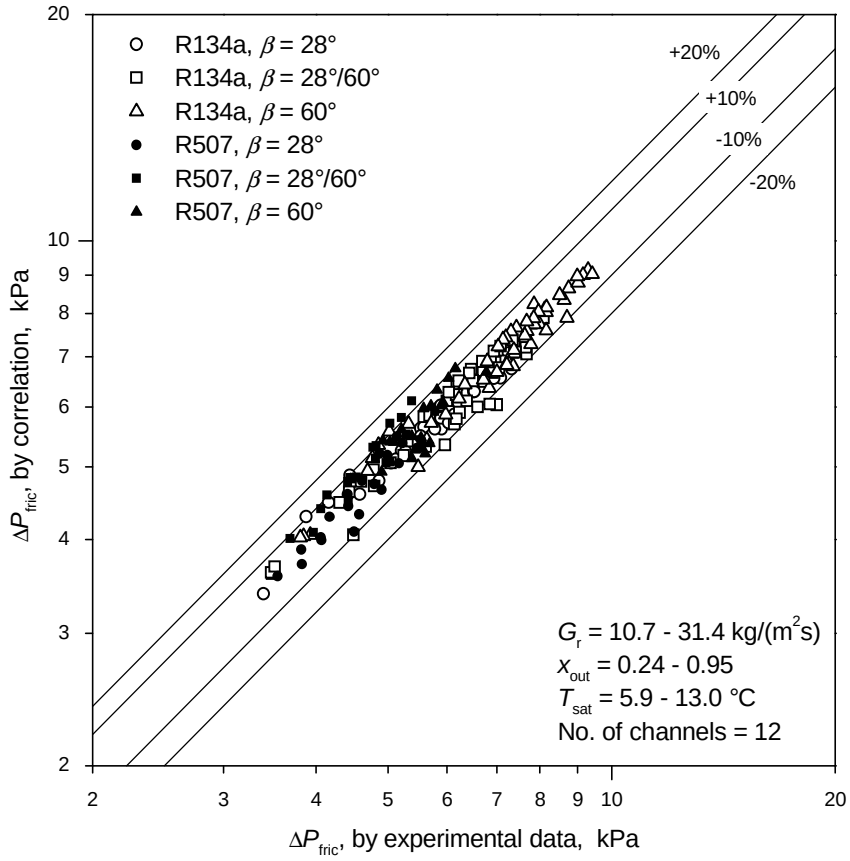


Figure 7.7: Comparison of predictions of ΔP_{fric} using Lockhart-Martinelli method with the experimental data

The calculated frictional pressure drop ΔP_{fric} using Equation (7.8) is compared with the experimental data, as given in Figure 7.7. This correlation agrees well with the experimental data; 93.7% of the data fall within 10% deviation bands, and 100% within 20% deviation bands. The mean absolute error is 4.2%.

Calculation of the total pressure drop using this method requires a stepwise integration of the local pressure gradients. This is usually done numerically with the aid of computer programs, and can be inconvenient for quick engineering calculations. It is to be noted that application of this correlation could not be performed using mean vapour quality x_m (to avoid the integration procedure), because doing so can result in errors as high as +40%, as verified with the present data.

Table 7.3: Comparison values of the Chisholm parameter C as reported by different authors

Author	Fluid	β, degrees	x	G, kg/(m^{2}s)	C	Description
Current study	R134a, R507A	28/28, 28/60, 60/60	0-0.95	10.7-31.4	$C = f\left(\mathrm{Re}_{fo}\right)$, 28.8-280	Liquid-overfeed evaporator
Kumar (1983)	-	-	-	-	~5.4-82	condensation, X = 0.01-100
Thonon (1995)	refrigerant	-	-	-	8	evaporation X by tube correlation
Winkelmann et al., (1999)	water-air	27°	0.05-0.9	35-142	6	adiabatic
Tribbe and Muller-Sterinhagen (2001)	water-air	30/30, 30/60, 60/60	0-1	50-600	$C = f\left(G, x\right)$	adiabatic
Asano et al. (2004)	water-air	60	-	-	2.73	adiabatic
Palm and Claesson (2006)	R134a	-	-	-	4.67	evaporation
Sterner and Sunden (2006)	ammonia	59-65	0.05-1	0.5-9.5	$C = f\left(\mathrm{Re}_{go}\right)$, 10-110	DX evaporator

A strong dependence of the Chisholm parameter C on the mass flux G is observed. This dependence was also reported by Sterner and Sunden (2006) for data obtained from ammonia DX evaporators. Other forms of $C-\phi_f{}^2$ relationship, such as suggested by Claesson and Simanic (2003), and by Tribbe and Müller-Steinhagen (2001), were tried but could not be fitted to the present data. Table 7.3 summarizes reported C values from some selected sources from the literature, for a comparison of the current correlation with those from other authors. It is noticed that the values of the parameter C vary considerably among those investigations. The disagreement is certainly relevant to the variety of channel geometries as tested; another possible reason, among others, could be due to the various means of determining the Martinelli parameter X. Many authors have chosen to use the original definition as given by Equation (2.60). This requires single-phase pressure drop correlations and is the approach adopted in this study. Some conveniently used the definition of X for circular tubes (Equation 2.61), for example in the correlation by Thonon (1995), some simply did not give this information. Also noticed from the table is that the parameter C obtained from phase changing processes such as condensing and evaporating tends to be much greater than that obtained in adiabatic conditions. This might, tentatively, be attributed to the non-physical treatment of linear change of x along the channel length as commonly used for evaporator analysis, but a more detailed explanation could not be obtained at this stage.

A Discussion of the Two Methods of Correlating the Frictional Pressure Drop Data

The two methods employed in the present study for correlating the frictional pressure drop data both provide good agreement with the data, with the Lockhart-Martinelli method predicting the data to some extent better than the homogeneous method. However, it is likely that the homogenous model is more physically sound for predicting the two-phase pressure drop in PHE channels for the following reasons:

1. The channel geometry is highly three-dimensional which promotes turbulence and mixing of the two phases to be “homogeneous”,
2. The flow is in the vertical direction, which prevents stratification of the two phases.

Yan and Lin (1999) observed, via flow visualization for R134a at G = 55 kg/(m^{2}s), x_m = 0.15 and higher, that a turbulent mist flow dominated in the channel with strong recirculation in each denting cavity on the channel wall. This observation suggests a homogeneous flow pattern in the corrugated channel. It could be argued that in PHE evaporators the mass flux is usually low (lower than

31.4 kg/m^{2}s in the current study, lower than 9.5 kg/m^{2}s in Sterner and Sunden's (2006) study on several ammonia evaporators) and for low flow rates the homogeneous model is usually considered not suitable, this is true at least for conventional ducts with uniform cross-section. Chisholm (1983) and also Thome (2004 b) pointed out that the homogeneous model gives reasonable results only at high mass fluxes exceeding 2000 kg/(m^{2}s) for tube flow . This criterion can not be applied directly to PHE's considering their unique channel geometry. It is known that the flow is usually turbulent at even very low Reynolds numbers in corrugated channels. Along with the generation of vapour and the strong inter-phase effects associated with swirling motion of the fluids and continuous change in flow direction and velocity, it is not unreasonable to assume that the flow is homogeneous at least for the upper part of the channel. The discussion of two-phase flow features in this type of channel still remains open awaiting further data and observations.

The correlations developed are both satisfactory to present the present data. In application, the correlation using the homogeneous method (Equation 7.7) is simple and straightforward, while the correlation using the Lockhart-Martinelli method (Equation 7.8) requires an integration procedure. It is to be noted that the equation forms and associated constants of both correlations, as for the two-phase friction factor f_{tp} and the Chisholm parameter C, were obtained using and heavily rely on, regression analysis. As such, it would be appropriate to regard the current correlations more as a statistical and empirical approach than flow model based analysis.

7.4 Conclusion

Based on the experimental and field testing data, correlations were developed for predicting the thermal and hydraulic performances of PHE liquid over-feed evaporators. Two correlations were obtained for predicting the refrigerant flow boiling heat transfer coefficient h_r, one of these reflecting the generally accepted h-q relationship in pool boiling with the exponent of q being 0.67, the other one having all its constants and components determined by regression analysis, with the exponent of q being 0.56. Both of these correlations reflect a nucleate boiling dominant process, in which the mass flux and vapour quality have a small influence on the heat transfer coefficient. The mean absolute errors of these two correlations are respectively 7.3% and 6.8%, compared with the 222 data points covering R134a, R507A, ammonia and R12. For two-phase frictional pressure drop, data were correlated with two established methods, namely the homogeneous and the Lockhart-Martinelli method. The homogeneous model

shows a slightly higher discrepancy with the experimental data but is likely to be more physically sound for PHE evaporators, and is much simpler to apply. The mean absolute errors are respectively 6.7% and 4.2% for these correlations, based on 206 data points covering R134a and R507A.

All obtained correlations are accurate for the tested refrigerants and evaporator working conditions. Validation of these correlations with other data has been difficult due to the lack of published information. For other refrigerants running at comparable conditions, these correlations could serve as a guide, while more accurate design or evaluation may still need to be based on further testing data.

CHAPTER 8

CONCLUSIONS AND RECOMMENDATIONS

8.1 Conclusions

The primary objective of this study was the performance assessment of plate heat exchangers used as refrigerant liquid over-feed evaporators. To this aim, experimental data were obtained from single-phase performance tests with water, two-phase evaporator performance tests with R134a and R507, and additional field tests with ammonia and R12. Reduction, analysis, and correlating of these data were carried out and presented in related chapters. A summary of the conclusions drawn from those chapters is given here, along with additional remarks on developing empirical correlations.

Experimental results of the exchanger single-phase water-water performance tests clearly showed that chevron angle has a strong influence on the water heat transfer rate and frictional pressure drop. High overall heat transfer coefficients and high friction factors were observed. Correlations were derived for the heat transfer coefficient using the familiar Sieder-Tate type of equation, and for friction factor expressed as a function of the Reynolds number. A collection of some published correlations were accessed and compared with the experimental data, some of those fit reasonably well with the data. However, in general, the disagreement between those correlations is rather high, which indicates that a general correlation might be difficult to achieve, due to the highly complex and flexible geometrical features of PHE's.

For the evaporator performance tests, the same three PHE units were arranged in parallel but operated and tested individually as liquid over-feed evaporators. Experimental data were obtained for the heat transfer and pressure drop analysis. Two refrigerants were used, namely R134a and R507A. The heat transfer data suggested a nucleate boiling-dominant process in the evaporators. For both refrigerants in the test range, the heat transfer coefficient h showed a strong dependence on the heat flux q, and weakly on mass flux G, vapour quality x, and the chevron angle β. On the other hand, the two-phase frictional pressure drop of the refrigerants showed strong dependence on mass flux and vapour quality, and

increased with higher chevron angles. The frictional pressure losses with both refrigerants were observed to increase almost linearly with the homogenous two-phase kinetic energy per unit volume. Based on the experimental data, two empirical correlations were developed for predicting the refrigerant flow boiling heat transfer coefficients covering refrigerants R134a, R507A, ammonia, and R12 data. These two correlations are given by Equations (7.1) and (7.2) and are reproduced as follows:

Correlation 1:

$$\mathrm{Nu}_{\mathrm{r}} = \frac{h_{\mathrm{r}} d_0}{k_{\mathrm{f}}} = 1.18\times10^{-4} \cdot \left(\frac{q d_0}{k_{\mathrm{f}} T_{\mathrm{sat}}}\right)^{0.67} \left(\frac{i_{\mathrm{fg}} d_0^{\,2}}{\alpha_{\mathrm{f}}^{\,2}}\right)^{0.42} \left(\frac{\rho_{\mathrm{f}}}{\rho_g}\right)^{-0.10} \mathrm{Pr}_{\mathrm{f}}^{\,0.31} \qquad (8.\ 1)$$

Mean absolute error 7.3% for all data. Specially, the percentage error is 6.4% for ammonia and 11.1% for R12.

Correlation 2:

$$\mathrm{Nu}_{\mathrm{r}} = \frac{h_{\mathrm{r}} d_0}{k_{\mathrm{f}}} = 1.87\times10^{-3} \cdot \left(\frac{q d_0}{k_{\mathrm{f}} T_{\mathrm{sat}}}\right)^{0.56} \left(\frac{i_{\mathrm{fg}} d_0^{\,2}}{\alpha_{\mathrm{f}}^{\,2}}\right)^{0.31} \mathrm{Pr}_{\mathrm{r}}^{\,0.33} \qquad (8.\ 2)$$

Mean absolute error 6.8% for all data. Specially, the percentage error is 4.1% for ammonia and 8.9% for R12.

The two correlations are of basically the same form with the difference that for Correlation 1 the exponent of the heat flux has been specially chosen as 0.67 to reflect the commonly accepted *h-q* relationship in pool boiling, and for Correlation 2 this component was found as 0.56, which best fits the data. Two-phase pressure drop data of R134a and R507A were correlated using two different approaches, namely the homogeneous model and the Lockhart-Martinelli method. These two correlations are given by Equations (7.7) and (7.8), and are reproduced as:

The homogeneous model:

$$f_{\mathrm{tp}} = \frac{3.81\times10^{4} \cdot F_{\mathrm{R,\,f}}}{\mathrm{Re}_{\mathrm{tp}}^{\,0.90} \left(\frac{\rho_{\mathrm{f}}}{\rho_{\mathrm{g}}}\right)^{0.16}} \qquad (8.\ 3)$$

where
$\mathrm{Re}_{\mathrm{tp}} = G d_{\mathrm{h}} / \mu_{\mathrm{tp}}$.

$$\mu_{tp} = \rho_m \left[x_m \frac{\mu_g}{\rho_g} + (1 - x_m) \frac{\mu_f}{\rho_f} \right],$$

$$\rho_m = \left[x_m / \rho_g + (1 - x_m) / \rho_f \right]^{-1}.$$

$$x_m = 0.5 (x_{in} + x_{out})$$

$F_{R,f}$ is a geometrical parameter catering for different chevron angles:

$$F_{R,f} = 0.183R^2 - 0.275R + 1.10, \quad R = \beta / 30^\circ$$

The Mean absolute error is 6.7%.

The Lockhart-Martinelli method using Chisholm parameter:

$$C = \frac{1 \times 10^6}{\left[\mathrm{Re}_{fo} \cdot (\rho_f / \rho_g) \right]^{F_{R,C}}} \tag{8. 4}$$

where $\mathrm{Re}_{fo} = G d_h / \mu_f$ is the liquid-only Reynolds number,

$F_{R,C}$ is a geometrical parameter catering for different chevron angles:

$$F_{R,C} = 0.0951R^2 - 0.114R + 1.07, \quad R = \beta / 30^\circ$$

The mean absolute error is 4.2% for this correlation. The homogeneous model showed a slightly higher discrepancy with the experimental data but is likely to be more physically sound for PHE evaporators, and is much simpler to apply.

All correlations were developed with the assistance of statistical regression techniques, and gave satisfactory agreements with the present data. Validation of these correlations by other data has been difficult due to the lack of published information.

As a concluding remark, some comments could be given regarding the assessment of empirical correlations. Empirical correlations contain constants and exponents which are evaluated from experimental data. For such a correlation, it is possible to find values for these constants and exponents which will give exact agreement with any *single* experimental point, and it is also possible that the correlation may be improved for each set of data by adjusting the value of the constants. A good correlation should be able to predict reasonable results over a wide range of conditions, and should always be based on data set which is accurate and reliable. This has proved to be no easy task for measurements of two-phase flow parameters. As pointed out by Dukler et al. (1964) concerning frictional pressure drop in two-phase *circular* tube flow: “claims of superiority of one correlation over another could usually be reversed simply by making the comparison for different data. It is easy to see why this is so when, for apparently

similar test conditions, pressure drop data of different investigators vary by 30 to 60 %". The situation could become even worse when it comes to the case of two-phase flow in PHE corrugated channels, where geometrical parameters include the chevron angle, corrugation depth, surface enlargement factor, plate aspect ratio, and possible usage of flow distributors, along with different flow channels in individual exchangers. Of the limited number of published works, it seems that no correlation obtained for specified equipment has found applicability in another situation. The highly complex feature of the two-phase flow, combined with many possible patterns of channel geometry, all makes it unlikely that any simple model will account for all situations. With this consideration, it might be true that a "generally applicable" model can be used as a rough guide of the range of possible pressure drops, while any serious and accurate design may need testing to obtain data for the specified equipment.

8.2 Suggestions for Future Work

This thesis is by no means regarded as complete. Some aspects of the two-phase flow and heat transfer mechanisms in the corrugated channels are not addressed, and some need further investigation. Some research areas are suggested here, which may help to achieve a better understanding of two-phase flows in PHE's.

A wide testing range is advantageous for experimental investigations, especially so if the aim is to obtain empirical correlations with wide applicability. In the current study the tested ranges of the evaporators' heat flux and mass flow rates were typical for PHE evaporators but were still relatively small. It would be desirable to expand this testing range to cover a greater spectrum. The easiest way of carrying out this work with the current facility is to replace the PHE units with smaller sizes. There is no information available that describes the possible operating limits of PHE evaporators in terms of those two parameters, but a heat flux up to 20 kW/m^2 and mass flux up to 100 kg/m^2 could be a first and reasonable estimation, and shoukld be considered for future works.

Flow visualization of two-phase flow in PHE channels is a topic rarely addressed and the two-phase flow patterns in this type of channel are very poorly understood. The purpose of flow visualization is to obtain qualitative information of the flow, based on which two-phase flow patterns could be identified. Even though the identification of flow patterns is always associated with subjective judgments, it is believed (Thome, 2002) that the best approaches for modelling two-phase heat transfer and pressure drops are those based on flow pattern analysis. Two-phase flow patterns in conventional pipes are well investigated and

documented, but this is not so for PHE's or similar corrugated channels. Two-phase flow visualization investigations for PHE channels (such as by Vlasogiannis et al, 2002, Shiomi et al, 2004) had often used transparent materials as a cover plate, and the obtained pictures were always vague and blurry because of metal reflection (this is a problem not suffered by investigations on pipe flows). This is an interesting topic but a successful investigation may need some novel design of the experimental facility.

The performance of PHE direct-expansion evaporators is not investigated in this study, though some experimental observations and conclusions from other researchers are discussed at certain points. DX evaporators are more commonly employed in small installations for example domestic heat pumps. At least two aspects need some consideration which are not as significant in liquid over-feed systems, these being the partition of the evaporator according to the flow pattern (two- and single-phase zones, or in other words, evaporation and superheating zones) and flow distribution for multi-channel units. These are briefly discussed in Section 2.7.2. It is possible to estimate the effects of these parameters by overall measurement and system analysis, a more profound investigation may need the help of other techniques, for example, the TLC (thermochromic liquid crystal) technique for determining regions of a DX evaporator as used by Claesson and Palm (1999), and evaporator inclination for evaluating the influence of flow distribution between channels as used by Kedzierski (1995).

8.3 Suggestions on Experimental Facility Design

There are certain criteria for evaluating an experimental facility, those including functionability, reliability, and flexibility. A good design must certainly be based on a deep understanding of the problem at hand, and can be improved by experience. The suggestions given here address refrigerant evaporator tests as carried out in this study, but some general features also apply to other types of heat transfer equipment.

For a fixed evaporator operating with a certain refrigerant, assume that the heat transfer coefficient h is a function of the heat flux q, mass flux G, vapour quality x, and the system pressure P. The aim of the experimentation is to find the influence of those parameters on h. q can be controlled by two factors: the evaporating temperature and the condensing temperature. The evaporating temperature can be controlled by a back pressure regulator installed upstream of the compressor; while this device was installed in the current equipment, the control was not effective. For an air-cooled condenser, the condensing temperature can be controlled by regulating the air flow rate, this proved very

effective in the current study, and can be achieved by any of the following methods: (1). speed control of one or more variable-speed fans, (2). operation of multiple fixed-speed fans, (3). use of dampers.

For liquid over-feed evaporators, the mass flow rate G is to be controlled by a liquid pump with by-passing arrangements. It is always preferable to use a by-passing arrangement for flow rate control rather than using a single valve in the main line, and this applies also to water flow control. This arrangement requires two valves, one on the main line and one on the by-pass line, and usually gives far more stable flows over a wide range. To use this arrangement, the pump must be sufficiently large, say capable of 1.5 times the maximum test flow rate. Furthermore, it is preferable to install the main line regulating valve on the evaporator return line rather than on the feed line. This is because the refrigerant liquid in the feed line is at or very close to saturation, and a sharp pressure drop across the valve may result in liquid flashing, a situation to be avoided. For DX evaporators, the mass flow rate G is controlled by thermal-expansion valves. It is preferable to use hand valves rather than automatically controlled valves for testing purposes.

The evaporator inlet vapour quality x_{in} can be controlled using a pre-heater upstream of the test evaporator, and calculated from measurements of the heat load of the pre-heater. The evaporator exit vapour quality x_{out} is determined by the cooling load of the evaporator. From the evaporator heat balance, i.e., $\dot{Q} = \dot{m} \cdot i_{fg} \cdot \Delta x$, where $\dot{Q}$ is a measure of q and $\dot{m}$ a measure of G, it is clear that the three variables of q, G, and Δx are coupled parameters, and it is not possible to investigate the individual influence of any one parameter on h without involving one or both of the other two parameters. One option, as performed in this study, is to run the evaporator at fixed heat fluxes, and for each heat flux change the flow rates which correspondingly determine Δx. This has the effect of treating q and the product of $\dot{m} \cdot \Delta x$ as two groups, arranged with the consideration that q is considered as a measure of the nucleate boiling effect, and G and x are both measures of forced convection effects, in flow boiling heat transfer.

REFERENCES

ASHRAE Handbook 2005: Fundamentals.

ASHRAE Handbook 2006: Refrigeration.

Ayub Z.H., 2003, Plate heat exchanger literature survey and new heat transfer and pressure drop correlations for refrigerant evaporators, *Heat Transfer Engineering*, vol.24, no.5, pp.3-16.

Avallone E.A. and T. Baumeister III, *Mark's Standard handbook for Mechanical Engineers,* 10th edition, McGraw-Hill, 1996.

Baehr and Stephan, 2006, *Heat and Mass Transfer*, 2nd ed., Springer, New York.

Bailey-McEwan M., 1994, *Surveys of performance of water chilling machines at surface water chilling installation* (unpublished), Consultancy Report, Chamber of Mines of South Africa.

Bailey-McEwan M., Serfontein J. and Cornelissen R.J.R., 1996, *Comparative performance before and after renewing plates of No.1 evaporator, 21-22 June 1996* (unpublished), Technical Report, Hartebeestfontein Gold Mining Co. Ltd.

Baroczy C.J., 1966, A systematic correlation for two-phase pressure drop, *Chemical Engineering Progress Symposium Series*, vol.62, no.64, pp.232-249.

Bassiouny M.K. and Martin H., 1984a, Flow distribution and pressure drop in plate heat exchangers – I, U-type arrangement, *Chemical Engineering Science*, vol.39, no.4, pp.693-700.

Bassiouny M.K. and Martin H., 1984b, Flow distribution and pressure drop in plate heat exchangers – II, Z-type arrangement, *Chemical Engineering Science*, vol. 39, no.4, pp.701-704.

Bejan and Kraus, 2003, *Heat Transfer Handbook*, John Wiley & Sons, New Jersey.

Bennett D.L. and Chen J.C., 1980, Forced convective boiling in vertical tubes for saturated pure components and binary mixtures, *AIChE Journal*, vol.26, no.3, pp.454-461.

Bergles A., Lienhard V J.H., Kendall G.E. and Griffith P., 2003, Boling and evaporation in small diameter channels, *Heat Transfer Engineering*, vol.24, no.1, pp.18-40.

Bertsch S.S., Groll E.A., and Garimella S.V., 2..8, Review and comparative analysis of studies on saturated flow boiling in small channels, *Nanoscale and Microscale Thermophysical Engineering*, vol. 12, pp.187-227.

Bjorge R.W., Hall R.G., and Rohsenow W.M., 1982, Correlation of forced convection boiling heat transfer data, *International Journal of Heat and Mass Transfer*, vo.25, no.6, pp.753-757.

Boccardi G., Celata G.P., Cumo M., Gerosa A., Giuliani A. and Zorzin A., 2000, The use of new refrigerants in compact heat exchangers for the refrigeration industry, *Heat Transfer Engineering*, vol.21, no.4, pp.53-62, 2000

Bond M.P., 1981, Plate heat exchangers for effective heat transfer, *The Chemical Engineer*, no.367, pp.162-167.

Buonopane R.A., Troupe R.A. and Morgan J.C., Heat transfer design method for plate heat exchangers, *Chemical Engineering Progress*, vol.59, no.7, pp.57-61, 1963

Carlson J.A., 1992, Understand the capabilities of plate-and-frame heat exchangers, *Chemical Engineering Progress*, vol.88, no.7, 26-31.

Chen J.C., 1966, Correlations for boiling heat transfer to saturated fluids in convective flow, *Industrial and Engineering Chemistry Process Design and Development*, vol.5, no.3, pp.322-329.

Chahabra R.P. and Richardson J.F., 1999, *Non-Newtonian Flow in the Process Industries*, Butterworth-Heinemann.

Chisholm D., 1967, A theoretical basis for the Lockhart-Martinelli correlation for two-phase flow, *International Journal of Heat and Mass Transfer*, vol.10, pp.1767-1778.

Chisholm D., 1973, Pressure gradients due to friction during the flow of evaporating two-phase mixtures in smooth tubes and channels, *International Journal of Heat and Mass Transfer*, vol.16, pp.347-358

Chisholm D., 1983, *Two-phase Flow in Pipelines and Heat Exchangers*, Longman Inc., New York.

Clark D.F., 1974. Plate heat exchanger design and recent developments, *The Chemical Engineer*, no.285, pp.275-279.

Claesson J. and Simanic B., 2003, Pressure drop and visualization of adiabatic R134a two-phase flow inside a chevron type plate heat exchanger, in: *Proceedings of the 21st International Congress of Refrigeration*, paper ICR0314, 2003, Washington D.C.

Claesson J. and Palm B, 1999, Boiling mechanism in a small compact brazed plate heat exchanger (CBE) determined by using thermochromic liquid crystals, in: *Proceedings of the 20th International Congress of Refrigeration*, Sydney, Australia, 19–24 September 1999, Paper 117.

Claesson J., Palm B., 2002, Discrepancy between calculated and measured superheated area in an evaporator plate heat exchanger, *in: Proceedings of the 1st International Conference on Heat Transfer, Fluid Mechanics and Thermodynamics*, South Africa, April 8-10, 2002, paper CJ1.

Claesson J., 2005a, Thermal and hydraulic characteristics of brazed plate heat exchangers - Part I: Review of single-phase and two-phase adiabatic and flow boiling characteristics, *ASHRAE Transactions*, vol.111, no.1, pp.822-833.

Claesson J., 2005b, Thermal and hydraulic characteristics of brazed plate heat exchangers - Part II: Current research on evaporators at KTH, *ASHRAE Transactions*, vol.111, no.1, pp.834-845.

Collier J.G., 1983, Boling and evaporation, in: Schlunder E.U. et al., eds., 1983, *Heat Exchanger Design Handbook*, Hemisphere Publishing Corporation, New York, section 2.7.

Collier J.G. and Thome J.R., 1994, *Convective Boiling and Condensation*, 3rd ed., Oxford University Press, New York.

Cooper A., 1974a, Recover more heat with plate heat exchangers, *The Chemical Engineer*, no.285, pp.280-285.

Cooper A., 1974b, Condensation of steam in plate heat exchangers, *AIChE Symposium*. vol.70, no.138, pp.172-177.

Cooper A. and Usher J.D., 1983, Plate heat exchangers, in: Schlunder E.U. et al., eds., 1983, *Heat Exchanger Design Handbook*, Hemisphere Publishing Corporation, New York, Section 3.7.

Cooper M.G., 1984, Saturation nucleate pool boiling: a simple correlation, *I.Chem Eng. Symposium Series*, vol.86, pp.785-793

Crozier R.D., Booth J.R. and Stewart J.E., 1964, Heat transfer in plate and frame heat exchangers, *Chemical Engineering Progress*, vol.60, no.8, pp.43-45.

Darabi J., Salehi M., Saeedi M.H., and Ohadi M.M., 1995, Review of available correlations for prediction of flow boiling heat transfer in smooth and augmented tubes, *ASHRAE Transactions*, vol.101, no.1, pp.965-975.

Donowski V.D. and Kandlikar S.G., 2000, Correlating evaporation heat transfer coefficient of refrigerant R-134a in a plate heat exchanger, in: *Proceedings of Boiling 2000: Phenomena and Emerging Applications, Engineering Foundation*, April 30-May 5, 2000, Alaska, Paper 154.

Dossat R.J., 1991, *Principles of Refrigeration*, 3rd edition, Prentice-Hall, New Jersey.

Dukler A.E., Wicks M. and Cleveland R.G., 1964, Frictional pressure drop in two-phase flow: B. An approach through similarity analysis, *AIChE Journal*, vol.10, no.1, pp.44-51.

Dummett G.A., 1964, The plate heat exchanger in the food industries, Part II-Development and Applications, *Chemistry and Industry*, vol.38, pp.1604-1612.

Edelstein S., Perez A.J., and Chen J.C., 1984, Analytic representation of convective boiling functions, *AIChE Journal*, vol.30, no.5, pp.840-841.

Edwards M.F., Changal A.A. and Parrott D.L., 1974, Heat transfer and pressure drop characteristics of a plate heat echanger using Newtonian and Non-Newtonian liquids, *The Chemical Engineer*, no.285, pp.286-288, 293.

Engelhorn and Reinhart, 1990, Investigations on heat transfer in a plate evaporator, *Chemical Engineering and Processing*, vol.28, pp.143-146.

Feener D.M., 1999, Applying flow conditioning, *Control Engineering*, vol.46, no.2, pp.107-109.

Fijas D.F., 1997, Brazed plate heat exchangers, in: Grimm N.R. and Rosaler R.C., eds., 1997, *HVAC Systems and Components Handbook*, 2nd ed., McGraw-Hill Professional, Section 5.2.

Focke W.W., 1983, Turbulent convective transfer in plate heat exchangers, *International Communications in Heat and Mass Transfer*, vol.10, no.3, pp.201-210, 1983

Focke W.W., 1985, Asymmetrically corrugated plate heat exchanger plates, *International Communications in Heat and Mass Transfer*, vol.12, no.1, pp.67-77.

Focke W.W., Zachariades J. and Olivier I., 1985, The effect of the corrugation inclination angle on the thermohydraulic performance of plate heat exchangers., *International Journal of Heat and Mass Transfer*, vol.28, no.8, pp.1469-1479.

Focke W.W. and Knibbe P.G., 1986, Flow visualization in parallel-plate ducts with corrugated walls, *Journal of Fluid Mechanics*, vol.165, pp.73-77.

Focke W.W., 1986, Selecting optimum plate heat exchanger surface patterns, Journal of Heat Transfer, vol.108, no.1, pp.153-160.

Friedel L., 1979, Improved friction pressure drop correlations for horizontal and vertical two-phase pipe flow, *European Two-phase Flow Group Meeting*, Paper E2, Ispra, Italy

Gaiser G. and Kottke V., 1989, Flow phenomena and local heat and mass transfer in corrugated passages, *Chemical Engineering and Technology*, vol.12, no.6, pp.400-405.

García-Cascales J.R., Vera-García F., Corberán-Salvador J.M. and Gonzálvez-Maciá J., 2007, Assessment of boiling and condensation heat transfer correlations in the modeling of plate heat exchangers, *International Journal of Refrigeration*, vol.30, no.6, pp.1029-1041.

Ghiaasiaan S.M., 2007, *Two-phase Flow, Boiling and Condensation: In Conventional and Miniature Systems*, Cambridge University Press.

Goldfinch S., 1994, The role of the plate heat exchanger in refrigeration, *Australian Refrigeration, Air Conditioning and Heating*, vol.48, no.11, pp.33-36.

Gorenflo D., 1993, Pool boiling, in: *VDI Heat Atlas*, 1st English edition, Springer.

Gorenflo D., 1999, State of the art in pool boiling heat transfer of new refrigerants, in: *Proceedings of the 20th International Congress of Refrigeration*, Sydney, Australia, 19–24 September 1999.

Gray R.M., 1984, Design and use of plate heat exchangers in boiling and condensing applications, *IChemE Symposium Series*, no.86, pp.685-694.

Grønnerud. R., 1972, Investigation of liquid hold-up, flow resistance and heat transfer in circulation type evaporators, Part IV: Two-phase Flow Resistance in Boiling Refrigerants, Annexe 1972-1, *Bulletin de L'Institut du Froid*

Gungor K.E. and Winterton R.H.S., 1986, A general correlation for flow boiling in tubes and annuli, *International Journal of Heat and Mass Transfer*, vol.29, no.3, pp.351-358.

Gungor K.E. and Winterton R.H.S., 1987, Simplified general correlation for saturated flow boiling and comparisons of correlations with data, *Chemical Engineering Research and Design*, vol.65, no.1, pp.148-159.

Han D. Lee K. and Kim Y., 2003, Experiments on the characteristics of evaporation of R410A in brazed plate heat exchangers with different geometric configurations, *Applied Thermal engineering*, vol.23, no.10, pp.1209-1225.

Hanssen R., 1997, The role of the plate heat exchanger in refrigeration, MSc (Eng) Selected Topic Report, University of the Witwatersrand, South Africa.

Heavner R.L., Kumar H. and Wanniarachchi A.S., 1993, Performance of an industrial plate heat exchanger: effect of chevron angle, *AIChE Symposium Series*, vol.89, no.295, pp.262-267.

Hsieh Y.Y. and Lin T.F., 2002, Saturated flow boiling heat transfer and pressure drop of refrigerant R 410A in a vertical plate heat exchanger, *Int. J. Heat Mass Transfer*, vol.45, no.5, pp.1033-1044.

Hsieh Y.Y. and Lin T.F., 2003, Evaporation heat transfer and pressure drop of refrigerant R-410A flow in a vertical plate heat exchanger, *Journal of Heat Transfer*, vol.125, no.5, pp.852-857.

Hewitt G.F., 1983, Gas-liquid flow, in: Schlunder E.U. et al., eds., 1983, *Heat Exchanger Design Handbook*, Hemisphere Publishing Corporation, New York, Section 2.3.2.

Hewitt N.J., McMullan J.T. and Moran D.G., 1993, The ccontrol of a refrigeration system using a compact plate heat exchanger as an evaporator, *International Journal of Energy Research*, vol.17, no.5, pp.393-399.

Incropera F.P. and DeWitt D.P., 1990, *Introduction to Heat Transfer*, 2nd ed., John Wiley & Sons.

Jassim E.W., Newell T.A. and Chato J.C., 2005, Refrigerant pressure drop in chevron and bumpy style flat plate heat exchangers, Experimental Thermal and Fluid Science, vol.30, pp.213-222.

Jokar A, Hosni M. and Eckels S.J., 2006, Dimensional analysis on the evaporation and condensation of refrigerant R-134a in mini-channel plate heat exchangers, *Applied Thermal Engineering*, vol.26, no.17-18, pp.2287-2300.

Kakac S. and Liu H., 2002, *Heat Exchangers: Selection, Rating, and Thermal Design*, 2nd ed., CRC Press.

Kanaris A.G., Mouza K.A. and Paras S.V., 2004, Designing novel compact heat exchangers for improved efficiency using a CFD code, in: *1st International Conference "From Scientific Computing to Computational Engineering"*, Athens, September 8-10 , 2004

Kandlikar S.G. and Shah R.K., 1989, Multipass plate heat exchangers-effectiveness-NTU results and guidelines for selecting pass arrangements, *Journal of Heat Transfer*, vol.111, no.2, pp.300-313, 1989

Kandlikar S.G., 1990, A general correlation for saturated two-phase flow boiling heat transfer inside horizontal and vertical tubes, *Journal of Heat Transfer*, vol.112, pp.219-228.

Kandlikar S.G., 1991, A model for correlating flow boiling heat transfer in augmented tubes and compact evaporators, *Journal of Heat Transfer*, vol.113, pp.966-972.

Kandlikar S.G. and Nariai H., 1999, Flow boiling in circular tubes, in: Kandlikar S.G., Shoji M., and Dhir V.K., eds., *Handbook of Phase Change: Boiling and Condensation*, CRC Press, Chpater 15.

Kandlikar S.G. and Steinke M.E., 2003, Predicting heat transfer during flow boiling in minichannels and microchannels, *ASHRAE Transactions*, vol.109, no.1, pp.1-9.

Katzel J., 2000, Heat exchanger basics, *Plant Engineering*, vol.54, no.4, pp.87-93.

Kedzierski. M.A., 1995, Effect of inclination on the performance of a compact brazed plate condenser and evaporator, *NISTIR Report, No. 5767*

Kumar H., 1983, Condensation duties in plate heat exchangers, *IChemE Symposium Series*, no.75, pp.478-486.

Kumar H., 1984, The plate heat exchanger: construction and design, *IChemE Symposium Series*, no.86, pp.1275-1288.

Kumar H., 1993, Evaporation in plate heat exchangers, *AIChE Symposium Series*, vol.89, no.295, pp.211-222.

Kumar H., Edwards M.F., Davison P.R., Jackson D.O. and Heggs P.J., 1994, The importance of corner header distributor designs in plate heat exchangers, in: Berryman R.J. eds. *Heat Transfer 1994, Proceedings of the 10th international Heat Transfer Conference*, Inst of Chemical Engineers UK, pp.81-86.

Kuppan T., 2000, *Heat Exchanger Design Handbook*, Marcel Dekker Inc.

Lemmon E.W., M.O. McLinden and D.G. Friend, "Thermophysical Properties of Fluid Systems" in: *NIST Chemistry WebBook, NIST Standard Reference Database Number 69*, Eds. P.J. Linstrom and W.G. Mallard, June 2005, National Institute of Standards and Technology, Gaithersburg MD, 20899 (http://webbook.nist.gov/chemistry/).

Liu Z. and Winterton R.H.S., 1991, A general correlation for saturated and subcooled flow boiling in tubes and annuli, based on a nucleate pool boiling equation, *International Journal of Heat and Mass Transfer*, vol.34, no.11, pp.2795-2766.

Lockhart R.W. and Martinelli R.C., Proposed correlation of data for isothermal two-phase, two-component flow in pipes, *Chemical Engineering Progress*, vol.45, no.1, pp.39-48, 1949

Longo G.A., Gasparella A. and Sartori R., 2004, Experimental heat transfer coefficients during refrigerant vaporization and condensation inside herringbone-type plate heat exchangers with enhanced surfaces., *International Journal of Heat and Mass Transfer*, vol.47, no.19-20, pp.4125-4136.

Longo G.A. and Gasparella A., 2007, Heat transfer and pressure drop during HFC refrigerant vaporization inside a brazed plate heat exchanger, International Journal of Heat and Mass Transfer, vol.50, no.25, pp.5204-5214.

Marriott J., 1971, Where and how to use plate heat exchangers, *Chemical Engineering*, vol.78, pp.127-134, April 5.

Martin H., 1996, A theoretical approach to predict the performance of chevron-type plate heat exchangers, *Chemical Engineering and Processing*, vol.35, no.4, pp.301-310.

Martin H., 2002, The generalized Lévêque equation and its practical use for the prediction of heat and mass transfer rates from pressure drop, *Chemical Engineering Science*, vol.57, no.16, pp.3217-3223.

Martinelli R. C. and Nelson D.B., 1948, Prediction of pressure drop during forced-circulation boiling of water, *Transactions of the ASME*, vol.70, pp.695-702.

Mehrabian M.A. and Poulter R., 2000, Hydrodynamics and thermal characteristics of corrugated channels: computational approach, *Applied Mathematical Modelling*, vol.24, no.5, pp.343-364.

McQuillan K.W. and Whalley P.B., 1985, Flow patterns in vertical two-phase flow, *International Journal of Multiphase Flow*, vol.11, no.2, pp.161-175.

Mencke E., Olsson A., Larsson J., Dahlquist A., Persson Y. and Eriksson P., 2005, Brazed plate heat exchangers and their applications, *ASHRAE Transactions*, vol.111, no.1, pp.813-821,

Muley A. and Manglik R.M., 1999, Experimental Study of turbulent flow heat transfer and pressure drop in a plate heat exchanger with chevron plates, *Journal of Heat Transfer*, vol.121, no.1, pp.110-117.

Müller-Steinhagen H. and Heck K., 1986, A simple friction pressure drop correlation for two-phase flow in pipes, *Chemical Engineering and Processing*, vol.20, pp.297-308, 1986

Nithiarasu P., 2005, Role of numerical modeling in compact heat exchanger analysis, in: Shah R.K. et al., eds., *Proceedings of Fifth International Conference on Enhanced, Compact and Ultra-compact Heat Exchangers*, Hoboken, NJ, USA, 2005

Ould Didi M.B., Kattan N., and Thome J.R., 2002, Prediction of two-phase pressure gradients of refrigerants in horizontal tubes, *International Journal of Refrigeration*, vol.25, no.7, pp.935-947,

Palm B. and Claesson J., 2006, Plate heat exchangers: calculation methods for single- an dtwo-phase flow, *Heat Transfer Engineering*, vol.27, no.4, pp.88-98.

Panchal C.B., Hills D.L. and Thomas A., 1983, Convective boiling of ammonia and Freon 22 in plate heat exchangers, *Argonne National Laboratory Report*, No. CONF-830301-13.

Panchal C.B. and Rabas T.J., 1993, Thermal performance of advanced heat exchangers for ammonia refrigeration systems, *Heat Transfer Engineering*, vol.14, no.4, pp.42-57.

Panchal C.B. and T.J. Rabas, 1999, Fouling characteristics of compact heat exchangers and enhanced tubes, in: *Proceedings of the Conference on Compact Heat Exchangers and Enhancement Technology for the Process Industries*, Banff, Canada, 1999.

Pelletier O., Stromer F. and Carlson A., 2005, CFD simulation of heat transfer in compact brazed plate heat exchangers, *ASHRAE Transactions*, vol.111, no.1, pp.846-854.

Peters J.V.S. and Kandlikar S.G., 2007, Further evaluation of a flow boiling correlation for microchannels and minichannels, in: *Proceedings of the Fifth International Conference on Nanochannels, Microchannels and Minichannels*, Puebla, Mexico, 2007.

Pierre B., 1964, Flow resistance with boiling refrigerants- part I, *ASHRAE Journal*, vol.6, no.9, pp.58-65.

Pioro I.L., Rohsenow W., Doerffer S.S., 2004, Nucelate pool-boiling heat transfer. I: review of parametric effects of boiling surface, *International Journal of Heat and Mass Transfer*, vol.47, no., pp.5033-5044.

Rao B.P. and Das S.K., 2004, An experimental study on the influence of flow maldistribution on the pressure drop across a plate heat exchanger, *Journal of Fluids Engineering*, vol.126, no.4, pp.680-691.

Raju K.S. and Chand J., 1980, Consider the plate heat exchanger, *Chemical Engineering*, vol.87, no.16, pp.133-144.

Reppich M., 1999, Use of high performance plate heat exchangers in chemical and process industries, *International Journal of Thermal Sciences*, vol.38, no.11, pp.999-1008.

Seligman R.J.S., 1964, The plate heat exchanger in the food industries, part I: genesis of an idea, *Chemistry and Industry*, vol.38, pp.1602-1603.

Shah M.M., 1976, A new correlation for heat transfer during boiling flow through pipes, *ASHRAE Transactions*, vol.82, no.2, pp.66-86.

Shah M.M., 1982, Chart correlation for saturated boiling heat transfer: equations and further study, *ASHRAE Transactions*, vol.88, no.1, pp.185-196.

Shah M.M., 2006, Evaluation of general correlations for heat transfer during boiling of saturated liquids in tubes and annuli, *HVAC & R Research*, vol.12, no.4, pp.1047-1063.

Shah R.K. and Focke W.W., 1988, Plate heat exchanger and their design theory, in: Shah R.K., Subbarao E.C. and Mashelkar R.A., eds., *Heat Transfer Equipment Design*, Hemisphere Publishing Corporation, Washington, pp.227-254.

Shah R.K. and Sekulic D.P., 2003. *Fundamentals of Heat Exchanger Design*, John Willey & Sons.

Shiomi Y., Nakanishi S. and Uehara T., 2004, Characteristics of two-phase flow in a channel formed by chevron type plates, *Experimental Thermal and Fluid Science*, vol.28, no.2-3, pp.231-235, 2004

Stasiek J., Collins M.W., Ciofalo M. and Chew P.E., 1996, Investigation of flow and heat transfer in corrugatred passages, Part I: Experimental results, *International Journal of Heat and Mass Transfer*, vol.39, no.1, pp.149-164

Steiner D. and Taborek J., 1992, Flow boiling heat transfer in vertical tubes correlated by an asymptotic model, *Heat Transfer Engineering*, vol.13, no.2, pp.43-69.

Sterner D. and Sunden B., 2006, Performance of Plate Heat Exchangers for Evaporation of Ammonia, *Heat Transfer Engineering*, vol.27, no.5, pp.45-55.

Stephan K. and Abdelsalam M., 1980, Heat-transfer correlations for natural convection boiling, *International Journal of Heat and Mass Transfer*, vol.23, no.1, pp.73-87.

Strömblad M., 1989, Plate heat exchanger characteristics in refrigerant systems, *SCANREF International*, no.4

Stoecker W.F., 1998, *Industrial Refrigeration Handbook*, McGraw-Hill.

Taitel Y. and Dukler A.E., 1976, A model for predicting flow regime transitions in horizontal and near horizontal gas-liquid flow, *AIChE Journal*, vol.22, no.1, pp.47-55.

Taitel Y., Bornea D., and Dukler A.E., 1980, Modelling flow pattern transitions for steady upward gas-liquid flow in vertical tubes, *AIChE Journal*, vol.26, no.3, pp.345-354.

Thome J.R., 2002, On recent advances in modelling of two-phase flow and heat transfer, *in: Proceedings of the 1st International Conference on Heat Transfer, Fluid Mechanics and Thermodynamics*, South Africa, April 8-10, 2002, paper TJ1.

Thome J.R., 2003, Boiling, in: Bejan A. and Kraus A.D., eds., 2003, *Heat Transfer Handbook*, Johan Willey & Sons, Chapter 9.

Thome J.R., 2004a, Boiling in microchannels: a review of experiment and theory, *International Journal of Heat and Fluid Flow*, vol.25, pp.128-139.

Thome J.R., 2004b, *Engineering Data Book III*, Wolverine Tube, Inc.

Thonon B., Vidil R. and Marvillet C., 1995, Recent research and developments in plate heat exchangers, *Journal of Enhanced Heat Transfer*, vol.2, no.1-2, pp.149-155.

Thonon B., Feldman A., Margat L. and Marvellet C., 1997, Transition from nucleate boiling to convective boiling in compact heat exchangers., International Journal of Refrigeration, vol.20, no.8, pp.592-597.

Thonon B., 2008, A review of hydrocarbon two-phase heat transfer in compact heat exchangers and enhanced geometries, *International journal of Refrigeration*, vol.31, pp.633-642.

Tribbe C and Muller-Steinhagen H.M., 2000, An evaluation of the performance of phenomenological models for predicting pressure gradient during gas-liquid flow in horizontal pipelines, *International Journal of Multiphase Flow*, vol.26, no.6, pp.1019-1036.

Tribbe C. and Müller-Steinhagen H.M., 2001a, Gas/liquid flow in plate-and-frame heat exchangers -part I: pressure drop measurements, *Heat Transfer Engineering*, vol.22, no.1, pp.5-11.

Tribbe C. and Müller-Steinhagen H.M., 2001b, Gas/liquid flow in plate-and-frame heat exchangers -part II: two-phase multiplier and flow pattern analysis, *Heat Transfer Engineering*, vol.22, no.1, pp.12-21.

Trifonov Yu. Ya., 1998, Viscous liquid film flows over a periodic surface, *International Journal of Multiphase Flow*, vol.24, no.7, pp.1139-1161.

Troupe R.A., Morgan J.C., and Prifti J., 1960, The plate heater – versatile chemical engineering tool, *Chemical Engineering Progress*, vol.56, no.1, pp.124-128.

Uehara H., Stuhltrager E., Miyara A., Murakami H. and Miyazaki K., 1997, Heat transfer and resistance of a shell and plate-type evaporator, *Journal of Solar Energy Engineering*, vol.119, pp.160-164.

Usher J.D., 1970, Evaluating plate heat exchangers, *Chemical Engineering*, vol.77, 23 February, pp.90-94.

Vlasogiannis P., Karagiannis G., Argyropoulos P. and Bontozoglou V., 2002, Air–water two-phase flow and heat transfer in a plate heat exchanger, *International Journal of Multiphase Flow*, vol.28, pp.757-772.

VDI Heat Atlas, 1993, 1st ed. in English, Springer.

Wanniarachchi A.S., Ratnam U., Tilton B.E. and Dutta-Roy K., Approximate correlations for chevron-type plate heat exchangers, *ASME HTD*, vol.314, *1995 National Heat Transfer Conference*, vol.12, , pp.145-151

Wilkinson W.L., 1974, Flow distribution in plate heat exchangers, *The Chemical Engineer*, vol.285, pp.289-292

Winkelmann D., Thonon B., Auracher H. and Bontemps A, 1999, Two-phase flow characteristics of a corrugated channel, in: *Proceedings of the 20th International Congress of Refrigeration*, IIR/IIF, Sydney, 1999, Paper 426.

Yan Y.Y. and Lin T.F., 1999, Evaporation heat transfer and pressure drop of refrigerant R-134a in a plate heat exchanger, *Journal of Heat Transfer*, vol.121, no.1, pp. 118-127.

Appendix A Plate Geometrical Information

Details of the three brazed plate heat exchangers are given in this section. All geometrical parameters were double checked and confirmed, in addition to the information supplied by the manufacturer, and may be regarded as accurate. Dimensions of the unit (outside) are given in Figure A.1.

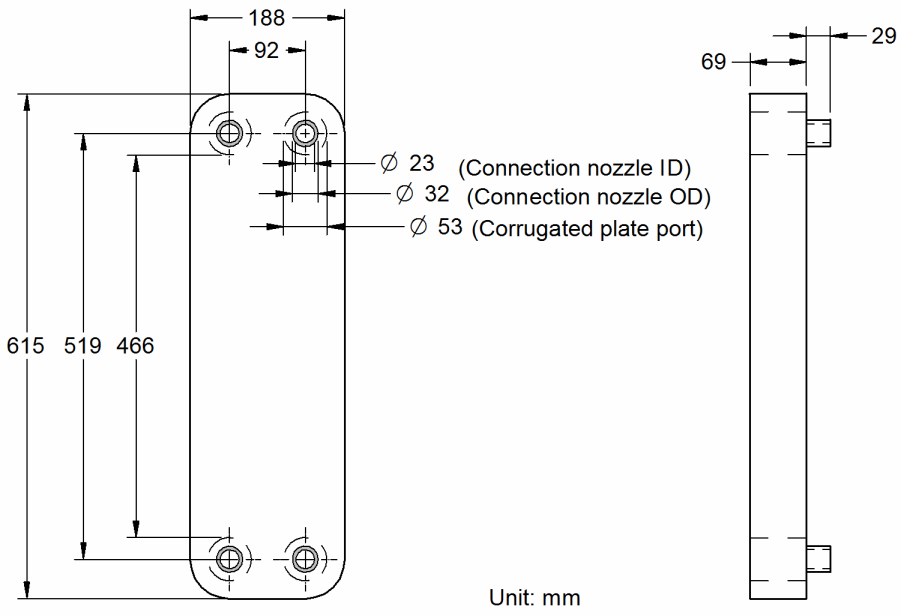


Figure A.1: BPHE B3-095-24-30 Unit dimensions

Plate Geometrical Parameters

Number of plates:	$N_{\mathrm{p}} = 24$
Number of effective plates:	$N_{\mathrm{p,eff}} = N_{\mathrm{p}} - 2 = 22$
Number of channels:	$N_{\mathrm{ch}} = N_{\mathrm{p}} - 1 = 23$, Q1-Q2 side: 12, Q3-Q4: 11
Plate port diameter:	$D_{\mathrm{p}} = 53$ mm
Mean flow channel gap:	$b = 2$ mm
Heat transfer area per plate:	$A_{\mathrm{p}} = 0.095$ m^2 (by manufacturer)
Plate thickness:	$\delta = 0.4$ mm[1]

[1] The manufacturer has given $b = 2$ mm and $\delta = 0.4$ mm. This was double-checked by the following measurements: Use a tape measure and probe it into the port hole, take the average of

Volume per channel:	$V_{ch} = 0.201$ l (10^{-3}m^3) [1]
Design pressure:	30 bar
Design temperature:	-196 to 200 °C
Port to port channel length:	$L_p = 519$ mm (by manufacturer, confirmed by measurement)
Effective channel length:	$L_{eff} = 466$ mm
Width of flow channel:	$w = 180$ mm (by manufacturer, confirmed by measurement)
Chevron angle:	H = 60, L = 27.5 degrees [2]
Corrugation wavelength:	$\lambda = 8.1$ mm[3]
Enlargement factor:	$\phi = 1.14$ [1]

---

readings from different ports. It is thus obtained that 24 plates have a thickness of 57.5 mm, and so one plate is $57.5/24 = 2.396$ mm. By using a micrometer, the plate thickness is obtained as 0.39 mm. The mean channel gap is thus 2.006 mm. Because of the small deviations, the values provided by the manufacturer are taken.

[1] The manufacturer has given the channel volume as 0.25 l, however, this value is apparently wrong, the unit dimension simply can not give this much volume. According to the plate dimension, the theoretical maximum volume one channel can possibly have is:

$$\left[607\times180-88^2(1-\tfrac{\pi}{4})\right]\times2 = 215200 \text{ mm}^3 = 0.2152 \text{ l}$$

It is obtained from the manufacturer that B3-095 is similar to the Alfa-Laval AC 120, which again from Alfa-Laval's catalogue has a channel volume of 0.201 l. A test was carried out on the three units; water was filled into the PHE channels to find the side volumes. Three repeated tests were done on each channel, the result shows:

BPHE	Side volume, ml	
	Q1-Q2 side	Q3-Q4 side
B3-095-24-H	2185	2350
B3-095-24-L	2200	2350
B3-095-24-M	2310	2180

Considering that some air might be trapped in connecting junctions, the maximum volume of the three is taken as the final result for side volume of each exchanger. Note that the two sides have a number of channels of 11 and 12. Thus, from the test on B3-095-24-L, 11 channels have a volume of 2200 ml, and the channel volume is then 0.200 l. It is reasonable to believe that the Alfa-Laval AC120 channel volume is applicable to present units, i.e., 0.201 l/ channel.

(A correspondence with the manufacturer later confirmed that the channel volume is indeed 0.2 l.)

[2] The manufacturer gave those values. The measurement on the plate top view photos shows slight difference, where the high chevron angle is 58.5, and the low chevron angle is 27.4 degrees.

[3] Measurements were taken on two types of plates, i.e., the high and low chevron angle plates, respectively. The result shows that the high angle plate has a corrugation wave length of 8.133 mm, while the low angle one has a wave length of 8.059 mm. Taking the average and rounding off, the value is 8.1 mm.

Single channel flow area: $A_{ch} = wb = 0.18 \times 2 \times 10^{-3} = 3.6 \times 10^{-4}$ m^2

Channel equivalent diameter: $d_e = 2b = 2 \times 2 = 4$ mm

Channel hydraulic diameter: $d_h = 2b / \phi = 2 \times 2 / 1.14 = 3.51$ mm

Total heat transfer area: $A = A_{plate} N_{p,eff} = 0.095 \times 22 = 2.09$ m^2

---

[1] ϕ is defined as: $\phi = \dfrac{\text{developed length}}{\text{projected length}}$. The value of ϕ is a function of the corrugation pitch and the corrugation depth. Martin (1996) suggested an equation to estimate λ : $\phi \approx \frac{1}{6}\left(1 + \sqrt{1 + X^2} + 4\sqrt{1 + X^2 / 2}\right)$, where $X = b\pi / \lambda$.

For the present plates, $X = 2 \times 3.142 / 8.1 = 0.776$, and thus :

$$\phi \approx \frac{1}{6}\left(1 + \sqrt{1 + X^2} + 4\sqrt{1 + X^2 / 2}\right) = 1.138$$

A further check of the value can be carried out using the following equation (Kakac and Liu, 2002):

$$\phi = \frac{A_{plate}}{L_{eff}\, w} = \frac{0.095}{0.466 \times 0.18} = 1.133$$

Appendix B Sensor Technical Data and Wire Connections

This section gives details of the technical data and wire connections, for the 14 sensors that have been used in the present study.

B.1 LM35DZ Temperature Sensors

Model: LM35 DZ
Manufacturer: National Semiconductors (USA)
Quantity used: 4

Technical Specifications:

Operating temperature range: 0 – 100 °C
Power supply: 4 to 30 VDC (use 9 V)
Signal output: linear +10 mV/°C.
Accuracy: ±0.6°C at 25 °C, ±0.9°C at 0 and 100 °C.
Nonlinearity: ± 0.2 °C
(Nonlinearity is defined as the deviation of the output-voltage-versus-temperature curve from the best-fit straight line)

Wire Connection

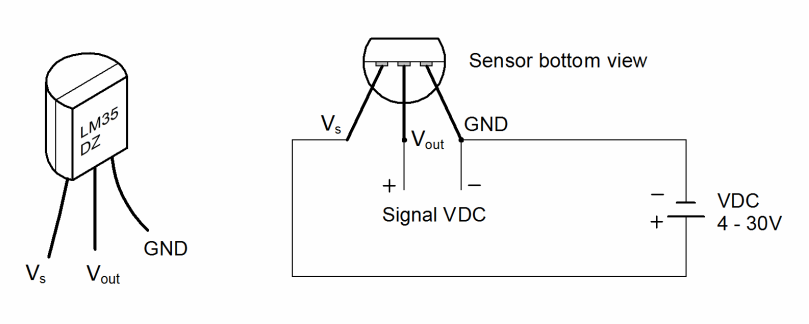


Figure B.1: Wire connection of LM35DZ

B.2 RS 257-026 Turbine Flow Meter

Model: RS 257-026 turbine flow meter
Manufacturer: RS Components, Ltd. (UK)
Quantity used: 2

Field Calibration

The unit is supplied factory calibrated to 4 – 100 l/min but may be field calibrated to have a maximum Flowrate of 150 l/min. The calibration shall be carried out as follows:

1. Set system to zero flow and connect a multimeter between terminals, adjust zero pot to read 4 mA on meter.
2. Set system to full flow (maximum = 150 l/min) with multimeter sill connected, adjust span pot to read 20 mA on meter.

Technical Specifications

Power supply: 24 VDC
Signal output: 4-20 mA
Flowrate range: 2 – 100 l/min
Maximum working pressure: 10 bar Oil/Water
Working temperature: 5 - 60 °C water
Accuracy: ±2 %

Wire Connection

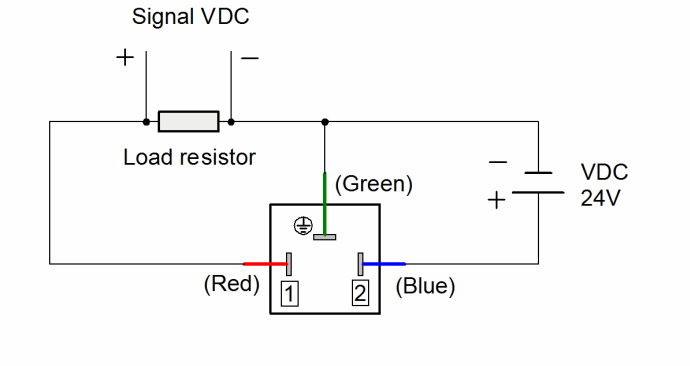


Figure B.2: Wire connection of RS257-026 turbine flow meter

B.3 Rosemount 3051 CD Differential Pressure Transmitter

Model: 3051CD
Manufacturer: Rosemount Inc. (USA)
Quantity used: 1

Technical Specifications

Power supply: 10.5-55 VDC (use 24)
Signal output: VDC 4 - 20 mA, linear with process pressure. Square root output optional.
Working range (factory calibrated): 0 to 80 kPa
Maximum working pressure: 250 bar
Accuracy: ±0.10% of span. For spans less than 2:1 of URL (Upper Range Limit), accuracy = ±0.05% of URL.

Wire Connection

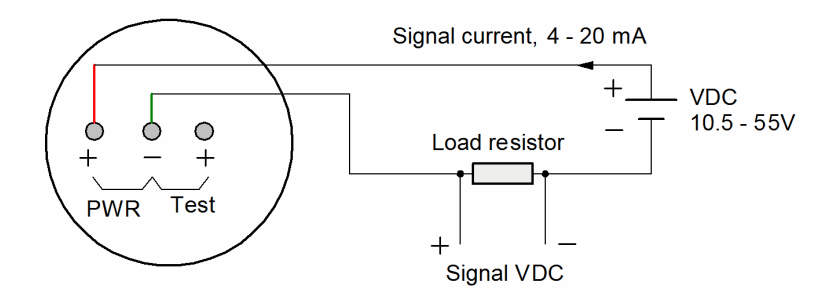


Figure B.3: Wire connection of Rosemount 3051 CD diff. pressure transmitter

B.4 Resistance Temperature Detectors (RTD's)

Four RTD's are used in the refrigeration system test, of those three are the RTXL model and one is the TCL model.

B.4.1 Pyrotec RTXL RTD's

Model: RTXL
Manufacturer: Pyrotec
Quantity used: 3

Technical Specifications

Power supply: 24 VDC
Signal output: 4-20 mA
Working range: 0-100 °C for 1 sensor, 0-200 °C for 2 sensors
Accuracy: ±0.1% of span

Wire Connection

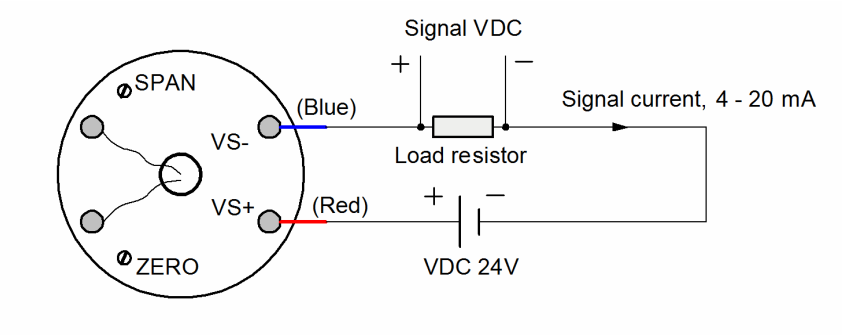


Figure B.4: Wire connection of Pyrotec RTXL RTD

B.4.1 TCL RTD's

Model: TCL
Manufacturer: Temperature Control, Johannesburg
Quantity used: 1

Technical Specifications

Power supply: 24 VDC
Signal output: 4-20 mA
Working range: 0-100 °C
Accuracy: ±0.1% of span

Wire Connections

See Figure B.4.

B.5 WIKA Static Pressure Transmitters

Model: WIKA 891.13.500
Manufacturer: WIKA Alexander Wiegand GMBH & Co. (Germany)
Quantity used: 2

Technical Specifications

Power supply: VDC 10 – 30 V
Signal output: 4 – 20 mA

Working range: 0 – 10 bar
Linearity error: ≤ 0.5% of span
Hysteresis error: ≤ 0.1% of span
Repeatability error: ≤ 0.05% of span

Wire Connection

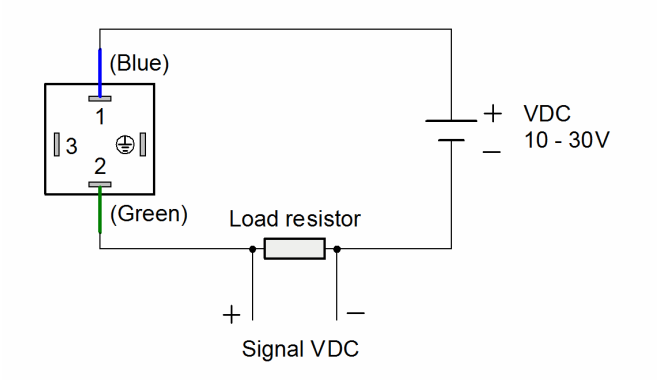


Figure B.5: Wire connection of WIKA pressure transmitter

B.6 Trimec MP15S Flowmeter

This flowmeter gives frequency signal, this signal need to be converted to current signal for the data acquisition system processing. A frequency-current converter is used Specifications of the two apparatus and wire connections are given.

B.6.1 Trimec MP15S Flowmeter

Model: MP15S 221-1 multi-pulse positive displacement flowmeter
Manufacturer: Trimec Industries (Australia)
Quantity used: 1

Technical Specifications:
Power input: 8 – 24 VDC maximum, 100 mA current maximum. Resistor of 500 Ω may be placed.
Signal output: frequency (pulse)
Flowrate range: 0.17 – 7.5 l/min
Maximum working pressure: 100 bar
Working temperature: -40 - 60 °C
Pulse output resolution: 200 pulse/ liter
Accuracy: ± 0.5% of reading

Repeatability: typically ± 0.03%
Pulses/liter: Reed switch 1: 204.26, Reed switch 2: 408.52, Hall effect: 408.52
(as given by the calibration certificate)

B.6.2 Frequency to Current Converter

Model: 1100P
Manufacturer: IQ Instruments cc. (South Africa)
Quantity used: 1

Technical Specifications

Power supply: 230V 50HZ
Signal input: VDC 0-60 HZ
Signal output: VDC 0-20 mA
Accuracy: 0.25% of span

B.6.3 Wire Connection

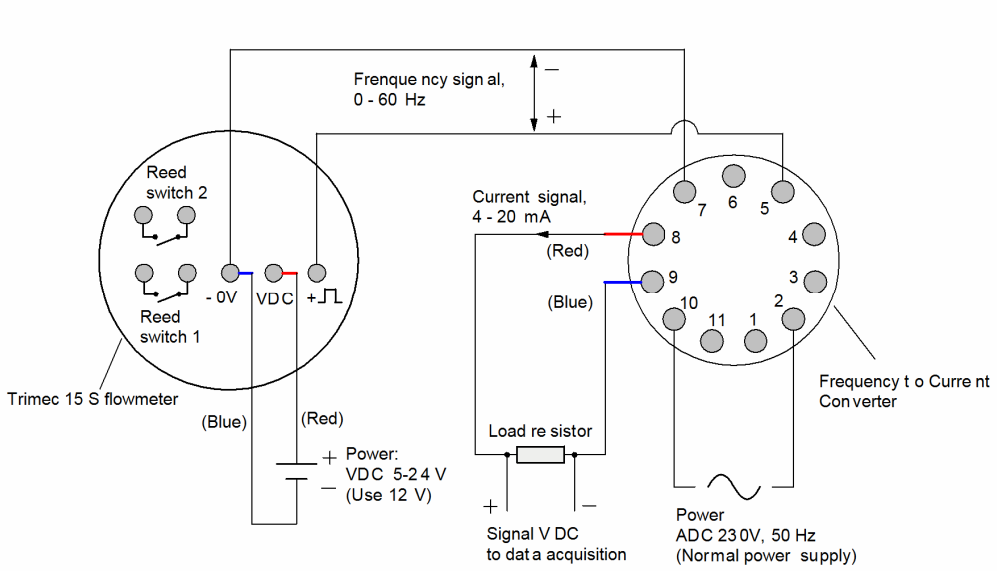


Figure B.6: Wire connection of Trimec MP15S and the frequency-current converter

Appendix C Sensor Calibration

C.1 Temperature Sensors
C.1.1 Reference Mercury Thermometer
C.1.2 LM35DZ Sensors
C.1.3 Resistance Temperature Detectors (RTD's)
C.2 RS 257-026 Turbine Flow Meters
C.3 Trimec MP15S Flowmeter
C.4 Rosemount 3051 CD Differential Pressure Transmitter
C.5 WIKA Static Pressure Transmitters

C.1 Temperature Sensors

The Temperature sensors were calibrated against a reference mercury thermometer, which was calibrated first to be the reference thermometer.

C.1.1 Reference Mercury Thermometer

The mercury thermometer has a minimum reading of 0.1 °C. First ice was filled into a 2-liter container to ¾ of its volume, the container was then stirred for about 1 minute and the thermometer was inserted into the bath water, the thermometer read 0.0 degrees. Then about 60 litres of tap water was filled into a bin and brought to boiling, the thermometer was completely immersed into the boiling water for more than 10 minutes, and the reading was 93.9 degrees. The calibration of the mercury thermometer was carried out on 23/09/2008, between 11-12 am, when the laboratory barometer read:

time	Barometer reading, kPa	Corresponding BP, °C[1]
11.00 am	827.0	94.34
12.45 am	824.9	94.26

[1] According to ASHRAE Handbook 2005 Fundamentals, the boiling point of water is:

Pressure, kPa	Boiling point, °C
701.8	90
846.1	95

From the above table, it is obtained by interpolation: $T = 0.03465P + 65.68$.
The equation means that 2.886 kPa of pressure difference will result in 0.1 °C change of boiling point.

Taking the boiling point as 94.3 °C, the thermometer underestimated the temperature by 0.4 °C at 94.3 °C, and was accurate at 0 degrees. Considering the mercury thermometer to be a linear device, a correction equation is obtained:

$$T_{\text{actual}} = 1.004 \cdot T_{\text{reading}} \tag{C.1}$$

C.1.2 LM35DZ Sensors

A well- insulated 2-litre flask was used as the calibrator. The temperature sensors and the mercury thermometer were put into the flask alongside each other for each temperature setting (using ice or boiling water to adjust the water temperature in the flask). 16 readings were taken in the temperature range of 18.3-63.6 °C (covers the testing temperature range), starting from the lowest value, rising to the maximum, and dropping to the lowest.

Calibration Curve The calibration data is plotted to obtain a fitted curve, the result is shown in Figure C.1 and Table C.2.

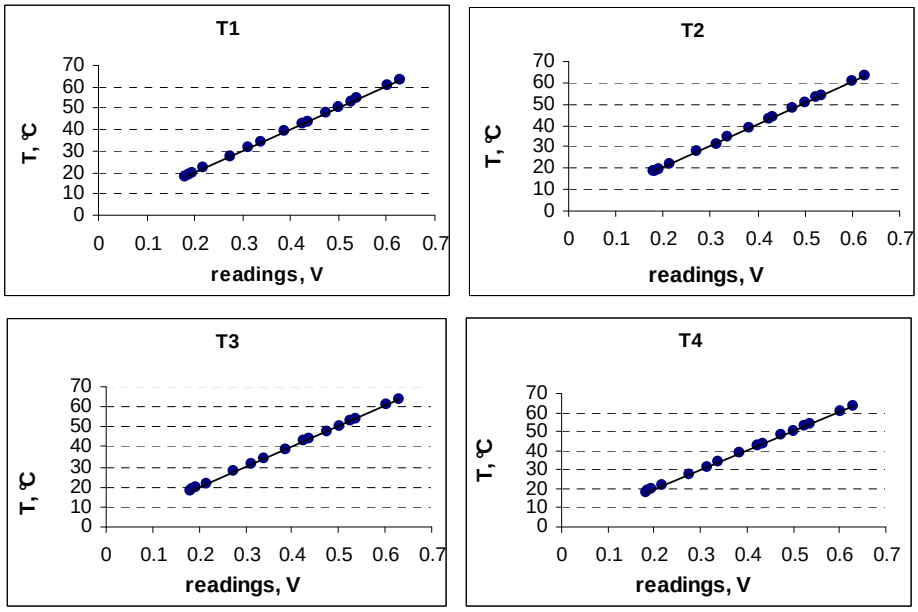


Figure C.1: Linear fitting for the four LM35DZ sensors calibration data

Table C.1: Calibration fitted curve

LM35DZ sensors calibration equation (x in V, y in ^{o}C):			
sensor	fitting	RMSE, ^{o}C	Rsquare
T1	$y = 100.87x - 0.0270,$	0.0289,	0.9999966
T3	$y = 100.80x - 0.0369,$	0.0271,	0.9999970
T2	$y = 100.92x + 0.0985,$	0.0297,	0.9999964
T4	$y = 100.84x - 0.0665,$	0.0282,	0.9999968

C.1.3 Resistance Temperature Detectors (RTD's)

The four RTD's were calibrated against the reference mercury thermometer. The RTD sensors and the mercury thermometer were put into the 2-litre flask alongside each other for each temperature setting (using ice or boiling water to adjust the water temperature in the flask). 17 readings were taken in the temperature range of 0 to 60 °C (covers the test temperature range needed), arranged in a sequence starting from the lowest value, rising up to highest, and dropping to the lowest. Calibration apparatus information is given as following:

Sensor power supply: 24 VDC
Sensor signal output: 4-20 mA
Load resistor: 47.0 ohm for all sensors

Calibration Curve Best fitting curves were obtained for the RTD sensors, as shown in Figure C.2 and Table C.2.

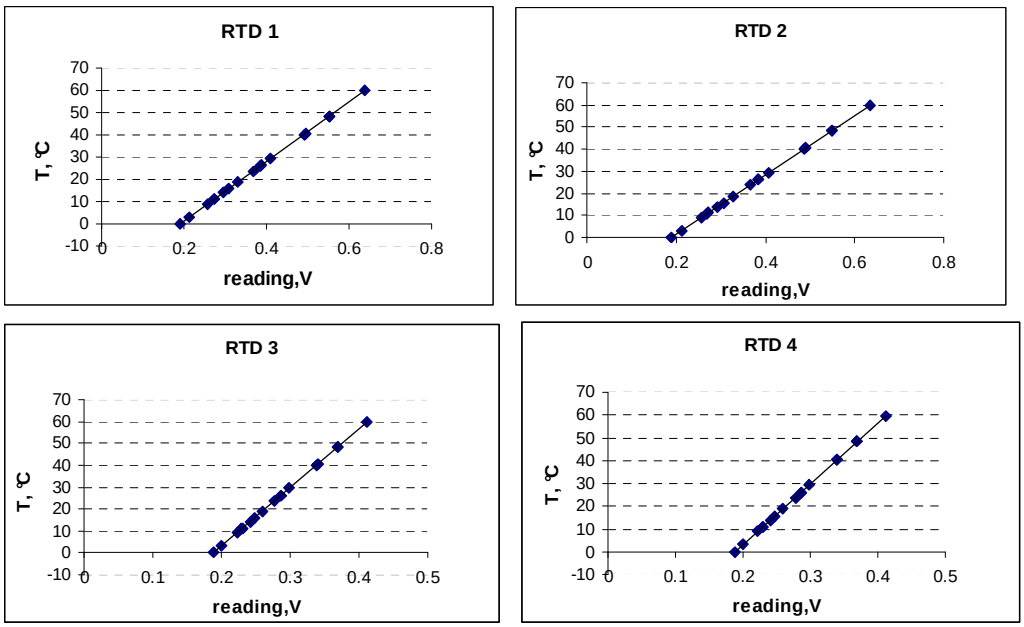


Figure C.2: Calibration curve of RTD sensors

Table C.2: Calibration equation of the four RTD sensors

RTD curve fitting equation (x in Volts, y in ^{o}C)			
sensor	fitting	RMSE, ^{o}C	Rsquare
RTD 1	$y = 133.02x - 25.1524$,	0.0257,	0.9999979
RTD 2	$y = 133.95x - 25.1882$,	0.0200,	0.9999987
RTD 3	$y = 268.36x - 50.6932$,	0.0328,	0.9999966
RTD 4	$y = 268.36x - 50.6793$,	0.0286,	0.9999974

C.2 RS 257-026 Turbine Flow Meters

Two identical flowmeters, termed as flowmeter 1 and 2, were calibrated with the same procedure. Water from the flowmeters was collected in a bin up to a marking line, and then put onto a mechanical scale to weigh. The calibration started with maximum flow (about 1.1l/s), then flow was dropped by steps to a minimum flow (about 0.22 l/s). The flow was then shut off and raised up again to repeat the previous points. 17 points were taken in total for each flowmeter. Calibration apparatus information is:.

Mechanical scale minimum reading: 100 g
Water temperature: 17 °C
Water density: 998.7 kg/m^3
Sensor power supply: 24 VDC
Sensor signal output: 40-20 mA
Load resistor: 46.8 ohm for flowmeter 1, 46.9 ohm for flowmeter 2

Calibration Curve Best fitting curves were obtained for the two flowmeters; see Figure C.3 for the calibration curve and Table C.3 for the fitted equation. It can be found that power law curves have a better fitting goodness, and it was then decided that for flow rates inside the calibration range, power law fitting curve is to be used, for flow rates beyond that, linear fitting curve was to be used, because the flow meter is designed as a linear output device.

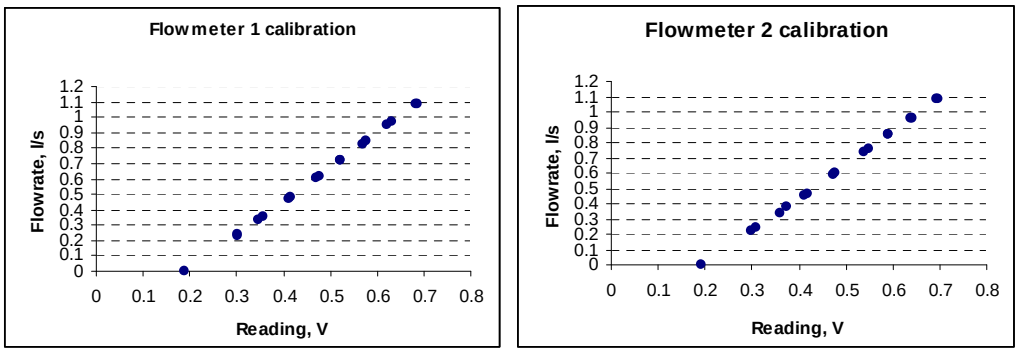


Figure C.3: Flowmeter calibration curve

Table C.3: Calibration equation of the two RS flowmeters

	Calibration curve equation, x in V, y in l/s			
	fitting	equation	RMSE, l/s	R-square
Flowmeter 1	Linear	$y = 2.219x - 0.4374$	0.005919	0.9997
	Power-law	$y = 2.188x^{1.1} - 0.3529$	0.00151	1
Flowmeter 2	Linear	$y = 2.171x - 0.4327$	0.006746	0.9996
	Power-law	$y = 2.137x^{1.098} - 0.3499$	0.003914	0.9999

C.3 Trimec MP15S Flowmeter

The Trimec MP15S multipulse flowmeter was calibrated using water. A frequency to current converter was connected to the flowmeter for the data acquisition system. Because the pump had a capacity which is too big for the flowmeter, a by-pass arrangement was made and the flowmeter was positioned in the main line. Centrifugal pumps operate in a certain range of flow rates, below that vibration and flow fluctuation occur. If a relatively small stable flow is required from a big capacity pump, a by-pass arrangement is necessary because it allows free adjustment of flow in the main line without much effect on the pump overall flow rate. Two valves were thus needed, one for the mainline and one for the by-pass line. Flow rates were controlled starting from 2.2 l/min, rising up to 8.4 l/min, then dropping down back to 0 l/min, 14 readings were taken. Water from the flowmeters was collected by a bucket up to a marking line, and then put onto a mechanical scale to weigh. Apparatus was set as:

Water temperature: 18.6 °C

Minimum reading of scale: 50 g

Flowmeter power supply: 12 VDC

Flowmeter signal output: frequency 0-60 HZ

Frequency to current converter signal output: 4-20 mA

Load resistor: 46.8 ohm

Calibration Curve Calibration curves of the linear and power-law type are obtained for the two sensors; the result is shown in Figure C.4 and Table C.4.

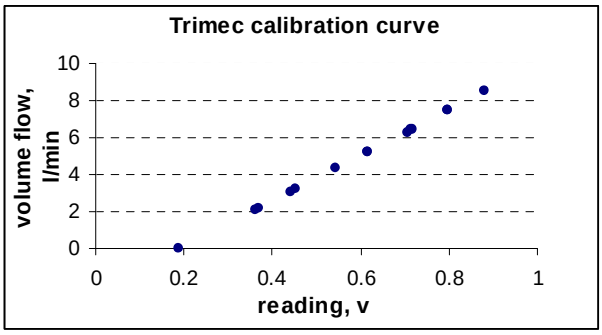


Figure C.4: Calibration curve of Trimec MP15S flowmeter

Table C.4: Calibration equation of Trimec MP15S

Trimec MP15S curve fitting equation, x in Volts, y in l/min			
	equation	RSME, l/min	R-square
linear	$y = 12.343x - 2.377$	0.03357	0.9998
power-law	$y = 12.12x^{1.056} - 2.061$	0.01715	1

C.4 Rosemount 3051 CD Differential Pressure Transmitter

Two rubber tubes with inside diameter of 4 mm were connected to the transmitter. The low-side tube had a water head of approximately 300 mm, and was attached to a wall and kept constant during the calibration. The high-side tube had a length of approximately 10 metres, one end of this tube was moved up with an interval of 1 m against a tape measure, up to 7.5 m (last movement was 0.5 m), and moved down in the same steps. 17 readings were taken. Calibration apparatus was set as:

Type measure minimum reading: 1 mm
Water density: 998.21 kg/m3 (at 20 °C)
Gravity: 9.79 m/s^2
Sensor power supply: 24 VDC
Sensor signal output: 4-20 mA
Load resistor: 46.6 ohm

Calibration Curve A Calibration curve was obtained, as shown in Figure C.5 and Table C.5.

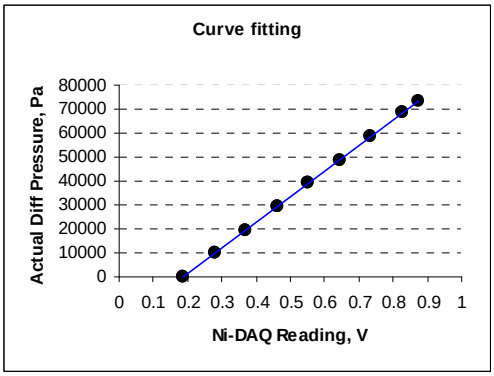


Figure C.5: Calibration curve of Rosemount 3051 CD

Table C.5: Calibration equation of Rosemount 3051 CD

Rosemount 3051 calibration equation (x in V, y in Pa):		
equation	RMSE, Pa	Rsquare
$y = 107067.3x - 20039.8$	18.58	1

C.5 WIKA Static Pressure Transmitters

The two WIKA static pressure transmitters were calibrated by a Budenberg dead weight pressure gauge calibrator. The calibrator consists of a precision machined piston and cylinder assembly mounted on an oil tank. Two tube connections allow the installation of a master gauge and the pressure transmitter which is to be calibrated. Weight is added onto the cylinder piston and lifted to a certain height by adjusting the hand pump linked to the oil tank. By adding different weights, various pressures are obtained. The calibrator works in accordance with the basic principle that $P = F / A$, where the pressure P acts on a known area of a sealed piston with area of A, generating a force F. This type of calibrator is the most accurate instrument for pressure sensor calibration. With high quality materials used, it has small uncertainties of measurement and excellent long term stability. 19 readings were taken for each sensor, in the range of 0-840 kPa. Weights were added starting from 10 psi (70 kPa), increasing to 120 psi (840 kPa), then decreasing to 50 psi (355 kPa). Calibration apparatus was set as:

Piston cross-section area: 0.0625 in^2
Sensor power supply: 24 VDC
Sensor signal output: 4-20 mA
Load resistor: 47.0 ohm for sensor 1, 46.8 ohm for sensor 2

Calibration Curve Calibration curves of the linear and power-law type are obtained for the two sensors; the result is shown in Figure C.6 and Table C.6.

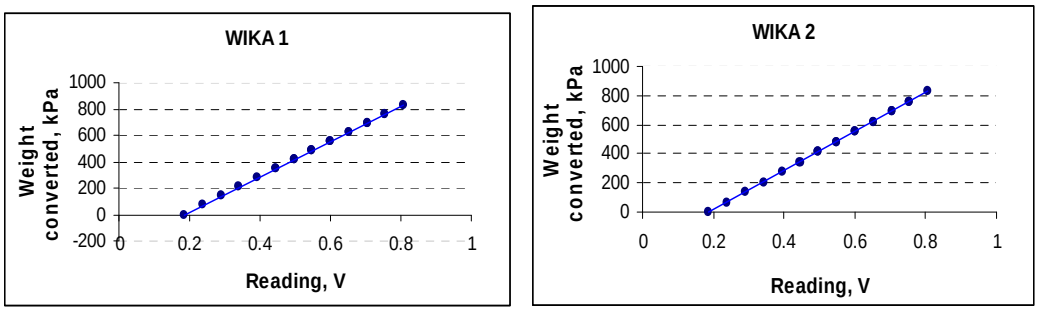


Figure C.6: Calibration curve of WIKA pressure sensors

Table C.6: Calibration equation of the WIKA pressure sensors

	Calibration curve equation, x in V, y in kPa			
	fitting	equation	RMSE, kPa	R-square
WIKA 1	Linear	$1330.07x - 247.45$	0.33	1
	Power-law	$1330x - 247.4$	0.34	1
WIKA 2	Linear	$1336.85x - 251.42$	0.21	1
	Power-law	$1337x^{1.001} - 251$	0.21	1

Appendix D Data Acquisition System Specifications

Technical Specifications:

Specifications listed below are typical at 25 °C unless otherwise noted.

Table D.1: NI PCI 6224 specifications

Analog Input			
Number of channels	16 differential or 32 single ended	**Settling time for multichannel measurements**	
		Accuracy, full scale step, all ranges	
ADC resolution	16 bits	±90 ppm of step (±6 LSB)	4 µs convert interval
Sampling rate			
Maximum	250 kS/s	±30 ppm of step (±2 LSB)	5 µs convert interval
Minimum	No minimum		
		±15 ppm of step (±1 LSB)	7 µs convert interval
		Calibration	
		Recommended warm-up time	15 minutes
Input range	±10V, ±5V, ±1V, ±0.2V	Calibration interval:	1 year
		Environmental	
Input FIFO size	4095 samples	Operating temperature	0 to 55 °C
		Maximum altitude	2,000m
Scan list memory	4095 entries		

Analog Input Circuitry

Figure D.1 shows the M series devices analog input circuitry

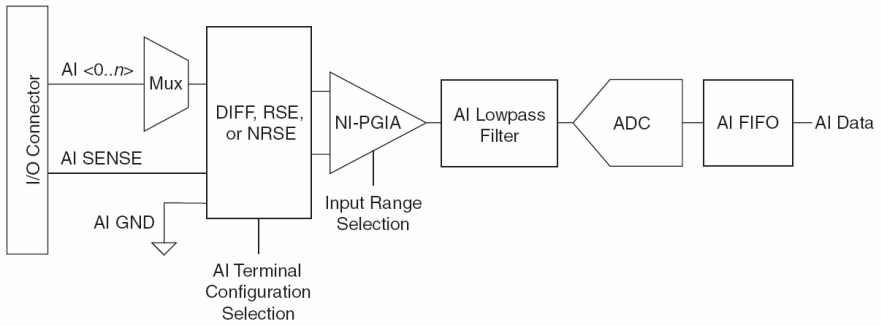


Figure D.1: M series analog input circuitry

For terms used in Figure D.1:

I/O Connector – analog input signals are connected to the I/O connector. The proper way of connection depends on the analog input ground-reference settings: DIFF, RSE, and NRSE modes.

MUX – Multiplexers. MUX route one AI channels at a time to the ADC through NI-PGIA.

NI-PGIA – NI programmable gain instrumentation amplifier. NI-PGIA amplifies or attenuates an AI signal to ensure the maximum resolution.

AI lowpass filter – A lowpass filter attenuates signals with frequencies above the cutoff frequency while passing signals below the cutoff frequency, this is used to reduce the noise level.

ADC – Analog to digital converter. ADC digitizes the AI signal by converting the analog voltage into a digital number.

AI FIFO – AI first-in-first-out. In multiple A/D conversions the FIFO buffer holds data during AI acquisitions to ensure that no data is lost.

Appendix E Experimental Results: Water Tests

E.1 Low Angle BPHE
E.2 Mixed Angle BPHE
E.3 High Angle BPHE

E.1 Low-angle BPHE Unit

	Observations							Calculation						
	$T_{h,in}$	$T_{h,out}$	$T_{c,in}$	$T_{c,out}$	Q_h	Q_c	LMTD	$\dot{Q}_h$	$\dot{Q}_c$	U	Re_h	Re_c	h_h	h_c
	°C	°C	°C	°C	l/s	l/s	°C	W	W	W/m^{2}K	-	-	W/m^{2}K	W/m^{2}K
1 *	55.9	39.64	18.65	45.89	0.397	0.245	14.82	26965	27732	870	562	283		
2 *	55.03	37.28	19.16	41.41	0.392	0.316	15.77	29080	29163	883	541	350		
3 *	55.88	37.12	18.64	41.27	0.394	0.329	16.47	30877	30875	897	547	362		
4	55.23	36.55	19.02	39.64	0.39	0.348	16.54	30494	29802	882	537	378	1895	1647
5	55.18	36	19.34	38.96	0.395	0.397	16.44	31665	32355	922	540	429	1905	1819
6	55.23	35.91	19.32	38.11	0.39	0.399	16.85	31477	31190	894	533	428	1884	1820
7	55.33	33.99	18.42	35.73	0.392	0.503	17.51	34987	36230	956	528	520	1871	2139
8	55.17	34.03	19.05	34.94	0.398	0.547	17.48	35155	36202	962	535	565	1889	2282
9	55.27	32.93	18.42	33.64	0.395	0.59	17.83	36945	37371	991	527	597	1868	2391
10	55.29	31.69	18.43	32.31	0.393	0.679	17.68	38841	39223	1051	519	678	1847	2646
11	55.24	32.12	18.62	31.98	0.396	0.693	17.94	38262	38524	1021	523	691	1857	2687
12	55.38	30.69	18.56	30.79	0.393	0.788	17.63	40579	40143	1101	514	775	1833	2945
13	56.03	31.34	18.6	30.85	0.394	0.791	18.26	40763	40387	1068	522	779	1848	2959
14	55.44	30.45	18.93	29.88	0.396	0.898	17.62	41450	40933	1126	518	877	1841	3247
15	56.01	30.41	18.55	29.95	0.396	0.898	18.03	42471	42680	1127	520	874	1844	3245
16	56.02	29.78	18.53	29.22	0.398	0.989	17.91	43684	44048	1167	519	954	1841	3477
17	55.46	29.71	18.9	29.13	0.396	0.995	17.44	42632	42431	1170	513	963	1830	3498
18	55.43	29.02	18.9	28.35	0.397	1.106	17.24	43908	43586	1219	512	1061	1828	3777
19	55.97	28.87	18.46	28.21	0.395	1.11	17.68	44834	45104	1213	511	1057	1821	3776
20	55.42	28.74	18.89	28.04	0.395	1.147	17.15	44108	43775	1231	508	1096	1816	3877
21	55.24	28.52	18.46	27.71	0.394	1.154	17.35	44107	44459	1216	505	1092	1809	3877
22	55.88	28.65	18.48	27.91	0.396	1.154	17.6	45143	45416	1227	511	1096	1821	3885

* Shaded cells: Laminar

	Observation		Calculation						
	Q	$DP_{mesurement}$	DP_{pipe}	$DP_{PHE,in}$	$DP_{PHE,out}$	DP_{port}	DP_{core}	Re	f
	l/s	Pa	Pa	Pa	Pa	Pa	Pa	-	-
1 *	0.305	825	34	177	105	14	495	282	1.13
2 *	0.345	1006	42	227	134	18	584	319	1.05
3	0.4	1311	55	306	181	25	744	354	0.99
4	0.443	1560	65	374	221	30	870	409	0.94
5	0.449	1646	68	385	227	31	935	397	0.99
6	0.543	2333	94	564	333	45	1297	481	0.93
7	0.545	2274	94	568	335	46	1232	504	0.88
8	0.643	3219	125	790	467	64	1773	595	0.91
9	0.647	3215	128	801	473	65	1748	573	0.89
10	0.742	4189	161	1052	621	85	2270	686	0.88
11	0.798	4808	183	1216	719	98	2592	738	0.87
12	0.84	5258	200	1348	796	109	2805	776	0.84
13	0.901	6014	226	1551	916	125	3196	833	0.84
14	0.945	6517	246	1705	1008	137	3421	873	0.81
15	1.052	8020	296	2113	1249	170	4192	972	0.81
16	1.089	8633	315	2265	1338	183	4532	1006	0.81
17	1.128	9270	347	2433	1437	196	4857	908	0.81

* Shaded cells: Laminar

E.2 Mixed-angle BPHE Unit

	Observations							Calculation						
	$T_{h,in}$	$T_{h,out}$	$T_{c,in}$	$T_{c,out}$	Q_h	Q_c	LMTD	$\dot{Q}_h$	$\dot{Q}_c$	U	Re_h	Re_c	h_h	h_c
	°C	°C	°C	°C	l/s	l/s	°C	W	W	W/m^{2}K	-	-	W/m^{2}K	W/m^{2}K
1	55.28	33.91	19.23	47.62	0.376	0.281	10.78	33578	33030	1490	505	331	3449	2860
2	55.35	32.64	19.14	46.2	0.375	0.309	11.18	35609	34719	1523	499	359	3426	3029
3	55.25	30.76	19	44.38	0.375	0.371	11.31	38387	39078	1624	490	423	3398	3380
4	55.39	29.05	18.87	42.18	0.373	0.425	11.63	41071	41119	1690	480	473	3363	3658
5	55.21	28.83	18.8	41.61	0.377	0.45	11.73	41673	42650	1700	485	498	3385	3789
6	55.18	27.39	18.7	39.12	0.375	0.521	12	43607	44252	1739	475	561	3347	4125
7	55.39	26.87	18.71	38.42	0.375	0.545	12.04	44830	44663	1782	475	582	3344	4234
8	55.15	26.29	18.63	37.17	0.373	0.588	12.1	45126	45325	1785	469	619	3319	4421
9	55.4	25.84	18.64	36.52	0.375	0.626	12.12	46401	46545	1832	470	654	3322	4593
10	55.09	24.97	18.52	34.47	0.371	0.702	12.19	46857	46580	1839	461	717	3282	4903
11	55.44	24.98	18.57	34.81	0.376	0.717	12.16	48022	48445	1890	469	736	3315	4981
12	55.03	24.22	18.47	32.89	0.369	0.788	12.16	47589	47341	1873	454	792	3251	5253
13	55.42	24.15	18.51	33.04	0.375	0.82	12.14	49135	49640	1936	463	826	3291	5395
14	55.46	23.62	18.47	31.74	0.376	0.915	12.16	50173	50594	1974	462	909	3285	5761
15	54.96	23.37	18.41	31.03	0.368	0.932	12.06	48690	49018	1932	449	917	3228	5808
16	55.48	23.11	18.43	30.52	0.374	1.019	12.11	50660	51375	2001	457	997	3260	6142
17	55.43	22.82	18.4	29.75	0.375	1.094	12.08	51243	51695	2030	458	1060	3260	6405
18	55.39	22.67	18.39	29.23	0.376	1.149	12.09	51566	51884	2041	458	1106	3261	6595

	Observation		Calculation						
	Q	$DP_{mesurement}$	DP_{pipe}	$DP_{PHE,in}$	$DP_{PHE,out}$	DP_{port}	DP_{core}	Re	f
	l/s	Pa	Pa	Pa	Pa	Pa	Pa	-	-
1	0.248	791	24	117	69	9	571	219	1.98
2	0.298	1076	33	170	101	14	759	264	1.81
3	0.397	1896	55	302	178	24	1338	352	1.8
4	0.434	2059	64	361	213	29	1392	384	1.57
5	0.481	2702	76	441	261	36	1888	425	1.74
6	0.536	3151	92	548	324	44	2142	474	1.59
7	0.594	3939	110	675	399	54	2701	526	1.62
8	0.67	4662	136	857	507	69	3093	593	1.46
9	0.697	5371	146	928	549	75	3674	617	1.61
10	0.741	6021	162	1050	620	85	4103	656	1.59
11	0.789	6727	181	1189	703	96	4559	698	1.56
12	0.848	7781	206	1374	812	111	5279	750	1.56
13	0.9	8596	228	1547	914	125	5781	796	1.52
14	0.965	9893	258	1779	1051	143	6661	854	1.52
15	1.008	10688	278	1943	1148	157	7162	892	1.5
16	1.115	13078	332	2374	1403	191	8778	986	1.5

E.3 High-angle BPHE

	Observations							Calculation						
	$T_{h,in}$	$T_{h,out}$	$T_{c,in}$	$T_{c,out}$	Q_h	Q_c	LMTD	$\dot{Q}_h$	$\dot{Q}_c$	U	Re_h	Re_c	h_h	h_c
	°C	°C	°C	°C	l/s	l/s	°C	W	W	W/m^{2}K	-	-	W/m^{2}K	W/m^{2}K
1	56.37	29.99	19.05	51.31	0.353	0.288	7.63	39009	38478	2446	463	351	5580	5125
2	56.34	29.22	19.02	50.66	0.352	0.304	7.72	39952	39835	2477	458	369	5557	5263
3	56.27	27.1	18.88	48.54	0.352	0.352	7.97	42985	43240	2581	450	417	5525	5651
4	56.44	25.01	18.72	45.93	0.354	0.414	8.22	46568	46763	2709	445	478	5508	6121
5	56.22	24.91	18.71	45.54	0.35	0.415	8.24	45892	46151	2665	438	476	5471	6117
6	56.45	23.38	18.59	42.89	0.354	0.488	8.43	49030	49245	2784	438	546	5477	6626
7	56.13	23.08	18.61	41.81	0.353	0.509	8.46	48887	49103	2764	435	564	5458	6759
8	56.49	22.4	18.52	40.63	0.355	0.555	8.51	50671	50960	2849	435	606	5460	7048
9	56.51	21.51	18.44	38.1	0.355	0.643	8.56	52049	52554	2910	432	682	5434	7572
10	56.07	21.49	18.46	37.78	0.351	0.644	8.49	50850	51727	2867	425	681	5396	7570
11	56.5	20.88	18.39	35.87	0.357	0.743	8.57	53231	54003	2970	431	769	5426	8125
12	55.99	20.67	18.37	34.87	0.356	0.781	8.49	52639	53589	2968	427	800	5405	8319
13	56.53	20.41	18.34	34.12	0.354	0.83	8.54	53616	54537	3004	427	844	5390	8581
14	56.52	20.1	18.31	32.73	0.355	0.923	8.5	54205	55397	3049	426	924	5385	9041
15	56.51	19.87	18.28	31.61	0.358	1.009	8.48	54968	56075	3100	429	999	5396	9450
16	56.44	19.82	18.26	31.18	0.358	1.045	8.51	54912	56247	3088	428	1029	5390	9613

	Observation		Calculation						
	Q	$DP_{mesurement}$	DP_{pipe}	$DP_{PHE,in}$	$DP_{PHE,out}$	DP_{port}	DP_{core}	Re	f
	l/s	Pa	Pa	Pa	Pa	Pa	Pa	-	-
1	0.265	1957	28	134	79	11	1705	213	5.15
2	0.293	2376	33	164	97	13	2068	236	5.1
3	0.326	2882	39	203	120	16	2504	262	5.01
4	0.348	3265	44	232	137	19	2833	280	4.96
5	0.393	4105	55	295	174	24	3557	316	4.89
6	0.398	4178	56	302	179	24	3617	320	4.86
7	0.441	5100	67	371	219	30	4413	355	4.83
8	0.474	5820	76	429	254	35	5027	381	4.75
9	0.529	7115	92	534	316	43	6130	425	4.66
10	0.591	8755	112	667	394	54	7529	475	4.58
11	0.728	12898	161	1011	598	82	11047	585	4.43
12	0.734	13086	164	1030	609	83	11201	591	4.41
13	0.811	15812	195	1258	744	101	13514	653	4.36
14	0.817	15958	197	1275	754	103	13629	657	4.34
15	0.902	19149	235	1555	919	125	16316	726	4.26
16	0.952	21131	258	1732	1023	140	17978	766	4.21
17	1.017	23844	290	1978	1169	159	20247	819	4.15
18	1.043	24946	302	2079	1228	168	21169	839	4.13

Appendix F Experiment Results: Refrigerant Evaporator Tests

F.1 R134a Low-angle BPHE Unit
F.2 R134a Mix-angle BPHE Unit
F.3 R134a High-angle BPHE Unit
F.4 R507A Low-angle BPHE Unit
F.5 R507A Mix-angle BPHE Unit
F.6 R507A High-angle BPHE Unit

F.1 R134a Low-angle BPHE Unit

Observations								
RTD1	RTD2	RTD3	RTD4	Trimec	WIKA 1	WIKA 2	RS 1	RM
$T_{w,out}$	$T_{w,in}$	$T_{r,in}$	$T_{r,out}$	Q_r	$P_{r,out}$	$P_{r,in}$	Q_w	ΔP_r
℃	℃	℃	℃	l/min	kPa	kPa	l/sec	kPa
10.85	14.66	6.79	6.85	5.015	288.2	298.4	0.7977	4.765
10.86	14.65	6.90	6.97	4.538	289.1	298.4	0.7995	3.874
10.84	14.64	6.91	6.96	4.051	288.2	296.7	0.7980	3.036
10.89	14.65	6.87	6.91	3.732	287.3	295.3	0.7966	2.401
11.00	14.54	6.89	6.76	5.202	288.4	298.5	0.8041	4.582
11.01	14.54	7.18	7.02	4.800	291.3	300.6	0.8009	3.871
11.10	14.52	7.50	7.25	4.419	294.1	302.7	0.8024	3.073
11.13	14.54	7.21	7.16	3.866	292.0	300.0	0.8010	2.218
10.97	14.51	6.93	6.89	3.587	287.1	294.5	0.7980	1.796
11.01	14.51	7.16	6.94	3.547	287.2	294.5	0.7997	1.632
12.34	15.98	8.65	8.43	5.324	309.1	319.4	0.7996	4.824
12.29	15.99	8.46	8.22	4.977	305.9	315.6	0.7987	4.227
11.50	14.47	8.03	7.89	5.614	303.5	313.7	0.7985	4.848
11.26	14.28	7.64	7.51	5.274	298.7	308.6	0.8043	4.391
11.30	14.28	7.81	7.57	4.784	299.5	308.7	0.8052	3.584
11.29	14.27	7.59	7.44	3.885	297.0	305.0	0.8045	2.291
11.31	14.28	8.03	7.55	3.658	297.4	305.0	0.8024	2.094
11.28	14.28	7.50	7.40	3.205	294.5	301.2	0.8034	1.064
9.01	13.76	5.44	5.17	5.258	269.2	278.6	0.5033	4.076
8.99	13.76	5.39	5.15	4.769	268.7	277.5	0.4996	3.450
8.96	13.74	5.45	5.12	4.259	268.2	276.3	0.4997	2.780
8.98	13.75	5.48	5.13	3.947	268.1	275.9	0.4996	2.319
8.96	13.74	5.44	5.12	3.632	267.5	274.9	0.4985	1.899
8.97	13.75	5.44	5.24	3.488	268.7	275.9	0.4993	1.664
8.98	13.70	5.38	5.24	3.142	268.1	274.7	0.5002	1.024
9.02	13.72	5.23	5.29	2.986	268.1	274.4	0.4992	0.753
9.58	14.21	5.65	5.65	6.149	272.9	283.4	0.4995	5.589
9.54	14.18	5.67	5.67	5.248	272.6	282.1	0.5000	4.415

9.52	14.17	5.76	5.70	4.570	272.6	281.2	0.4991	3.438
9.52	14.16	5.78	5.72	4.153	272.5	280.5	0.5001	2.802
9.51	14.16	5.79	5.73	3.736	271.9	279.4	0.4993	2.146
9.55	14.16	5.83	5.74	3.388	271.5	278.3	0.5003	1.531
9.54	14.15	5.73	5.73	3.151	270.6	277.0	0.4996	1.104
9.63	14.16	5.45	5.74	2.803	268.3	274.1	0.5000	0.437
11.72	15.72	8.14	8.20	4.645	309.8	318.6	0.5012	2.959
11.70	15.70	8.01	8.15	4.279	309.1	317.6	0.5007	2.433
11.63	15.67	8.07	8.12	3.732	308.3	316.0	0.5007	1.745
11.61	15.68	8.10	8.10	3.314	307.9	315.0	0.5011	1.080
11.66	15.67	8.29	8.23	3.058	308.6	315.0	0.5005	0.223
11.62	15.66	8.22	8.10	2.786	307.0	313.2	0.5006	0.023
11.63	15.66	8.14	8.07	2.491	305.1	310.8	0.4998	-0.372
11.56	15.64	8.13	8.50	2.283	306.7	311.9	0.4973	-0.383
12.90	15.76	10.15	10.13	5.145	335.7	343.7	0.4959	1.897
12.90	15.78	10.25	10.17	4.031	336.1	343.1	0.4965	0.676
12.87	15.75	10.31	10.20	3.283	336.1	342.5	0.4951	-0.103
12.92	15.77	10.34	10.28	2.859	336.9	342.9	0.4938	-0.380
12.94	15.78	10.30	10.33	2.533	337.4	343.1	0.4951	-0.384
12.98	15.78	10.27	10.40	2.243	337.9	343.3	0.4947	-0.384
12.96	15.75	10.19	10.38	1.998	336.8	341.9	0.4941	-0.384
13.00	15.77	10.10	10.39	1.788	336.0	340.8	0.4951	-0.384
13.90	15.82	11.54	11.52	4.814	355.1	362.2	0.4993	0.732
13.89	15.82	11.63	11.55	4.001	355.2	361.8	0.5005	0.053
13.88	15.80	11.65	11.56	3.530	355.6	361.9	0.5006	-0.329
13.89	15.81	11.65	11.62	3.072	356.2	362.2	0.5011	-0.386
13.91	15.82	11.61	11.68	2.543	356.8	362.5	0.5015	-0.387
13.92	15.81	11.55	11.75	1.953	357.2	362.5	0.5017	-0.386
13.92	15.81	11.50	11.80	1.555	356.9	361.8	0.5011	-0.387
13.97	15.81	11.36	11.70	1.155	353.7	358.1	0.5013	-0.387

Red colored data are not used for ΔP_{fric} data processing.

Calculations

$Q_{coolling}$ kW	LMTD ℃	U kW/(m^2·K)	q kW/m^2	G_r kg/(m^2·s)	x_{out} –	h_r kW/(m^2·K)	$\Delta P_{fric, expe}$ kPa
12.74	5.32	1.145	6.096	24.61	0.62	2.194	7.413
12.68	5.21	1.166	6.067	22.27	0.68	2.265	6.943
12.69	5.19	1.170	6.071	19.88	0.76	2.287	6.520
12.55	5.26	1.142	6.004	18.31	0.82	2.182	6.151
11.91	5.35	1.066	5.697	25.52	0.56	1.910	7.094
11.85	5.06	1.121	5.670	23.53	0.60	2.101	6.738
11.47	4.81	1.142	5.489	21.64	0.64	2.171	6.271
11.45	5.06	1.083	5.478	18.95	0.72	1.968	5.860
11.83	5.24	1.081	5.658	17.60	0.80	1.968	5.660
11.73	5.08	1.104	5.610	17.39	0.81	2.043	5.529
12.18	4.99	1.168	5.827	26.00	0.57	2.239	7.259
12.38	5.17	1.147	5.922	24.31	0.61	2.163	6.954
9.94	4.46	1.065	4.755	27.46	0.44	1.911	7.095
10.18	4.64	1.050	4.870	25.82	0.47	1.861	6.911

10.07	4.52	1.065	4.816	23.41	0.52	1.907	6.513
10.06	4.70	1.023	4.812	19.02	0.63	1.776	5.925
9.99	4.38	1.090	4.779	17.89	0.67	1.992	5.899
10.10	4.78	1.012	4.835	15.70	0.77	1.744	5.204
10.03	5.25	0.914	4.800	25.90	0.46	1.935	6.577
10.01	5.27	0.908	4.788	23.49	0.51	1.920	6.362
10.01	5.21	0.919	4.789	20.98	0.57	1.966	6.107
9.99	5.20	0.920	4.779	19.43	0.61	1.971	5.893
9.98	5.22	0.915	4.774	17.89	0.66	1.952	5.716
10.00	5.19	0.923	4.784	17.18	0.69	1.985	5.591
9.90	5.22	0.908	4.736	15.48	0.76	1.917	5.209
9.83	5.34	0.882	4.705	14.71	0.80	1.805	5.052
9.69	5.50	0.844	4.638	30.27	0.38	1.642	7.329
9.73	5.43	0.857	4.655	25.83	0.45	1.693	6.940
9.71	5.34	0.870	4.647	22.49	0.51	1.747	6.525
9.72	5.32	0.873	4.649	20.44	0.57	1.758	6.220
9.73	5.30	0.878	4.655	18.38	0.63	1.778	5.887
9.67	5.29	0.874	4.627	16.67	0.69	1.761	5.532
9.65	5.36	0.861	4.615	15.51	0.74	1.710	5.279
9.49	5.61	0.810	4.542	13.81	0.82	1.517	4.861
8.38	4.90	0.819	4.011	22.71	0.44	1.516	6.028
8.39	4.99	0.805	4.016	20.93	0.48	1.472	5.778
8.47	4.90	0.828	4.053	18.25	0.56	1.549	5.492
8.53	4.87	0.838	4.081	16.20	0.63	1.587	5.122
8.40	4.72	0.851	4.019	14.95	0.68	1.632	4.438
8.48	4.78	0.849	4.056	13.62	0.75	1.625	4.424
8.42	4.86	0.829	4.029	12.18	0.83	1.556	4.223
8.50	4.65	0.875	4.065	11.16	0.92	1.732	4.353
5.94	3.63	0.783	2.843	25.02	0.29	1.399	4.580
5.99	3.55	0.807	2.868	19.60	0.37	1.474	4.160
5.97	3.46	0.824	2.854	15.96	0.45	1.535	3.879
5.89	3.45	0.816	2.819	13.90	0.52	1.509	3.868
5.88	3.49	0.807	2.815	12.31	0.58	1.475	4.066
5.81	3.51	0.792	2.781	10.91	0.65	1.428	4.238
5.76	3.54	0.778	2.757	9.72	0.72	1.385	4.382
5.74	3.63	0.755	2.744	8.69	0.80	1.312	4.506
4.01	2.87	0.668	1.917	23.32	0.21	1.061	3.515
4.03	2.80	0.689	1.929	19.38	0.25	1.114	3.401
4.03	2.76	0.699	1.929	17.10	0.29	1.142	3.330
4.04	2.75	0.702	1.932	14.88	0.33	1.149	3.567
4.00	2.77	0.690	1.913	12.32	0.40	1.116	3.891
3.98	2.78	0.684	1.906	9.46	0.51	1.101	4.245
3.97	2.80	0.679	1.901	7.53	0.64	1.087	4.479
3.87	2.96	0.624	1.850	5.60	0.84	0.954	4.706

F.2 R134a Mix-angle BPHE Unit

Observations								
RTD1	RTD2	RTD3	RTD4	Trimec	WIKA 1	WIKA 2	RS 1	RM
$T_{w,out}$	$T_{w,in}$	$T_{r,in}$	$T_{r,out}$	Q_r	$P_{r,out}$	$P_{r,in}$	Q_w	ΔP_r
℃	℃	℃	℃	l/min	kPa	kPa	l/sec	kPa
10.97	14.83	8.16	7.70	5.022	300.1	311.4	0.7984	5.726
10.72	14.76	7.58	7.11	4.878	293.0	304.2	0.7967	5.778
10.98	14.70	7.73	7.29	4.352	296.0	306.0	0.7907	4.522
11.01	14.69	7.48	7.39	3.859	296.3	305.3	0.8058	3.356
11.24	14.76	8.25	8.12	5.325	307.4	318.6	0.8024	5.868
11.22	14.74	8.29	8.17	4.725	307.7	317.9	0.7995	4.729
11.24	14.71	8.32	8.17	4.393	307.5	317.2	0.8012	4.073
11.19	14.71	8.33	8.15	3.967	306.6	315.5	0.7995	3.207
11.08	14.66	8.16	8.06	3.707	304.4	312.7	0.7980	2.689
11.15	14.74	8.21	8.25	3.497	304.8	312.8	0.7982	2.302
11.49	14.45	8.26	7.95	5.240	305.6	316.7	0.7976	5.580
11.41	14.41	8.43	8.10	4.658	307.3	317.5	0.7975	4.455
11.42	14.41	8.55	8.19	4.023	307.8	316.8	0.7987	3.278
11.43	14.41	8.64	8.25	3.681	307.6	316.0	0.7996	2.657
11.29	14.36	8.46	8.32	3.281	306.2	313.7	0.8005	1.725
11.31	14.39	8.35	8.72	2.950	303.4	310.5	0.8002	1.477
9.01	13.84	6.20	6.01	5.444	279.1	289.8	0.5001	5.508
8.97	13.82	6.16	5.99	4.987	278.8	288.9	0.4989	4.803
8.95	13.80	6.27	5.99	4.309	278.4	287.5	0.4989	3.767
8.90	13.81	6.28	5.96	3.901	277.6	286.1	0.4990	3.124
8.90	13.80	6.30	5.97	3.732	277.7	285.9	0.4984	2.775
8.91	13.79	6.18	6.00	3.504	277.7	285.5	0.4985	2.382
8.88	13.79	6.14	6.01	3.158	276.9	284.1	0.4994	1.728
8.91	13.75	6.06	6.07	2.873	276.5	283.2	0.4976	1.174
9.60	14.24	6.58	6.48	5.514	282.3	293.1	0.5002	5.873
9.55	14.24	6.56	6.46	5.041	281.9	292.2	0.5007	5.172
9.52	14.21	6.56	6.46	4.516	281.5	291.0	0.5012	4.448
9.49	14.21	6.59	6.46	4.250	281.1	290.4	0.4999	4.050
9.50	14.25	6.57	6.48	4.023	281.1	290.1	0.5013	3.710
9.44	14.21	6.55	6.44	3.784	280.2	288.8	0.5018	3.310
9.44	14.20	6.59	6.52	3.404	280.3	288.2	0.5005	2.628
9.45	14.23	6.53	6.57	3.219	280.0	287.6	0.5002	2.335
9.42	14.17	6.44	6.61	3.069	278.9	286.3	0.5014	2.099
9.47	14.21	6.36	7.13	2.845	278.5	285.6	0.4990	1.749
11.98	15.78	9.21	9.10	4.700	320.9	331.5	0.4980	4.327
11.78	15.78	8.93	8.96	4.129	318.7	328.6	0.4985	3.694
11.74	15.76	8.89	8.96	3.921	318.9	328.5	0.5001	3.270
11.71	15.76	8.91	8.99	3.521	319.0	327.9	0.5005	2.525
11.70	15.74	9.00	9.03	3.015	318.9	326.8	0.4994	1.431
11.70	15.74	9.01	9.06	2.844	318.9	326.4	0.5022	1.057
11.69	15.73	8.97	9.06	2.526	317.3	324.2	0.4983	0.354
11.69	15.73	8.85	9.92	2.200	313.3	319.7	0.4995	-0.191
12.88	15.80	10.66	10.61	4.775	343.3	352.1	0.4991	2.419
12.87	15.79	10.75	10.63	3.950	343.3	351.3	0.5001	1.493
12.87	15.81	10.85	10.68	3.178	343.7	351.0	0.4994	0.734

12.87	15.81	10.84	10.71	2.842	343.9	350.9	0.5004	0.315
12.87	15.80	10.79	10.72	2.601	343.7	350.4	0.5001	0.020
12.90	15.79	10.77	10.81	2.284	344.3	350.6	0.4987	-0.320
12.89	15.77	10.67	10.81	2.076	343.8	349.8	0.4997	-0.383
12.94	15.80	10.52	10.83	1.760	341.8	347.4	0.5017	-0.384
13.98	15.85	12.05	11.96	5.079	362.3	370.3	0.5015	1.444
14.00	15.86	12.17	12.05	4.022	363.6	370.7	0.5019	0.414
13.98	15.85	12.22	12.06	3.509	363.7	370.5	0.5007	0.018
13.91	15.84	12.14	12.01	3.089	363.0	369.5	0.5013	-0.259
13.86	15.84	12.05	12.01	2.655	362.6	368.8	0.5023	-0.386
13.88	15.82	11.98	12.08	2.144	363.2	369.1	0.5010	-0.387
13.90	15.82	11.88	12.11	1.392	361.9	367.2	0.5022	-0.386
13.94	15.82	11.61	12.25	1.183	358.7	363.5	0.5017	-0.387

Red colored data are not used for ΔP_{fric} data processing.

Calculations

$Q_{coolling}$ kW	LMTD ℃	U kW/(m^2·K)	q kW/m^2	G_r kg/(m^2·s)	x_{out} –	h_r kW/(m^2·K)	$\Delta P_{fric, expe}$ kPa
12.91	4.19	1.473	6.176	24.55	0.63	2.523	7.932
13.45	4.62	1.393	6.437	23.89	0.68	2.301	8.100
12.30	4.62	1.274	5.883	21.30	0.69	1.997	7.402
12.42	4.78	1.244	5.943	18.90	0.79	1.913	6.708
11.83	4.16	1.361	5.662	26.03	0.55	2.206	7.803
11.78	4.08	1.380	5.634	23.09	0.61	2.260	7.267
11.65	4.07	1.369	5.572	21.47	0.65	2.230	6.935
11.79	4.03	1.399	5.641	19.39	0.73	2.312	6.470
11.96	4.08	1.401	5.721	18.12	0.79	2.321	6.192
11.98	4.06	1.412	5.733	17.10	0.84	2.350	6.000
9.88	4.27	1.106	4.727	25.62	0.46	1.608	7.681
10.03	4.03	1.192	4.801	22.76	0.53	1.798	7.104
10.00	3.92	1.221	4.784	19.65	0.61	1.865	6.503
10.00	3.83	1.248	4.786	17.97	0.67	1.928	6.181
10.28	3.82	1.287	4.918	16.03	0.77	2.023	5.593
10.31	3.77	1.309	4.932	14.42	0.86	2.078	5.624
10.12	4.40	1.099	4.842	26.76	0.45	1.828	7.346
10.14	4.40	1.103	4.854	24.51	0.49	1.840	7.091
10.13	4.29	1.130	4.845	21.17	0.57	1.916	6.703
10.27	4.25	1.155	4.912	19.17	0.64	1.990	6.431
10.24	4.22	1.161	4.900	18.34	0.67	2.009	6.234
10.18	4.32	1.128	4.873	17.22	0.71	1.912	6.042
10.26	4.33	1.133	4.910	15.52	0.79	1.925	5.690
10.10	4.38	1.104	4.834	14.13	0.85	1.846	5.379
9.74	4.55	1.024	4.659	27.07	0.43	1.626	7.674
9.83	4.53	1.038	4.702	24.75	0.47	1.660	7.432
9.85	4.49	1.049	4.715	22.17	0.53	1.689	7.204
9.87	4.46	1.059	4.722	20.87	0.57	1.716	7.050
9.99	4.49	1.066	4.781	19.75	0.60	1.732	6.914
10.02	4.45	1.077	4.793	18.58	0.64	1.762	6.727
9.98	4.39	1.089	4.777	16.72	0.71	1.796	6.378
10.03	4.43	1.083	4.797	15.81	0.76	1.780	6.244

9.98	4.45	1.073	4.774	15.07	0.79	1.753	6.136
9.92	4.37	1.087	4.747	13.98	0.85	1.792	5.974
7.92	4.02	0.943	3.791	22.92	0.42	1.420	6.995
8.34	4.12	0.968	3.991	20.14	0.50	1.476	6.846
8.43	4.11	0.981	4.035	19.13	0.53	1.506	6.596
8.48	4.07	0.996	4.056	17.18	0.60	1.542	6.180
8.44	3.97	1.017	4.039	14.71	0.69	1.595	5.486
8.49	3.96	1.026	4.064	13.87	0.74	1.613	5.247
8.44	3.97	1.016	4.037	12.32	0.83	1.592	4.785
8.43	3.74	1.078	4.035	10.74	0.95	1.747	4.488
6.10	3.10	0.943	2.919	23.19	0.32	1.414	5.039
6.10	3.01	0.972	2.920	19.17	0.39	1.480	4.778
6.15	2.91	1.010	2.942	15.42	0.49	1.573	4.602
6.16	2.91	1.013	2.947	13.79	0.54	1.578	4.425
6.15	2.94	1.000	2.941	12.63	0.59	1.547	4.300
6.02	2.95	0.977	2.882	11.09	0.66	1.494	4.173
6.02	3.01	0.957	2.880	10.08	0.73	1.447	4.251
6.00	3.16	0.909	2.870	8.55	0.85	1.338	4.462
3.93	2.42	0.777	1.882	24.57	0.20	1.068	3.696
3.89	2.33	0.800	1.861	19.45	0.24	1.111	3.495
3.92	2.26	0.829	1.876	16.96	0.28	1.170	3.483
4.07	2.28	0.854	1.947	14.94	0.33	1.220	3.525
4.14	2.31	0.858	1.982	12.84	0.39	1.227	3.708
4.07	2.35	0.830	1.949	10.37	0.48	1.172	4.044
4.03	2.42	0.797	1.928	6.74	0.73	1.107	4.529
3.94	2.57	0.735	1.886	5.73	0.84	0.990	4.660

F.3 R134a High-angle BPHE Unit

Observations								
RTD1	RTD2	RTD3	RTD4	Trimec	WIKA 1	WIKA 2	RS 1	RM
$T_{w, out}$	$T_{w, in}$	$T_{r, in}$	$T_{r, out}$	Q_r	$P_{r, out}$	$P_{r, in}$	Q_w	ΔP_r
℃	℃	℃	℃	l/min	kPa	kPa	l/sec	kPa
11.20	15.20	8.45	8.23	5.156	307.6	320.1	0.7965	7.300
11.23	15.19	8.65	8.26	5.047	307.9	320.2	0.7960	7.037
10.87	14.89	8.04	7.69	4.856	300.2	312.6	0.8055	7.117
11.22	15.16	8.57	8.27	4.587	307.9	319.4	0.7993	6.155
11.07	14.86	8.22	7.97	4.301	303.5	314.8	0.8044	5.748
11.07	14.89	8.14	7.99	3.815	301.1	311.3	0.8035	4.620
11.12	14.76	8.36	8.27	5.274	306.7	319.0	0.7927	7.106
11.11	14.74	8.60	8.38	4.729	307.6	319.0	0.7933	6.039
11.13	14.75	8.75	8.49	4.269	308.1	318.8	0.7928	5.183
11.15	14.74	8.80	8.52	4.228	308.0	318.7	0.7933	5.191
11.09	14.71	8.72	8.50	3.902	307.3	317.5	0.7924	4.584
11.19	14.75	8.83	8.61	3.442	305.8	314.9	0.7903	3.624
10.47	14.97	7.76	7.56	4.824	298.7	310.6	0.7048	6.666
9.50	14.96	7.29	7.40	4.429	294.8	305.0	0.4995	5.107

11.60	14.62	8.93	8.53	5.274	312.3	324.4	0.7960	6.718
11.59	14.60	9.00	8.58	4.378	312.1	323.0	0.7993	5.305
11.51	14.53	8.99	8.63	3.836	312.6	322.8	0.7971	4.427
11.44	14.53	9.13	8.92	3.555	315.5	325.1	0.7938	3.797
11.54	14.54	8.95	8.87	3.363	311.8	321.2	0.8036	3.503
9.03	13.87	6.80	6.58	5.396	286.5	298.0	0.5005	6.358
9.02	13.85	6.82	6.58	4.976	286.2	297.2	0.5011	5.725
9.02	13.87	6.82	6.59	4.490	286.0	296.4	0.5013	5.131
9.02	13.86	6.87	6.55	3.963	285.2	295.1	0.4993	4.481
9.02	13.86	6.87	6.55	3.807	285.1	294.8	0.5020	4.281
8.97	13.84	6.87	6.57	3.444	284.6	293.8	0.5006	3.697
8.97	13.81	6.87	6.60	3.188	284.0	292.8	0.5014	3.298
9.03	13.84	6.90	6.74	2.896	284.3	292.6	0.5021	2.674
9.66	14.23	7.38	7.25	5.501	293.7	304.7	0.4980	5.920
9.68	14.23	7.52	7.35	4.884	294.5	304.8	0.4981	5.068
9.70	14.29	7.57	7.43	4.518	295.2	305.1	0.4973	4.600
9.69	14.28	7.72	7.46	4.201	295.2	304.7	0.4978	4.193
9.67	14.26	7.64	7.47	4.081	295.4	304.7	0.4965	4.017
9.66	14.28	7.66	7.49	3.781	295.4	304.3	0.4967	3.644
9.64	14.31	7.70	7.56	3.366	295.0	303.4	0.4950	3.045
9.83	14.30	8.07	8.12	3.026	301.0	308.8	0.4968	2.301
11.99	15.85	9.80	9.65	5.030	327.1	338.4	0.5006	5.066
11.88	15.84	9.76	9.57	4.533	326.0	336.7	0.5005	4.466
11.93	15.84	9.82	9.65	4.128	327.0	337.2	0.4993	3.894
11.84	15.82	9.75	9.60	3.565	325.8	335.4	0.5008	3.140
11.93	15.82	9.98	9.76	3.109	327.6	336.4	0.4995	2.288
11.91	15.80	9.97	9.72	2.797	326.3	334.7	0.4992	1.796
11.98	15.81	10.14	9.83	2.485	326.4	334.3	0.4993	1.216
11.95	15.83	9.81	11.21	2.238	324.2	331.7	0.4951	0.876
12.80	15.85	10.78	10.74	4.845	345.3	354.9	0.4973	3.225
12.77	15.83	10.82	10.77	4.003	345.5	354.1	0.4992	2.127
12.77	15.84	10.92	10.83	3.258	346.0	353.8	0.4982	1.241
12.78	15.83	10.99	10.87	2.761	346.1	353.4	0.4982	0.702
12.80	15.84	10.97	10.92	2.456	346.3	353.4	0.4977	0.388
12.81	15.83	10.94	10.96	2.252	346.3	353.2	0.4970	0.180
12.82	15.81	10.93	11.05	2.045	346.6	353.2	0.4979	-0.100
12.84	15.81	10.89	11.30	1.778	346.4	352.5	0.4983	-0.382
13.93	15.87	12.31	12.24	5.120	366.3	374.6	0.4955	1.825
13.94	15.87	12.35	12.23	4.019	366.2	373.8	0.4934	0.884
13.96	15.86	12.45	12.30	3.405	366.9	374.0	0.4943	0.347
13.98	15.86	12.49	12.33	3.068	367.0	373.9	0.4947	0.073
13.81	15.86	12.27	12.24	2.547	365.5	372.0	0.4955	-0.310
13.88	15.87	12.32	12.37	2.158	366.9	373.1	0.4953	-0.375
13.89	15.86	12.31	12.51	1.514	367.3	373.1	0.4954	-0.386
13.88	15.86	12.22	12.95	1.203	366.2	371.5	0.4958	-0.387

Red colored data are not used for ΔP_{fric} data processing.

Calculations

$Q_{coolling}$ kW	LMTD ℃	U kW/(m^2·K)	q kW/m^2	G_r kg/(m^2·s)	x_{out} –	h_r kW/(m^2·K)	$\Delta P_{fric, expe}$ kPa
13.34	4.10	1.559	6.384	25.19	0.64	2.276	9.288
13.20	3.95	1.598	6.314	24.64	0.65	2.361	9.152
13.59	4.23	1.537	6.500	23.75	0.69	2.227	9.408
13.19	3.99	1.583	6.310	22.40	0.71	2.327	8.750
12.77	4.14	1.477	6.110	21.03	0.73	2.104	8.632
12.84	4.20	1.462	6.142	18.66	0.83	2.075	7.989
12.08	3.93	1.470	5.781	25.77	0.56	2.094	9.008
12.05	3.69	1.562	5.764	23.09	0.63	2.285	8.510
12.02	3.56	1.616	5.752	20.84	0.70	2.404	8.115
11.91	3.52	1.618	5.699	20.63	0.70	2.407	8.164
12.02	3.54	1.624	5.749	19.05	0.76	2.421	7.871
11.78	3.50	1.611	5.635	16.80	0.85	2.393	7.344
13.29	4.21	1.510	6.359	23.61	0.68	2.220	8.988
11.43	3.83	1.428	5.469	21.71	0.63	2.175	7.861
10.06	3.73	1.289	4.811	25.73	0.47	1.744	8.713
10.06	3.65	1.321	4.814	21.36	0.57	1.802	8.160
10.09	3.55	1.361	4.826	18.71	0.65	1.878	7.776
10.29	3.28	1.499	4.922	17.34	0.72	2.153	7.396
10.11	3.52	1.375	4.836	16.41	0.74	1.903	7.267
10.15	3.75	1.295	4.858	26.48	0.46	1.885	8.175
10.15	3.71	1.309	4.858	24.42	0.50	1.914	7.965
10.19	3.71	1.313	4.876	22.03	0.55	1.922	7.846
10.13	3.68	1.318	4.846	19.44	0.62	1.933	7.694
10.19	3.68	1.324	4.875	18.68	0.65	1.944	7.637
10.22	3.61	1.354	4.892	16.90	0.72	2.011	7.381
10.17	3.59	1.354	4.868	15.64	0.78	2.012	7.209
10.12	3.59	1.350	4.841	14.21	0.85	2.002	6.839
9.55	3.70	1.234	4.567	26.95	0.42	1.757	7.675
9.50	3.56	1.276	4.545	23.92	0.48	1.843	7.437
9.56	3.54	1.294	4.573	22.12	0.52	1.880	7.316
9.56	3.37	1.355	4.573	20.56	0.56	2.013	7.205
9.55	3.42	1.336	4.569	19.98	0.57	1.972	7.137
9.62	3.39	1.358	4.603	18.51	0.62	2.020	7.033
9.67	3.33	1.392	4.627	16.48	0.71	2.097	6.798
9.31	2.98	1.494	4.454	14.80	0.76	2.335	6.338
8.09	3.40	1.137	3.869	24.48	0.40	1.559	7.371
8.29	3.37	1.178	3.966	22.07	0.46	1.638	7.216
8.17	3.33	1.175	3.909	20.09	0.49	1.633	6.999
8.33	3.33	1.199	3.988	17.36	0.58	1.679	6.719
8.13	3.15	1.235	3.892	15.13	0.65	1.750	6.232
8.14	3.15	1.235	3.893	13.61	0.73	1.751	5.983
8.00	3.02	1.268	3.830	12.09	0.80	1.817	5.636
8.05	2.81	1.372	3.851	10.89	0.90	2.042	5.487
6.35	2.91	1.044	3.039	23.52	0.33	1.389	5.719
6.38	2.84	1.075	3.055	19.43	0.40	1.445	5.326
6.41	2.74	1.119	3.065	15.81	0.49	1.526	5.023
6.35	2.67	1.136	3.039	13.40	0.58	1.557	4.850

6.34	2.69	1.127	3.031	11.92	0.65	1.540	4.755
6.28	2.71	1.110	3.005	10.93	0.70	1.509	4.688
6.24	2.69	1.112	2.987	9.92	0.77	1.512	4.550
6.19	2.65	1.118	2.960	8.63	0.87	1.523	4.448
4.02	2.11	0.914	1.925	24.75	0.20	1.167	3.979
3.98	2.08	0.917	1.907	19.43	0.25	1.173	3.927
3.93	1.99	0.943	1.879	16.45	0.29	1.215	3.847
3.89	1.96	0.950	1.862	14.82	0.32	1.227	3.814
4.26	2.03	1.002	2.037	12.31	0.42	1.316	3.841
4.11	2.01	0.980	1.968	10.43	0.48	1.279	4.027
4.08	1.98	0.987	1.951	7.32	0.68	1.290	4.438
4.11	1.87	1.049	1.965	5.82	0.87	1.398	4.644

F.4 R507A Low-angle BPHE Unit

Observations								
RTD1	RTD2	RTD3	RTD4	Trimec	WIKA 1	WIKA 2	RS 1	RM
$T_{w, out}$	$T_{w, in}$	$T_{r, in}$	$T_{r, out}$	Q_r	$P_{r, out}$	$P_{r, in}$	Q_w	ΔP_r
℃	℃	℃	℃	l/min	kPa	kPa	l/sec	kPa
12.51	16.49	8.36	8.52	6.140	722.4	732.2	0.7980	3.510
12.91	16.57	9.09	9.38	6.538	746.2	756.6	0.7966	3.418
12.52	16.49	8.35	8.54	6.222	723.3	733.2	0.7954	3.562
12.55	16.53	8.17	8.43	6.002	720.0	729.9	0.7947	3.335
12.60	16.51	7.82	8.17	5.965	713.2	722.4	0.8009	3.378
12.60	16.48	7.83	8.20	5.598	712.8	721.5	0.7968	2.759
12.67	16.50	7.80	8.26	5.125	710.6	718.6	0.7969	2.173
12.63	16.47	7.50	8.16	4.772	703.6	711.2	0.7911	1.608
12.85	16.46	8.61	8.93	6.256	732.1	741.4	0.7972	3.308
12.89	16.47	8.70	9.00	5.918	733.7	742.6	0.7959	2.835
12.92	16.47	8.68	8.99	5.241	731.2	739.6	0.7968	2.177
12.84	16.47	8.12	8.78	4.529	717.4	724.9	0.7964	1.404
13.44	16.43	9.16	9.43	6.906	745.7	755.3	0.7939	3.465
13.48	16.43	9.15	9.41	5.559	743.5	752.0	0.8077	2.282
13.43	16.43	9.03	9.45	4.839	741.6	749.6	0.8083	1.619
13.47	16.44	8.92	9.60	4.244	738.7	746.2	0.8058	0.907
13.57	16.40	8.88	9.57	4.077	735.3	742.5	0.8046	0.573
13.94	16.37	10.28	10.56	6.383	773.9	782.6	0.8066	2.721
13.97	16.35	10.22	10.40	5.250	768.1	775.9	0.8036	1.753
13.93	16.34	10.08	10.32	4.484	763.8	771.2	0.8037	1.163
13.94	16.35	10.05	10.49	3.912	763.1	769.9	0.8006	0.601
13.84	16.33	9.55	10.34	3.700	752.3	758.8	0.8014	0.162

Calculations							
$Q_{coolling}$ kW	LMTD ℃	U kW/(m^2·K)	q kW/m^2	G_r kg/(m^2·s)	x_{out} –	h_r kW/(m^2·K)	$\Delta P_{fric, expe}$ kPa
13.28	5.66	1.123	6.356	26.58	0.75	2.261	5.547
12.19	5.14	1.134	5.831	28.22	0.65	2.304	5.143
13.21	5.67	1.115	6.320	26.93	0.74	2.234	5.539
13.24	5.86	1.081	6.333	25.99	0.76	2.100	5.469
13.12	6.20	1.012	6.275	25.89	0.76	1.847	5.537
12.93	6.18	1.002	6.186	24.29	0.80	1.818	5.170
12.76	6.22	0.981	6.107	22.24	0.86	1.751	4.902
12.71	6.40	0.949	6.080	20.73	0.91	1.658	4.573
12.07	5.55	1.041	5.774	27.07	0.67	1.949	5.234
11.92	5.49	1.038	5.701	25.60	0.70	1.940	4.992
11.83	5.52	1.026	5.662	22.67	0.78	1.896	4.790
12.07	5.90	0.979	5.775	19.63	0.92	1.743	4.496
9.94	5.36	0.887	4.754	29.83	0.50	1.472	4.872
9.98	5.39	0.887	4.776	24.01	0.63	1.459	4.614
10.14	5.42	0.896	4.853	20.91	0.73	1.485	4.421
10.01	5.45	0.879	4.790	18.34	0.82	1.441	4.072
9.55	5.52	0.828	4.569	17.62	0.82	1.308	3.815
8.20	4.48	0.875	3.922	27.45	0.45	1.427	4.412
8.02	4.59	0.835	3.835	22.59	0.54	1.325	4.174
8.11	4.68	0.828	3.879	19.30	0.64	1.308	4.061
8.08	4.64	0.833	3.866	16.84	0.73	1.322	3.835
8.36	4.92	0.813	4.001	15.96	0.79	1.273	3.545

F.5 R507A Mix-angle BPHE Unit

Observations								
RTD1 $T_{w, out}$ ℃	RTD2 $T_{w, in}$ ℃	RTD3 $T_{r, in}$ ℃	RTD4 $T_{r, out}$ ℃	Trimec Q_r l/min	WIKA 1 $P_{r, out}$ kPa	WIKA 2 $P_{r, in}$ kPa	RS 1 Q_w l/sec	RM ΔP_r kPa
12.14	16.32	8.36	8.70	6.027	726.2	735.7	0.8025	4.019
12.23	16.32	8.41	8.80	5.560	726.4	735.3	0.8024	3.152
12.18	16.30	8.29	8.87	5.151	723.3	731.6	0.8001	2.565
12.21	16.29	8.28	8.83	5.108	722.4	730.6	0.7970	2.476
12.65	16.28	9.09	9.40	6.639	744.1	754.1	0.7957	4.179
12.70	16.27	9.07	9.42	5.852	743.3	752.5	0.8037	3.187
12.80	16.28	9.19	9.58	5.301	745.1	753.7	0.8043	2.505
12.63	16.25	8.77	9.55	4.724	736.2	744.1	0.8068	1.687
13.31	16.26	9.53	9.78	7.273	754.1	764.3	0.8078	4.572
13.25	16.29	9.86	9.99	5.634	756.0	764.7	0.7936	2.875
13.34	16.28	9.96	10.22	4.768	759.1	767.0	0.7919	1.865
13.33	16.28	9.64	10.21	4.402	753.6	761.1	0.7919	1.307
13.30	16.27	9.41	10.95	4.172	748.0	755.3	0.7926	1.057

13.87	16.30	10.57	10.68	7.060	775.9	785.6	0.8008	4.057
13.80	16.26	10.50	10.66	5.415	773.8	782.3	0.7984	2.503
13.82	16.26	10.45	10.65	4.540	771.6	779.4	0.7977	1.780
13.83	16.24	10.37	10.90	3.844	771.4	778.6	0.7962	0.869
13.76	16.19	9.69	14.10	3.698	754.7	761.9	0.7969	0.477

Calculations

$Q_{coolling}$ kW	LMTD ℃	U kW/(m^2·K)	q kW/m^2	G_r kg/(m^2·s)	x_{out} –	h_r kW/(m^2·K)	$\Delta P_{fric, expe}$ kPa
14.03	5.29	1.270	6.712	26.11	0.81	2.133	5.775
13.76	5.27	1.250	6.584	24.08	0.86	2.078	5.287
13.81	5.28	1.252	6.606	22.32	0.93	2.086	5.034
13.59	5.32	1.223	6.504	22.13	0.92	2.008	4.969
12.08	4.85	1.191	5.779	28.68	0.63	1.923	5.381
12.00	4.88	1.176	5.743	25.28	0.72	1.879	5.031
11.70	4.81	1.164	5.598	22.89	0.77	1.846	4.769
12.21	4.97	1.176	5.844	20.43	0.90	1.876	4.414
9.98	4.83	0.988	4.776	31.37	0.48	1.438	5.205
10.08	4.51	1.069	4.824	24.27	0.63	1.623	4.824
9.75	4.41	1.059	4.666	20.53	0.72	1.600	4.436
9.78	4.61	1.016	4.681	18.98	0.78	1.504	4.141
9.86	4.41	1.071	4.718	18.00	0.83	1.626	4.058
8.11	4.18	0.928	3.881	30.33	0.41	1.314	4.811
8.22	4.17	0.943	3.934	23.27	0.54	1.345	4.527
8.13	4.22	0.922	3.892	19.51	0.63	1.305	4.417
8.04	4.17	0.923	3.845	16.53	0.74	1.306	3.967
8.12	2.85	1.362	3.884	15.94	0.77	2.404	3.688

F.6 R507A High-angle BPHE Unit

Observations

RTD1 $T_{w, out}$ ℃	RTD2 $T_{w, in}$ ℃	RTD3 $T_{r, in}$ ℃	RTD4 $T_{r, out}$ ℃	Trimec Q_r l/min	WIKA 1 $P_{r, out}$ kPa	WIKA 2 $P_{r, in}$ kPa	RS 1 Q_w l/sec	RM ΔP_r kPa
12.00	16.29	8.94	9.38	5.943	737.5	747.8	0.8019	5.013
12.67	16.26	9.67	10.00	6.510	757.8	768.3	0.8023	4.946
12.59	16.26	9.60	9.95	6.015	755.4	765.4	0.8012	4.394
12.65	16.27	9.63	10.05	5.276	755.1	764.8	0.8004	3.654
12.69	16.26	9.42	10.18	4.590	749.0	757.9	0.8007	2.925
12.60	16.24	9.19	12.54	4.474	743.2	752.0	0.7997	2.734
13.32	16.27	10.23	10.39	6.143	766.6	776.8	0.7996	4.470
13.22	16.26	10.15	10.36	5.733	765.1	775.0	0.8007	3.918
13.31	16.25	10.19	10.50	4.742	764.2	773.3	0.7992	3.000
13.28	16.26	10.08	10.57	4.437	761.1	769.9	0.7995	2.674

13.31	16.25	9.95	10.68	4.274	759.1	767.8	0.7992	2.505
13.28	16.30	11.65	11.88	7.073	794.8	805.4	0.8043	5.139
13.13	16.29	11.48	11.74	5.598	788.6	798.1	0.8049	3.672
13.12	16.25	11.27	11.73	4.795	785.5	794.4	0.8043	2.852
13.13	16.24	11.08	11.73	4.668	782.4	791.0	0.8033	2.417
13.85	16.28	12.13	12.38	7.351	808.8	819.3	0.8024	4.830
13.89	16.29	12.27	12.46	5.963	808.6	818.2	0.8022	3.586
13.73	16.28	12.06	12.35	5.364	805.9	815.0	0.8024	2.933
13.93	16.29	12.31	12.60	4.428	808.3	816.7	0.8019	2.280
13.86	16.23	11.43	12.41	4.113	788.3	796.3	0.8012	1.598

Red colored data not stable for heat transfer rate.

Calculations

$Q_{coolling}$ kW	LMTD ℃	U kW/(m ^{2}·K)	q kW/m^2	G_r kg/(m^2·s)	x_{out} –	h_r kW/(m^2·K)	$\Delta P_{fric,\ expe}$ kPa
14.37	4.52	1.520	6.876	25.69	0.84	2.398	6.781
12.05	4.24	1.360	5.764	28.06	0.65	2.020	6.157
12.29	4.25	1.383	5.879	25.93	0.72	2.072	6.032
12.13	4.23	1.371	5.802	22.75	0.81	2.046	5.891
11.98	4.35	1.319	5.731	19.80	0.91	1.932	5.694
12.20	3.41	1.714	5.836	19.32	0.95	2.916	5.609
9.88	4.16	1.137	4.727	26.42	0.57	1.565	5.925
10.18	4.15	1.174	4.871	24.66	0.63	1.635	5.714
9.85	4.12	1.144	4.711	20.40	0.73	1.578	5.538
9.96	4.15	1.149	4.768	19.10	0.79	1.587	5.443
9.82	4.20	1.120	4.701	18.40	0.81	1.532	5.385
10.16	2.59	1.879	4.861	30.26	0.51	3.421	5.823
10.65	2.65	1.923	5.096	23.96	0.68	3.570	5.584
10.55	2.79	1.810	5.046	20.54	0.78	3.199	5.375
10.46	2.93	1.709	5.004	20.01	0.80	2.897	5.032
8.16	2.48	1.574	3.904	31.39	0.40	2.529	5.213
8.05	2.37	1.627	3.853	25.45	0.49	2.667	5.089
8.56	2.45	1.671	4.094	22.91	0.57	2.790	4.921
7.92	2.32	1.634	3.792	18.90	0.65	2.688	4.901
7.96	2.90	1.313	3.810	17.61	0.69	1.917	4.454

Appendix G Sample Calculation: Refrigerant Evaporator Tests

A sample calculation for the refrigerant evaporator tests is given, according to the data reduction method as specified in Section 6.3. This sample calculation is based on the first set of measurement readings of the R134a test on the Low-angle PHE (β = 28°/28°). The experimental readings can be found in *Appendix F* (first line in *Section 1*, in the subsection of *Observations*). Some selected calculation results are also given in *Appendix F* (in *Section 1*, in the subsection of *Calculations*.)

Constants

Plates:

$A = 2.09\ \text{m}^2,\ A_{\text{ch}} = 3.60\times10^{-4}\ \text{m}^2,\ L_{\text{p}} = 0.519\ \text{m},\ d_{\text{h}} = 3.51\ \text{mm},$

$N_{\text{ch, r}} = 12,\ N_{\text{ch, w}} = 11.$

System:

$R_{\text{wall}} = 0.03\times10^{-3}\ \text{m}^2\cdot\text{K/W},\ R_{\text{foul}} = 0.04\times10^{-3}\ \text{m}^2\cdot\text{K/W},\ h_{\text{leg}} = 0.66\ \text{m}.$

R134a:

$M = 102\ \text{kg/kmol},\ P_{\text{crit}} = 4059\ \text{kPa},\ \rho_{\text{f}} = 1270,\ \rho_{\text{g}} = 18.59,\ \text{kg/m}^3,$

$\mu_{\text{f}} = 0.0002467,\ \mu_{\text{g}} = 0.00001104,\ \text{Pa}\cdot\text{s},\ c_{\text{p, f}} = 1362\ \text{J/(kg}\cdot\text{K)},$

$k_{\text{f}} = 0.08876\ \text{W/(m}\cdot\text{K)},\ \sigma = 0.01050\ \text{N/m}$

Heat Transfer Parameters

$$\dot{Q}_{\text{cooling}} = \dot{m}_{\text{w}} c_{\text{p, w}} \left(T_{\text{w, in}} - T_{\text{w, out}}\right) = \frac{0.7977\times999.4}{1000}\times4192\times(14.66-10.86) = 12.70\ \text{kW}$$

$$\Delta P_{\text{leg}} = \rho_{\text{r, in}} g h_{\text{leg}} = 1272\times9.79\times0.66 = 8.219\ \text{kPa}$$

$$\Delta T_{\text{sub}} = \frac{7.25}{\left(P_{\text{r, in}} + \text{atm}\right)^{0.7647}} \Delta P_{\text{leg}} = \frac{7.25}{(298.4+82.7)^{0.7647}}\times8.219 = 0.6330\ ^{\circ}\text{C}$$

$$\dot{Q}_{\text{sub}} = \dot{m}_{\text{r}} c_{\text{p, r}} \Delta T_{\text{sub}} = \frac{5.015\times1272}{60\times1000}\times1.360\times0.633 = 0.09153\ \text{kW}$$

$$T_{\text{sat}} = T_{\text{r, in}} + \Delta T_{\text{sub}} = 6.785 + 0.633 = 7.418\ ^{\circ}\text{C}$$

$$LMTD = \frac{\left(T_{\text{w, in}} - T_{\text{r, out}}\right) - \left(T_{\text{w, out}} - T_{\text{sat}}\right)}{\ln\left(\left(T_{\text{w, in}} - T_{\text{r, out}}\right) / \left(T_{\text{w, out}} - T_{\text{sat}}\right)\right)} = \frac{(14.66 - 6.85) - (10.85 - 7.42)}{\ln\left((14.66 - 6.85) / (10.85 - 7.42)\right)} = 5.323 \ \ ^{\circ}\text{C}$$

$$U = \frac{\dot{Q}_{\text{cooling}}}{A \cdot LMTD} = \frac{12.70}{2.09 \times 5.323} = 1.142 \ \ \text{kW/}\left(\text{m}^2 \cdot \text{K}\right)$$

$$\text{Re}_{\text{w}} = \frac{G d_{\text{h}}}{\mu} = \frac{0.7977 \times 999.4}{1000 \times 3.6 \times 10^{-4} \times 11} \times \frac{3.51 \times 10^{-3}}{0.001213} = 582.5$$

$$\text{Pr}_{\text{w}} = \frac{\mu c_{\text{p}}}{k} = \frac{0.001213 \times 4192}{0.5852} = 8.689$$

$$\text{Nu}_{\text{w}} = c\,\text{Re}^{\text{m}}\,\text{Pr}^{0.33} = 0.059 \times 582.5^{0.78} \times 8.689^{0.33} = 17.28$$

$$h_{\text{w}} = \frac{\text{Nu}_{\text{w}}\, k}{d_{\text{h}}} = \frac{17.28 \times 0.5852}{0.00351} = 2.881 \ \ \text{kW/}\left(\text{m}^2 \cdot \text{K}\right)$$

$$q = \frac{\dot{Q}_{\text{cooling}}}{A} = \frac{12.7}{2.09} = 6.077 \ \ \text{kW/}\left(\text{m}^2 \cdot \text{K}\right)$$

$$G_{\text{r}} = \frac{\dot{m}_{\text{r}}}{A_{\text{ch}} N_{\text{ch, r}}} = \frac{5.015 \times 1272}{60 \times 1000 \times 3.6 \times 10^{-4} \times 12} = 24.61 \ \ \text{kg/}\left(\text{m}^2 \cdot \text{s}\right)$$

$$x_{\text{out}} = \frac{\dot{Q}_{\text{cooling}}}{i_{\text{fg}} \dot{m}_{\text{r}}} = \frac{12.7}{193.4 \times \dfrac{5.015 \times 1272}{60 \times 1000}} = 0.6176$$

$$h_{\text{r}} = \frac{1}{\dfrac{1}{U} - \dfrac{1}{h_{\text{w}}} - R_{\text{foul}} - R_{\text{wall}}} = \frac{1}{\dfrac{1}{1142} - \dfrac{1}{2881} - 0.00003 - 0.00004} = 2.181 \ \ \text{kW/}\left(\text{m}^2 \cdot \text{K}\right)$$

Pressure Drop Parameters

$$P_{\text{pipe, elev}} = \rho_{\text{r, in}} g h_{\text{pipe, elev}} = 1272 \times 9.79 \times 0.47 = 5.853 \ \ \text{kPa}$$

(see Figure 6.1 for the pipe elevation)

$$\Delta P_{\text{tot}} = \Delta P_{\text{meas}} + P_{\text{pipe, elev}} = 4.765 + 5.853 = 10.62 \ \ \text{kPa}$$

$$\Delta P_{\text{elev}} = \frac{\rho_{\text{f}} \rho_{\text{g}}}{\rho_{\text{f}} - \rho_{\text{g}}} \frac{L_{\text{p}} g}{x_{\text{out}} - x_{\text{in}}} \ln \frac{1 + x_{\text{out}}\left(\frac{\rho_{\text{f}}}{\rho_{\text{g}}} - 1\right)}{1 + x_{\text{in}}\left(\frac{\rho_{\text{f}}}{\rho_{\text{g}}} - 1\right)}$$

$$= \frac{1270 \times 18.59}{1270 - 18.59} \times \frac{0.519 \times 9.79}{0.6197} \times \ln \frac{1 + 0.6197 \times \left(\frac{1270}{18.59} - 1\right)}{1} = 0.5810 \ \ \text{kPa}$$

$$\Delta P_{\text{acce}} = G^2 \left(x_{\text{out}} - x_{\text{in}}\right)\left(\frac{1}{\rho_{\text{g}}} - \frac{1}{\rho_{\text{f}}}\right) = 24.61^2 \times 0.6197 \times \left(\frac{1}{18.59} - \frac{1}{1270}\right) = 0.01989 \ \ \text{kPa}$$

$$G_{\text{port}} = \frac{\dot{m}_{\text{r}}}{\frac{1}{4}\pi D_{\text{port}}{}^2} = \frac{5.015 \times 1272}{60 \times 1000 \times 0.25 \times 3.142 \times 0.053^2} = 48.18 \ \ \left(\text{kg/m}^2 \cdot \text{s}\right)$$

$$\Delta P_{\text{port, Shah}} = 0.75\left(\frac{G_{\text{port}}^2}{2\rho_{\text{r, in}}}\right) + 0.75\left(\frac{G_{\text{port}}^2}{2\rho_{\text{r, out}}}\right)$$

$$= 0.75\times\frac{48.18^2}{2\times 1272} + 0.75\times\frac{48.18^2}{2\times\left(\frac{0.6197}{18.59}+\frac{1-0.6197}{1270}\right)^{-1}} = 0.02996 \text{ kPa}$$

ΔP, inlet pipe (liquid only)

$$G_{\text{pipe-in}} = \frac{\dot{m}_{\text{r}}}{\frac{1}{4}\pi d^2} = \frac{5.015\times 1272}{60\times 1000\times 0.25\times 3.142\times 0.0132^2} = 776.8 \text{ kg/}\left(\text{m}^2\cdot\text{s}\right)$$

$$\text{Re}_{\text{pipe-in}} = \frac{Gd}{\mu_{\text{f}}} = \frac{776.8\times 0.0132}{0.0002467} = 41564$$

$$f = \frac{0.184}{\text{Re}^{0.2}} = \frac{0.184}{41564^{0.2}} = 0.02193$$

$$\Delta P_{\text{fric, pipe-in}} = f\cdot\frac{L}{d}\cdot\left(\frac{G^2}{2\rho}\right) = 0.02193\times\frac{1.12}{0.0132}\times\left(\frac{776.8^2}{2\times 1272}\right) = 0.4414 \text{ kPa}$$

$$\Delta P_{\text{local, pipe-in}} = f\cdot\left(\frac{L}{d}\right)_{\text{eq}}\cdot\left(\frac{G^2}{2\rho}\right) = 0.02193\times 160\times\left(\frac{776.8^2}{2\times 1272}\right) = 0.8323 \text{ kPa}$$

(excluding the inlet connection)

$$\Delta P_{\text{acce, connection-in}} = -\left(\frac{G_{\text{pipe-in}}^2}{2\rho_{\text{f}}}\right)\cdot\left[1-\left(\frac{d_{\text{pipe-in}}}{d_{\text{port}}}\right)^4\right] = -\left(\frac{776.8^2}{2\times 1270}\right)\cdot\left[1-\left(\frac{0.0132}{0.053}\right)^4\right]$$

$$= -0.2367 \text{ kPa}$$

$$\Delta P_{\text{fric, connection-in}} = K\cdot\left(\frac{G_{\text{pipe-in}}^2}{2\rho_{\text{f}}}\right) = 0.88\times\left(\frac{776.8^2}{2\times 1270}\right) = 0.2091 \text{ kPa}$$

$$\left(K = \left[1-\left(d/D\right)^2\right]^2 = \left[1-\left(0.0132/0.053\right)^2\right]^2 = 0.88\text{, see Table 4.1 }\right)$$

$$\Delta P_{\text{pipe-in}} = \Delta P_{\text{fric, pipe-in}} + \Delta P_{\text{local, pipe-in}} + \Delta P_{\text{acce, connection-in}} + \Delta P_{\text{fric, connection-in}}$$

$$= 0.4414 + 0.8323 - 0.2367 + 0.2091$$

$$= 1.246 \text{ kPa}$$

ΔP, outlet pipe (two-phase)

$$X_{\text{tt}}^2 = \left(\frac{\mu_{\text{f}}}{\mu_{\text{g}}}\right)^{0.2}\left(\frac{1-x}{x}\right)^{1.8}\frac{\rho_{\text{g}}}{\rho_{\text{f}}} = \left(\frac{0.0002467}{0.00001104}\right)^{0.2}\times\left(\frac{1-0.6176}{0.6176}\right)^{1.8}\times\frac{18.59}{1270}$$

$$= 0.01150$$

$$G_{\text{pipe-out}} = \frac{\dot{m}_{\text{r}}}{\frac{1}{4}\pi d^2} = \frac{5.015\times 1272}{60\times 1000\times 0.25\times 3.142\times 0.03^2} = 150.4 \text{ kg/}\left(\text{m}^2\cdot\text{s}\right)$$

$$\mathrm{Re}_{\mathrm{f}}=\frac{G(1-x)d}{\mu_{\mathrm{f}}}=\frac{150.4\times(1-0.6176)\times 0.03}{0.0002467}=6994$$

$$f_{\mathrm{f}}=\frac{0.184}{\mathrm{Re}_{\mathrm{f}}{}^{0.2}}=\frac{0.184}{6994^{0.2}}=0.03132$$

$$\Delta P_{\mathrm{f}}=f_{\mathrm{f}}\cdot\frac{L}{d}\cdot\frac{G^2(1-x)^2}{2\rho_{\mathrm{f}}}=0.03132\times\frac{0.43}{0.03}\times\frac{150.4^2\times(1-0.6176)^2}{2\times 1270}$$

$$=0.0005846\ \text{kPa}$$

$$\phi_{\mathrm{f}}{}^2=1+\frac{C}{X_{\mathrm{tt}}}+\frac{1}{X_{\mathrm{tt}}{}^2}=1+\frac{20}{0.0115^{0.5}}+\frac{1}{0.0115}=274.5$$

$$\Delta P_{\text{fric, pipe-out}}=\Delta P_{\mathrm{f}}\cdot\phi_{\mathrm{f}}{}^2=0.0005846\times 274.5=0.1605\ \text{kPa}$$

$$\Delta P_{\text{f, Tee-branch}}=f_{\mathrm{f}}\cdot\left(\frac{L}{d}\right)_{\mathrm{eq}}\cdot\left(\frac{G^2(1-x)^2}{2\rho_{\mathrm{f}}}\right)=0.03132\times 60\times\frac{150.4^2\times(1-0.6176)^2}{2\times 1270}$$

$$=0.002447\ \text{kPa}$$

$$C_{\text{Tee-branch}}=\left[\lambda+(c_2-\lambda)\left(1-\frac{\rho_{\mathrm{g}}}{\rho_{\mathrm{f}}}\right)^{0.5}\right]\left[\left(\frac{\rho_{\mathrm{f}}}{\rho_{\mathrm{g}}}\right)^{0.5}+\left(\frac{\rho_{\mathrm{g}}}{\rho_{\mathrm{f}}}\right)^{0.5}\right]$$

$$=\left[1+(1.75-1)\left(1-\frac{18.59}{1270}\right)^{0.5}\right]\left[\left(\frac{1270}{18.59}\right)^{0.5}+\left(\frac{18.59}{1270}\right)^{0.5}\right]=14.63$$

$$\phi_{\text{f, Tee-branch}}{}^2=1+\frac{C_{\text{Tee-branch}}}{X_{\mathrm{tt}}}+\frac{1}{X_{\mathrm{tt}}{}^2}=1+\frac{14.63}{0.0115^{0.5}}+\frac{1}{0.0115}=224.4$$

$$\Delta P_{\text{Tee-branch, pipe-out}}=\Delta P_{\text{f, Tee-brach}}\cdot\phi_{\text{f, Tee-branch}}{}^2=0.002447\times 224.4=0.5491\ \text{kPa}$$

$$\Delta P_{\text{f, ball-valve}}=f_{\mathrm{f}}\cdot\left(\frac{L}{d}\right)_{\mathrm{eq}}\cdot\left(\frac{G^2(1-x)^2}{2\rho_{\mathrm{f}}}\right)=0.03132\times 20\times\frac{150.4^2\times(1-0.6176)^2}{2\times 1270}$$

$$=0.0008157\ \text{kPa}$$

$$C_{\text{ball-valve}}=\left[\lambda+(c_2-\lambda)\left(1-\frac{\rho_{\mathrm{g}}}{\rho_{\mathrm{f}}}\right)^{0.5}\right]\left[\left(\frac{\rho_{\mathrm{f}}}{\rho_{\mathrm{g}}}\right)^{0.5}+\left(\frac{\rho_{\mathrm{g}}}{\rho_{\mathrm{f}}}\right)^{0.5}\right]$$

$$=\left[1+(1.5-1)\left(1-\frac{18.59}{1270}\right)^{0.5}\right]\left[\left(\frac{1270}{18.59}\right)^{0.5}+\left(\frac{18.59}{1270}\right)^{0.5}\right]=12.54$$

$$\phi_{\text{f, ball-valve}}{}^2=1+\frac{C_{\text{ball-valve}}}{X_{\mathrm{tt}}}+\frac{1}{X_{\mathrm{tt}}{}^2}=1+\frac{12.54}{0.0115^{0.5}}+\frac{1}{0.0115}=204.9$$

$$\Delta P_{\text{ball-valve, pipe-out}}=\Delta P_{\text{f, Tee-brach}}\cdot\phi_{\text{f, Tee-branch}}{}^2=0.0008157\times 204.9=0.1671\ \text{kPa}$$

$$\rho_{\mathrm{m}}=\left(\frac{x}{\rho_{\mathrm{g}}}+\frac{1-x}{\rho_{\mathrm{f}}}\right)^{-1}=\left(\frac{0.6176}{18.59}+\frac{1-0.6176}{1270}\right)^{-1}=29.83\ \text{kg/m}^3$$

$$\Delta P_{\text{acce, connection-out}} = \left(\frac{G_{\text{pipe-out}}^2}{2\rho_{\text{m}}}\right)\cdot\left[1-\left(\frac{d_{\text{pipe-out}}}{d_{\text{port}}}\right)^4\right] = \left(\frac{150.4^2}{2\times 29.83}\right)\cdot\left[1-\left(\frac{0.03}{0.053}\right)^4\right]$$

$$= 0.3402 \text{ kPa}$$

$$\Delta P_{\text{fric, connection-out}} = K\cdot\left(\frac{G_{\text{pipe-out}}^2}{2\rho_{\text{m}}}\right) = 0.3\times\left(\frac{150.4^2}{2\times 29.83}\right) = 0.1137 \text{ kPa}$$

($K = 0.3$, see Table 4.1)

$$\Delta P_{\text{pipe-out}} = \Delta P_{\text{fric, pipe-out}} + \Delta P_{\text{Tee-branch, pipe-out}} + \Delta P_{\text{ball-valve, pipe-out}} + \Delta P_{\text{acce, connection-out}} + \Delta P_{\text{fric, connection-out}}$$

$$= 0.1605 + 0.5491 + 0.1671 + 0.3402 + 0.1137$$

$$= 1.331 \text{ kPa}$$

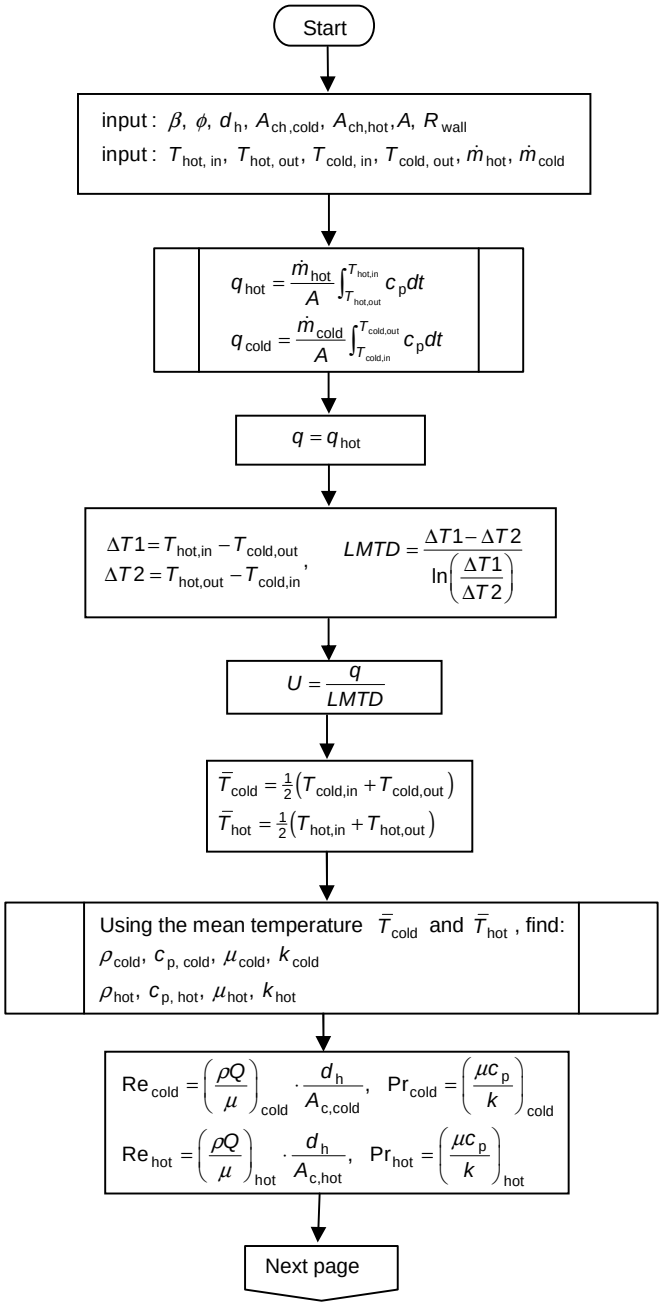
Frictional Pressure drop in PHE

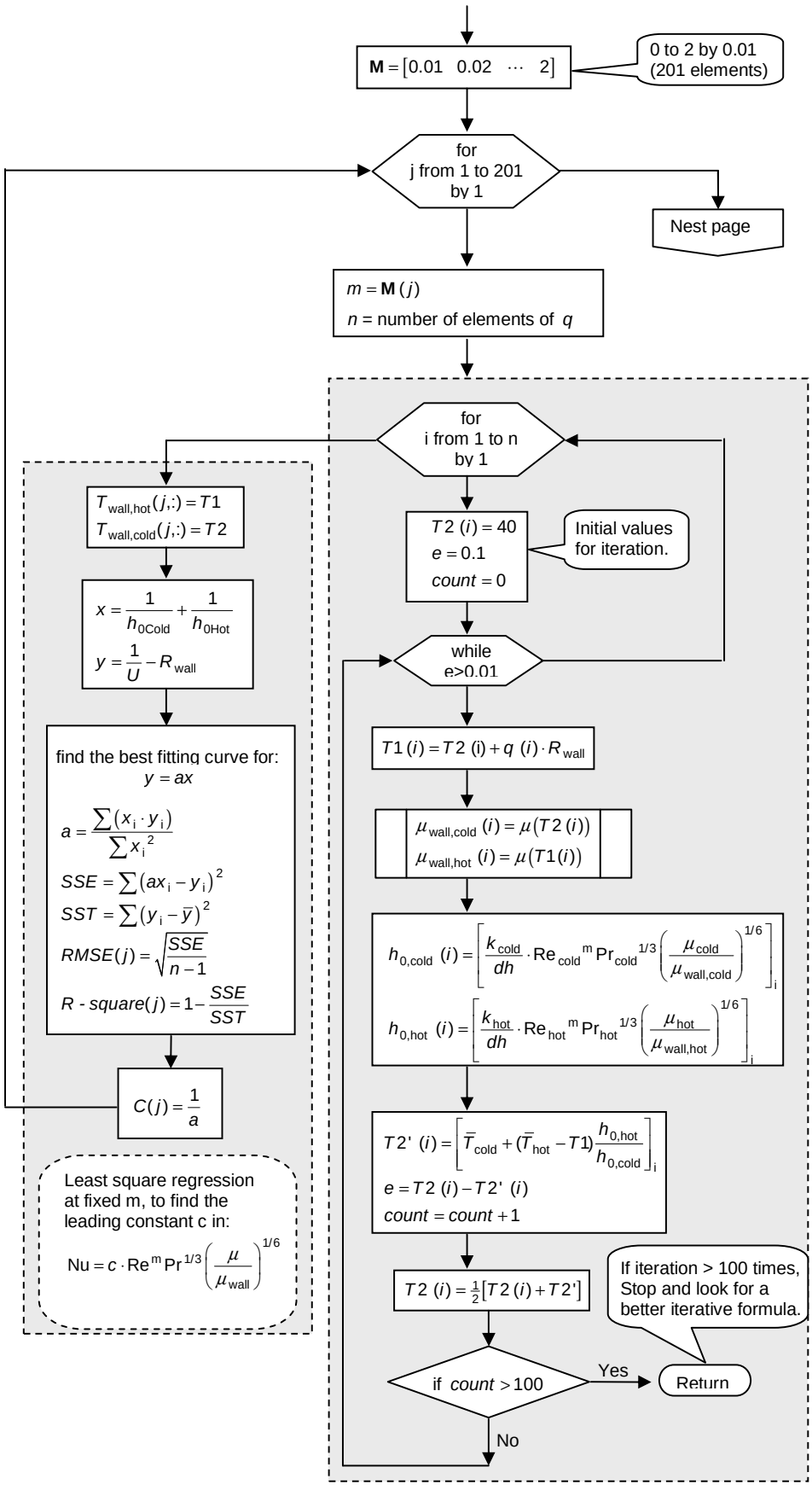
$$\Delta P_{\text{fric}} = \Delta P_{\text{tot}} - \Delta P_{\text{elev}} - \Delta P_{\text{acce}} - \Delta P_{\text{port}} - \Delta P_{\text{pipe-in}} - \Delta P_{\text{pipe-out}}$$

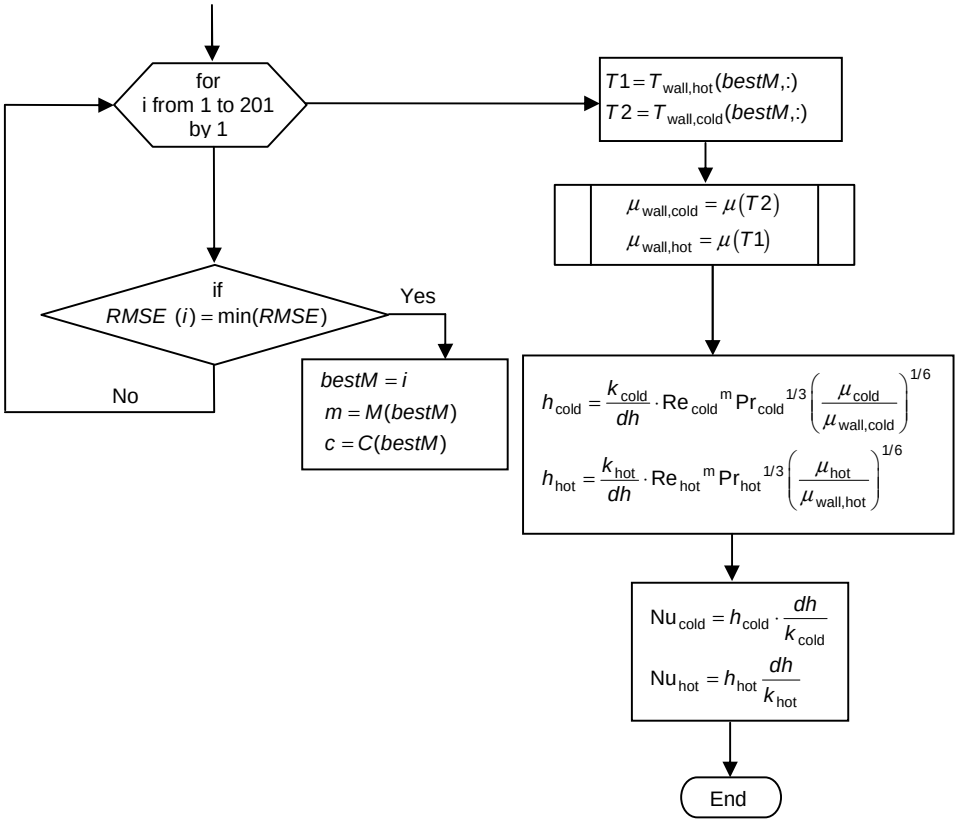
$$= 10.62 - 0.5810 - 0.01989 - 0.02996 - 1.246 - 1.331$$

$$= 7.412 \text{ kPa}$$

Appendix H MATLAB Program Flowchart: Water Test Heat Transfer Coefficients




M = [0.01 0.02 ⋯ 2]
0 to 2 by 0.01 (201 elements)
for j from 1 to 201 by 1
Nest page
m = M(j)
n = number of elements of q
for i from 1 to n by 1
T_wall,hot(j,:) = T1
T_wall,cold(j,:) = T2
T2(i) = 40
e = 0.1
count = 0
Initial values for iteration.
x = 1/h_0Cold + 1/h_0Hot
y = 1/U − R_wall
while e>0.01
find the best fitting curve for:
y = ax
a = Σ(x_i · y_i) / Σx_i^2
SSE = Σ(ax_i − y_i)^2
SST = Σ(y_i − ȳ)^2
RMSE(j) = √(SSE/(n−1))
R - square(j) = 1 − SSE/SST
T1(i) = T2(i) + q(i) · R_wall
μ_wall,cold(i) = μ(T2(i))
μ_wall,hot(i) = μ(T1(i))
h_0,cold(i) = [k_cold/dh · Re_cold^m Pr_cold^1/3 (μ_cold/μ_wall,cold)^1/6]_i
h_0,hot(i) = [k_hot/dh · Re_hot^m Pr_hot^1/3 (μ_hot/μ_wall,hot)^1/6]_i
T2'(i) = [T̄_cold + (T̄_hot − T1) h_0,hot/h_0,cold]_i
e = T2(i) − T2'(i)
count = count + 1
T2(i) = ½[T2(i) + T2']
if count > 100
Yes
Return
If iteration > 100 times, Stop and look for a better iterative formula.
No
C(j) = 1/a
Least square regression at fixed m, to find the leading constant c in:
Nu = c · Re^m Pr^1/3 (μ/μ_wall)^1/6



Variables list (names are case-sensitive)

Variable	Name in Matlab	Description	Variable	Name in Matlab	Description
A	AHeatTransfer	Total heat transfer area	q_{cold}	qCold	Heat load, $q = \frac{\dot{m}}{A}\int_{t1}^{t2} c_{\text{p}} dt$
$A_{\text{c,cold}}$	AcCold	Flow cross-section area	q_{hot}	qHot	
$A_{\text{c,hot}}$	AcHot		R_{wall}	RWall	Wall thermal resistance
c_{p}	cp	Specific heat	Re	Re	Reynolds number
d_{h}	dh	Hydraulic diameter	$T_{\text{cold,in}}$	TColdIn	Temperatures of hot and cold streams at inlet and outlet
k_{wall}	kWall	Wall thermal conductivity	$T_{\text{cold,out}}$	TColdOut	
$LMTD$	LMTD	Log mean temperature difference	$T_{\text{hot,in}}$	THotIn	
$\dot{m}_{\text{cold}}$	massFlowCold	Mass flow rate	$T_{\text{hot,out}}$	THotOut	
$\dot{m}_{\text{hot}}$	massFlowHot		β	beta	Chevron angle
Nu	Nu	Nusselt number	δ_{wall}	wallThickness	Wall thickness
Pr	Pr	Prandtal number	ϕ	fai	Enlargement factor
Q_{cold}	voluFlowCold	Volumetric flow rates	μ	miu	viscosity
Q_{hot}	voluFlowHot		ρ	rho	density
q	q	Heat load, $q = \frac{1}{2}(q_{\text{hot}} + q_{\text{cold}})$			

Appendix I Uncertainty Analysis: General Theory, the ASME and ISO Methods

I.1 Introduction
I.2 Basic Mathematics of Uncertainty Calculation
I.3 Traditional Classifications of Errors: Random and Systematic Errors
I.4 The ASME Method
  I.4.1 Types of Errors
  I.4.2 Precision Error, *P*
  I.4.3 Bias Error, *B*
  I.4.4 Combining Errors
  I.4.5 Uncertainty of a Parameter
  I.4.6 Uncertainty of a Result
I.5 The ISO Method (GUM Method)
  I.5.1 Basis of GUM
  I.5.2 Terms Used in GUM
  I.5.3 Type A Evaluation of Standard Uncertainty, u_A
  I.5.4 Type B Evaluation of Standard Uncertainty, u_B
  I.5.5 Combined Standard Uncertainty
  I.5.6 Expanded Uncertainty, *U*
Additional References

I.1 Introduction

All measurements have errors, due to measurement procedures, instrumental inaccuracy, and environmental influences. By definition, errors are the differences between the measurements and the true values. Even the most carefully calibrated instruments will have errors. In practice, the true values of measured quantities are rarely known, thus, the best one can do is to obtain the "best estimate" of the true value, along with the estimate of the error. This is the task of uncertainty analysis. Uncertainty analysis is imperative when using data directly or in calibrating or validating simulation methods (Stem et. al., 1999).

The fact is that until today, there is not a uniform and unambiguous method of uncertainty analysis, though some general mathematics applies to all possible methods. There are two widely accepted methods from two organizations: the ASME method and the ISO method. The main difference between the two methods is the way in which the random and systematic uncertainty estimates are handled (though the terms "random" and "systematic" are not recommended in the ISO method). Moffat (1982, 1985, and 1988) also proposed a method but his approach is not consistent with either of those standards. Other approaches

include those of NIST and AIAA, as briefly introduced by Coleman and Steele (1995).

The ASME method was briefly described by Abernethy et al. (1985) and the updated revision can be found in the standard: ANSI/ASME PTC 19.1, 2005. ISO published the document "Guide to the Expression of Uncertainty in Measurement" in 1993, revised in 1995 and usually referred to as the "GUM" method. This method was developed by a joint committee of seven international organizations (BIPM, IEC, IFCC, ISO, IUPAC, IUPAP and OIML) and is gaining wider applications.

Steele et al. (1994) made a comparison between the two methods applying the Monte Carlo techniques in a series of example experiments. It was shown that the ISO model is more consistent in providing an uncertainty interval. Coleman and Steele (1995) represented (but not with the same terminology) a discussion of the assumptions and approximations used in the method and also a brief overview of uncertainty analysis. Also found in Kirkup 's web article, the ISO method is well summarized and represented. Another good literature source is the UKAS (United Kingdom Accreditation Service) document on measurement uncertainty (Publication reference: M3003, 2nd edition, 2007).

The ISO method of uncertainty analysis is followed in this study.

I.2 Basic Mathematics of Uncertainty Calculation

Kline and McClintock (1953) showed (as described in the article by Moffat, 1988) that the uncertainty in a computed result could be estimated with good accuracy using a root-sum-square (RSS) combination of the effects of each of the individual inputs. This treatment is shown below.

The result of the experiment is assumed to be calculated from a set of measurements using a data interpretation program:

$$R = R\ (X_1,\ X_2,\ \ldots,\ X_n) \tag{I. 1}$$

The effect of an error in one measurement on the error of the calculated result is:

$$\delta R_{x_i} = \frac{\partial R}{\partial X_i}\delta X_i \tag{I. 2}$$

The term $\frac{\partial R}{\partial X_{\mathrm{i}}}$ is often called the *sensitivity factor* (or *sensitivity coefficient*) and denoted as θ_{i}. When several independent variables are used in the function *R*, the terms are combined by a root-sum-square method:

$$\delta R = \sqrt{\sum_{i-1}^{n} \left(\frac{\partial R}{\partial X_{\mathrm{i}}} \delta X_{\mathrm{i}} \right)^2} \tag{I. 3}$$

This single equation is the basic equation of all types of uncertainty analysis. Equation (I. 3) applies when:

1. Each measurement (X_{i}) is independent,
2. Each measurement fits a Gaussian distribution,

It would be straightforward in applying Equation (I. 3) to the following two basic conditions:

1. for $R = X_1 + X_2$,

$$\delta R = \sqrt{\left(\delta X_1 \right)^2 + \left(\delta X_2 \right)^2} \tag{I. 4}$$

2. for $R = X_1 X_2$,

$$\delta R = \sqrt{\left(X_2 \cdot \delta X_1 \right)^2 + \left(X_1 \cdot \delta X_2 \right)^2} = R \cdot \sqrt{\left(\frac{\delta X_1}{X_1} \right)^2 + \left(\frac{\delta X_2}{X_2} \right)^2} \tag{I. 5}$$

Note that Equation (I. 5) applies also to $R = X_1 / X_2$, this can be proved by:

$$\frac{\partial R}{\partial X_1} = \frac{1}{X_2}, \quad \frac{\partial R}{\partial X_2} = \frac{X_1}{-X_2{}^2}, \quad \rightarrow$$

$$\delta R = \sqrt{\left(\frac{1}{X_2} \delta X_1 \right)^2 + \left(\frac{X_1}{-X_2{}^2} \delta X_2 \right)^2} = \frac{X_1}{X_2} \sqrt{\left(\frac{\delta X_1}{X_1} \right)^2 + \left(\frac{\delta X_2}{X_2} \right)^2}$$

In general, when an equation describing the results is a pure ‘product form’, then the *relative* uncertainty can be found directly. That is, if

$$R = X_1{}^{\mathrm{a}} X_2{}^{\mathrm{b}} \cdots X_{\mathrm{n}}{}^{\mathrm{m}} \tag{I. 6}$$

then

$$\frac{\delta R}{R} = \sqrt{\left(a \frac{\delta X_1}{X_1} \right)^2 + \left(b \frac{\delta X_2}{X_2} \right)^2 + \cdots + \left(m \frac{\delta X_{\mathrm{n}}}{X_{\mathrm{n}}} \right)^2} \tag{I. 7}$$

This can be proved by:

$$\frac{\partial R}{\partial X_1} = X_2^{\,b} \cdots X_n^{\,m} \cdot a X_1^{\,a-1} = R\frac{a}{X_1} \rightarrow$$
$$\frac{\partial R}{\partial X_1}\delta X_1 = R\left(a\frac{\delta X_1}{X_1} \right)$$

apply the same principle to other terms, substitute into Equation (I. 3), and the result is Equation (I. 6).

There is no particular difficulty in the evaluation of Equation (I. 3), provided that each δX_i is known. The central problems are the assignment of the proper value to the uncertainty of each input item and the selection of which items to be included in the analysis. This is where the various methods differ from each other. It is important to recognize that Equation (I. 3) applies regardless of different methods used for uncertainty analysis.

In most situations, the overall uncertainty is dominated by only a few of its terms. Terms that are smaller than the largest term by a factor of 3 or more can usually be ignored. This is due to the RSS combination: small terms have very small effects (Moffat, 1988).

I.3 Traditional Classifications of Errors: Random and Systematic Errors

Errors are traditionally classified as random or systematic. Random errors (also called precision errors) follow a Normal distribution (Gaussian distribution), and so can be determined by statistical tools. Systematic errors (also called fixed errors, bias errors) are fixed in repeated trials (or readings) at a measurement point, and cause the measured value to be consistently above or consistently below the true value.

Briefly, an instrument's bias error is the difference between the average and true values, the precision error is the scatter about the bias. In other words, if only random errors exist then the mean of an infinite number of readings will be the true value. On the other hand, if only systematic errors exist then there is only one reading (no scatter and all readings are one) and that reading is away from the true value by the systematic error (so it is called "bias"). Precision can be

improved only by selecting another measuring device, but bias error, if known, can be eliminated by correction. A particular device can be considered precise but biased, or biased but precise.

I.4 The ASME Method

I.4.1 Types of Errors

At a single measurement point, the total error has two components, bias error (*B*) and precision errors (*P*). The total error is then expressed as:

$$\delta = B + P \tag{I. 8}$$

Both the bias and precision are presumed to represent statistical properties of a Gaussian distributed data set.

I.4.2 Precision Error, *P*

The precision error *P* can be determined by statistical tools, from a number of repeated measurements. In the ASME method of uncertainty analysis, it is assumed that measurements without bias error will represent a Gaussian distribution around the true value of the parameter. Thus, the true value is the population mean. However, because the population has an infinite number of measurements, the population mean can only be estimated by a sample mean, and this brings the application of the Student's *t*-distribution.

The Student's *t*-distribution (or *t*-distribution) is a probability distribution usually used to estimate the mean of a Normal population when the sample size is small. For a sample of size *n* drawn from a Normal population with mean μ and standard deviation σ, the quality

$$t = \frac{\overline{x} - \mu}{s / \sqrt{n}} \tag{I. 9}$$

has a *t* distribution with *n* -1 degrees of freedom, where the $\overline{x}$ is the sample mean, *s* is the *sample standard deviation* and is called the "precision index":

$$\overline{x} = \frac{1}{n} \sum_{i=1}^{n} x_i \tag{I. 10}$$

$$s = \sqrt{\frac{1}{n-1}\sum_{i=1}^{n}\left(x_i - \bar{x}\right)^2} \qquad \text{(I. 11)}$$

Since the true value of the variable is the population mean μ, the error between the measured value and the true value, defined as the precision error P, is:

$$P = t\frac{s}{\sqrt{n}} \qquad \text{(I. 12)}$$

The student's t value is a function of the degrees of freedom of the data set, and can be found in statistics and probability reference books. For a sample size of n, the number of degrees of freedom is $v = n - 1$. t value is always associated with a confidence level, it is a common practice to choose a t value where the confidence level is 95% in the two-tailed t-table. t is usually set equal to 2 for large samples, as a general rule, when $n > 30$.

I.4.3 Bias Error, *B*

The bias error B is constant during a given set. In repeated measurements of a given set, each measurement has the same bias. There is no statistical equation to calculate the bias error; instead, it must be estimated from the best available information (Moffat, 1982). The estimation of the bias error is not an easy task since the true value is not known. Calibration information and comparison of measurements by different methods can help but **in general the estimate of bias must be based on judgment and is often subjective** and hard to quantify or defend rigorously. Usually one must rely on the engineering judgment of instrumentation and measurement engineers to provide an upper limit on the bias.

The bias errors include those which are known and can be calibrated out, those which are negligible and can be ignored and those which are estimated and included in the uncertainty analysis. An example of a bias error is the sensor uncertainty as specified by the sensor manufacturer. In some cases an instrument will be calibrated against a known standard, and the precision of the calibration (being a *random* error in the calibration procedure) can be used as an estimate of the *bias* error.

I.4.4 Combining Errors

In the measurement of a parameter, errors can arise from many sources; these basically include calibration errors, data acquisition errors, and data reduction errors. For each of the sources there will be bias and precision components. To obtain the precision of each measured value (like temperature, pressure, or flow rate), the root sum square (RSS) method is used to combine the two components from the *k* sources of error.

$$P = \sqrt{\left(P_1^{\,2} + P_2^{\,2} + \ldots + P_K^{\,2} \right)} \tag{I. 13}$$

$$B = \sqrt{\left(B_1^{\,2} + B_2^{\,2} + \ldots + B_K^{\,2} \right)} \tag{I. 14}$$

I.4.5 Uncertainty of a Parameter

Now the precision error and bias error for a measured parameter are obtained. To express the total error for that parameter using a single number *U*, the two components need to be combined. The expression for the measured value, in the form of an interval within which the true value of the parameter is expected to lie, is:

$$\overline{x} \pm U \tag{I. 15}$$

Two methods can be used to combine the bias error with the precision error, addition of the two components (ADD) and combination by root sum square (RSS). It remained an argument as which method should be used till the late 1970s. The NBS (National Bureau of Standards, USA) suggested in late 1980 that either method should be accepted if:

1. the bias and precision components are propagated separately from the measurements to the final test result,
2. the method of combination is clearly stated.

(Abernethy et al., 1985)

It is not possible to define a rigorous confidence level for either method because the bias is an upper limit based on judgment which has unknown characteristics. It is usually recommended the ADD method has a 99% confidence level and the RSS has 95%. Thus

$$U_{\text{ADD}} = B + P \quad \text{with 99\% confidence level}$$
$$U_{\text{RSS}} = \sqrt{B^2 + P^2} \quad \text{with 95\% confidence level} \tag{I. 16}$$

I.4.6 Uncertainty of a Result

A result is derived by measured parameters through the functional relationship, and errors of independent variables propagate into the result. The bias and precision error are kept separate until the last step of computing the uncertainty of a result. The precision and bias errors of a result are calculated separately by Equation (I. 3). Thus if the result is a function of independent parameters: $R = R(X_1, X_2, \ldots, X_n)$, the precision error of a result is given by:

$$P_R = \sqrt{\sum_{i-1}^{n} \left(\frac{\partial R}{\partial X_i} P_{X_i} \right)^2} \tag{I. 17}$$

and the bias error of a result is given by:

$$B_R = \sqrt{\sum_{i-1}^{n} \left(\frac{\partial R}{\partial X_i} B_{X_i} \right)^2} \tag{I. 18}$$

Again the total uncertainty of a result is given by the two models of ADD and RSS.

I.5 The ISO Method (GUM Method)

The ISO method is generally referred to as the GUM method, as an abbreviation of the standards (*Guide to the Expression of Uncertainty in Measurement*) that describes this method, and this term will be used in the following.

I.5.1 Basis of GUM

1. Uncertainties are categorized in two ways according to how they are estimated:
   Type A: evaluated by the statistical analysis of a series of measurements,

Type B: evaluated by other means.
The traditional classification of uncertainties, "random" and "systematic" errors is not recommended by GUM.

2. Combined uncertainty of the two types is calculated by taking the square root of the sum of the variances due to Type A and Type B uncertainties.
3. In situations where it may be necessary to quote a "confidence level" within which the true value of the measurement is likely to lie, a coverage factor k shall be stated.

I.5.2 Terms Used in GUM

Standard uncertainty, u
Uncertainty of the result of a measurement expressed as a standard deviation.

Combined standard uncertainty, u_c
The positive root of the sum of the variances of the standard uncertainties of all contributing quantities (whether these be Type A or Type B uncertainties).

Expanded uncertainty, U
Quantity defining an interval which is expected to encompass a confidence level (usually 95%)

Coverage factor, k
This is used to obtain the expanded uncertainty, U, given the combined standard uncertainty, u_c. Specifically,

$$U = k \cdot u_c \tag{I. 19}$$

For an expanded uncertainty where the confidence level is 95%, k usually lies between 2 and 3.

I.5.3 Type A Evaluation of Standard Uncertainty, u_A

It is assumed that repeated measurements of a quantity X will represent a Gaussian distribution. The best estimate of the true value is found by the arithmetic mean of the measurements from n measurements:

$$\overline{X} = \frac{\sum_{i=1}^{n} X_i}{n} \tag{I. 20}$$

To show the variability of the measured values of the quantity X, we use the *sample standard deviation*:

$$s = \sqrt{\frac{\sum_{i=1}^{n}\left(X_i - \bar{X}\right)^2}{n-1}} \qquad \text{(I. 21)}$$

The measurement of the variability of the means (if an experiment consisting of measurements is repeated many times, then the distribution of means has its own standard deviation) is represented by the *standard deviation of the means* (often called standard error of the mean) as $s(\bar{X})$:

$$s(\bar{X}) = \frac{s}{\sqrt{n}} \qquad \text{(I. 22)}$$

In GUM $s(\bar{X})$ is called by a new term, *standard uncertainty*, and represented by the symbol, u. Thus, if $\bar{X}$ is the best estimate of X, then the standard uncertainty is written as $u(\bar{X})$.

I.5.4 Type B Evaluation of Standard Uncertainty, u_B

Where the best estimate of an input quantity is not determined by repeated measurements, we cannot use the type A evaluation methods to establish the standard uncertainty. In such a situation to evaluate the uncertainty we must use:

1. previous measurement data,
2. experience with or general knowledge of the behavior and properties of relevant materials and instruments,
3. calibration certificates, manufacturers' specifications,
4. data tables from handbooks.

An uncertainty determined in this manner is referred to as a "Type B" uncertainty. The proper use of available information for a Type B evaluation of standard uncertainty calls for insight based on experience and general knowledge, and is a skill that can be learned with experience. It should be recognized that a Type B evaluation of standard uncertainty can be as reliable as a Type A evaluation, especially when a Type A evaluation is based on a comparatively small number of statistically independent observations.

Care must be taken to ensure that the uncertainty, as given in the manufactures' specifications, calibration certificates, and so on, is correctly interpreted.

- If (from manufacturer's specification, calibration certificate, handbook, or other sources) the quoted uncertainty is stated to be a multiple of a standard deviation, the standard uncertainty $u(X_i)$ is simply the standard deviation (the quoted value divided by the multiplier).
- If the quoted uncertainty is stated to have a confidence level of 90, 95, or 99%, one may assume a normal distribution of the quoted uncertainty, unless otherwise indicated, and recover the standard uncertainty of X_i by dividing the quoted uncertainty by a appropriate factor. As for a normal distribution, the factor is 1.64, 1.96, and 2.58 for the above three levels of confidence.
- If the quoted uncertainty is stated as "there is a *x*% chance that the quantity X_i lies within the interval of a- to a+", one may also assume a normal distribution of the uncertainty of X_i and recover the standard uncertainty (standard deviation for that distribution).
- In cases where only the upper and lower limits are given, and there is no specific knowledge about the possible values of X_i within the interval, one

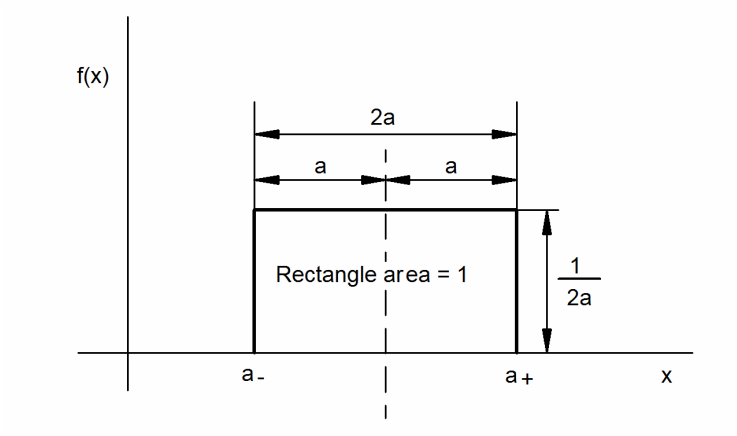


Figure I.1: Rectangular probability distribution

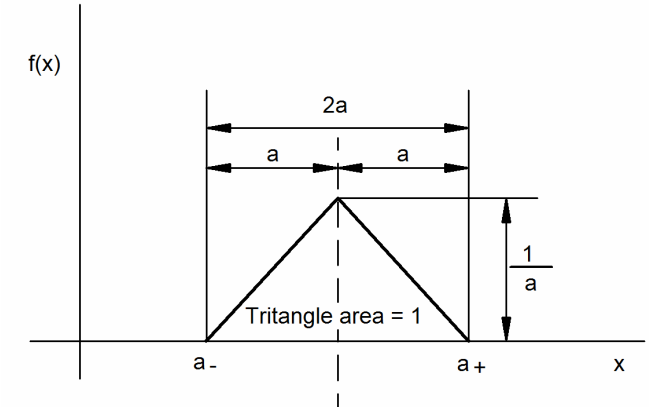


Figure I.2 : Triangular probability distribution

can only assume that it is equally probable for X_i to lie anywhere within it. This is a rectangular distribution. Denoting the upper limit as a_+ and the lower limit as a_-, and every value between those limits is equally probable to be the true value, as shown in Figure I.1. In a rectangular distribution the best estimate of σ^2 is given by:

$$s^2 = \sigma^2 = \frac{a^2}{3} \tag{I. 23}$$

where *a* is the half width of the distribution.

The standard deviation, which is called the Type B standard uncertainty, *u*, of the rectangular distribution is:

$$u = s = \frac{a}{\sqrt{3}} \tag{I. 24}$$

- In cases when it is more realistic to expect that values near the bounds are less likely than those near the midpoint, a symmetric trapezoidal distribution having equal sloping sides (isosceles trapezoid) is assumed. Set the trapezoidal base width $a+ - a- = 2a$, and a top of width $2a\beta$ where $0 \le \beta \le 1$. As $\beta \to 1$ this trapezoidal distribution approaches the rectangular distribution (Figure I.1), while $\beta = 0$ it is triangular distribution (Figure I.2). At this distribution, the expectation (best estimation) of X_i is $\frac{1}{2}(a_- + a_+)$ and the standard uncertainty is:

$$u = s = a\sqrt{\frac{1+\beta^2}{6}} \tag{I. 25}$$

- If the measuring instrument has a resolution of δx, a rectangular distribution is assumed where the true value *x* can lie with equal probability anywhere in the interval $x - \delta x/2$ to $x + \delta x/2$. And thus the standard uncertainty is $u = \frac{\delta x}{2\sqrt{3}} = 0.29\delta x$. (Gum F.2.2.1)

I.5.5 Combined Standard Uncertainty

Combine type A uncertainty with Type B uncertainty for the same variable

This is the common situation where a quantity is measured using a calibrated sensor. The Type A uncertainty is obtained by repeat measurements and Type B uncertainty is evaluated by a manufacturer's specification or calibration certificate. (GUM examples in 4.3.7 and 5.1.5). In this case, The GUM method treats the Type B uncertainty as providing bounds to an additive correction to the measured quantity X and thus the quantity is expressed as: $X = \overline{X} + \Delta\overline{X}$. The Type A uncertainty of X is expressed as $u(\overline{X})$ and Type B $u(\Delta\overline{X})$, respectively. Since the quantity X is now treated as the addition of two terms, the standard uncertainty of X is the combined standard uncertainty of Type A and Type B uncertainty (Equation I. 4):

$$u_{\mathrm{c}}(X) = \sqrt{u(\overline{X})^2 + u(\Delta\overline{X})^2} \qquad \text{(I. 26)}$$

Or, more generally, if the contributions to $u_{\mathrm{c}}(y)$ of the Type A and Type B standard uncertainties alone are denoted, respectively, by $u_{\mathrm{c,\,A}}(y)$ and $u_{\mathrm{c,\,B}}(y)$, the combined standard uncertainty of y can be expressed as (GUM G.4.1, note 3):

$$u_{\mathrm{c}}(y) = \sqrt{u^2_{\mathrm{c,\,A}}(y) + u^2_{\mathrm{c,\,B}}(y)} \qquad \text{(I. 27)}$$

Combined standard uncertainty of independent input quantities

If quantity Y depends on independent quantities (i.e., not related) X_1, X_2, …, X_{N} in the form:

$$Y = f(X1, X2, \cdots, X_{\mathrm{N}}) \qquad \text{(I. 28)}$$

The standard uncertainty of y, where y is the *best estimate* of the quantity Y (take note of the terminology) and thus the result of the measurement, is obtained by appropriately combining the standard uncertainties of the input estimates x_1, x_2, …, x_{N}. The combined standard uncertainty of the estimate y is denoted by $u_{\mathrm{c}}(y)$ and given by:

$$u_{\mathrm{c}}(y) = \sqrt{\sum_{i=1}^{N}\left[\frac{\partial f}{\partial x_{\mathrm{i}}}u(x_{\mathrm{i}})\right]^2} \qquad \text{(I. 29)}$$

Note that this equation is the same as Equation (I. 3) (Equation 10 in GUM), and it can be deduced from this equation:

1. for $Y = X_1 + X_2$,

$$u_c(y) = \sqrt{u_c^2(x_1) + u_c^2(x_2)} \tag{I.30}$$

2. for $Y = X_1 X_2$, or $Y = X_1 / X_2$

$$\frac{u_c(y)}{y} = \sqrt{\left(\frac{u_c(x_1)}{x_1}\right)^2 + \left(\frac{u_c(x_2)}{x_2}\right)^2} \tag{I.31}$$

I.5.6 Expanded Uncertainty, *U*

Expanded uncertainty *U* and combined standard uncertainty u_c

The standard uncertainty, u_c, is the basic measure of uncertainty in the GUM method. However, there are situations in which it is preferable to quote an interval of confidence *p* (usually 95%) within which the true value will lie. Specifically, we can write:

$$Y = y \pm U \tag{I. 32}$$

where *Y* is the true value of the quantity, *y* is the best estimate of *Y*, and *U* is the ***expanded uncertainty***. The equation is also expressed as $y - U \le Y \le y \pm U$.

The expanded uncertainty, *U*, is related to the combined standard uncertainty, $u_c(y)$, by the equation:

$$U = k \cdot u_c(y) \tag{I. 33}$$

k is referred to as the ***coverage factor***. In general, *k* is in the range 2 to 3.

It should be recognized that multiplying $u_c(y)$ by a constant provides no new information but presents the previously available information in a different form. It should also be recognized that in most cases the level of confidence *p* is rather uncertain, not only because the limited knowledge of the probability distribution characterized by *y* and $u_c(y)$, but also because of the uncertainty itself. (GUM, 6.2.3)

Coverage factor in type A evaluation of uncertainty

If u_c is determined through a Type A evaluation of uncertainty, it is usual to assume that the *t* distribution may be applied when determining the coverage factor, and $t = \frac{y - Y}{u_c(y)}$.

The Student's *t*-distribution (or *t*-distribution) is a probability distribution usually used to estimate the mean of a Normal population when the sample size is small. For a sample of size *n* drawn from a Normal population with population mean μ and standard deviation σ, the quality

$$t = \frac{\bar{X} - \mu}{s / \sqrt{n}} \tag{I. 34}$$

has a *t* distribution with *n* - 1 degrees of freedom. In the equation $\bar{X}$ is the sample mean, *s* is the sample deviation defined by:

$$s = \sqrt{\frac{1}{n-1} \sum \left(x_i - \bar{x} \right)^2} \tag{I. 35}$$

The student *t* value is a function of the degrees of freedom of the data set, for a sample size of n, the degrees of freedom is $v = n - 1$. At the level of confidence of 95% (i.e., the probability that the true value lies within a specified interval is 0.95), Table I.1 gives the coverage factor for various degrees of freedom. For values of v >10, k tends towards a value close to 2 and experimenters often use 2 as the coverage factor when the level of confidence required is 95%. For level of confidence of other values, for example, 99%, the t-table can be consulted to find out the *k* value with corresponding degrees of freedom. Specially, for v >10 and p = 95%, k = 3.

Table I.1: Coverage factors in Type A evaluation of uncertainty
at level of confidence of 95%

v	1	2	3	4	5	6	7	8	9	10
k	12.706	4.303	3.182	2.776	2.571	2.447	2.365	2.306	2.262	2.228

In the situation of $Y = f(X_1, X_2, \cdots, X_N)$ where the estimate for each of $X_1, X_2, \cdots, X_N$ is obtained from a different number of repeated observations, to obtain the coverage factor for $u_c(y)$, the effective degrees of freedom, v_{eff}, shall be calculated using the Welch-Satterthwaite formula:

$$\nu_{\text{eff}} = \frac{u_{\text{c}}{}^4(y)}{\sum_{i=i}^{N} \frac{u_{\text{i}}{}^4(y)}{\nu_{\text{i}}}} \qquad \text{(I. 36)}$$

where ν_{i} is the degrees of freedom of X_{i}, and $u_{\text{i}}(y) = \frac{\partial f}{\partial x_{\text{i}}} u_{\text{c}}(x_{\text{i}})$.

Coverage factor in Type B evaluation of uncertainty

If u_{c} is determined through a Type B evaluation based on an assumed probability distribution, the *k* value is not evaluated by the *t*-distribution. For example, when $u(x)$ is obtained from a rectangular probability distribution of assumed half-width of *a*, $u(x) = \text{a}/\sqrt{3}$ is viewed as a constant with no uncertainty (i.e., the uncertainty has no uncertainty for itself). The expanded uncertainty of a 95% level of confidence is simply 0.95 *a*, or $k = 1.65$ using the equation of $U = ku(x)$.

In the situation of $Y = f(X1, X2, \cdots, X_{\text{N}})$ where $u(x_{\text{i}})$ are obtained from both Type A and Type B evaluations, the probability distribution of the function $t = (y - Y)/u_{\text{c}}(y)$ can still be approximated by the *t*-distribution. the Welch-Satterthwaite formula also applies, and the degrees of freedom for a standard uncertainty which is determined by a Type B evaluation is assigned by:

$$\nu = \frac{1}{2}\left[\frac{u}{\Delta u}\right]^2 \qquad \text{(I. 37)}$$

where Δu is the standard deviation of the standard uncertainty, and $\Delta u = 0$ for rectangular distribution. At $\Delta u = 0$ it follows that $\nu = \infty$, in such a case, any term in the Welch-Satterthwaite formula with an infinite number of degrees of freedom is zero.

Additional References

Abernethy R.B., R.P. Benedict, R.B. Dowdell, ASME measurement uncertainty, *Journal of Fluids Engineering*, vol.107, pp.161-164, 1985

BIPM, IEC, IFCC, ISO, IUPAC, IUPAP, OIML, *Guide to the Expression of Uncertainty in Measurement*, ISO/1995, ISBN: 92-67-10188-9, First Edition 1993

Coleman H.W. and Steele W.G., Engineering application of experimental uncertainty analysis, *AIAA Journal*, vol.33, no.10, pp.1888-1896, 1995

Kline S.J., The purpose of uncertainty analysis, *Journal of Fluid Engineering*, vol.107, pp.153-160, 1985.

Kirkup L., Calculating and expressing uncertainty in measurement, Downloaded from: *http://www.science.uts.edu.au/physics/uncertainty.pdf*

Moffat R.J., Contributions to the theory of single sample uncertainty analysis, *Journal of fluids engineering*, vol.104, pp.250-260, 1982

Moffat R.J., Using uncertainty analysis in the planning of an experiment, *Journal of Fluids Engineering*, vol.107, pp.173-178, 1985.

Moffat R.J., Describing the uncertainties in experimental reports, *Experimental Thermal and Fluid Science*, vol.1, pp.3-17, 1988.

Steele W.G., R.A. Ferguson, R.P. Taylor, H.W. Coleman, Comparison of ANSI/ASME and ISO models for calculation of uncertainty, *ISA Transactions*, vol.33, pp.339-352, 1994

Stem F., Muste M., Beninati M-L, and Eichinger W.E., Summary of experimental uncertainty assessment methodology with example, IIHR Technical Report No.406, Iowa Institute of Hydraulic Research, College of Engineering, The University of Iowa, 1999.

UKAS, *The expression of Uncertainty and Confidence in Measurement*, UKAS Publication reference: M3003, 2nd edition, 2007.

Appendix J Uncertainty Analysis: Sensor Calibration

The accuracy of a sensor can be obtained through either the manufacturer's specification or a calibration procedure, and will contribute to the uncertainty of a measurement conducted by this sensor. There are two standards of uncertainty analysis one can follow: the ASME method and the ISO method. In this study, the ISO method of uncertainty analysis is used.

J.1 Calculation Method
J.2 Temperature sensors
  J.2.1 Mercury Thermometer
  J.2.2 LM35DZ Sensors
  J.2.3 Resistance Temperature Detectors (RTD's)
J.3 RS 257-026 Turbine Flow Meters
J.4 Trimec MP15S Flowmeter
J.5 Rosemount 3051 CD Differential Pressure Transmitter
J.6 WIKA Static Pressure Transmitters

J.1 Calculation Method

For a sensor which measures the quantity *x*, the uncertainty (accuracy) of the sensor is obtained by both Type A and Type B evaluation of standard uncertainty.

Type A evaluation has two components:

- $u_{A1}(x) = \frac{s}{\sqrt{n}}$, where *s* is the sample standard deviation, and *n* is the sample size
- $u_{A2}(x) = \text{RMSE of calibration curve fitting}$ [1]

Type B evaluation evaluates the standard uncertainty of the actual value of the quantity being measured, and is denoted by $u_B(x)$. This means the actual flow rate for a flowmeter, the actual temperature for a temperature sensor, for example.

[1] RMSE = Root Mean Squared Error. This error evaluates the goodness of the curve fitting. RMSE is calculated by $\text{RMSE} = \sqrt{\frac{\sum (y'_i - y_i)^2}{n-p}}$, where y_i is the original respond to x_i, y'_i is the response from the fitting curve $y' = f(x)$. n is number of data points, p is the number of unknown coefficients, called the degrees of freedom.

In most cases, the quantity of interest is a function of many other quantities, for example, in the water flowmeter calibration, the actual volume flow rate is calculated by : $Q = M / (t \cdot \rho)$, where M is the total mass of collected water. To be able to evaluate the uncertainty, a probability distribution must be assumed for each of the component quantities.

The sensor's accuracy, or the combined standard uncertainty, $u_c(x)$, is obtained by:

$$u_c(x) = \sqrt{u_A^2(x) + u_B^2(x)} = \sqrt{u_{A1}^2(x) + u_{A2}^2(x) + u_B^2(x)} \qquad \text{(J. 1)}$$

J.2 Temperature sensors

J.2.1 Mercury Thermometer

Appendix C gives details of the mercury thermometer calibration, it is not to be repeated here. From the result of the calibration, the correction equation, as given by Equation (C.1), is reproduced as:

$$T_{\text{actual}} = 1.004 \cdot T_{\text{reading}} \qquad \text{(J. 2)}$$

Now assume that the water not being distilled and errors due to the lab barometer will bring an uncertainty of ± 0.1 °C to the actual boiling temperature, also, the resolution of the thermometer will bring another error of ±0.029 °C [1], thus at 94.3 °C the mercury thermometer has a standard uncertainty of ± 0.104°C [2]. This final error distributes linearly along the range of 0 to 94.3 °C, for the thermometer itself, which is 0.0011 °C per degree.

At each reading of the thermometer, considering the resolution error of the thermometer (0.029 °C), the standard uncertainty is thus:

$$u(T) = \frac{0.11}{100} \times \text{Reding(corrected)} + 0.029\ ^\circ\text{C} \qquad \text{(J. 3)}$$

---

[1] For sensor resolution of δx, under rectangular distribution, the standard deviation is $0.29\delta x$.

[2] $\sqrt{0.1^2 + 0.029^2} = 0.104$

which can be represented as:

$$u(T_{\text{thermo}})_{\min} = 0.029\ ^{\circ}\text{C}, \quad \text{at reading}=0^{\circ}\text{C}$$
$$u(T_{\text{thermo}})_{\max} = 0.139\ ^{\circ}\text{C}, \quad \text{at reading}=100^{\circ}\text{C} \qquad \text{(J. 4)}$$

J.2.2 LM35DZ Sensors

Type A evaluation of standard uncertainty

The sample size, standard deviation, and calibration RMSE for the four temperature sensors are:

Sensors	T1	T2	T3	T4
No. Sam, n	60	60	60	60
Max. Sam. Std. Dev., V	8.4×10^{-5}	9.3×10^{-5}	8.3×10^{-5}	9.2×10^{-5}
Max. Sam. Std. Dev. [1], °C	0.0084	0.0093	0.0083	0.0092
Calibration curve fitting RMSE, °C	0.0289	0.0297	0.0271	0.0282

The uncertainty of the four temperature sensors can now be calculated as:

Sensor	T1	T2	T3	T4
$u_{\text{A},1} = \frac{s}{\sqrt{n}}$	0.001	0.001	0.001	0.001
$u_{\text{A},2} = \text{RMSE}$	0.029	0.030	0.027	0.028
$u_{\text{A}} = \sqrt{u_{\text{A},1}^2 + u_{\text{A},2}^2}$	0.029	0.030	0.027	0.028

Type B evaluation of standard uncertainty

This is the mercury thermometer uncertainty: $u_{\text{B}} = 0.0011\,T + 0.029\ ^{\circ}\text{C}$

Combined standard uncertainty

[1] Converted from the reading Std. Dev. The reading standard deviation at each point is (in volts):

Sensor	T1	T2	T3	T4
Std. Dev.	8.4×10^{-5}	9.3×10^{-5}	8.3×10^{-5}	9.2×10^{-5}

The calibration equation for each sensor indicates that 1 V reading is compounding to 100 °C.

It can be obtained from the above calculation that for all the four sensors, the standard uncertainty can be approximated as:

$$u_{\mathrm{A}}(T) = 0.03 \quad ^{\circ}\mathrm{C}$$
$$u_{\mathrm{B}}(T) = 0.0011 \cdot T + 0.03$$
$$u(T) = \left(u_{\mathrm{A}}^2 + u_{\mathrm{B}}^2 \right)^{0.5}$$

The calibration of the four RTD's has been in the range of about 0 to 60 °C, similar to that for the LM35's. The maximum uncertainty is also the same:

$$\left(u_{\mathrm{c}}(T) \right)_{\max} = \left(0.03^2 + \left[0.0011 \times 60 + 0.03 \right]^2 \right)^{0.5} = 0.07524 \quad ^{\circ}\mathrm{C}$$

J.2.3 Resistance Temperature Detectors (RTD's)

Type A evaluation of standard uncertainty

The sample size, standard deviation, and calibration RMSE for the four RTD's are:

Sensors	RTD 1	RTD 2	RTD 3	RTD 4
No. Sam, n	60	60	60	60
Max. Sam. Std. Dev., V	10×10^{-5}	10×10^{-5}	7.3×10^{-5}	9.9×10^{-5}
Max. Sam. Std. Dev., °C	0.013	0.013	0.027	0.027
Calibration curve fitting RMSE, °C	0.026	0.020	0.033	0.029

The uncertainty of the four temperature sensors can now be calculated as:

Sensor	RTD 1	RTD 2	RTD 3	RTD 4
$u_{\mathrm{A},1} = \frac{s}{\sqrt{n}}$	0.0017	0.0017	0.0035	0.0035
$u_{\mathrm{A},2} = \mathrm{RMSE}$	0.029	0.030	0.027	0.028
$u_{\mathrm{A}} = \sqrt{u_{\mathrm{A},1}^2 + u_{\mathrm{A},2}^2}$	0.026	0.020	0.033	0.029

Type B evaluation of standard uncertainty

This is the mercury thermometer uncertainty: $u_{\mathrm{B}} = 0.0011\,T + 0.029 \quad ^{\circ}\mathrm{C}$

Combined standard uncertainty

It can be obtained from the above calculation that for all the four sensors, the standard uncertainty can be approximated as:

$$u_{\mathrm{A}}(T) = 0.03 \quad ^{\circ}\mathrm{C}$$
$$u_{\mathrm{B}}(T) = 0.0011 \cdot T + 0.03$$
$$u(T) = u_{\mathrm{A}}^2 + u_{\mathrm{B}}^2$$

where T = 0 ~ 100 °C, is the measured value. The result shows that the maximum uncertainty is with the maxim measured temperatures. In the current calibration the maximum temperature was around 60 °C, the maximum uncertainty is then:

$$\left(u_{\mathrm{c}}(T)\right)_{\max} = \left(0.03^2 + \left[0.0011 \times 60 + 0.03\right]^2\right)^{0.5} = 0.07524 \quad ^{\circ}\mathrm{C}$$

J.3 RS 257-026 Turbine Flow Meters

Type A evaluation of standard uncertainty

At maximum and minimum calibrated flow rates, The sample size, standard deviation, and calibration RMSE for flowmeter One and Two are:

Flow rates	Flowmeter 1		Flowmeter 2	
	$Q = Q_{\min}$	$Q = Q_{\max}$	$Q = Q_{\min}$	$Q = Q_{\max}$
No. Sam., *n*	564	136	532	136
Sam. Std. Dev [1], l/s	0.00084	0.0058	0.0014	0.0039
Calibration curve fitting RMSE, l/s	0.00151		0.00391	

$$u_{\mathrm{A},1}(Q) = \frac{s}{\sqrt{n}} = \frac{0.0058}{\sqrt{136}} = 0.0005 \quad \text{l/s, at maximum}$$
$$u_{\mathrm{A},2}(Q) = \mathrm{RMSE} = \begin{cases} 0.0015 \text{ l/s, Flowmeter 1} \\ 0.0039 \text{ l/s, Flowmeter 2} \end{cases}$$
$$u_{\mathrm{A}}(Q) = \sqrt{u_{\mathrm{A},1}^2 + u_{\mathrm{A},2}^2} = \begin{cases} 0.0015 \text{ l/s, Flowmeter 1} \\ 0.0039 \text{ l/s, Flowmeter 2} \end{cases}$$

[1] Converted from the reading Std. Dev., which is in V.

Type B evaluation of standard uncertainty

The flow rate is calculated by: $Q = M/(t \cdot \rho)$, where M is the total mass of collected water.

1. The weight scale has a resolution of 0.1 kg, a rectangular distribution of the true value is assumed, for which it is equally probable for the true value X to lie anywhere within the band $[X - 0.05\ \text{kg},\ X + 0.05\ \text{kg}]$.
2. Same distribution assumption is made for the time counted which is assigned with an uncertainty limit of 1s, and the density with an uncertainty limit of 1 kg/m^3.

Now the uncertainty of components for actual flow rates of flowmeter One and Two can be determined as:

Quantity X_i	unit	Error limits, δx_i	Standard uncertainty, $u(x_i) = 0.29\delta x_i$	Value of X_i	
				Flowmeter One	Flowmeter Two
M	kg	0.1	0.029	$M_{min} = 61.25$, $M_{max} = 62.35$	$M_{min} = 61.2$, $M_{max} = 62.2$
t	s	1	0.29	$t_{min} = 56.5$, $t_{max} = 264.7$	$t_{min} = 56.5$, $t_{max} = 278.3$
ρ	kg/m^3	1	0.29	998.7	998.7

$$\frac{u_B(Q)}{Q} = \sqrt{\frac{u^2(M)}{M} + \frac{u^2(t)}{t} + \frac{u^2(\rho)}{\rho}} = \sqrt{\left(\frac{0.029}{62}\right)^2 + \left(\frac{0.29}{M/(\rho Q)}\right)^2 + \left(\frac{0.29}{998.7}\right)^2}$$

$$= 10^{-2}\sqrt{0.003 + 0.22Q^2},\quad Q \text{ in l/s}$$

(where $M/(\rho Q) \approx \frac{62}{1000Q} = 0.062/Q$)

Combined standard uncertainty

The combined standard uncertainties are:

Flowmeter	Flowmeter 1	Flowmeter 2
$u_A(Q)$, l/s	0.0015	0.0039
$u_B(Q)$, l/s	$Q \cdot 10^{-2}\sqrt{0.003 + 0.22Q^2}$, Q in l/s	
$u_c(Q)$, l/s	$\sqrt{u_A^2 + u_B^2}$	

This result shows that the maximum uncertainty is with the maxim measured flow rates. In the current calibration the maximum flow was around 1.2 l/s. the maximum percentage uncertainty is then:

$$\left(\frac{u_c(Q)}{Q}\right)_{max} = \frac{\left(0.0039^2 + \left[1.2\times10^{-2}\times\sqrt{0.003+0.22\times1.2^2}\right]^2\right)^{0.5}}{1.2} = 0.006522$$

J.4 Trimec MP15S Flowmeter

Type A evaluation of standard uncertainty

At maximum and minimum calibrated flow rates, The sample size, standard deviation, and calibration RMSE for the Trimec MP15S flowmeter are:

Flow rates	$Q = Q_{min}$	$Q = Q_{max}$
No. Sam., *n*	644	218
Sam. Std. Dev, l/min	0.0073	0.034
Calibration curve fitting RMSE, l/min	0.0172	

$$u_{A,1}(Q) = \frac{s}{\sqrt{n}} = \frac{0.034}{\sqrt{218}} = 0.0023 \quad \text{l/min, at maximum}$$

$$u_{A,2}(Q) = \text{RMSE} = 0.0172 \quad \text{l/min}$$

$$u_A(Q) = \sqrt{u_{A,1}^2 + u_{A,2}^2} = 0.0174 \quad \text{l/min}$$

Type B evaluation of standard uncertainty

Following the same procedure as for the 257-026 Turbine Flow Meters, the flow rate is calculated by: $Q = M/(t\cdot\rho)$, where M is the total mass of collected water.

1. The weight scale has a resolution of 0.05 kg, assuming rectangular distribution of the weights, the true value X to lie anywhere within the band $[X - 0.025\ \text{kg},\ X + 0.025\ \text{kg}]$.
2. Same distribution assumption is made for the time counted which is assigned with an uncertainty limit of 1s, and the density with an uncertainty limit of 1 kg/m^3.

Now the uncertainty of components for actual flow rates of the flowmeter is :

Quantity X_i	unit	Error limits, δx_i	Standard uncertainty, $u(x_i) = 0.29\delta x_i$	Value of X_i
M	kg	0.05	0.015	$M_{min} = 21.1$, $M_{max} = 20.9$
t	s	1	0.29	$t_{min} = 140.9$, $t_{max} = 582.7$
ρ	kg/m^3	1	0.29	998.7

$$\frac{u_B(Q)}{Q} = \sqrt{\frac{u^2(M)}{M} + \frac{u^2(t)}{t} + \frac{u^2(\rho)}{\rho}} = \sqrt{\left(\frac{0.015}{21}\right)^2 + \left(\frac{0.29}{M/(\rho Q)}\right)^2 + \left(\frac{0.29}{998.7}\right)^2}$$
$$= 10^{-2}\sqrt{0.006 + 0.00052Q^2}, \quad Q \text{ in l/min}$$

Combined standard uncertainty

The combined standard uncertainties are:

$u_A(Q)$, l/min	0.0174
$u_B(Q)$, l/min	$Q \cdot 10^{-2}\sqrt{0.006 + 0.00052Q^2}$, Q in l/min
$u_c(Q)$, l/min	$\sqrt{u_A^2 + u_B^2}$

This result shows that the maximum uncertainty is with the maxim measured flow rates. In the current calibration the maximum flow was around 8.5 l/min. the maximum percentage uncertainty is then:

$$\left(\frac{u_c(Q)}{Q}\right)_{max} = \frac{\left(0.0174^2 + \left[8.5\times10^{-2}\times\sqrt{0.006 + 0.00052\times8.5^2}\right]^2\right)^{0.5}}{8.5}$$
$$= 0.002924$$

J.5 Rosemount 3051 CD Differential Pressure Transmitter

Type A evaluation of standard uncertainty

The sample size, standard deviation, and calibration RMSE for the transmitter are:

Water head	$h = 0 \sim 7.5$ m

No. Sam., n	60
Max. Sam. Std. Dev., Pa	6.72
Calibration curve fitting RMSE, Pa	18.6

$$u_{\mathrm{A},1}(DP) = \frac{s}{\sqrt{n}} = \frac{6.72}{\sqrt{60}} = 0.87 \ \text{Pa, at maximum}$$

$$u_{\mathrm{A},2}(DP) = \mathrm{RMSE} = 18.6 \ \text{Pa}$$

$$u_{\mathrm{A}}(DP) = \sqrt{u_{\mathrm{A},1}^2 + u_{\mathrm{A},2}^2} = 18.6 \ \text{Pa}$$

Type B evaluation of standard uncertainty

Differential pressure is calculated by: $DP = \rho g h$.

1. The Type measure has a resolution of 1 mm, a rectangular distribution of the true value is assumed, for which it is equally probable for the true value X to lie anywhere within the band [$X - 0.5$ mm, $X + 0.5$ mm].
2. Same assumption is made for the gravity which is assigned with an uncertainty limit of 0.01 m/s^2, and the density with an uncertainty limit of 1 kg/m^3.

The uncertainty of components for actual differential pressure are:

Quantity X_{i}	unit	Error limits, δx_{i}	Std. uncertainty, $u(x_{\mathrm{i}}) = 0.29\delta x_{\mathrm{i}}$	Value of X_{i}
ρ	kg/m^3	1	0.29	998.2
g	m/s^2	0.01	0.0029	9.79
h	m	0.001	0.00029	$h_{\min} = 0\mathrm{m}$, $h_{\max} = 7.5\mathrm{m}$

$$\frac{u_{\mathrm{B}}(DP)}{DP} = \sqrt{\left[\frac{u(\rho)}{\rho}\right]^2 + \left[\frac{u(g)}{g}\right]^2 + \left[\frac{u(h)}{h}\right]^2} = \sqrt{\left(\frac{0.29}{998.2}\right)^2 + \left(\frac{0.0029}{9.79}\right)^2 + \left(\frac{0.00029}{DP/\rho g}\right)^2}$$

$$= \sqrt{17.1\times10^{-8} + \left(\frac{2.9}{DP}\right)^2} \quad \text{DP in Pa}$$

Combined standard uncertainty

At any reading of DP where $0 \le DP \le 73.3\times10^3$ Pa :

$u_A(DP)$, Pa	18.6
$u_B(DP)$, Pa	$DP \cdot \sqrt{17.1\times10^{-8}+\left(\frac{2.9}{DP}\right)^2}$, DP in Pa
$u_c(DP)$	$\sqrt{u_A^2+u_B^2}$

The application of this device in the current study is in the range of 1-30 kPa in the current study. For this range:

$$\left(\frac{u_c(DP)}{DP}\right)_{DP=30kPa} = \frac{\left(18.6^2+\left[30000\times\sqrt{17.1\times10^{-8}+\left(2.9/30000\right)^2}\right]^2\right)^{0.5}}{30\times10^3} = 0.00075$$

$$\left(\frac{u_c(DP)}{DP}\right)_{DP=1kPa} = \frac{\left(18.6^2+\left[1000\times\sqrt{17.1\times10^{-8}+\left(2.9/1000\right)^2}\right]^2\right)^{0.5}}{1000} = 0.0188$$

J.6 WIKA Static Pressure Transmitters

Type A evaluation of standard uncertainty

The sample size, standard deviation, and calibration RMSE for the transmitter are:

Weight pressure	0 - 840 kPa	0 - 840 kPa
No. Sam., n	60	60
Max. Sam. Std. Dev., kPa	0.57	0.149
Calibration curve fitting RMSE, kPa	0.33	0.34

$$u_{A,1}(DP) = \frac{s}{\sqrt{n}} = \frac{0.57}{\sqrt{60}} = 0.074 \text{ kPa, at maximum}$$

$$u_{A,2}(DP) = \text{RMSE} = 0.33 \text{ kPa}$$

$$u_A(DP) = \sqrt{u_{A,1}^2+u_{A,2}^2} = 0.34 \text{ kPa}$$

Type B evaluation of standard uncertainty

Differential pressure is calculated by: $P = Mg / A$.

1. The weights and the calibrator were in good maintained condition, it is safe to evaluated the relative uncertainty of the weights and the calibrator to be ± 0.5%.
2. Assuming rectangular distribution for g with an uncertainty limit of 1 kg/m^3.

The uncertainty of components for actual differential pressure are:

Quantity X_i	unit	Error limits, δx_i	Std. uncertainty, $u(x_i) = 0.29\delta x_i$	Value of X_i
M	kg	-	-	-
A	m^2	-	-	-
g	m/s^2	0.01	0.0029	9.79

$$\frac{u_B(P)}{P} = \sqrt{\left[\frac{u(M)}{M}\right]^2 + \left[\frac{u(A)}{A}\right]^2 + \left[\frac{u(g)}{g}\right]^2} = \sqrt{0.005^2 + 0.005^2 + \left(\frac{0.0029}{9.79}\right)^2}$$
$$= 0.0071$$

Combined standard uncertainty

At any reading of DP where $0 \le DP \le 840$ kPa :

$u_A(P)$, kPa	0.34
$u_B(P)$, kPa	$P \cdot 0.0071$
$u_c(DP)$	$\sqrt{u_A^2 + u_B^2}$

The application of this device in the current study is around 300 kPa for R134a tests and 800 kPa for R507 tests. For this range:

$$\left(\frac{u_c(P)}{P}\right)_{P=300} = \frac{\left(0.34^2 + (300 \times 0.0071)^2\right)^{0.5}}{300} = 0.0072$$

$$\left(\frac{u_c(P)}{P}\right)_{P=800} = \frac{\left(0.34^2 + (800 \times 0.0071)^2\right)^{0.5}}{800} = 0.0071$$

Appendix K Uncertainty Analysis: Water Tests

K.1 Calculation Method
K.2 Experimental Results
Mass Flow Rate, $\dot{m}$
Log Mean Temperature Difference, ΔT_{LM} (LMTD)
Differential pressure, ΔP
Heat Flux, q
Overall Heat Transfer Coefficient, U
Heat Transfer Coefficient, h_c
Reynolds Number, Re
Nusselt Number, Nu
Friction Factor, f

K.1 Calculation Method

For any measured quantity x, the standard uncertainty $u(x)$ is calculated by:

$$u(x) = \sqrt{u_A^2(x) + u_B^2(x)} \qquad \text{(K. 1)}$$

where $u_A(x) = \frac{s}{\sqrt{n}}$, is the Type A evaluation, s is sample standard deviation, and n is sample size, $u_B(x)$ is the Type B evaluation, taken as the sensor calibration uncertainty, or quoted uncertainty from the manufacturer.

K.2 Experimental Results

Mass Flow Rate, $\dot{m}$

Mass flow rate of the water streams is calculated by: $\dot{m} = \rho Q$. The standard uncertainty of $\dot{m}$ is calculated as:

unit	No. of data points	Hot stream (Flowmeter 1)				Cold stream (Flowmeter 2)			
		$u(\dot{m})$, kg/s		$u(\dot{m})/\dot{m}$, %		$u(\dot{m})$, kg/s		$u(\dot{m})/\dot{m}$, %	
		min	max	min	max	min	max	min	max
Low angle	19	0.002	0.002	0.43	0.43	0.004	0.007	0.60	1.13

Mix angle	18	0.002	0.002	0.44	0.45	0.004	0.007	0.60	1.40
High angle	16	0.002	0.002	0.46	0.46	0.004	0.006	0.61	1.36

$u(\dot{m})$ values are rounded to 0.001 kg/s

Sample Calculation

As an example, the calculation for first point in Low angle unit (19 points for this test) is shown below. The measurements are given as:

Water stream	Reading, l/s	Std. Dev., l/s	No. Sample
Hot, Flowmeter 1	0.396	0.0006	40
Cold, Flowmeter 2	1.154	0.0013	40

For hot water:

$$u_A(Q) = \frac{s}{\sqrt{40}} = \frac{0.0006}{\sqrt{40}} = 9.5\times10^{-5} \quad \text{l/s}$$

$$u_B(Q) = \sqrt{0.0015^2 + \left[10^{-2} Q\sqrt{0.003 + 0.22Q^2}\right]^2} = 0.0017 \quad \text{l/s}$$

$$u_c(Q) = \sqrt{u_A^2 + u_B^2} = 0.0017 \quad \text{l/s}$$

To calculate $u(\dot{m})$, Assume rectangular distribution of uncertainty band of 1 kg/m3 for density ρ and so $u(\rho) = 0.29 \quad \text{kg/m}^3$:

$$\frac{u_c(\dot{m})}{\dot{m}} = \sqrt{\left(\frac{u(Q)}{Q}\right)^2 + \left(\frac{u(\rho)}{\rho}\right)^2} = \sqrt{\left(\frac{0.0017}{0.396}\right)^2 + \left(\frac{0.29}{1000}\right)^2} = 0.0043$$

$$u_c(\dot{m}) = 0.396\times1000\times0.0042 = 0.0017 \quad \text{kg/s}$$

For cold water:

$$u_A(Q) = \frac{0.0013}{\sqrt{40}} = 0.00021 \quad \text{l/s}$$

$$u_B(Q) = \sqrt{0.0039^2 + \left[10^{-2} Q\sqrt{0.003 + 0.22Q^2}\right]^2} = 0.0074 \quad \text{l/s}$$

$$u_c(Q) = \sqrt{u_A^2 + u_B^2} = 0.0074 \quad \text{l/s}$$

$$\frac{u_c(\dot{m})}{\dot{m}} = \sqrt{\left(\frac{0.0074}{1.154}\right)^2 + \left(\frac{0.29}{1000}\right)^2} = 0.0064$$

$$u_c(\dot{m}) = 1.154\times1000\times0.0064 = 0.0074 \quad \text{kg/s}$$

Log Mean Temperature Difference, ΔT_{LM} (LMTD)

For clarity, the equation for log mean temperature difference is rewritten as:

$$y = \mathrm{LMTD} = \frac{x_1 - x_2}{\ln(\frac{x_1}{x_2})} \qquad \text{(K. 2)}$$

where $x_1 = \Delta T_1 = T_{\mathrm{h,in}} - T_{\mathrm{c,out}}$, $x_2 = \Delta T_2 = T_{\mathrm{h,out}} - T_{\mathrm{c,in}}$. The combined uncertainty for ΔT_{LM} is:

$$u_{\mathrm{c}}(y) = \sqrt{\left[\frac{\partial y}{\partial x_1} u(x_1)\right]^2 + \left[\frac{\partial y}{\partial x_2} u(x_2)\right]^2} \qquad \text{(K. 3)}$$

where the partial differentials are:

$$\frac{\partial y}{\partial x_1} = \frac{1}{\ln(\frac{x_1}{x_2})} - \frac{(x_1 - x_2)\cdot\frac{1}{x_1}}{\left[\ln(\frac{x_1}{x_2})\right]^2}, \quad \frac{\partial y}{\partial x_2} = -\left\{\frac{1}{\ln(\frac{x_1}{x_2})} - \frac{(x_1 - x_2)\cdot\frac{1}{x_2}}{\left[\ln(\frac{x_1}{x_2})\right]^2}\right\}$$

Results for the current water test are:

unit	No. of data points	$u(LMTD)$, °C (round to 0.01)		$\frac{u(LMTD)}{LMTD}$, %	
		min	max	min	max
Low angle	19	0.08	0.08	0.4	0.5
Mix angle	18	0.08	0.09	0.7	0.8
High angle	16	0.08	0.14	0.9	1.6

Sample Calculation

As an example, the calculation for first point in Low angle unit test (19 points for this test) is given below. The measurement readings are:

Sensor	$T_{\mathrm{h,in}}$	$T_{\mathrm{h,out}}$	$T_{\mathrm{c,out}}$	$T_{\mathrm{c,in}}$
Reading, °C	55.88	26.85	27.91	18.48
Std. Dev., °C	0.008	0.009	0.06	0.005

Sample size	40	40	40	40

Calculation:

$x_1 = \Delta T_1 = T_{\text{h,in}} - T_{\text{c,out}} = 27.97$, $x_2 = \Delta T_2 = T_{\text{h,out}} - T_{\text{c,in}} = 10.17$, ℃

$$\frac{\partial y}{\partial x_1} = \frac{1}{\ln(\frac{x_1}{x_2})} - \frac{(x_1 - x_2)\cdot\frac{1}{x_1}}{\left[\ln(\frac{x_1}{x_2})\right]^2} = \frac{1}{\ln(2.75)} - \frac{17.8\cdot\frac{1}{27.97}}{\left[\ln(2.75)\right]^2} = 0.367$$

$$\frac{\partial y}{\partial x_2} = -\left\{\frac{1}{\ln(\frac{x_1}{x_2})} - \frac{(x_1 - x_2)\cdot\frac{1}{x_2}}{\left[\ln(\frac{x_1}{x_2})\right]^2}\right\} = -\frac{1}{\ln(2.75)} + \frac{17.8\cdot\frac{1}{10.17}}{\left[\ln(2.75)\right]^2} = 0.722$$

For each sensor, from: $u_{\text{B}}(T) = 0.04 + 0.001 \times \text{reading}$ ℃

$u(T_{\text{h,in}}) = 0.096$, $u\left(T_{\text{h,out}}\right) = 0.069$, $u\left(T_{\text{c,out}}\right) = 0.068$, $u\left(T_{\text{c,in}}\right) = 0.058$, ℃

Uncertainty of individual temperatures:

sensor	$T_{\text{h,in}}$	$T_{\text{h,out}}$	$T_{\text{c,out}}$	$T_{\text{c,in}}$
$u_{\text{A}} = \frac{s}{\sqrt{n}}$, ℃	0.001	0.001	0.01	0.001
$u_{\text{B}} = 0.04 + 0.001 \times \text{reading}$ *, ℃	0.096	0.069	0.068	0.058
$u_{\text{c}} = \sqrt{u_{\text{A}}^2 + u_{\text{B}}^2}$, ℃	0.096	0.069	0.069	0.058

* u_{B} is the sensor calibration uncertainty

Uncertainty of temperature differences:

$$u(x_1) = \sqrt{u^2(T_{\text{h,in}}) + u^2(T_{\text{c,out}})} = \sqrt{0.096^2 + 0.068^2} = 0.118 \quad ^\circ\text{C}$$

$$u(x_2) = \sqrt{u^2(T_{\text{h,out}}) + u^2(T_{\text{c,in}})} = \sqrt{0.069^2 + 0.058^2} = 0.090 \quad ^\circ\text{C}$$

Result:

$$u_{\text{c}}(y) = \sqrt{\left[\frac{\partial y}{\partial x_1}u(x_1)\right]^2 + \left[\frac{\partial y}{\partial x_2}u(x_2)\right]^2} = \sqrt{(0.367\times 0.118)^2 + (0.722\times 0.090)^2}$$

$$= 0.078 \quad ^\circ\text{C}$$

$$\frac{u_{\text{c}}(y)}{y} = \frac{0.078}{17.8/\ln 2.75} = 0.0044 = 0.4\%$$

Differential pressure, Δ*P*

Result:

unit	No. of data points	No. of samples at each measuring point	$u(\Delta P)$, Pa (Round to 1)		$u(\Delta P)/\Delta P$, %	
			min	max	min	max
Low angle	17	40	19	22	0.2	1.9
Mix angle	16	40	19	27	0.2	2.4
High angle	18	40	19	33	0.1	1.0

Sample calculation

For first point in Low angle unit test. Measurement readings are:

Reading, Pa	Std. Dev., Pa	No. Sample
9475	49	40

For hot water:

$$u_A(DP) = \frac{s}{\sqrt{n}} = \frac{49}{\sqrt{40}} = 7.7 \quad \text{Pa}$$

$$u_B(DP) = \sqrt{18.6^2 + \left[DP \cdot \sqrt{17.1\times10^{-8} + \left(\frac{2.9}{DP}\right)^2} \right]^2} = 19.2 \quad \text{Pa}$$

$$u_c(DP) = \sqrt{u_A^2 + u_B^2} = 20.7 \quad \text{Pa}$$

$$\frac{u_c(DP)}{DP} = \frac{20.7}{9475} = 0.0022$$

Heat Flux, *q*

Heat flux is calculated by:

$$q = \frac{1}{A}\dot{m}\int_{t1}^{t2} c_p dT \qquad \text{(K. 4)}$$

For the calculation of the standard uncertainty, the equation is modified as:

$$q = \frac{1}{A}\dot{m} c_p \Delta T \qquad \text{(K. 5)}$$

Heat load can be calculated by either hot water side of the cold water side. A rectangular distribution is assumed for heat transfer area A with an uncertainty band of 3%, also a rectangular distribution is assumed for specific heat with an uncertainty band of 1%.

Result:

unit	No. of data points	Hot stream		Cold stream	
		$u(q)/q$, %		$u(q)/q$, %	
		min	max	min	max
Low angle	19	1.1	1.2	1.3	1.5
Mix angle	18	1.1	1.2	1.3	1.7
High angle	16	1.1	1.1	1.2	1.7

Sample Calculation

For the first point in Low angle unit test, readings are:

Quantity	$T_{h,in}$	$T_{h,out}$	$T_{c,out}$	$T_{c,in}$	$\dot{m}_{hot}$	$\dot{m}_{cold}$
unit	°C	°C	°C	°C	kg/s	kg/s
Value, x_i	55.88	28.65	27.91	18.48	0.396	1.154
$u(x_i)$	0.10	0.07	0.07	0.06	-	-
$u(x_i)/x_i$, %	-	-	-	-	0.43	0.64

Uncertainty of heat transfer area, $\frac{u(A)}{A} = \frac{0.29 \times 0.03A}{A} = 0.0087$

Uncertainty of specific heat, $\frac{u(c_p)}{c_p} = \frac{0.29 \times 0.01 c_p}{c_p} = 0.0029$

For hot stream:

$$\frac{u(\Delta t)}{\Delta t} = \frac{\sqrt{0.1^2 + 0.07^2}}{55.88 - 28.65} = 0.0045$$

$$\frac{u(q)}{q} = \sqrt{\left[\frac{u(\Delta t)}{\Delta t}\right]^2 + \left[\frac{u(\dot{m})}{\dot{m}}\right]^2 + \left[\frac{u(A)}{A}\right]^2 + \left[\frac{u(c_p)}{c_p}\right]^2} = \sqrt{\frac{0.45^2 + 0.43^2 + 0.87^2 + 0.29^2}{100^2}}$$

$$= 0.011$$

For cold stream:

$$\frac{u(\Delta t)}{\Delta t} = \frac{\sqrt{0.07^2 + 0.06^2}}{27.91 - 18.48} = 0.0098$$

$$\frac{u(q)}{q} = \sqrt{\frac{0.98^2 + 0.64^2 + 0.87^2 + 0.29^2}{100^2}} = 0.015$$

Overall Heat Transfer Coefficient, *U*

U is calculated by

$$U = \frac{q}{LMTD} \qquad \text{(K. 6)}$$

where *q* is calculated from the hot stream (lower uncertainty compared with the cold side). The standard uncertainty is:

$$\frac{u(U)}{U} = \sqrt{\left(\frac{u(q)}{q}\right)^2 + \left(\frac{u(\Delta T_{\mathrm{LM}})}{\Delta T_{\mathrm{LM}}}\right)^2} \qquad \text{(K. 7)}$$

Result:

unit	No. of data points	$u(U)/U$, %	
		min	max
Low angle	19	1.2	1.3
Mix angle	18	1.3	1.4
High angle	16	1.4	1.9

Heat Transfer Coefficient, h_c

The film coefficient is obtained from:

$$\frac{1}{U} - R_{\mathrm{wall}} = \frac{1}{h_{\mathrm{h}}} + \frac{1}{h_{\mathrm{c}}} \qquad \text{(K. 8)}$$

where $R_{\mathrm{wall}} = \left(\delta / k\right)_{\mathrm{wall}}$. Only the cold side water stream is of interest, based on which the final correlation

$$\mathrm{Nu} = f\left(\mathrm{Re}, \mathrm{Pr}, \left(\frac{\mu}{\mu_{\mathrm{wall}}}\right)\right) \qquad \text{(K. 9)}$$

is drawn. Uncertainty of U and thus $1/U$ can be obtained from previous sections. The uncertainty of the wall resistance, R_{wall}, is calculated based on the assumptions that:

1. a rectangular distribution of wall thickness with an uncertainty band of 3%, and so: $\frac{u(\delta)}{\delta} = \frac{0.29 \times 0.03\delta}{\delta} = 0.0087$
2. a rectangular distribution of wall thermal conductivity with an uncertainty band of 1%, and so: $\frac{u(k)}{k} = \frac{0.29 \times 0.01k}{k} = 0.0029$

The relative standard uncertainty of wall resistance is thus:

$$\frac{u(R_{\mathrm{wall}})}{R_{\mathrm{wall}}} = \sqrt{\left[\frac{u(\delta)}{\delta}\right]^2 + \left[\frac{u(k)}{k}\right]^2} = \sqrt{0.0087^2 + 0.0029^2} = 0.0092$$

The uncertainties of the film coefficients of both sides are coupled, to find the uncertainty of $u(h_{\mathrm{c}})$ some assumptions must be made. In the extreme case where $u(h_{\mathrm{c}}) = 0$ the uncertainty of cold side film coefficient will have its maximum value. From this assumption, it can be calculated:

$$\frac{u(h_{\mathrm{c}})}{h_{\mathrm{c}}} = \frac{u(\frac{1}{U} - R_{\mathrm{wall}})}{\frac{1}{U} - R_{\mathrm{wall}}}$$

Result:

unit	No. of data points	$u(h_{\mathrm{c}})/h_{\mathrm{c}}$, %	
		min	max
Low angle	19	1.2	1.3
Mix angle	18	1.3	1.5
High angle	16	1.6	2.1

Reynolds Number, Re

Reynolds number is calculated by:

$$\mathrm{Re} = \frac{\rho u d_\mathrm{h}}{\mu} = \frac{\rho d_\mathrm{h}}{A_\mathrm{c}\mu} \cdot Q \qquad \text{(K. 10)}$$

Assuming rectangular distribution for $\rho, \mu, d_\mathrm{h}, A_\mathrm{c}$ with uncertainty bands of 0.1%, 1%, 3%, 3%, respectively, and it is obtained that:

$$\frac{u(\rho)}{\rho} = \frac{0.29 \times 0.001\rho}{\rho} = 0.00029$$
$$\frac{u(\mu)}{\mu} = \frac{0.29 \times 0.01\rho}{\rho} = 0.0029$$
$$\frac{u(d_\mathrm{h})}{d_\mathrm{h}} = \frac{0.29 \times 0.03 d_\mathrm{h}}{d_\mathrm{h}} = 0.0087$$
$$\frac{u(A_\mathrm{c})}{A_\mathrm{c}} = \frac{0.29 \times 0.03 A_\mathrm{c}}{A_\mathrm{c}} = 0.0087$$

And:

$$\frac{u(\mathrm{Re})}{\mathrm{Re}} = \sqrt{\left[\frac{u(\rho)}{\rho}\right]^2 + \left[\frac{u(\mu)}{\mu}\right]^2 + \left[\frac{u(d_\mathrm{h})}{d_\mathrm{h}}\right]^2 + \left[\frac{u(A_\mathrm{c})}{A_\mathrm{c}}\right]^2 + \left[\frac{u(Q)}{Q}\right]^2} = \sqrt{0.00016 + \left[\frac{u(Q)}{Q}\right]^2}$$

Result:

unit	No. of data points	$u(\mathrm{Re}_\mathrm{c})/\mathrm{Re}_\mathrm{c}$, %	
		min	max
Low angle	19	1.4	1.7
Mix angle	18	1.4	1.9
High angle	16	1.4	1.9

Nusselt Number, Nu

Nusselt number is calculated by:

$$\mathrm{Nu} = \frac{h d_\mathrm{h}}{k} \qquad \text{(K. 11)}$$

Assuming rectangular distribution for k, d_h with uncertainty bands of 1%, 3%, respectively, it is obtained:

$$\frac{u(k)}{k} = \frac{0.29 \times 0.01k}{k} = 0.0029, \quad \frac{u(d_\mathrm{h})}{d_\mathrm{h}} = \frac{0.29 \times 0.03 d_\mathrm{h}}{d_\mathrm{h}} = 0.0087$$

$$\frac{u(\mathrm{Nu})}{\mathrm{Nu}} = \sqrt{\left[\frac{u(k)}{k}\right]^2 + \left[\frac{u(d_\mathrm{h})}{d_\mathrm{h}}\right]^2 + \left[\frac{u(h)}{h}\right]^2} = \sqrt{0.00008 + \left[\frac{u(h)}{h}\right]^2}$$

Result:

unit	No. of data points	$u(\mathrm{Nu})/\mathrm{Nu}$, %	
		min	max
L angle	19	1.5	1.6
M angle	18	1.6	1.7
H angle	16	1.8	2.2

Friction Factor, *f*

The Darcy friction factor is calculated by:

$$f = \frac{DP/L}{\frac{1}{2}\rho u^2/d_\mathrm{h}} = \frac{DP}{Q^2}\cdot\frac{d_\mathrm{h}}{L}\cdot\frac{2A_\mathrm{c}^2}{\rho} \qquad \text{(K. 12)}$$

Assuming rectangular distribution for $\rho, d_\mathrm{h}, L, A_\mathrm{c}$ with uncertainty bands of 0.1%, 3%, 3%, 3% respectively, it is obtained:

$$\frac{u(\rho)}{\rho} = \frac{0.29\times 0.001\rho}{\rho} = 0.00029$$
$$\frac{u(d_\mathrm{h})}{d_\mathrm{h}} = \frac{0.29\times 0.03 d_\mathrm{h}}{d_\mathrm{h}} = 0.0087$$
$$\frac{u(L)}{L} = \frac{0.29\times 0.03 L}{L} = 0.0087$$
$$\frac{u(A_\mathrm{c})}{A_\mathrm{c}} = \frac{0.29\times 0.03 A_\mathrm{c}}{A_\mathrm{c}} = 0.0087$$

Use 1.4% as the relative uncertainty for Q:

$$\frac{u(f)}{f} = \sqrt{\left[\frac{u(\rho)}{\rho}\right]^2 + \left[\frac{u(d_\mathrm{h})}{d_\mathrm{h}}\right]^2 + \left[\frac{u(L)}{L}\right]^2 + \left[\frac{u(A_\mathrm{c})}{A_\mathrm{c}}\right]^2 + \left[\frac{u(Q)}{Q}\right]^2 + \left[\frac{u(DP)}{DP}\right]^2} = \sqrt{0.00042 + \left[\frac{u(DP)}{DP}\right]^2}$$

Result:

unit	No. of data points	$u(f)/f$, %	
		min	max
L angle	17	2.1	3.1
M angle	16	2.1	3.1
H angle	18	2.1	2.3

Appendix L Uncertainty Analysis: Refrigerant Evaporator Tests

L.1 Calculation Method
L.2 Experimental Results
Water Mass Flow Rate, $\dot{m}_w$
Heat Flux, q
Log Mean Temperature Difference, ΔT_{LM} (LMTD)
Overall Heat Transfer Coefficient, U
Refrigerant Heat Transfer Coefficient, h_r
Refrigerant Mass Flow Rate $\dot{m}_r$
Outlet Vapour Quality, x
Total Pressure Drop, ΔP_{tot}
Frictional Pressure Drop, ΔP_{fric}
Friction Factor, f

L.1 Calculation Method

For any measured quantity x, the standard uncertainty $u(x)$ is calculated by:

$$u(x) = \sqrt{u_A^2(x) + u_B^2(x)} \qquad \text{(L. 1)}$$

where $u_A(x) = \frac{s}{\sqrt{n}}$, is the Type A evaluation, s is sample standard deviation, and n is sample size, $u_B(x)$ is the Type B evaluation, taken as the sensor calibration uncertainty, or quoted uncertainty from the manufacturer.

L.2 Experimental Results

Water Mass Flow Rate, $\dot{m}_w$

Mass flow rate of the water streams is calculated by: $\dot{m}_w = (\rho Q)_w$. The standard uncertainty of $\dot{m}$ is calculated as:

unit	R134a	R507

	No. data	$u(\dot{m})/\dot{m}$, %		No. data	$u(\dot{m})/\dot{m}$, %	
		min	max		min	max
Low angle	58	0.38	0.43	22	0.42	0.42
Mix angle	58	0.38	0.42	18	0.42	0.42
High angle	59	0.39	0.42	20	0.42	0.42

Sample Calculation

A sample calculation is given here for the first reading of the Low angle unit with R134a. The measurements are:

Reading, l/s	Std. Dev., l/s	No. Sample
0.7977	0.000972	60

Result:

$$u_A(Q) = \frac{s}{\sqrt{n}} = \frac{0.000972}{\sqrt{60}} = 1.255\times10^{-4} \quad \text{l/s}$$

$$u_B(Q) = \sqrt{0.0015^2 + \left[10^{-2} Q \sqrt{0.003 + 0.22Q^2}\right]^2} = 0.0034 \quad \text{l/s}$$

$$u_c(Q) = \sqrt{u_A^2 + u_B^2} = 0.0034 \quad \text{l/s}$$

To calculate $u(\dot{m})$, Assume rectangular distribution of uncertainty band of 1 kg/m3 for density ρ and so $u(\rho) = 0.29 \quad \text{kg/m}^3$:

$$\frac{u_c(\dot{m})}{\dot{m}} = \sqrt{\left(\frac{u(Q)}{Q}\right)^2 + \left(\frac{u(\rho)}{\rho}\right)^2} = \sqrt{\left(\frac{0.0034}{0.7977}\right)^2 + \left(\frac{0.29}{1000}\right)^2} = 0.0043$$

Heat Flux, *q*

Heat flux is calculated from:

$$q = \frac{1}{A}\left(\dot{m} c_p \Delta T\right)_w \qquad \text{(L. 2)}$$

A rectangular distribution is assumed for heat transfer area A with an uncertainty band of 3%, also a rectangular distribution is assumed for specific heat with an uncertainty band of 1%.

Result:

unit	R134a	R507

	No. data	$u(q)/q$, %		No. data	$u(q)/q$, %	
		min	max		min	max
Low angle	58	1.8	4.3	22	2.2	3.4
Mix angle	58	1.8	4.3	18	2.1	3.4
High angle	59	1.7	4.3	20	2.1	3.5

Sample Calculation

A sample calculation is given here for the first reading of the Low angle unit with R134a. The measurements are:

Quantity	$T_{w,in}$	$T_{w,out}$	$\dot{m}_w$
unit	°C	°C	kg/s
Value, x_i	16.49	12.51	0.798
$u(x_i)$	0.056	0.053	-
$u(x_i)/x_i$, %	-	-	0.42

Uncertainty of heat transfer area, $\frac{u(A)}{A} = \frac{0.29 \times 0.03A}{A} = 0.0087$

Uncertainty of specific heat, $\frac{u(c_p)}{c_p} = \frac{0.29 \times 0.01 c_p}{c_p} = 0.0029$

$$\frac{u(\Delta t)}{\Delta t} = \frac{\sqrt{0.056^2 + 0.053^2}}{16.49 - 12.51} = 0.01937$$

$$\frac{u(q)}{q} = \sqrt{\left[\frac{u(\Delta t)}{\Delta t}\right]^2 + \left[\frac{u(\dot{m})}{\dot{m}}\right]^2 + \left[\frac{u(A)}{A}\right]^2 + \left[\frac{u(c_p)}{c_p}\right]^2} = \sqrt{\frac{1.94^2 + 0.42^2 + 0.87^2 + 0.29^2}{100^2}}$$

$$= 0.0219$$

Log Mean Temperature Difference, ΔT_{LM} (LMTD)

For clarity, the equation for log mean temperature difference is rewritten as:

$$y = \mathrm{LMTD} = \frac{x_1 - x_2}{\ln(\frac{x_1}{x_2})} \qquad \text{(L. 3)}$$

where $x_1 = \Delta T_{max}$, $x_2 = \Delta T_{min}$. The combined uncertainty for ΔT_{LM} is:

$$u_c(y) = \sqrt{\left[\frac{\partial y}{\partial x_1} u(x_1)\right]^2 + \left[\frac{\partial y}{\partial x_2} u(x_2)\right]^2} \qquad \text{(L. 4)}$$

where the partial differentials are:

$$\frac{\partial y}{\partial x_1} = \frac{1}{\ln(\frac{x_1}{x_2})} - \frac{(x_1 - x_2)\cdot\frac{1}{x_1}}{\left[\ln(\frac{x_1}{x_2})\right]^2}, \quad \frac{\partial y}{\partial x_2} = -\left\{\frac{1}{\ln(\frac{x_1}{x_2})} - \frac{(x_1 - x_2)\cdot\frac{1}{x_2}}{\left[\ln(\frac{x_1}{x_2})\right]^2}\right\}$$

Results:

unit	R134a			R507		
	No. data	$u(\Delta T_{LM})/\Delta T_{LM}$, %		No. data	$u(\Delta T_{LM})/\Delta T_{LM}$, %	
		min	max		min	max
Low angle	58	0.8	1.9	22	0.8	1.2
Mix angle	58	0.9	2.3	18	1.0	1.9
High angle	59	1.2	2.9	20	1.2	2.3

Sample Calculation

A sample calculation is given here for the first reading of the Low angle unit with R134a.

Measurements:

Sensor	$T_{w,\,out}$	$T_{w,\,in}$	$T_{r,\,in}$	$T_{r,\,out}$
Reading, °C	10.85	14.66	6.29	6.25
Std. Dev., °C	0.002258	0.001306	0.03164	0.004135

Uncertainty of individual temperatures (sample size = 60):

Sensor	$T_{w,\,out}$	$T_{w,\,in}$	$T_{r,\,in}$	$T_{r,\,out}$
$u_A = \frac{s}{\sqrt{n}}$, °C	0.0003	0.0002	0.0041	0.0005
$u_B = 0.04 + 0.001 \times \text{reading}$ *, °C	0.0508	0.0547	0.0463	0.0462
$u_c = \sqrt{u_A^2 + u_B^2}$, °C	0.0508	0.0547	0.0465	0.0463

* u_B is the sensor calibration uncertainty

Uncertainty of temperature differences:

$$u(x_1)=\sqrt{u^2(T_{\mathrm{w,\,in}})+u^2(T_{\mathrm{r,\,out}})}=\sqrt{0.0547^2+0.0463^2}=0.072\ \ ^\circ\mathrm{C}$$

$$u(x_2)=\sqrt{u^2(T_{\mathrm{w,\,out}})+u^2(T_{\mathrm{r,\,in}})}=\sqrt{0.0508^2+0.0465^2}=0.069\ \ ^\circ\mathrm{C}$$

Calculation:

$$x_1=\Delta T_{\max}=T_{\mathrm{w,\,in}}-T_{\mathrm{r,\,out}}=8.41,\ x_2=\Delta T_{\min}=T_{\mathrm{w,\,out}}-T_{\mathrm{r,\,in}}=4.56,\ ^\circ\mathrm{C}$$

$$\frac{\partial y}{\partial x_1}=\frac{1}{\ln(\frac{x_1}{x_2})}-\frac{(x_1-x_2)\cdot\frac{1}{x_1}}{\left[\ln(\frac{x_1}{x_2})\right]^2}=\frac{1}{\ln(1.84)}-\frac{3.85\cdot\frac{1}{8.41}}{\left[\ln(1.84)\right]^2}=0.41$$

$$\frac{\partial y}{\partial x_2}=-\left\{\frac{1}{\ln(\frac{x_1}{x_2})}-\frac{(x_1-x_2)\cdot\frac{1}{x_2}}{\left[\ln(\frac{x_1}{x_2})\right]^2}\right\}=-\frac{1}{\ln(1.84)}+\frac{3.85\cdot\frac{1}{4.56}}{\left[\ln(1.84)\right]^2}=0.63$$

Result:

$$u_{\mathrm{c}}(y)=\sqrt{\left[\frac{\partial y}{\partial x_1}u(x_1)\right]^2+\left[\frac{\partial y}{\partial x_2}u(x_2)\right]^2}=\sqrt{(0.41\times0.072)^2+(0.63\times0.069)^2}$$

$$=0.053\ \ ^\circ\mathrm{C}$$

$$\frac{u_{\mathrm{c}}(y)}{y}=\frac{0.053}{3.85/\ln1.84}=0.0084=0.84\%$$

Overall Heat Transfer Coefficient, *U*

U is calculated by

$$U=\frac{q}{\mathrm{LMTD}} \qquad \text{(L. 5)}$$

The standard uncertainty of *U* is:

$$\frac{u(U)}{U}=\sqrt{\left(\frac{u(q)}{q}\right)^2+\left(\frac{u(\Delta T_{\mathrm{LM}})}{\Delta T_{\mathrm{LM}}}\right)^2} \qquad \text{(L. 6)}$$

Results:

unit	R134a	R507

	No. data	$u(U)/U$, %		No. data	$u(U)/U$, %	
		min	max		min	max
Low angle	58	2.0	4.7	22	2.4	3.6
Mix angle	58	2.1	4.9	18	2.3	3.9
High angle	59	2.2	5.1	20	2.4	4.2

Refrigerant Heat Transfer Coefficient, h_r

The film coefficient is obtained from:

$$\frac{1}{U} = \frac{1}{h_w} + \frac{1}{h_r} + R_{wall} + R_f \qquad \text{(L. 7)}$$

where $R_{wall} = (\delta / k)_{wall}$, R_f is the fouling factor. Uncertainty of U and thus $1/U$ can be obtained from previous sections. The uncertainty of the wall resistance, R_{wall}, was obtained in the water test as:

$$\frac{u(R_{wall})}{R_{wall}} = \sqrt{\left[\frac{u(\delta)}{\delta}\right]^2 + \left[\frac{u(k)}{k}\right]^2} = \sqrt{0.0087^2 + 0.0029^2} = 0.0092$$

As a safe estimation, the percentage uncertainty of the fouling factor is set as 20%. Uncertainties of the water side heat transfer had been previously obtained in the water test as:

unit	No. data points	$u(h_w)/h_w$, %	
		min	max
Low angle	19	1.2	1.3
Mix angle	18	1.3	1.5
High angle	16	1.6	2.1

The maximum values for $u(h_w)/h_w$ are to be used in this analysis. Uncertainties of the refrigerant side heat transfer coefficient can now be calculated:

$$\frac{u(h_r)}{h_r} = \frac{u\left(\frac{1}{U} - \frac{1}{h_w} - R_{wall} - R_f\right)}{\frac{1}{U} - \frac{1}{h_w} - R_{wall} - R_f} \qquad \text{(L. 8)}$$

Result:

unit	R134a			R507		
	No. data	$u(h_r)/h_r$, %		No. data	$u(h_r)/h_r$, %	
					min	max
Low angle	58	4.2	7.6	22	5.0	6.5
Mix angle	58	3.8	7.0	18	5.0	7.9
High angle	59	3.7	6.7	20	4.9	8.6

Refrigerant Mass Flow Rate $\dot{m}_r$

The R134a mass flow rate is calculated by: $\dot{m}_r = (\rho Q)_r$. Assume a rectangular distribution of uncertainty band of 1 kg/m3 for density ρ and so $u(\rho) = 0.29 \ \text{kg/m}^3$. The standard uncertainty of $\dot{m}$ is calculated as:

unit	R134a			R507		
	No. data	$u(\dot{m})/\dot{m}$, %		No. data	$u(\dot{m})/\dot{m}$, %	
		min	max		min	max
Low angle	58	0.3	1.8	22	0.3	0.5
Mix angle	58	0.4	1.9	18	0.3	0.6
High angle	59	0.4	2.0	20	0.3	0.9

Outlet Vapour Quality, *x*

The refrigerant outlet vapour quality is calculated from:

$$\dot{Q} = \dot{m}_r \cdot \Delta x \cdot i_{fg} \qquad \text{(L. 9)}$$

where the inlet vapour quality is assumed as 0. Assume a rectangular distribution of uncertainty band of 1 kJ/kg for enthalpy of vaporization and so $u(i_{fg}) = 0.29 \ \text{kJ/kg}$. The results are:

unit	R134a		R507	
	No. data	$u(x_{out})/x_{out}$, %	No. data	$u(x_{out})/x_{out}$, %

		min	max		min	max
Low angle	58	1.7	4.6	22	2.0	3.3
Mix angle	58	1.6	4.6	18	2.0	3.3
High angle	59	0.3	4.5	20	1.9	3.4

Total Pressure Drop, ΔP_{tot}

The total pressure drop is a direct measurement. The results are:

unit	R134a			R507		
	No. data	ΔP_{tot}, Pa		No. data	ΔP_{tot}, Pa	
		min	max		min	max
Low angle	58	20	43	22	20	24
Mix angle	58	21	32	18	20	26
High angle	59	20	50	20	20	74

Frictional Pressure Drop, ΔP_{fric}

The frictional pressure drop is calculated by the measured pressure drop less the pressure drop through pipeline and all fittings, given by:

$$\Delta P_{fric} = \Delta P_{measurement} - \Delta P_{pipeline} \qquad \text{(L. 10)}$$

Assume the calculation of $\Delta P_{pipeline}$ has uncertainty of 20%. The results for the frictional pressure drop are:

unit	R134a			R507		
	No. data	$\frac{u(\Delta P_{fric})}{\Delta P_{fric}}$, %		No. data	$\frac{u(\Delta P_{fric})}{\Delta P_{fric}}$, %	
		min	max		min	max
Low angle	58	7	12.4	22	9.5	12.4
Mix angle	58	5.1	12.1	18	10.8	12.5
High angle	59	5.0	11.6	20	8.2	12.8

Friction Factor, *f*

The Darcy friction factor is calculated by:

$$f = \frac{DP / L}{\frac{1}{2}\rho u^2 / d_h} = \frac{DP}{Q^2} \cdot \frac{d_h}{L} \cdot \frac{2A_c^2}{\rho} \qquad \text{(L. 11)}$$

Assuming rectangular distribution for ρ, d_h, L, A_c with uncertainty bands of 0.1%, 3%, 3%, 3% respectively, it is obtained:

$$\frac{u(\rho)}{\rho} = \frac{0.29 \times 0.001\rho}{\rho} = 0.00029$$
$$\frac{u(d_h)}{d_h} = \frac{0.29 \times 0.03 d_h}{d_h} = 0.0087$$
$$\frac{u(L)}{L} = \frac{0.29 \times 0.03 L}{L} = 0.0087$$
$$\frac{u(A_c)}{A_c} = \frac{0.29 \times 0.03 A_c}{A_c} = 0.0087$$

Results:

unit	R134a			R507		
	No. data	$u(f)/f$, %		No. data	$u(f)/f$, %	
		min	max		min	max
Low angle	58	7.3	12.5	22	9.7	12.5
Mix angle	58	5.6	12.2	18	10.9	12.6
High angle	59	5.4	11.7	20	8.4	12.9

Appendix M Heat Transfer Surface Partition for A DX Evaporator

The heat transfer surface of the evaporator is divided into two regions: evaporating and superheating. To be able to calculate individual area of these two regions, single-phase heat transfer correlation must be known for refrigerant gas at the superheating region. Now consider only the most basic conditions:

1. no non-equilibrium between the two-phases, at x=1, flow enters the region of superheating,
2. no flow maldistribution, channel-average values of flow rate is taken for analysis,
3. saturation temperature is constant in the evaporating region, this will ignore the influence of pressure drop.

the temperature profile in such an evaporator is schematically shown by Figure M.1 (Classon and Palm, 2002, Sterner and Sunden, 2006). The heat transfer rate superheating the vapour (single-phase) is:

$$\dot{Q}_{\text{sup}} = \dot{m}_{\text{r}} \Delta h_{\text{r, sup}} = c_{\text{p, r}} \left(T_{\text{r, o}} - T_{\text{r, i}} \right) \tag{M. 1}$$

where $\Delta h_{\text{r,sup}}$ is the refrigerant enthalpy change due to superheating. The temperature of water at the dividing point, $T_{\text{w,b}}$, can now be determined from:

$$\dot{Q}_{\text{sup}} = \dot{m}_{\text{w}} c_{\text{p, w}} \left(T_{\text{w, i}} - T_{\text{w, b}} \right) \tag{M. 2}$$

The superheating area, A_{sup}, can now be determined from:

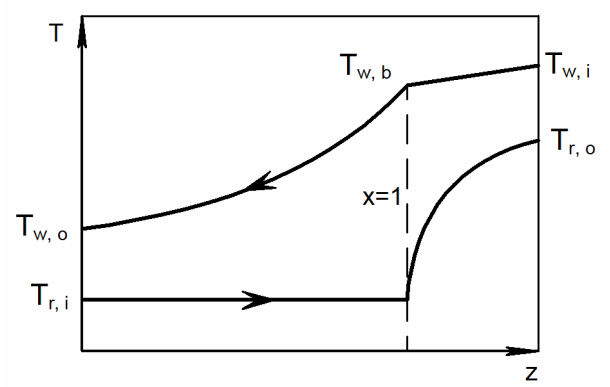


Figure M.1:Temperature profile of a DX PHE evaporator

$$\frac{1}{U_{\text{sup}}} = \frac{1}{h_{\text{w}}} + \left(\frac{\varepsilon}{k}\right)_{\text{wall}} + \frac{1}{h_{\text{r, g}}} \qquad \text{(M. 3)}$$

$$U_{\text{sup}} = \frac{\dot{Q}_{\text{sup}}}{A_{\text{sup}} \Delta T_{\text{lm, sup}}} \qquad \text{(M. 4)}$$

where $\Delta T_{\text{lm, sup}}$ is the log mean temperature difference at the superheating region. The total heat transfer area is usually known, and the evaporating area A_{tp} can be obtained from:

$$A_{\text{tot}} = A_{\text{sup}} + A_{\text{tp}} \qquad \text{(M. 5)}$$

Appendix N Operating Instructions for the Refrigerant Evaporator Test Facility

The experimental facility used in this study was designed and built as a liquid over-feed system. Refrigerant evaporator tests were carried out on three middle-size industrial brazed plate heat exchangers. The three units were installed in parallel, and the test was carried out individually for each unit. The detailed operating instruction of the facility, for each evaporator test, are given as following.

i. Before the refrigeration system is started, the compressor should be checked for any refrigerant accumulation in the crank case.

   Liquid refrigerant in the crank case will boil upon starting the compressor as a result of sudden pressure drop, and the lubricant oil in the crank case will be brought into compressor cylinders by refrigerant foams and further into the system. A convenient method to avoid this situation is to install a heater inside the crack case, and to allow the oil to be warmed for some time, say 30 minutes, before starting the system. As a heater is not available for the current equipment, a mini flow torch was used. Before starting the compressor, the blow torch was placed on the underside of the compressor just below the sight glass of the crank case. If the fluid as seen from the sight glass begins to boil then there is refrigerant in the compressor. Allow the fluid to boil until the boiling appears to have stooped completely. Once this has occurred then there should be only oil left in the crank case.

ii. Start the water pump, open the inlet and outlet valves for the evaporator to be opened while also making sure the water line valves for other evaporators are closed.

iii. Start the compressor of the refrigeration system, open the inlet and outlet valves for the evaporator while also making sure the refrigerant line valves for other evaporators are closed.

iv. Switch the data acquisition system, launch the measurement software, and carried out a self-calibration of the software.

v. Adjust the water flow rate at a fixed value at approximately 0.8 kg/s, and maintain at this flow rate for all tests. This is done by operating the bypass valve and the main line valve.

vi. Fully open the refrigerant bypass valve to achieve the maximum possible flow rate of the refrigerant, allow the system to run 40 minutes to stabilize.

vii. Once the system is stabilized, record the first reading by the data acquisition system. the data recording takes 30 seconds, as the sample rate is 2, therefore 60 data samples are taken, for each measured quantity.

viii. Reduce the refrigerant flow rate by adjusting the bypass valve, to preset values. Allow the system to run for approximately 10 minutes to stabilize, once the system is stabilized, another reading is to be taken.

ix. Follow the previous step until the flow rate is reduced to the lowest possible of the system.

x. Once all the readings are taken for the first cooling load, reduce the system cooling load, repeat steps vi – ix.

Three methods were used for controlling the cooling load: (1) by the surge drum back pressure regulator, (2) by the surge drum isolating valve, and (3) by damping the condenser surface. Of these the method (3) proved the most effective. Dampers made of cardboard strips were used, those strips were placed to over the condenser surface and the air flow rate across the condenser was controlled by adjusting the number of dampers.

xi. After all readings are saved, shut down the system and close all inlet and outlet refrigerant valves.

xii. Steps i -xi are to be repeated for other evaporators.